Hydrogel biocomposites for bone tissue regeneration

Nkhwa, Shathani

Awarding institution:
King's College London

Hydrogel biocomposites for bone tissue regeneration

Shathani Nkhwa

Thesis submitted for the degree of Doctor of Philosophy at King's College London

Tissue engineering and Biophotonics

Dental Institute, King's College London

August 2016

Abstract

The biomedical burden of large bone defects caused by trauma, infection, tumours or inherent genetic disorders remains a clinical challenge. Autologous bone or autograft continue to be the clinical “gold standard” for most effective bone regeneration, which is limited by bone supply and donor site morbidity. Thus, current synthetic substitutes need to be improved to match the performance of autografts.

Bone tissue engineering is an attractive approach for regeneration of bone especially in relation to critical sized defects and a scaffold with osteoinductive properties and adequate mechanical properties is expected to enhance bone formation. The aim of the study is to enhance bone regeneration and the concept is based on adequate design of three dimensional scaffolds that mimic the structure of bone, which by virtue of its inherent properties have the ability to localise fluids rich in osteoinductive factors.

The hydrogels and composites were all synthesized with a base polymer polyvinyl alcohol (PVA), which is both robust, biocompatible and FDA approved material. Facile methods of crosslinking such as air-drying and freeze-drying which introduces a level of porosity in the materials due to the lyophilisation process, were used to render the hydrogels insoluble, and conditions optimised to yield materials with properties suitable for soft bone tissue applications.

PVA hydrogels were synthesized and characterised, results indicated that water uptake, glass transition and tensile strength were influenced by varying concentration of the polymer solution.

A new type of dual network (DN) hydrogel composed of PVA and alginate was developed and optimised. Characterisations by spectral and thermal analysis, confirmed incorporation of alginate within the PVA network structure. Hydration dynamics and tensile properties, indicated that DN formed from a PVA base crosslinked by two freeze thaw cycles yielded tough hydrogels with controlled swelling, making them suitable for

soft tissue applications as well as the diversity of being further incorporated with ceramic fillers for the development of bone composite substitutes.

Incorporation of bioglass® 45S5 within the polymeric network structure of the DN led to enhancement of the mechanical properties such as tensile strength and fracture toughness as well as imparting bioactivity within the hydrogel composites, which was demonstrated by the development of hydroxy carbonated apatite on the surface and internal structure of the composites, this result was further corroborated by the increase in tensile strength and stiffness of the composites when placed in simulated body fluid over a period of 28 days.

The second group of hydrogel composites was composed of a PVA fluid phase and calcium metaphosphate (CMP) ceramic phase, crosslinked by freeze drying. This hydrogel composite was developed to have a high mineral content with properties that closely resemble the properties of bone based on its inorganic/organic nanocomposite structure. Compression and water uptake behaviour of the composite could be modulated by varying concentration of PVA and the composite system properties were found to be suitable and lie within the range values for trabecular bone.

In vitro cell culture tests were used to assess biocompatibility and the selected scaffolds were seeded with human osteoblast cells (HOB) and were evaluated by MTT, and live dead staining. All the systems were found to be biocompatible and cells were able to attach and proliferate within the scaffolds. Biofunctionality was assessed on the scaffolds which all showed a peak increase in alkaline phosphatase activity (ALP) at day 14, an important bone marker indicating osteoblast differentiation.

Acknowledgements

First and foremost I would like to take this opportunity to thank King's College London, for giving me the opportunity to fulfil my career aspirations, goals and dreams. I would like to thank my supervisor Dr Deb for giving me the opportunity to work in her lab, providing me with mentorship and guidance during my study period at Kings. She has played a pivotal role in my development and growth as a researcher, she has pushed me to be the best I can be in my work, introduced me to the rapidly developing world of biomaterials and has allowed me to draw on her knowledge and experience whilst completing my research. Her counsel and friendship has also helped me through some difficult times during the course of my studies, and I would like to humbly thank her for that. It has been an honour to have her as my 1st supervisor. I would also like to thank my 2nd supervisor Dr Ines Reichert for her expertise in orthopaedic surgery and the guidance she provided with surgical handling of biomaterials. I would like to give a big thanks to Richard Mallet, Neelam Gurav, Hassan Farah, Peter Pilecki, Dr Giuseppe Cama and Evren Kemal for all the insightful knowledge assistance and guidance they provided in the labs, providing a perfect environment with platforms for discussions on matters of research.

To my Family first I would like to thank my mother Unami, the great woman who sired me. As a single parent I know it must have not been easy, but your constant support and motivation from a young age has played a pivotal role in this current journey of my life. I want to take this opportunity to thank you for being a great and wonderful mother. I want to thank my father Isaac, your motivation, guidance and support of me and my career aspirations have truly been wonderful. Your words of wisdom in good and tough times have led me to become the woman I am now. Your belief in me to achieve all my dreams helped me believe in myself even more. To my aunt Taboka AKA mum/mmaMothusi/Tabs you have truly been an angel sent by god. When everything fell apart you were there for me, provided me with a support structure, you held me up when I couldn't hold myself up. Your role in my life has been beyond measure. I want to take

this opportunity to thank you for everything you are and all that you do. You are a great mother and aunt, and you have been god sent. To my grandparents my aunts, uncles, the whole family (both living and past), although too many to mention all by name I thank you too, for the provision of great family (sisterly love (Joy and Bangu), brotherly love (Mothusi, uncle Bets, Moesi)) I love you all so much. To the government of Botswana and the University of Botswana, School of Medicine, I would like to take this opportunity to thank you for all the study opportunities you have provided as well as financial provisions and support, through the course of my life, it has truly been an honour to be a child and citizen of Botswana. “Pula”.

Table of Contents

List of Figures

List of Tables

Abbreviations

3D	- 3 dimensional
AD	- Air-drying
ALP	- Alkaline phosphatases
ATR-FTIR	- Attenuated total reflectance – Fourier transform infrared spectroscopy
BG	- Bioglass®
BMP	- Bone morphogenetic protein
CMP	- Calcium metaphosphate
DbN	- Double Network
DSC	- Differential scanning calorimetry
DMA	- Dynamic mechanical analysis
DN	- Dual Network
DNBG	- Dual network Bioglass®
ECM	- Extracellular matrix
EDAX	- Energy dispersive X-ray
EWC	- Equilibrium water uptake
FT	- Freeze thawing (24hrs freeze drying followed by thawing)
HOB	- Human osteoblast
HA	- Hydroxyapatite
IPN	- Interpenetrating network
PBS	- Phosphate buffered saline
PRP	- Platelet rich plasma
PVA	- Poly vinyl alcohol
SA	- Sodium alginate
SBF	- Simulated body fluid
SEM	- Scanning electron microscopy

Chapter 1
Introduction to thesis

The musculoskeletal system of the human body acts as a scaffold providing mechanical support, protecting vital internal organs and, assisting in movement. The skeleton is composed of bones supported by ligaments, tendons, muscles and cartilage. Bone function includes storage of crucial nutrients, lipids and minerals, production of blood cells that nourish the body and play a vital role in protecting the body against infection, and storage of chemical energy. Bone is highly dynamic and is constantly remodelling and changing shape to adapt to the daily forces which it incurs. It has remarkable regenerative properties with the capability of scar-less self-renewal. Bone cells and osteoid make up the organic component of bone, and hydroxyapatite (HA) the inorganic component [2]. Natural bone has elastic modulus and tensile strength in the ranges 0.05 – 30 GPa and 10 – 150 MPa respectively, with properties dependent on its inorganic/organic nano-composite structure containing approximately 70% mineral (HA), 22% proteins (type I collagen) ad 8% water by weight [3].

Musculoskeletal disorders are the most common cause of severe long term pain and physical disability affecting hundreds of millions of people around the world. There are more than 150 different musculoskeletal disorders which encompass a range of acute onset conditions to life-long disorders, some of which are accompanied by symptoms of pain and or inflammation and can involve limitation of motion, disability and even death [4, 5]. In some cases day to day functioning can be severely restricted due to significantly high levels of pain and limitation in movement which can result in serious complications such as pressure sores or increased infections. All these factors combined can lead to negative psychological developments due to potential deformity and consequential fears of failing or social interactions.

According to the World Health Organisation (W.H.O), skeletal trauma, violence and road traffic accidents are listed by as the leading causes of disability and injury accounting for 16% of the global burden of disease [6]. Trauma can result in large or critical bone size defects impairing revascularisation, leading to insufficient provision of nutrients and oxygen to the bone cells. This results in compromised bone healing, delayed union, mal-union and non-union, thus leading to significant clinical problems. Non-union can also be associated with poor nutrition, pre-existing diseases such as diabetes, HIV and AIDS, cancer, poor and compromised blood supply, medication, and old-age due to decline in regenerative abilities such as in cases of osteoporosis, inflammation and infection of the bone and surrounding tissue [3]. These are major health concerns with huge socioeconomic implications.

Reconstruction of extensive bone defects still remains a technical challenge, bone grafting is often used to provide an osteoconductive, osteoinductive and osteogenic environment to promote bone healing and repair. Osteoconductive material is one that acts as a scaffold, supporting the attachment of osteoprogenitor cells and ingrowth of capillaries. Osteoinduction refers to the process where host mesenchymal stem cells are recruited from the surrounding tissues and differentiate into bone forming osteoprogenitor cells characterised by the presence of bone morphogenetic proteins (BMPs) and their growth factors. Osteogenesis is the ability of the graft to produce new bone, and this process is dependent on the presence of live bone cells (i.e. osteoprogenitor cells) in the graft. Autografts remain the gold standard as they are histocompatible and non-immunogenic, and they offer essential components to achieve osteoinduction, osteogenesis and osteoconduction, all of the imperative properties required of a bone graft material. Allografts represent the second most common bone-grafting technique, they are available in various forms including demineralised bone matrix (DBM), morselised and cancellous chips, cortico-cancellous and cortical grafts. Several studies have however highlighted considerable shortcomings, limitations and

complications of autologous and allogenic transplantations [7]. Reconstructive surgeries are still limited by the paucity of autologous materials available and donor site morbidity. The limitations in the application of autografts and allografts have necessitated research for alternatives and the development of synthetic bone graft substitutes. Given the continuing research in this area, the understanding on the biological aspects of bone regeneration, tissue engineering and regenerative medicine has significantly improved the new knowledge created and presents an exciting platform and new prospects in addressing development of synthetic bone grafts, these developments give surgeons new options for restoring bone form and function.

Bone tissue engineering focuses on alternative treatment options that will enhance bone repair and regeneration. Ideally bone scaffolds should be biocompatible and closely mimic the natural bone extracellular matrix niche and should allow for sufficient vascularisation to meet the needs of the growing tissue. The philosophy of tissue engineering is to aim to develop synthetic materials that establish key interactions with cells in ways that unlock the body's innate powers of organisation and self repair, as opposed to attempting to recreate complex living tissues ex vivo [8].

The purpose of the scaffold is to provide mechanical support and function as the extracellular matrix to facilitate cell infiltration, adhesion, and proliferation whilst enabling delivery of growth factors. Synthetic, natural and decellularized tissues have been widely explored as scaffolds substitutes that have led to the development of several bone substitutes such as hydroxyapatite, β-tricalcium phosphate and bioactive glasses and composites thereof. Ceramic components enables mimicking the inorganic component of bone, it lacks the organic counterpart, which creates the adequate microenvironment for osteogenesis to take place. Thus, polymers including both natural and synthetic polymers such as Polyvinyl alcohol (PVA), polycaprolactone (PCL), poly(lactic-co-glycolic acid) (PLGA), poly(l-lactic acid) (PLLA), alginate (Alg), collagen (Col), gelatine (Gn), Chitosan, silk fibroin (SF) and glycosaminoglycans (GAGs) have been employed and studied [9-11]. A number of in vitro studies proved that using polymer gels of stiffness between 10s to 100s KPa, increased the potential of materials

to foster cell proliferation, migration and differentiation [12]. This has been attributed to the fact that hydrogels have some similarity to natural soft tissues due to their highly hydrated 3D structures that can resist dissolution in aqueous environment, and they have the advantage of relative ease of fabrication, with modifiable physicochemical properties and tailorable architecture [9]. Biocomposites have been developed from calcium phosphates, ceramics and polymers to balance out limitations of the individual ceramics and polymer phases. Examples of composites currently being investigated for bone and soft tissue engineering include but are not limited to chitosan in combination with nano hydroxyapatite (nHA) or bioactive glass [13, 14], Gelatine with bioactive glass [15], Alginate with β-TCP [16], silk fibroin with nHA [17], and PVA and biphasic calcium phosphate [18]. In most of the previous studies undertaken, different methods have been applied to assess cell attachment, proliferation and differentiation as well as the biomechanical function of the composites. However, recent studies have used orthobiologics and mechanobiology, and it is imperative that future research directions consider both approaches in order to provide an overlap in bone development as well as to respond to variations in the stiffness of bone as these are influenced by the type and anatomical location of different bone.

Another important aspect in tissue engineering is the capability to translate research and technology innovations into the clinical field. Lessons learnt from the short history of industrial tissue engineering are that the provision of effective products is not in itself sufficient to ensure commercial success. Success in the market often depends on a combination of clinical performance marketing and cost effectiveness. It is important to identify the simplest functional performance required to resolve a defined clinical problem, as financial considerations dictate that the complexity of biomaterial designs be kept at a minimum because over engineering devices or materials may lead to unlikely and unsuccessful translations to clinical use [8].

The goal of this study was to design and fabricate hydrogel composite scaffolds with features to promote bone tissue regeneration with optimal trade-off between the

biological and mechanical criteria towards clinical translation. Translation requires that the process meets the FDA system requirements and hence reproducibility and ease of manufacture were important considerations. The selection of biomaterials, process and design methods were aimed to decrease micro-motion in situ, enhance toughness, be conducive to entrapping growth factors, specifically platelet rich plasma and be applicable both as cell free and cell loaded scaffolds. In this study simple and facile methods were employed to crosslink and fabricate PVA hydrogels, and the key processing parameters were systematically varied and their influence on the architecture and mechanical features of the hydrogels was assessed. The most effective method of crosslinking of PVA was then employed in the next stage to create a composite with a high ratio of calcium metaphosphate (CMP) as the filler in order to decrease the rigidity of the CMP scaffold and further allow controlled expansion to closely fit the bone defect and enhance the clinical applicability towards a bone plug. However, PVA is brittle in nature, hence a toughening of this matrix was then studied using the analogy of double networks hydrogels and dual networks where tough interpenetrating dual networks of PVA and SA were developed. Therefore the dual network phase of development was carried out with the hypothesis that, by combining the two polymers, mechanical properties would be enhanced whilst lowering the swelling ratio, which would in turn improve cell attachment and proliferation on the surface and internal structure of the hydrogels. The dual network system was then further developed to form bone composites by incorporating fillers such as bioglass, which would enhance the mechanical properties, impart bioactivity to the hydrogels via apatite formation, enhancing biomaterial/host integration and the attachment of osteoblast cells. All developed composites were fully characterised and their biocompatibility determined.

This thesis is divided into 7 chapters. Chapter 1 provides an introduction to the thesis whilst Chapter 2 highlights the literature review relevant to this study. Chapters 3, 4, 5 and 6 are the experimental chapters. Each experimental chapter is comprised of an introduction with a mini review of the specific materials used for fabrication of scaffolds in

the respective chapter, followed by results, discussion and conclusion. Chapter 7 presents an overall summary and future work.

Chapter 3 describes the fabrication of PVA single network hydrogels which were fully characterised. The hydrogels were fabricated via simple methods of crosslinking i.e. freeze thawing, freeze thawing+air-drying and air-drying for three varying concentrations of PVA polymer at different concentration to identify an optimal processing route.

Chapter 4 focusses on the fabrication of PVA and CMP composites via freeze drying. Varying concentrations of PVA were used in the development of the composites and these, were fully characterised. Selected composites on the basis of optimal properties were further assessed for biocompatibility and functionality, and the outcomes have been reported.

Chapter 5 describes a study on the fabrication of dual networks. The dual networks were fabricated using PVA and sodium alginate and the processing parameters are described followed by their characterisation. Since the properties of the dual networks were deemed suitable for both wound dressings and drug delivery vehicles, a preliminary study on the ability of the dual networks to release vancomycin is reported and finally evaluation of biocompatibility of the hydrogels was assessed.

Chapter 6 focusses on the development of dual network composites with Bioglass®, where non-porous and porous composites were developed and fully characterised. Bioactivity of the composites was also assessed with characterisation of the apatite formed on the surface of the composites. Biocompatibility of the hydrogel composites were assessed.

Chapter 7 provides an overall discussion and conclusion of the study, which provides a platform for the potential benefits and applications of this biomedical engineering innovation in the medical field and its potential application in musculoskeletal disorders.

Chapter 2
Literature review

2.1 OVERVIEW

There is a global demand for bone substitutes due to the prevalence of bone diseases encountered in the clinical environment, as well as trauma cases. Bone graft substitutes which are often incorporated during reconstructive procedures, improve the healing rates and provide a clinical response to pathologies such as degenerative diseases, congenital deformity, tumour and avascular necrosis [19]. In oral and maxillofacial treatment, dental implantation in the posterior maxilla often requires bone augmentation procedures, maxillary sinus grafting procedures have been performed with autografts or non-autogenous grafting materials [20], bone augmentation is also required to reconstruct the alveolar ridge so as to provide a base sufficient for functional and aesthetic implants [21]. Osteoporosis as well as bone loss due to failed hip and knee replacements is increasingly becoming a major problem and this has been exacerbated by the increase in the number of joint replacements. The morbidity of fractures and the consequent delays in unions and non-unions remains a technical challenge to date [22]. Bone is reported to be the second most transplanted tissue in the world and a major financial burden to the world economies [23]. The main contributory factors have been reported as accidents, bad health (obesity, diabetes), ageing population, infections and degenerative diseases.

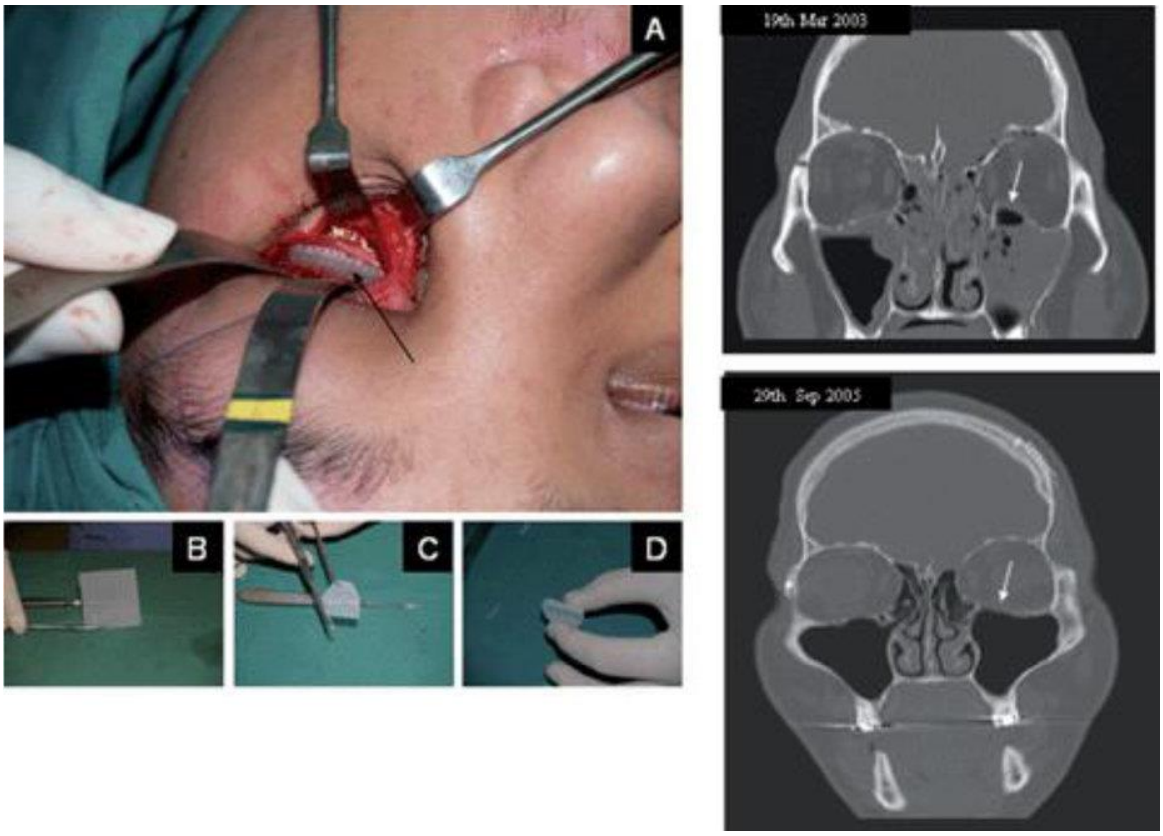

Figure 2-1: [**A,B,C,D**] Clinical case showing the craniofacial scaffold applications for orbital floor fractures, using a mouldable medical grade polycaprolactone (mPCL) scaffold sheet. CT images show defect site (above) before surgery and clinical follow up 2.5years (below) post-surgery. Adapted from Henkel et al [24].

The reports on the incidence and prevalence of non-union vary significantly based on anatomic region and the criteria used to define non-union [25]. “In the UK, there are approximately 850 000 new fractures seen each year of which the majority heal without difficulty. Rates of non-union of 5–10% of fractures have been indicated, there is however insufficient data available to validate the estimates. The cost to the National Health Service (NHS) of treating non-union has been reported to range between £7000 and £79 000 per person. However, this does not take into account the morbidity and loss of earnings of the individual nor any long-term health burden [26].” A 2012 comparative report by Frost & Sullivan on the global investment in Tissue Engineering Research reported that the United States contributes 48.6%, while Europe contributes 40.2% of global market revenue to tissue engineering solutions and that the USA is the leading country dedicating 60% of the global tissue engineering expenditure to research and development (R&D), while the UK dedicates 8% [22].

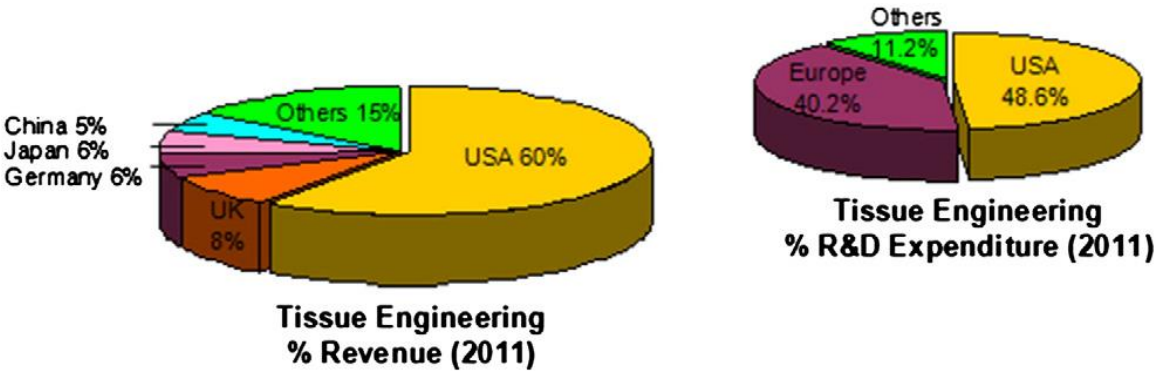

Figure 2-2: Frost & Sullivan analysis on countries leading in the area of tissue engineering, as represented by their revenue and R&D expenditure. Adapted from Liu et al [22].

2.2 BIOLOGY OF BONE

Bone composition

Bone tissue is comprised of two distinct structures being cortical and cancellous bone. Cortical bone (80%), is a dense and heavily calcified structure found at the surface and is responsible for the stability of the skeleton. Cancellous bone (20%) is found in deeper areas of the bone and is less heavily calcified with a greater surface area. The proportion of trabecular and cortical bone varies by skeletal site. The bone matrix is composed of 70% inorganic components which include mineral hydroxy apatite, bicarbonate, potassium and magnesium ions and 30% of organic components such as collagen, proteins (22%) and water (8%).

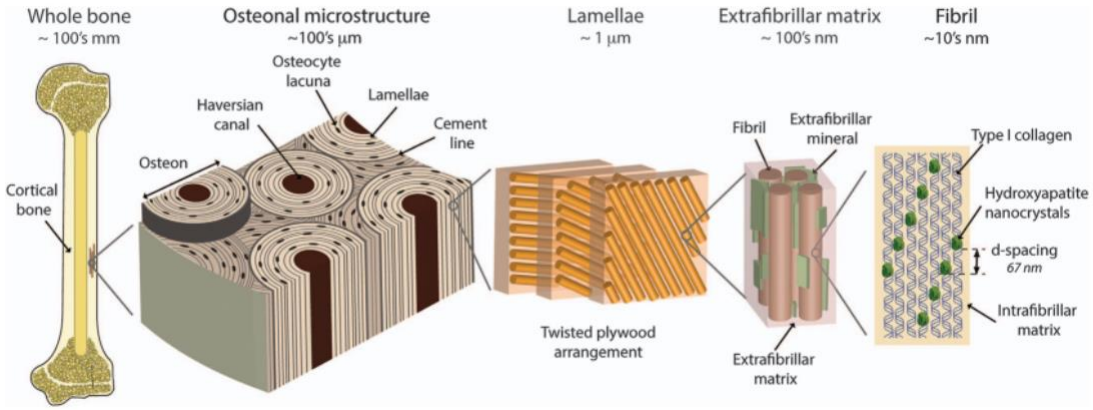

Figure 2-3: Hierarchical structure of human cortical bone. The structure of bone spans numerous length-scales from the macroscopic whole-bone structure to the nanoscale collagen and mineral components. Adapted from Zimmermann et al [27].

This specialised connective tissue has 3 dominant types of cells being osteoblasts (mononuclear cells 15-30µm in size), osteocytes (15µm in length) and osteoclasts (large multi-nucleated). Osteoblasts synthesize and release organic material of bone i.e. collagen rich osteoid containing type I collagen and proteins such as osteopontin, osteocalcin, osteonectin, osteoprotegrin (OPG), bone morphogenetic proteins (BMPs), and glycoproteins, in which mineralisation occurs. Osteocytes are derivatives of terminally differentiated osteoblasts, they are the most abundant and are present in the lacunae within the mineralised matrix (calcified bone) as they develop from osteoblasts that are trapped in newly formed extracellular matrix. They are sensory cells in the bone for mechanotransduction, enabled by their interconnected 3 dimensional cellular network. Osteoclasts play a key role in bone resorption to maintain bone homeostasis [28, 29]. All these cells form an interconnected network allowing for communication and transport between the osteocytes deep within the tissue and the osteoblasts and osteoclasts located within the vicinity of vascular spaces and bone surfaces to which the loads are conveyed. The neighbouring osteoblasts and osteocytes are connected with numerous gap junctions that allow coordinated cellular activity, whereas the intracellular communication in the form of a calcium signal exists between osteoblasts and osteoclasts and among osteoclast via receptors [28].

Biomechanics

Tissues of the body have a wide range of mechanical properties, as bone, connective tissue, cartilage and epithelial tissue all have varying properties. Cartilage is reported to behave like a viscoelastic material, epithelial tissue behaves like a synthetic elastomer [30], and bone is said to exhibit a tough behaviour at low strain rates, attributed mostly to its hierarchical, as well as porous structure, which is able to stop crack propagation after small amounts of cracking. However bone fractures more like a brittle material at high strain rates [31]. The properties of compact, cancellous bone, and some soft tissues usually affected during bone injury are listed on Table 2-1.

Property	Cortical bone	Cancellous bone	Cartilage	Skin
Compressive strength (MPa)	100 - 230	2 - 12		
Tensile strength (MPa)	50 - 150	10 - 20	9 - 40	1 – 20
Strain to failure (%)	1 - 3	5 - 7	60 – 120	30 – 70
Young's modulus (GPa)	7 - 30	0.5 - 0.05		

Table 2-1: Comparative table of mechanical properties of different tissue types. Adapted from Henkel et al [24].

Process of bone healing

When bone is injured, the trauma results in the interruption of skeletal integrity as well as disruption of vascular structures and nutrient flow in the bone leading to reduced oxygen tension and disruption of marrow architecture. The healing process to restore the tissue to its original physical and mechanical properties is influenced by a highly regulated multi stage process involving a variety of systemic and local factors. Bleeding, extracellular matrix, growth factors and stem cells are necessary factors that play a key role in the healing of fractured bone, their cellular and molecular components are present at elevated levels around the fracture site. At the cellular level, there are inflammatory cells, vascular cells, osteochondral progenitors and osteoclasts. At molecular level pro-inflammatory cytokines and growth factors, pro-osteogenic factors and angiogenic factors drive fracture repair [32]. There are two processes of healing; primary and secondary healing.

Primary bone healing: This is mainly known to occur in cortical bone repair, it is initiated when bone fragment ends are aligned and fixed avoiding any relative movements at the fracture site. This allows osteoblasts to lay across the fracture lines and rebuild new bone oriented along the dominant mechanical loading direction [33].

Secondary bone healing: Secondary healing occurs when there is a remaining gap between the bone fragment ends and a complete anatomic reconstruction of the

displaced fragments is not possible. In this case healing occurs in three distinct but overlapping stages: 1) the early inflammatory stage 2) the repair stage and 3) the late remodelling stage.

The inflammation stage begins the moment the bone is broken or injured, bleeding around the injured area leads to the formation of a haematoma during the first few hours and days. Inflammatory cells like granulocytes, macrophages, lymphocytes, monocytes, degranulating platelets and fibroblasts infiltrate the haematoma in-between the fracture. This helps combat infections as secreted cytokines such as tumour necrosis factor-alpha (TNF-α), and interleukin-1, -6, -11 and -18 (IL-1, -6, -11 and -18) lead to the recruitment of inflammatory cells which in turn recruit mesenchymal stem cells to the site of injury [29]. The clot eventually advances into a fibrous thrombus, leading to ingrowth of vascular tissue, and migration of mesenchymal cells. At this stage the exposed cancellous bone and muscle aid in providing nutrients and oxygen supply to the injured site.

During the repair stage, intramembraneous ossification starts to consolidate the injured area in the periosteal regions distant of the fracture ends (due to sufficient provision of oxygen in that area), fibroblast cells that are present in the granulation tissue begin to form cartilage and fibrocartilage (endochondral ossification, occurring in hypoxic environment) [34]. The cartilage formed in this process is usually the primary tissue to bridge the fractured zone, which helps support vascular ingrowth, as the process is accompanied by trafficking of stem cells and progenitor cells with regenerative potential, and provides substantial stability to the bone fragments and reduces inter-fragmentary movement during healing.

As vascular ingrowth progresses, a collagen matrix is laid down while osteoid is secreted and subsequently mineralized, which leads to the formation of a soft callus around the repair site. The callus remains quite weak to external stresses for around six weeks and eventually ossifies allowing for osteoblasts at the periosteum to begin laying down woven bone. The woven bone results in a callus that has a larger diameter than the original bone which in turn provides sufficient mechanical stability with an increased polar

moment of inertia against torsion and also withstanding bending loads. Due to the formation of the external callus, the internal callus becomes mineralised with calcium hydroxyapatite forming a hard callus of woven bone.

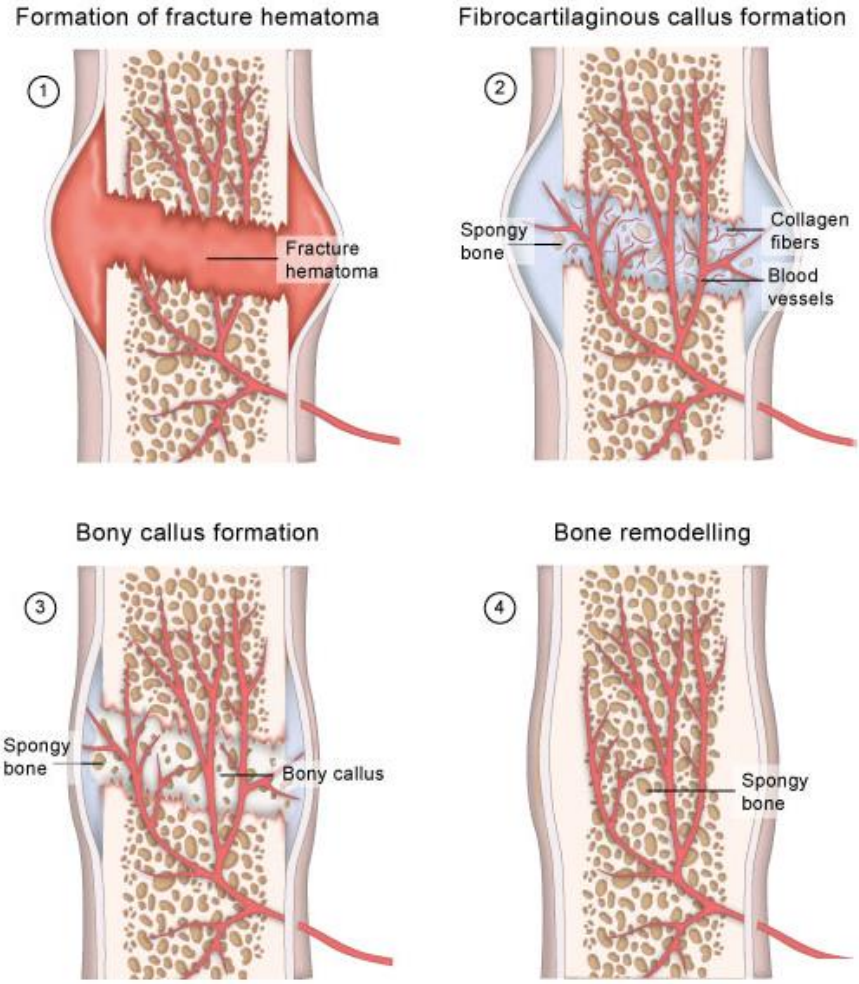

Figure 2-4: Schematic diagram illustrating consecutive phases of bone healing. Adapted from Pearson education [35].

In the final stage of remodelling the large fracture callus is replaced by secondary lamellar bone, restoring the size of the new bone to that of the original bone's shape, structure and mechanical strength, accompanied by reversion of vascular supply to the normal state. This phase of remodelling occurs slowly over a period of months to years influenced by mechanical loads and stresses incurred on the bone, however it has been reported that adequate strength is typically achieved within 3 to 6 months [33, 36, 37].

Disorders of bone union

Severe trauma can result in open fractures with tissue devascularisation and bone loss and if a fracture or wound site is not healed after 4 months, it can be considered a delayed union. If no bony healing is obtained in 6 months after the fracture, it can be clinically considered as non-union [38]. Delayed union occurs when the fracture gap is more than 1mm, resulting in reduced blood supply or infection at the wound site. Non-unions occur when there is a wide separation of bone ends resulting in soft tissue interposition, lack of blood supply, infection or an adverse biomechanical environment. The pathophysiology of non-unions has not been clearly established and consequently a variety of patient attributes and lifestyle factors such as, age, sex, diabetes, use of medications such as corticosteroids and non-steroidal anti-inflammatory drugs (NSAIDs), smoking, excessive alcohol intake and poor nutrition, have been hypothesised to contribute to the development of complications encountered in bone healing [38]. Non-union fractures can be categorised as being hypertrophic or atrophic non-unions presented in Figure 2-5.

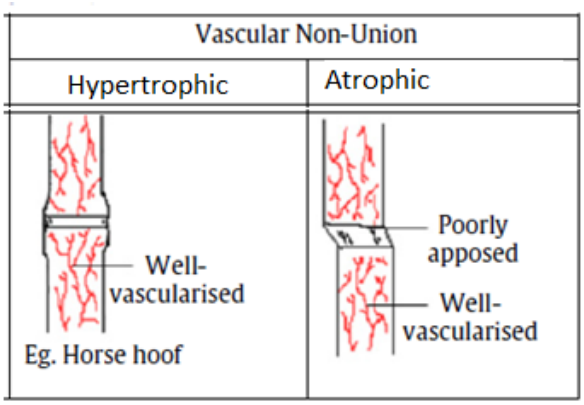

Figure 2-5: Types of non-unions, including avascular and vascular non-unions. Adapted from Liu et al [22].

Hypertrophic: It presents with a large broad vital callus that is inefficient to regenerate and form a bone union. The bone ends appear sclerotic and flared owing to excess callus formation, the non-union is also termed elephants foot due to its radiographic appearance. The gap between the bone ends is filled by cartilage and inefficient and

unstable fixation of the wound is attributed to multidirectional motion of the fracture fragments [39, 40].

Atrophic: It presents with a wound site that has no attempt in healing, due to impaired biological support, damaged vascular supply, and the destruction of the periosteum and endosteum. The bone ends are usually resorbed and rounded, and in most cases associated with soft tissue damage accompanied by detraction of the surrounding tissues. The gap between the bone ends is often very wide, filled with fibrous tissue and can be classified as a critical sized bone defect [39, 40]. The treatment of atrophic bone non-unions requires a surgical intervention that will reduce fracture gap and allow for distribution of mechanical loads while allowing for introduction of new cells, vascular supply and healthy bone tissue formation in the fracture gap.

2.3 BONE GRAFTS AND SUBSTITUTES

Various forms of bone grafts are available and classified into 3 categories: autogenous bone, allografts and synthetic graft substitutes.

Autografts (autogenous bone grafts): They are currently the gold standard for bone replacement and involves the harvesting of cortical or cancellous bone from the patient's own donor site. The most common sites of sourcing the autograft is the anterior and posterior iliac crest of the pelvis. This form of grafting provides minimum immunological rejection and histocompatibility as the graft acts as an osteoconductive scaffold, providing osteoinduction from bone morphogenetic proteins (BMPs) and other growth factors, and also allowing osteogenesis of osteoprogenitor cells [41, 42]. This method has some disadvantages as the length of time for surgery is increased and complication due to second site morbidity. It is reported that the complication rates are within the range of 8.5-20% and this includes complications such as haematoma formation, blood loss, nerve injury, ureteral injury, fracture, pelvic instability as well as cosmetic defects. In addition, the amount of healthy bone that can be harvested from the patient at any one time also poses a major limitation [43].

Although autografts are considered the ‘gold standard’, complications have been reported. A study published in 2013 where a cortico-cancellous block bone was grafted into the maxillary sinus, underwent a negative remodelling of its volume during the first period of healing. The authors argued that this was most likely due to graft resorption of the cortex, coupled with, primarily, an increase in the density of the spongious area [20]. A reduction of graft height after alveolar ridge reconstruction using iliac bone has also been reported [44], whereas calvarial bone grafts have been reported to have minimal bone resorption [45]. Graft resorption in extensive bone transplantation has been identified as a major concern and it presents a risk which can lead to insufficient bone regeneration and further complications [21].

***Allografts (allogenic banked bone grafts)*:** Bone harvested from a different donor to that of the patient mainly referred to as cadaver from other humans. Cadaveric allograft bone is available in either cancellous, cortical forms or demineralised bone matrix (DBM). In the United Kingdom allografts are mainly used in arthroplasty and are sourced from osteo-arthritic femoral heads removed during total hip replacement [46]. Allogenic bone has been found to have both osteoinductive and osteoconductive properties, but due to sterilisation and purification procedures this is limited [47] due to absence of viable cells, which leads to lack of osteogenic properties. However, the advantages are that it is readily available in various shapes, form and sizes, and there is no donor site morbidity. Allografts are available in frozen and freeze dried forms, and can be sterilised using ethylene oxide, gamma-irradiation or autoclaving, however these processes reduce mechanical integrity and osteoinductive capabilities of the graft. These methods of sterilisation have also been reported to be ineffective towards prion proteins, including variant Creutzfeldt-Jakob disease, raising the possibility of iatrogenic transmission [46]. Other limitations include harvesting and conservation of the grafts, higher risk of rejection and it does not vascularise as well as autografts [42, 47]. A study on logistic regression analysis of existing foot and ankle fusion literature, suggested that patients treated with cancellous autograft, structural autograft, and cancellous allograft have odds of fusion equal with or better than those treated either without graft or with structural allograft [19].

DBM is available in different forms such as powder, putty, crushed granules and gel filled syringes, and can be used alone or in combination with other materials such as allogeneic bone chips and calcium sulphate granules. DBM has been used in spinal infusions, healing of unicameral bone cysts, and treatment of long bone lesions and management of stiff non-unions. The osteoinductive ability of a particular DBM product is highly dependent on the type and specific preparation of bone used [48, 49].

***Xenogenic*:** Harvested from non-human species usually of bovine origin, they are considered to carry the risk of transmitting zoonotic diseases as well as triggering certain immune responses [3, 50] despite the xenograft material being processed at very high temperatures (up to 1000°C) to remove all proteins. Systematic reviews have shown that bovine derived graft materials may carry risk of prion transmission to patients [51].

***Synthetic grafts*:** Grafts are synthesized and fabricated from natural or synthetically derived materials which do not originate from humans or animals. Research in this area was primarily aimed at counteracting disadvantages and limitations of the aforementioned bone graft substitutes by providing an osteoconductive framework for bone growth while eliminating risk of infection and disease transmissions. Synthetic grafts can be fabricated from various types of materials either individually or in combination to form composites. They can be designed to be bioactive, interact and integrate with biological tissue assisting in regeneration. A major advantage is that synthetic grafts can be designed and tailored to have specific degradation rates, mechanical properties as well as be incorporated with biological molecules and drugs, to improve osteoinduction, enhance regeneration and recovery time whilst drugs may be incorporated to counteract infections during healing. Synthetic bone grafts commonly comprise of; ceramics and glasses such as, calcium phosphates, hydroxyapatite, bioactive glass, and polymer or polymer composites. Biological polymers usually employed include collagen, gelatine, chitosan and hyaluronic acid, whilst synthetic polymers include polyfumarates, polylactic acid (PLA), polyglycolic acid (PGA), polycaprolactone, poly vinyl alcohol (PVA) and copolymers of PLA and PGA (PLGA).

Commercial bone grafts

A review on bone graft substitutes currently available in orthopaedic practice identified a total of 59 bone graft substitutes marketed by 17 different companies in the United Kingdom [46]. However, internationally there are currently over 200 different bone grafts available, and many of the commercially available bone grafts have not been peer reviewed to assess their clinical efficacy.

Category	Bone graft	Form	material	Mechanism of action			Recommended use
				Osteoconduction	Osteoinduction	Resorbable	
Autografts	Extra-oral -Iliac crest -Tibial plateau	Various	Patient source	✓	✓	✓	Small to large reconstructions.
	Intra-oral -Symphysis -Tuberosity Ramus						Small reconstructions. Resorption can take up to 6 months but occurs faster in the case of extra-oral sources.
Allografts	Allomatrix®	-Injectable -formable putty	DBM with calcium sulphate carrier	✓	✓	✓	Bone void filler in trauma surgery, lumbar spine surgery, tumour resection surgery and long bone non-union. Applicable in Non-loadbearing situations.
	Plexure	-Granules -Wedge	DBM and Polylactide-	✓	✓		Void filler, oncology bone surgery, tibial

		-Block sheet	coglycolide				plateau fractures, and arthroplasty surgery.
Xenograft	CopiOs®	-Cancellous chips, -Cancellous cubes -Cortico-cancellous wedges	Bovine bone	✓			Bone void filler
	Bio-Oss®, Bio-Oss-PEN, Bio-Oss-Collagen		Bovine bone	✓			Small to moderate reconstructions in defects with moderate to high osteogenic potential. The graft has very slow resorption up to 36 months.
Synthetic graft	Osteoset	-Pellets -Beads	Calcium sulphate	✓		✓	Spinal surgery, trauma, treatment of benign cysts and adult reconstruction
	GeneX	-Paste, -Putty	Calcium phosphate and calcium sulphate	✓		✓	Scaphoid non-union, trauma and bone void filler
	ChronOS®	-Granules, -Blocks -Wedges 60% to 70% porosity	β-TCP	✓		✓	Bone Void filler where cancellous bone is required. Non-load-bearing applications in trauma, spinal and reconstruction surgery. Resorbable at 6 to 18 months.
	Norian® SRS® and Norian® SRS® Fast Set Putty	-Cement -Injectable paste -mouldable putty	Calcium phosphate	✓		✓	Bone void filler, applicable in distal radial, proximal and distal tibia, calcaneum, proximal

							and distal femur, proximal humerus and acetabulum fractures
	INFUSE® Bone Graft	-Multiple kit sizes	rhBMP-2 protein on an absorbable collagen sponge	✓	✓	✓	Approved for fusion with spinal cage, open tibia fractures with IM nail
	Endobon	-Block -Cylinder -Granules 60% to 80% porosity	HA	✓		✓	Tibial plateau, distal tibial, calcaneal, distal radial fractures and in bone tumour surgery

Table 2-2: Summary of commercially available, currently used bone graft substitutes in orthopaedic practice. Adapted from Kurien et al [46].

A report on currently available bone grafts for implantation in the UK suggests that only Alpha-BSM, Cortoss, Norian SRS and Vitoss can be clinically considered as equal or superior to autografts [46]. Clinical trials on bone non-union augmentation with graft substitutes highlight some of the limitations of current commercial grafts, for example; Ziran et al [52] reviewed 41 patients with various non-union treated with Allomatrix where they found a total of 20 patients (51%) developed post-operative drainage problems and 13 required debridement (removal of dead and damaged tissue), and the non-union persisted, with 11 developing deep infection. Similar problems have arisen when Osteoset was used in non-union surgery [53]; Chu and Shih recently described the treatment of 15 patients with non-union of the scaphoid using percutaneous fixation supplemented with GeneX, where union was confirmed in 14 patients (93%) at a mean of 15.3 weeks [46, 54]. More recently, a novel system for harvesting autologous intramedullary reamings as a bone graft from the canal of the femur or tibia called reamer-irrigator-aspirator (RIA), has been reported with emerging evidence that RIA possesses equivalent osteoconductive and vascular properties. Clinical evidence also suggests that larger volumes of graft can be obtained with RIA and that it causes less

harvest site morbidity and pain [55]. Thus, the current bone graft biomaterials tend to suffer from lack of integration with the host tissue, and in some cases bone formation is limited only to the ends of the grafts which again lead to non-union [56, 57]. In other cases late allograft graft fractures at ~10 years have been reported to be as high as 60%, with 50% loss in bone strength [58].

2.4 BONE TISSUE ENGINEERING

Strategies in design

Bone tissue engineering (BTE) focusses on the development of alternative solutions for fracture repairs in order to improve and enhance the quality of clinical responses to bone grafting procedure. In addressing the challenges of BTE therapies, it is not only important to understand the underlying causes resulting in non-union repair but, it is also critical to understand the material properties of native tissue, as each tissue serves a specific function and purpose. Parameters such as hydration dynamics and material stiffness are known to provide substantial feedback in cell-scaffold interactions and dictate cell phenotype, it is therefore imperative that these properties be understood and emulated for enhanced integration and performance of the scaffold in its biological role. Scaffolds should be tailored for different types of bone and fracture sites and it is essential that their design should take into consideration the ease of manufacturing and clinical handling of the graft in the operating room. Requirements for an ideal scaffold should include the following;

Biocompatibility: Can be defined as “the ability of a material to locally trigger and guide non-fibrotic wound healing, reconstruction and tissue integration” [59]. An ideal scaffold must be osteoconductive and osteoinductive. The osteoconductive properties provide a guide for newly forming bone by allowing bone cells to adhere, proliferate and form extracellular matrix on the surface and internal structure of the scaffold. This process supports normal cellular activity without being toxic on native tissue. The osteoinductivity induces bone formation through the recruitment and stimulation of progenitor cells and biomolecular signalling.

Mechanical properties: Mechanical properties and architecture of ideal bone substitute scaffolds should closely mimic those of the native tissue they are intended to augment, as proper load transfer is important. Inappropriate stiffness and material strength may result in consequential resorption of native bone tissue, which may severely impede the progression of bone repair, of which functional union repair may take up to several years [60, 61].

Porosity: There is a greater degree vascular infiltration, and faster rate of bone tissue ingrowth or apposition with percentage of porosity, as higher porosity is expected to enhance osteogenesis. Macropores (>100μm) are believed to favour cell migration and enhance bone ingrowth and osseointegration, whereas micropores (<5μm) results in larger surface area that is believed to contribute to higher bone inducing protein adsorption. An integral and essential property for scaffolds is interconnected porosity, which impacts ingrowth of new bone especially in long term tissue interface maintenance. Pore size should be at least 100μm in diameter for successful diffusion of essential nutrients and oxygen for cell survivability and at least > 300μm for improved osteogenesis, these values have been reported to be sufficient to support vascularisation and blood vessel invasion [62]. The pattern of bone ingrowth is reported to vary according to the scaffold architecture, this was demonstrated in a study where continuous bone-forming pattern was observed inwards of scaffolds with a random pore size, while scaffolds with pores of the same size but with solid walls led to the formation of discontinuous bone islets throughout the scaffold [63]. Even though porosity reduces the mechanical properties of scaffolds and increases the complexity for reproducible fabrication, studies have established that multi-scale porous scaffolds involving both micro and macro porosities can perform better than only macro porous scaffolds [64].

Biodegradability/Bioresorbability: An ideal scaffold should be able to degrade in vivo at a rate that is proportional to new tissue formation whilst maintaining some mechanical integrity during tissue regeneration process. The degradation behaviour of the scaffolds should vary based on applications such as 9 months or more for scaffolds in spinal fusion or 3 to 6 months for scaffolds in cranio-maxillofacial applications [65].

These requirements lay the groundwork and foundation of the 4Fs (form, function, fixation, formation) for the design of an effective scaffold. A scaffold must conform to the 3D shape of the defect (form), while maintaining mechanical properties to the bone in repair (function),and allowing for the ability of integration and attachment to the existing bone and neighbouring soft tissue (fixation), as well as providing an osteoconductive environment (formation) [23].

Types of scaffolds

Different materials have been used to fabricate an increasing number of novel scaffolds for bone tissue engineering over the past years and different methods of fabrication have been applied [29]. Composites of polymers and ceramics are the most popular class of composites investigated, due to the ability to mimic the bone architecture, with an ever increasing number of publications in this area. The criteria for selecting materials for application as biomaterials for tissue engineering is based on the materials chemistry, molecular weight, solubility, hydrophilicity/hydrophobicity, surface energy, degradation, structure, and erosion mechanism.

Polymers

Natural and synthetic polymers have been widely researched as scaffolds for tissue engineering due to their versatile properties. Natural polymers are biodegradable and are characterised by biocompatibility, enabling the adhesion and migration of cells within their structures [22]. The most commonly used natural polymers in bone tissue engineering include collagen, alginate, fibrin, hyaluronic acid, silk, gellan gum and chitosan. The main advantage of natural polymers is their ability to support tissue growth and remodelling, however they are mechanically weak.

There are biologically inspired synthetic polymers that have also been investigated for tissue repair and regeneration, which are derived from amino acids, such as tyrosine-derived polycarbonates, polyethers and, to a lesser extent polyarylates, [66, 67]. Synthetic polymers have an advantage of the ability to tailor their micro- (composition,

architecture and binding groups) and macro-scale (porosity, stiffness and elasticity) features for specific applications. Synthetic polymers such as poly (lactic acid) (PLA), poly (glycolic acid) (PGA), and polycaprolactone (PCL), Poly (vinyl alcohol) (PVA), polyethylene glycol (PEG) and poly (methyl methacrylate) (PMMA), among others are commonly used in bone tissue engineering. Some of the polymers can be degraded via the natural physiological pathway, however for some, the degradation mechanism results in a local acidic environment (e.g. PLA or PGA) that can have adverse tissue responses [65].

Currently polymers have been employed in the development of; smart hydrogels which allow for tailoring properties such as mechanical stability and release kinetics for the desired application, therefore rendering them as multicomponent hydrogels capable of responding to multiple triggers or forming mechanically strong hydrogels. They include in situ chemically crosslinkable hydrogels, double network hydrogels, combinations of natural and synthetic polymers as well as composite hydrogels [9, 68, 69]; hydrogels used as delivery vehicles for drugs and osteogenic factors [70-72]. Polymers have also been explored as coating materials for permanent bone implants to improve the interface integration with native tissue, examples include coating of ceramics (polymer coated HA graft [73]), titanium (titanium coated with a microwave plasma polymer made from allylamine (PPAAm) [74]), hard polymer scaffolds and even allografts. One successful study aimed at developing a novel scaffold for bone tissue engineering, worked on bone xenografts coated with degradable synthetic poly(L-lactide-co-Ɛ-caprolactone) (PLCL) and with natural polysaccharide polymers in order to increase their mechanical properties on one side and to improve cell adhesion on the other [75].

Limitations of polymers include difficulties in processing and purification as well as concerns regarding immunogenicity for natural polymers. The potential also exists for batch-to-batch variability in materials, diminishing the predictability of results in the clinic, and lastly natural polymers are not capable of matching the mechanical properties of bone tissue. Limitations of synthetic polymers include lack of bioactivity which restricts

positive biomaterial–host interactions, particularly in comparison to naturally derived polymers that have ECM-binding domains [76].

Ceramics

Inorganic materials, such as calcium phosphate (CaPs) and bioactive glasses, are known to have good biocompatibility. They form bonds with hard and in some cases soft tissue. CaPs have been studied extensively as scaffolds for bone tissue engineering as they are a major constituent of bone. Majority of research has been focused on hydroxyapatite (HA), beta-tricalcium phosphate (β-TCP) or mixture of HA and β-TCP, known as biphasic calcium phosphate (BCP), which have been found to successfully support new bone formation [65]. Inorganic materials vary in terms of mechanical properties and the rate at which they are resorbed. Calcium sulphate is reported to have the fastest resorption of between 4 to 12 weeks whilst hydroxyapatite has slow resorption and has been observed radiographically 10 years after implantation. Calcium phosphates depending on the characteristic phase exhibit slow to rapid resorption that can range from around 6 months to 10 years, while TCP resorption occurs between 6 to 18 months [77].

Recently the addition of dopants such as zinc and strontium into β-TCP structure have shown an increase in type I collagen gene expression and extracellular signal regulated kinases (ERK) secretion that positively regulates angiogenesis, osteoblast proliferation, differentiation and morphogenesis [78]. The addition of dopants into the β-TCP structure was also found to allow for control of dissolution rates, densification behaviour, mechanical strength, and biocompatibility [79, 80]. Many different compositions of bioactive glasses have been explored, with their main attribute being able to form a layer of hydroxy carbonate apatite (HCA) on the surface of the scaffold when placed in physiological conditions. This HCA layer significantly enhances osteoblast activity and adsorbs proteins and growth factors that facilitate new bone formation in vivo. These characteristics make them highly desirable material in bone tissue engineering [81, 82]. However, ceramics are limited by their brittleness and have low fracture toughness

usually with a comparatively high compressive modulus and in some cases their biocompatibility and biodegradability is often insufficient.

Composites

The current strategies to enhance clinical success of scaffolds have been focussed on the development of composites and hybrid scaffolds, which combine the desirable properties of individual material components to achieve a synergistic effect in their resultant properties. Composites properties can be modulated according to need and application by controlling the volume fraction of components as well as composition, this process results in scaffolds with strength that is able to match that of the properties of bone [65]. Composites can be broadly categorised into particle-reinforced, fibre-reinforced and structural composites, arising in numerous composites available for review in bone tissue engineering. However the review of composites in this section is limited to providing a background on hydrogel composites, which relate to biocomposites that can be used in conjunction with orthobiologics for bone healing, fabricated in this study.

Ceramic fillers such as calcium phosphates and hydroxyapatite can be incorporated with polymers to create hydrogel composites with enhanced mechanical properties with the ability to promote bioactivity in vitro and vivo. They can be tailored to have controlled porosity as well as be incorporated with drugs for drug delivery [83, 84]. Nano particles can be engineered from a variety of sources (e.g. polymers, minerals, metals and semiconductors) into various shapes, and have been incorporated in hydrogels to form composites [85]. Organic clay nanoparticles have been used to reinforce hydrogels for example, polymer/clay nano-composites composed of N-isopropyl acrylamide and hectorite clay Laponite XLG were formed by free radical polymerisation of the polymer in an aqueous suspension of clay. The resulting hydrogel had tensile modulus in the range of 270-300kPa and elongation of up to 1300%. The nano-composite gels could also withstand high levels of deformation in twisting bending and knotting [86]. A PVA

hydrogel reinforced with organic substituted clay nanoparticles was reported to have enhanced tensile strength and diminished microbial penetration, while maintaining high water absorbency [87]. Polymeric NP such as dendrimers and micelles have been incorporated into hydrogels for drug delivery systems [88].

Gold nanoparticles (AuNPs) possess useful electronic and optical properties and are being actively explored as biosensors (e.g. quantized capacitance and surface plasmon resonance) [89]. Gold nano particles/Poly(acrylamide) (AuNP/PAAm) composite hydrogels have been reported to demonstrate significant increase in electrical conductivity. Silver nano particles (AgNPs) have unique antibacterial properties and have been investigated for their use as antibacterial wound dressings [90] with a specific one being marketed by Smith and Nephew for wound dressings.

Strategies of coating magnetic nanoparticles (MNPs) with hydrogels have been explored to increase their hydrophilicity and biocompatibility, as well as reduce non-specific protein absorption e.g. a sol-gel reaction was utilised to coat iron oxide MNPs with silica hydrogel [91]. Because MNPs have the ability to produce heat under applied magnetic field ("magnetocaloric effect"), they have been explored in hyperthermia-based cancer therapies for use as thermal ablation and temperature sensitive drug delivery, where one study showed that magnetisation of PEG-MNP composite hydrogels generated enough heat to kill glioblastoma cells [92, 93].

Carbon based nanoparticles (CBNs) such as carbon nanotubes (CNTs) and graphene have excellent multi-functions such as mechanical strength, electrical, thermal and optical conductivity. They have been researched for a variety of applications such as high strength materials, nano scale electronic circuitry, sensors and actuators, as well as to reinforce hydrogel for biomedical applications [94, 95].

Fabrication of scaffolds

Various methods have been employed in the fabrication of scaffolds, the primary requirement has been that techniques selected should ensure consistency in the fabrication processes and reproducible results, and that simultaneously the material

properties and the desired scaffold design requirements should not be adversely affected. Fabrication of scaffolds can be grouped by their various processing techniques presented on Table 2-3.

Fabrication Method	Description
Solvent casting	Consists in dispersing calibrated mineral (e.g., sodium chloride, sodium tartrate and sodium citrate) or organic (e.g., sucrose) particles in a polymer solution. This dispersion is then processed either by casting or by freeze-drying in order to produce porous scaffolds.
Particulate leaching	Polymer is mixed with a porogen (e.g. sodium chloride, sucrose) and loaded into a mould, followed by subjection to heat treatment, freeze drying or air-drying, after which the polymer-porogen composite is immersed in a solvent for the selective dissolution of the porogen. Various shapes can be produced to form 3D porous scaffolds by simply changing the mould geometry.
Fibre bonding	Consists of individual fibres woven or knitted into 3-D patterns of variable pore size. Its main advantage is the large surface area, for cell attachment and rapid diffusion of nutrients.
High pressure based methods	Based on the CO_2 saturation of polymer disks, through their exposure to high-pressure CO_2. A thermodynamic instability is then created by reducing the CO_2 gas pressure to an ambient level, which results in nucleation and expansion of the dissolved CO_2, generating macropores.
Freeze drying	Relies on a thermally induced phase separation, which occurs when the temperature of a homogeneous polymer solution, previously poured into a mould, is decreased. Once the phase-separated system is stabilized, the solvent-rich phase is removed by vacuum sublimation leaving behind the polymeric foam. This methodology has been used to develop scaffolds from natural and synthetic origin.
Rapid prototyping	It is a computerized fabrication technique that can produce highly complex three dimensional physical objects using data generated by computer assisted design (CAD)

	systems, computer based medical imaging, digitizers and other data makers. It is also known as solid freeform fabrication (SFF).

Table 2-3: Summary of some commonly used conventional fabrication techniques of 3-D scaffolds. Adapted from Salgado et al [96].

Biomolecules/orthobiologics to promote bone healing

It has been stated that "the enormous anticipated promise of gene therapy in the 1990s has not been realized, mainly due to safety concerns related to adverse immune responses that have led to some well-publicized patient deaths in clinical trials. For clinical applications, gene therapy requires extensive information regarding the safety and efficacy of the expressed target gene as well as its delivery vehicles." [23]. This has led to the much safer use of orthobiologics in the clinical field. Orthobiologics can be defined as materials made from high concentration of substances that are naturally found within the body and can be used to help improve healing time of the injured tissue. With bone being highly vascularized, the performance of a bone scaffold is dictated by its ability to induce new blood vessel formation, as improper and insufficient vascularization leads to oxygen and nutrient deficiency, which may result in non-uniform cell differentiation and cell death. It is known that growth factors control osteogenesis, bone tissue regeneration and ECM formation via recruiting and differentiating osteoprogenitor cells to specific lineages [97]. Therefore, incorporating different growth factors and other biomolecules are of special interest for bone tissue engineering [65]. The most commonly applied growth factors are bone morphogenetic proteins (BMPs) as they have been reported to have the capability to modulate stem cell activity towards bone regeneration [98]. Current strategies have also adopted the inclusion and use of platelet rich plasma (PRP) to enhance regeneration and recovery time [99].

Bone Morphogenetic Proteins (BMPs)

Bone morphogenetic proteins (BMPs) are considered to be the gold standard for promoting bone fusion. They have been commercially available for a decade, and this has enabled surgeons to work with the osteoinductive product, however there are

collateral effects in its clinical interaction and use, most specifically its prohibitive high cost, which has limited its accessibility and use. BMPs are multifunctional growth factors which induce formation of both bone and cartilage, and are known to also play a role in a number of non-osteogenic developmental processes. BMP-2, -4, -5, -6, and -7 have the greatest osteogenic properties and extensive studies have demonstrated that they are important factors in regulating chondrogenesis and skeletogenesis during normal embryonic development [100, 101].

BMP	Function
BMP-2	Induces bone cartilage formation, as it is expressed in areas surrounding initial cartilage condensation periosteal and osteogenic zones. Plays a key role in osteoblast differentiation as it induces expression of RUNX2 and osterix.
BMP-4	Expressed in perichondrium. It also regulates the formation of teeth, limbs and bone from mesoderm, and plays a key role in fracture repair.
BMP-5	Performs functions in cartilage development. Mutations of which have been found to be a direct cause of skeletal defects.
BMP-6	Plays a key role in joint integrity of adults.
BMP-7	High levels expressed in perichondrium, and plays a key role in osteoblast differentiation as it induces of critical transcript factors RUNX2 and Osterix. Received approval for long bone non-union and has been demonstrates to be equivalent to autogenous bone grafting in the setting of tibial non-unions [77].

Table 2-4: BMPs with high osteogenic capacity and a description of their function [100, 101].

The use of BMP's in bone healing has been on the rise in the last decade [101], however there are controversial outcomes being reported past animal and human studies. Of the known bone morphogenetic proteins, only BMP-2 and BMP-7 have been approved by the United Sates Food and Drug Administration (FDA), which have also shown to encourage neovascularisation [77]. BMPs have generally been substantial to restore bone defects in animal models as well as humans. Segmental defects in the mandible of young monkeys implanted with rhBMP-2 in a poly-D, L-lacticco-glycolic acid coated

gelatine sponge showed successful regeneration [102], whilst a clinical study on 14 patients with mandibular continuity defects showed successful osseointegration with rhBMP-2 in a collagen carrier without a concomitant bone grafting material [103]. Several clinical studies have been summarised in a review by Asahina, et al, (2014) where the use of BMP led to comparable results obtained on the use of autogenous bone grafts [104]. Despite the benefits reported on BMPs, clinical translation to induce new bone formation requires a larger amount of BMPs 10~100 times more in humans as compared to smaller animal species (rodents). However, high doses of BMPs have been reported to induce significant edema or swelling, a case study example whereby a high dose of rhBMP-2 was used in anterior cervical spinal fusion procedures, caused an inflammatory response resulting in upper airway obstruction between post-operative days. As a result these patients were noted to have significantly longer stays in the hospital [105], similar observations were reported elsewhere [106] as well as in a study where a high dose of INFUSE graft was used for a similar application [107]. Other clinical studies reported that using off-label rhBMP-2 failed to restore mandibular bone defects in 2 out of 5 of their patients [108], with [109] adding to their findings potential contribution of the off-label BMP2 to abnormal neurologic findings in their patients. With these varying reports on BMPs it can be suggested that, the growth factors are able to regenerate small bony defects such as extraction sockets or the sinus floor, but are not conclusive in restoration of large bony defects such as segmental bone defects in the mandible [22, 104].

Platelet Rich Plasma (PRP)

PRP is a volume of plasma fraction from autologous blood with a platelet concentration 49 times that of the baseline level, it can be activated by thrombin or calcium chloride which induces the platelets to secrete growth factors. Enhancement or clinical efficacy in healing can be expected with platelet concentration of 1000000 platelets/µl in 5ml of plasma [110, 111], due to the high concentration of growth factors and secretory proteins present. The clinical use of platelet-rich plasma for a wide variety of applications has been reported, most prevalently in the problematic wound, maxillofacial, and orthopaedic

literature[112], and currently being explored the use of platelet concentrates to improve healing and replace fibrin glues [99, 113]. Examples of biologically active factors released by activated platelets are presented on Table 2-5.

Growth factors	Biologic Activities
PD-EGF	Promotes wound healing by encouraging cell growth recruitment and differentiation. Basically stimulating the proliferation of keratinocytes and dermal fibroblasts. Also responsible for cytokine secretion [99, 114].
PDGF A + B	Stimulates production of other growth factors, chemo-attraction, cell recruitment & proliferation as well as blood vessel growth and granulation. Leads to matrix formation with BMPs (collagen & bone) via growth factor secretions. Promotes messenchymal stem cell, and endothelial cell replication, & osteoid production [99, 110, 114].
PDAF	Has the capacity to induce vascularisation by stimulating the vascular endothelial cells [99].
PF-4	This is a chemo-attractant for fibroblasts and a potent anti-heparin agent and is known to stimulate the initial influx of neutrophils into wounds [99].
FGF	Potent inductor in cell proliferation. Responsible for cell migration and growth. As well as angiogenesis (blood vessel growth) and fibroblast proliferation [110, 115].
EGF	Responsible for cell proliferation and differentiation of epithelial cells [110].
VEGF	Main inducer for formation of blood vessels (angiogenesis), vessel lumen, migration and mitosis of endothelial cells and also responsible for vasodilation by indirectly releasing nitrous oxide. Creates fenestrations and chemotactic for macrophages and granulocytes [99, 115].
ECGF	Responsible for angiogenesis and endothelial cell proliferation [114].
TGF-β1	Promotes bone matrix synthesis and enhances proliferative activity of

	fibroblasts. Stimulates cell replication, biosynthesis of type I collagen and fibronectin as well as blood vessels. Responsible for growth inhibition and apoptosis (cell death) by inhibiting osteoclast formation, bone resorption, differentiation and activation [99, 114].
IGF-I, II	Enhances bone formation by proliferation and differentiation of osteoblasts and responsible cell growth, differentiation, recruitment and collagen synthesis with PDGF, as well as being chemotactic for fibroblast and stimulating protein synthesis [99, 114, 115].

Table 2-5: Biomolecules found in platelet granules; PD-EGF(platelet-derived endothelial growth factor); PDGF (platelet derived growth factor); PDAF (platelet derived angiogenesis factor) FGF (fibroblast growth factor); EGF (epidermal growth factor); VEGF (vascular endothelial growth factor); ECGF (endothelial cell growth factor); TGF (transforming growth factor); IGF (insulin like growth factor).

PRP also contains white blood cells such as monocytes and polymorphonuclear neutrophils, which trigger a localised inflammatory effect beneficial to tissue healing, but neutrophils have been hypothesized to impede healing. PRP is used in orthopaedic applications to enhance bone healing, especially in fracture repair as a method of improving fusion or non-union rates [116]. However, the use of PRP continues to be controversial in terms of its effect on enhanced or accelerated bone healing which may be attributed to the lack of localisation of PRP at the wound site, or due to rapid distribution within the body. Tricalcium phosphate/chitosan in combination with autologous PRP, have been reported to enhance osteogenic differentiation of MSC's in vivo (in goats), indicating induction of significant osteogenesis with PRP [117], however another study comparing the bone regenerative effect of PRPs of different species (rat, goat, human) using human bone graft and HA/TCP reported that in rats and goats, PRP did not enhance bone regeneration, but human PRP combined with HA/TCP resulted in significant bone regeneration [16]. The combination of CPC's with PRP in conjunction with polymers also indicate contradicting reports on the effect of the inclusion of PRP on the properties. CPC's in combination with 10% PRP were reported to cause a reduction in the modulus of the cements by 20-50%, it however resulted in greater new bone tissue

formation at 9 weeks in rabbits in comparison to cements with no PRP [118], whereas a PRP/TCP collagen cement reported no loss in the properties of the CPC. A clinical trial on twenty three patients with periradicular bony defect, evaluating the osteogenic potential of alloplastic (G-bone synthetic composed of TCP and HA) bone substitute with and without PRP, reported early bone regeneration in grafts with PRP [119]. An observational study that examined the clinical results and complications after the use of autologous platelet concentrate (APC) in 62 patients undergoing a variety of foot and ankle surgery with risk of non-union and 56 patients with APC and bone graft, concluded that the platelet concentration may be beneficial [120]. A similar study using APC with local autograft plus tricalcium phosphate and hydroxyapatite (TCP/HA) reported that addition of autologous platelet concentration to a mixture of autologous bone graft plus TCP/HA decreased the rates of posterolateral lumbar fusion [121]. One study examining a two year follow up on determining the efficacy of platelet glue in instrumented posterolateral lumbar fusion with local bone graft in 67 patients 34 of whom were treated with platelet glue concluded that there was not enough evidence to support the advantages of using platelet glue [122]. A retrospective study evaluating two groups undergoing lumbar fusion (one with and one without autologous growth factors) in lumbar intertransverse fusions, concluded that the use of autologous growth factors resulted in inferior rates of arthrodesis as compared to autogenous bone grafts alone [123]. A review by Hsu et al, on PRP in orthopaedic applications concluded that there is limited clinical evidence demonstrating any beneficial effects from the use of PRP in bone healing applications, citing that “clinical evidence indicates that PRP is not efficacious either alone or as an adjunct to local bone in these applications” [124], however a correspondence to this publication by Padilla et al, stated that “we should no longer compare the biologic and therapeutic efficacy of very distinct products in musculoskeletal orthopaedic surgery by lumping all autologous platelet- and plasma-derived products together. In the field of PRP products, we must not take oranges for apples simply because they are both fruit [125].”

2.5 CLINICAL TRANSLATION – Challenges for the future of bone tissue engineering

In order to translate scaffolds from bench to bedside, it is imperative to precisely assess the clinical demands for specific scaffold characteristics. To achieve a broad and optimised range of clinical applications, the scaffold is required to perform as a developmentally conducive extracellular niche with a dynamically long-lasting yet degradable three-dimensional architecture, which over time, can be replaced by cell-derived tissue function. An important gate keeper to the translation of scaffolds for clinical use is the design and manufacturing processes [24]. Therefore new scaffolds should meet the following clinical translation requirements:

- FDA approval.
- Cost effective manufacturing process.
- Ability to be sterilised by industrial techniques.
- Must be user friendly and easy to handle with minimal preparatory procedures and turnaround time in the operation theatre.
- Scaffolds should be radiographically distinguishable from newly formed tissue. [24]

Advancement in bone tissue engineering remains a challenge, the progress achieved to date is very low with limited clinical solutions attained, despite the significant investment in research and development. Intensive investigations with large numbers of publications yearly have been undertaken as well as various clinical translation studies. The most pressing challenge remains to be the issue of long term mechanical integrity as well as insufficient vascularisation in the grafts which limits the cell survival rate thus resulting in poor osseointegration, a few of these factors are summarised in Table 2-6.

Factors	**Challenge**
Vascularisation	Poor vascularisation within large grafts, attributed to the porosity within the graft/scaffold.
Osseointegration	Poor osseointegration of implant with host bone.
Infection	Wound site susceptible to infection depending on sterility techniques adopted during scaffold fabrication, and implantation. Lack of/slow resorption of grafts, typically HA increases the possibility of infection over long term.
Degradability	Ability to degrade and resorb, ideally in tandem with rate of new bone formation. Hydroxyapatite (HA) scaffolds used are non-resorbable and in some cases take years to resorb. Calcium sulphates undergo fast resorption which is not in proportion to the rate of new bone ingrowth.
Strength	Low stiffness and strength.

Table 2-6: Main factors that limit success in clinical orthopaedic applications. adapted from Liu et al [22].

It has been hypothesised that the inconclusive reports obtained from the use of orthobiologics such as PRP have been due to the limited ability to retain the product within the graft and localisation of the product at the wound site. Some studies have also reported that incorporating the product in the stages of scaffold fabrication results in growth factors that are not fresh nor the patient's own(autologous) at the time of transplantation. These factors have limited the use of orthobiologics in clinical practice. Additionally the cost of current commercial bone grafts to date, are high and even more expensive when incorporated with orthobiologics such as BMPs, and therefore representing an enormous cost to the health system [46]. However the current ability of doctors to spin autologous blood to obtain PRP therefore increases the feasibility for it to be incorporated within the scaffolds during surgical procedures.

CONCLUSION AND AIMS

The drawbacks and limitations associated with the use of autografts, allografts and xenografts are a significant factor indicating the need for focussed research and development in synthetic bone grafts. The review of literature confirmed that composite biomaterials have the potential to significantly improve bone regeneration. The complexity in the challenges of tissue engineered bone formulations need to extend beyond simple void fillers to more challenging biomimetic, biofunctional constructs, which will then be subjected to the standard lengthy approval process for clinical translation. Despite the challenges encountered in bone tissue engineering, there is tremendous optimism on the potential to replace damaged and degenerate structures and tissues. Undoubtedly, there is a large and essentially unmet clinical need for highly effective smart bone substitutes that can be used in conjunction with orthobiologics. Ideal characteristics of a bone substitute should be;

- Non immunogenic and non-toxic.
- Design controllable, inexpensive and readily available.
- Contain minimal number of components so as to reduce its complexity.

The overall objectives of this study were therefore to;

- Develop a clinically viable technology to repair, regenerate and enhance bone healing across bone defects.
- Develop an osteoconductive bone substitute with good structural properties.
- Develop a graft that can readily absorb autologous PRP becoming rich in growth factors, as well as retaining them, allowing for their local delivery at the wound site, so as to imbibe osteoinductive properties, which assist in the process of bone healing.

The following steps were followed with the aim of accomplishing this goal.

1) **Development of matrix:** Matrices were fabricated via facile methods of crosslinking

I. PVA hydrogels and composites,

II. PVA-alginate dual network hydrogels and their composite networks,

For applications as scaffolds for soft tissue and bone augmentation and regeneration, specifically focusing on the ability of the fabricated materials to be able to absorb and retain biological fluids rich in growth factors (orthobiologics) which aid in enhancing tissue regeneration. In addition the composite hydrogels were synthesised in micro and macroporous form, which is expected to confer the ability of these materials to support functional extracellular matrix.

2) **Composite systems for load bearing:** The functional stiffness of bone varies depending on its type of collagen content and its recognised effect on fracture healing. This concept was applied to develop optimum formulations of composite hydrogel systems. Physico chemical and mechanical properties to understand the potential limits of applications the hydrogels and composites can address.

Biocompatibility and functionality assessment: Preliminary studies were carried out and various in vitro assays were used to assess the cell material interaction. However further in-depth evaluation of in vitro studies will be required prior to in vivo implantation and finally to clinical translation. The study however represents facile methodologies towards fabrication of bone substitutes to enable clinical translation.

Chapter 3
Poly(vinyl alcohol) hydrogels fabricated using facile methods of crosslinking

3.1 INTRODUCTION TO HYDROGELS

Hydrogels are three dimensional polymeric networks that are able to absorb and retain large amounts of water or biological fluids. A strong gel consists of an almost frequency independent G' and G'' moduli, where G' values are typically 1-2 orders of magnitude greater than G'' (G'>>G'', G''/G'<0.1). A weak gel has a profile G' and G'' moduli with a slight frequency dependence (G''/G'>0.1) [126]. The fluid retaining polymers result in soft tissue like consistency with a relatively porous structure that resembles living tissues thereby minimizing inflammatory response to the surrounding cells [127]. Hydrogels can be 'reversible', which are primarily formed via the molecular entanglements or through involvement of secondary forces such as ionic, H bonding and hydrophobic forces and these physical gels can be reversed by altering the environment, whilst 'permanent' gels are obtained via covalent bonding through cross linking of the macromolecular chains. Chemical crosslinking has permanent junctions formed by covalent bonds, while physical crosslinking has transient junctions arising from either polymer chain entanglements, crystallite formation, or weaker physical interactions such as ionic interactions, hydrogen bonding, or hydrophobic interactions [127]. Both physical and chemically crosslinked hydrogels are not homogenous, due to inhomogeneities arising from clusters of molecular entanglements, or hydrophobically or ionically associated domains. Transient network defects also contribute arising from, free chain ends or chain loops in physical hydrogels and or due to cluster formation. Cluster formation occurs due to regions of low water swelling and high crosslink density, that are dispersed within regions of high swelling, and as well as low crosslink density in chemical hydrogels [128].

A gel consists of continuous solid with fluid phases of colloidal dimensions, gelation of the gel can be induced by rapid evaporation of the solvent. Drying under normal conditions gives rise to capillary pressure that causes shrinkage of the gel network resulting in a dried gel called a xerogel. If the gel is dried under supercritical conditions, where there is no interface between liquid and vapour, so there is no capillary pressure and relatively little shrinkage, this results in an aerogel. Hydrogels can absorb from 10-20% up to thousands of times their dry weight in water, many of these properties are governed not only by degree of swelling, but also directly by the chemical nature of the polymer network and network morphology [9]. The interactions responsible for water sorption include capillary, osmotic and hydration forces exerted by the crosslinked polymer chains resulting in expansion of the polymer chains. The magnitude of these opposing effects determines the equilibrium swollen state, which to a large extent determine some important properties of the hydrogel, including internal transport and diffusion characteristics and mechanical strength.

The suitability of hydrogels as biomedical materials and their performance in a particular application depend to a large extent on their bulk structure. The most important parameters used to characterise the network structure of hydrogels are:

- The polymer volume fraction in a swollen state (a measure of the amount of fluid imbibed and retained by the hydrogel).
- The molecular weight of the polymer chain between two neighbouring crosslinking points which can either be chemical or physical in nature (a measure of the degree of crosslinking of the polymer).
- The corresponding mesh size (a measure of space available between the macromolecular chains, very useful for diffusion of drugs).

These parameters are inter-related and can be determined by applying the equilibrium – swelling theory and rubber elasticity theory. With neutral gels, Flory–Rehner theory is also useful for analysis [129], this theory describes swelling by stating that “crosslinked polymers will reach equilibrium in a fluidic environment by the thermodynamic force to

reduce entropy via mixing as opposed to by the elastic or retractile force of the polymer chains themselves to contract."

Hydrogels have numerous applications in the pharmaceutical and medical industry, due to their ability to be fabricated in many different physical forms, such as solid moulded forms in the case of soft contact lenses, membranes or sheets for use as a reservoir in a transdermal drug delivery patch, or for 2D electrophoresis gels, pressed powder matrices applied as pills or capsules, micro particles applied as bio adhesive carriers or wound dressings, and coatings on implants or catheters [128].

3.2 CLASSIFICATION OF HYDROGELS

Hydrogels can be characterised based on their derivation and composition which can be divided into natural polymer hydrogels, synthetic polymer hydrogels and combinations of the two classes (bio hybrid hydrogels).

Natural polymers are derived from natural sources such as marine and algae that yield polysaccharides such as alginate and agarose, or can be obtained from mammalian extracellular matrix, examples include, collagen, hyaluronic acid, fibrin, gelatine, chondroitin sulphate, elastin and heparin. They are appealing for biological applications since they are biocompatible and have low toxicity, which has rendered them as effective matrices for cellular growth especially as they contain many cell signalling domains present in the in vivo extracellular matrix. However, hydrogels from natural polymers are mechanically weak and can seldom be used in native form.

Synthetic polymers offer great versatility in controlling polymer architecture, which is essential to prepare hydrogels with structured network, mechanical properties, degradation rates, chemical and biological response to stimuli. Some examples of synthetic hydrogels in biomedical use are poly ethylene glycol (PEG), poly(hydroxyethyl methacrylate) (PHEMA), polyvinyl alcohol (PVA) and polyacrylamide (PAM).

Hybrid hydrogels are derived from the integration of natural and synthetic polymers to create novel systems with high affinity specificity of binding with tailorable properties [129].

Ullah et al. 2015 stated that “The classification of hydrogels depends on their physical properties, nature of swelling, method of preparation, origin, ionic charges, sources, rate of biodegradation and observed nature of crosslinking.” [130]. However other modes of classification of hydrogels have been proposed [Peppas [127]], which include the method of preparation, ionic charge and physical structural features.

Hydrogels based on method of preparation: Hydrogels have been classified further into four groups of, homopolymer, copolymer, multipolymer and interpenetrating hydrogels. Homopolymer hydrogels are cross-linked networks of one type of hydrophilic monomer unit, whereas copolymer hydrogels are produced by cross-linking of two comonomer units, at least one of which must be hydrophilic to enable swelling of the hydrogel. Multipolymer hydrogels are produced from three or more comonomers reacting together. Finally, interpenetrating polymeric hydrogels are produced by preparing a first network that is then swollen in a monomer, the latter reacts to form a second intermeshing network structure which can be further crosslinked or not [127].

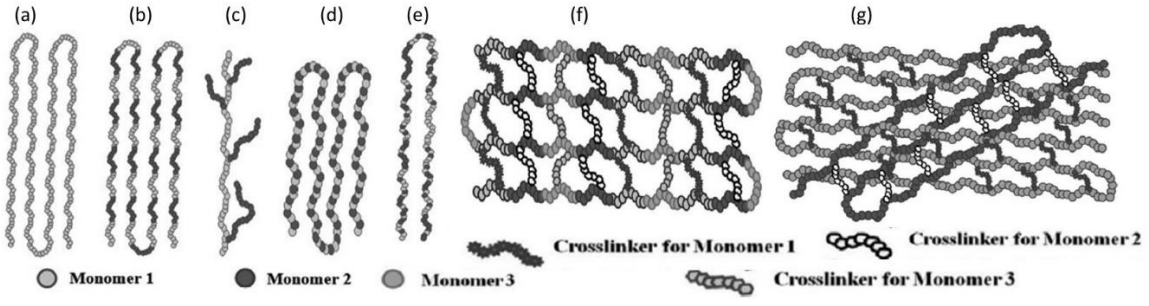

Figure 3-1: Schematic diagram for molecular structure of (a) Homopolymeric hydrogel, (b) Block copolymeric hydrogel, (c) Graft copolymeric hydrogel, (d) Alternating copolymeric hydrogel, (e) Random type copolymeric hydrogel, (f) multi-polymeric hydrogel and (g) interpenetrating network (IPN) hydrogel. Adapted from Singhal et al [131].

Ionic charge: The hydrogels have been classified as neutral, cationic, anionic, or ampholytic hydrogels. This refers to the overall charge of the hydrogel, where neutral hydrogels have no charged groups; anionic hydrogels have negatively charged groups (they dissociate more in higher pH media, and hence, display superior swelling in neutral basic solutions); cationic hydrogels have positively charged groups (their swelling is dependent on pH of the aqueous medium, which determines the degree of dissociation of the ionic chains. Cationic hydrogels display superior swelling in acidic media since their chain dissociation is favoured at low pH); whilst ampholytic hydrogels have both negative and positive charged groups rendering them with a dual behaviour (a change in pH can change the overall ionic properties). The anionic, cationic and ampholytic groups are described as ionic hydrogels or polyelectrolytes [127].

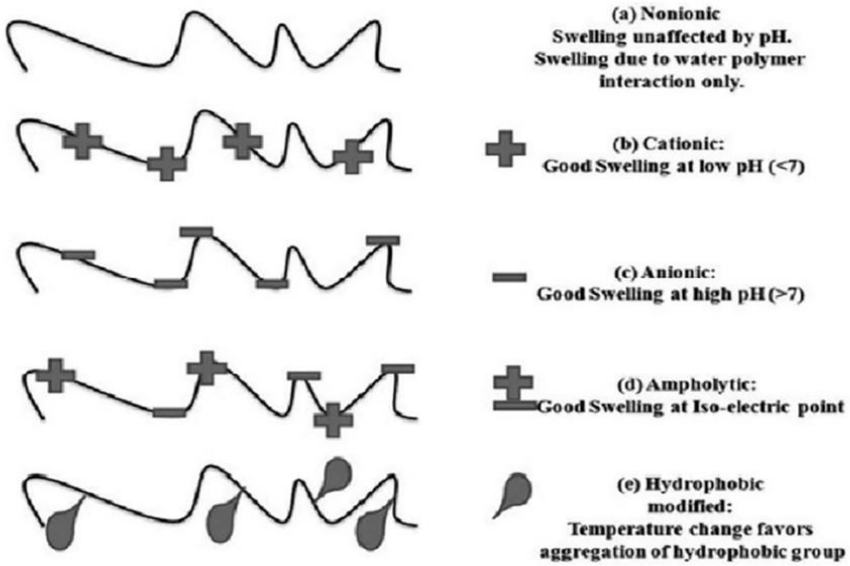

Figure 3-2: Schematic representation of different hydrogels based on presence of electric charge (a) non-ionic, (b) cationic, (c) anionic, (d) ampholytic and (e) hydrophobic modified hydrogels. Adapted from Singhal et al [131].

Physical structural features: Hydrogels can be classified as amorphous, semi crystalline, hydrogen bonded or complexation structures. In amorphous (non-crystalline) hydrogels, the macromolecular chains are arranged randomly; semi crystalline hydrogels include a mixture of amorphous and crystalline phases possessing dense regions of ordered macromolecular chains (crystallites); hydrogen bonds (if the hydrogel network is

based on electrostatic interactions) and complexation structures may be responsible for the three-dimensional structure formed [132, 133].

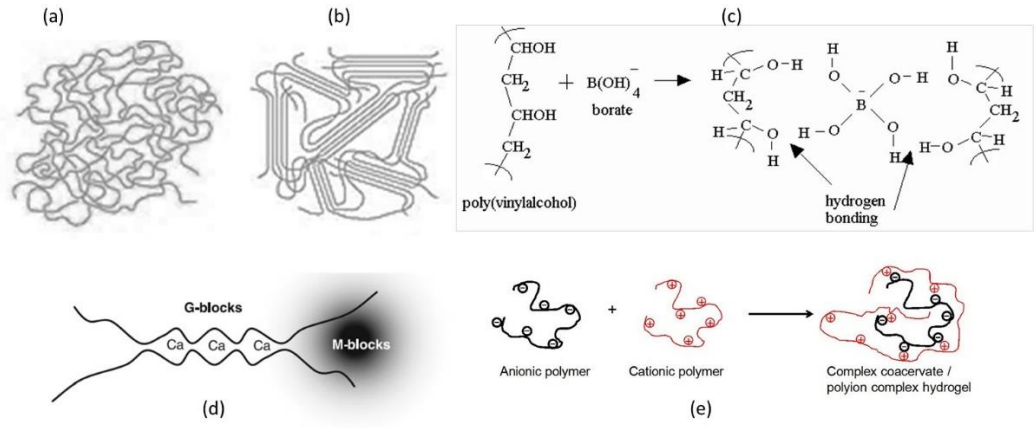

Figure 3-3: Schematic illustration of physical features of polymers (a) amorphous (b) semi-crystalline and physical crosslinking of polymers via (c) hydrogen bonding, (d) ion-polymer complexation and (e) polymer-polymer complexation. Adapted from Singhal et al [131].

3.3 SYNTHESIS OF HYDROGELS

Many different routes have been employed in the design and synthesis of hydrogels, either via chemical or physical crosslinking.

Chemical crosslinking of hydrogels

Chemically crosslinked hydrogels can be synthesized by chain growth polymerisation, addition or condensation polymerisation. Copolymerization or cross-linking free-radical polymerizations are commonly used to produce hydrogels by reacting hydrophilic monomers with multifunctional cross-linkers. The reaction can be initiated by photo-initiators, radiation, ultraviolet or chemical catalysts and the choice of the initiator depends on the type of monomer used. The reaction can be carried through bulk, suspension or solution polymerisation methods. However, all the methods used for biomedical applications need to consider the biological effects of the initiators and reaction conditions. This becomes further challenging if in vivo gelation is desirable, which may impair cellular functions.

Physical cross linking of hydrogels

On the other hand physical hydrogels are crosslinked via physical means, and these include ionic interaction, stereocomplex formation, hydrophobic association, protein interaction, crystallization and hydrogen bonding [130].

Hydrogen bonding can also function as a crosslinking tool in polymers containing a multitude of hydroxyl groups such as poly-vinyl alcohol. Aqueous solutions of polymers (gelatine, PVA etc.) are able to gradually gel and experience a small increase in elasticity upon standing at room temperature, with increase in time at this temperature partial and complete drying of the polymer solution can be achieved resulting in hydrogels with varying strengths depending on the polymer concentration, but in most cases weak physical gels with reversible links are formed from temporary associations between chains (e.g. hydrogen bonds). This form of drying is termed **air-drying**.

Crystallization involves a freezing and thawing process and creates a strong and highly elastic gel. PVA is an example of hydrogels that can be formed by physically crosslinking through repeated freezing/thawing cycles. Freeze thawing entails repeated cycles of freezing polymer solutions at temperatures below ~ -10°C and thawing with repeated cycles for constant known periods of time. This process produces dense thermo-reversible gel that are physically crosslinked polymers, which may contain uncrosslinked polymer and water. Properties of the resultant hydrogel are highly dependent on the molecular weight of the uncrosslinked polymer, concentration of the aqueous solution, temperature with length of time of freezing, and number of freeze-thaw cycles [134].

Principles of freeze-drying

Freeze drying or lyophilisation is an effective drying process, mostly done with water as a solvent. The first step entails freezing the product (polymer solution) to a minimum of -40°C, so as to allow for the water and solids to be fully crystallized whereby ice and solids are enclosed in zones in which amorphous concentrated solids and water remain in a mechanically solid state.

Once the suspension is crystallized, moisture (ice or water in an amorphous phase) can be extracted through sublimation from solid state (ice) directly to vapour phase (gas), whilst maintaining the materials crystalline structure. This method of drying results in scaffolds with random pore structure and network (porosity is achieved from the areas that had been previously occupied by the sublimated solvent.) The initial concentration of the polymer solution, the end temperature of cooling, and the length of time at this temperature are some of the factors that determine crystallisation [135].

The principle of sublimation can be explained with reference to a vapour pressure phase diagram (Figure 3-4), which demonstrates that at normal atmospheric pressure, water freezes below 0°C and boils at 100°C. The boiling point is reduced at lower pressures (principle on which vacuum distillation is based) and conversely raised at higher pressure (principle on which the pressure cooker operates). The triple point exists at exactly 6.11mbar and this is where the melting-point curve, vapour-pressure curve and sublimation-pressure curve meet. Below 6.11mbar H_2O passes directly from a solid to a gaseous state.

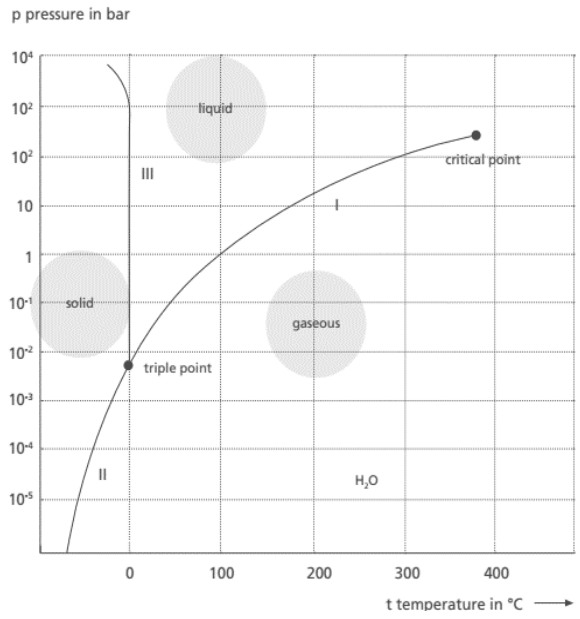

Figure 3-4: The phase diagram of water and the area in which this transfer from solid to vapour is possible. NB: atmospheric pressure = 101325 Pa (1.01325 bar).

Freeze-drying technique are widely used in pharmaceutical, biotechnology and food industry, where it has been used for: preserving characteristics of a substances such as

conserving archaeological finds, pharmaceutical products and milk; or for conditioning materials in cases of dried fruits in yoghurts; and also in chemical analysis of soils and organic substances in foodstuffs.

In recent years this drying technique has found use in the biomaterial industry as a process of physically crosslinking hydrogels with the use of bench top freeze driers to fabricate materials for tissue engineering applications. These freeze-dryers consist of, a vacuum system and condenser chamber (-55°C to -105°C) depending on the type of system. The vacuum, creates a pressure free environment which facilitates easy flow and migration of moisture as well as extraction of non-condensable vapours from the frozen gel and the shelf unit of which the sample is placed, to the condenser chamber as vapour naturally travels towards cooler surfaces.

The freeze drying technique of crosslinking to obtain hydrogels has advantages in that chemicals are not required for crosslinking, which may affect the biocompatibility of the resultant hydrogel, or require multiples washes to remove remnants of toxic substances, however this method does have limitations in that :

- There is limited control in the tailoring of porosity.
- The process of crosslinking is lengthy and time consuming.
- Benchtop freeze dryers are expensive.

Hydrogels fabricated in this manner have been found to be highly applicable in regenerative medicine, due to the nontoxic manner of fabrication and resultant micro and macroporous structure. Regenerative medicine relies on imbibing appropriate cellular activity through a combination of cells and a matrix. The matrix is usually a 3 dimensional biodegradable matrix with structural features emulating the extra cellular matrix (ECM) that supports tissue regeneration. Research pertaining to the criteria of selection and application of biodegradable matrices are still mainly empirical, however it is now recognised that the structural support, stiffness of the substrate, chemical composition and the signalling molecules provided, play an important role in controlling cell

behaviour. These parameters gives rise to a complex set of requirements and need consideration in conjunction with the already established correlation of biomaterials and cell behaviour [7].

3.4 POLY (VINYL ALCOHOL) HYDROGELS

Poly(vinyl alcohol), PVA is a water soluble semi crystalline synthetic polymer, produced via partial or full hydrolysis of polyvinyl acetate (PVAc) by replacement of the acetate group in vinyl acetate with the hydroxyl group in the polymer chain, in the presence of either a base or acid catalyst. Vinyl acetate is polymerised followed by alkaline hydrolysis with e.g. sodium hydroxide, which is an important catalyst for alcoholysis in the presence of an alcohol such as methanol and ethanol [136] (Figure 3-5). The level of hydrolysis governs the physical, chemical and mechanical properties of the resultant PVA [137]. PVA is commercially available in different grades based on their degree of hydrolysis and are classified as: partially hydrolysed 84.2 to 89.0% (can be considered as a polymer mixture of vinyl alcohol and vinyl acetate), moderately hydrolysed grade ranges from 92.5 to 96.5%, and completely hydrolysed ranges from 98.0 to 99.0% [138]. The degree of hydrolysis has a significant effect on solubility, which decreases with increase in the level of hydrolysis, as more hydroxyl groups cause strong intra and inter hydrogen bonding, whilst viscosity increases with degree of hydrolysis.

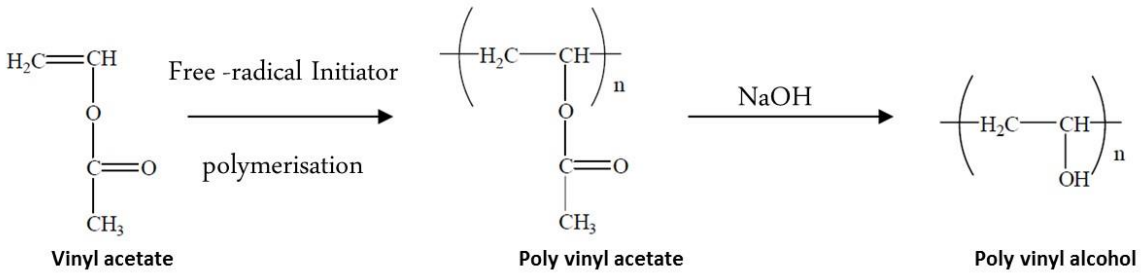

Figure 3-5: The reaction sequence for synthesis of PVA.

Crosslinking PVA

PVA contains a secondary hydroxyl group, which can be crosslinked either via chemical or physical crosslinking. Chemical crosslinking can be carried out by reacting with

aldehydes such as formaldehyde, glyoxal, glutaraldehyde [139, 140]; dicarboxylic acids [141] or inorganic compounds i.e. borate [142]. Physical crosslinking of PVA can be achieved via radiation photo-crosslinking [143, 144], air drying and repeated freeze-thawing cycles. Chemical crosslinking usually has residual amounts of the crosslinking agents (initiators, chain transfer agents and stabilisers) in the PVA hydrogel, which then require time consuming extraction procedure in order to remove the residue, so as to render the hydrogel applicable for biomedical and pharmaceutical applications. To counteract this, crosslinking of aqueous PVA solutions via freeze-thawing technique was pioneered by Peppas (1975). Crosslinking via freeze thawing process not only obviates the use of chemical cross linking agents but is reported to yield PVA hydrogels with higher mechanical strength than those crosslinked by chemicals or irradiation techniques. Repeated freezing and thawing of PVA induces crystal formation in the materials that allows for the formation of a network structure crosslinked with the quasi-permanent crystallites. The resultant hydrogel obtained, thus possess a macro porous structure, imprinted by the formation of ice crystals within the homogenous aqueous PVA system during the freezing step. Ice crystals expel amorphous polymer segments that finally separate the initial PVA aqueous solution into polymer-rich parts and polymer poor parts of a porous network. Polymer chain folded micro crystallites are formed in polymer rich phases as network junctions in physical PVA cryogels [145]. The properties of the resultant PVA hydrogel are dependent on the molecular weight of the polymer, temperature, duration and the number of freeze-thawing cycles. This method is the preferred method for preparation of PVA hydrogels as it allows for the formation of an ultrapure network without the use of crosslinking reagents, resulting in hydrogels with high degree of swelling in water, a rubbery and elastic nature and high mechanical strength. There have been many investigations of the molecular structure of PVA gels formed via freeze-thaw cycling [146-149]. A schematic representation of the freeze thawing processes is presented on Figure 3-6.

PVA homogenous aqueous solution

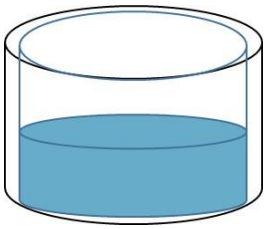

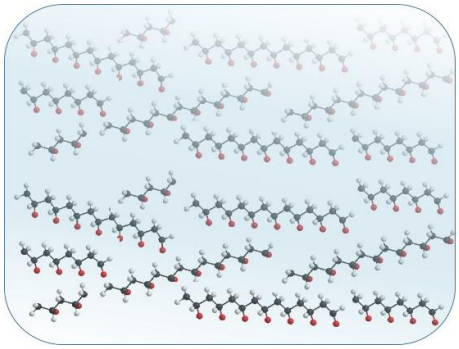

PVA aqueous solution frozen at -80°C prior to freeze drying

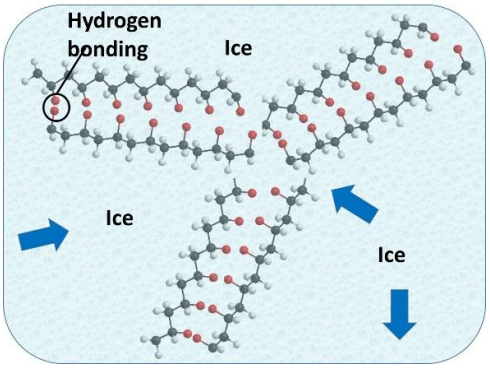

PVA subjected to freeze drying

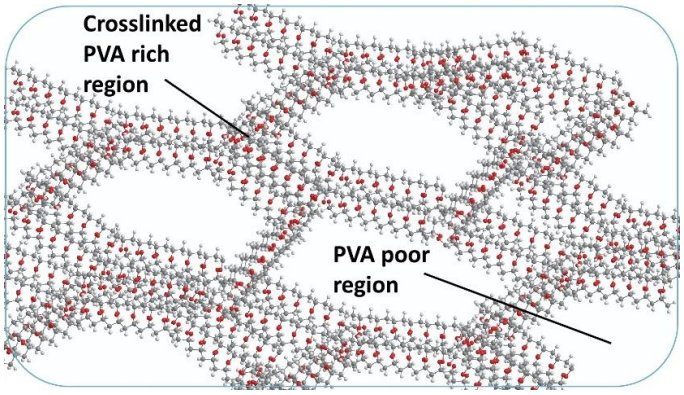

Figure 3-6: Schematic representation of PVA hydrogels prepared freeze drying method highlighting the microstructure of PVA through the processes of crosslinking with PVA-rich polymer phase and PVA poor polymer phase.

Applications of PVA

PVA has a well-documented history of successful applications in areas such as food chemistry, biotechnology, pharmaceuticals, medicine and tissue engineering. PVA exhibits excellent mechanical properties, good biocompatibility and biodegradability in human tissues and fluids, which has led to several biomedical applications [150]. PVA has been employed in the design and manufacture of tri-leaflet heart valve prosthesis whose design incorporated precisely defined geometries [151]. The authors found PVA to have a significant advantage which allowed replacement of heart valves via closed chest surgery, as well as pose as a superior alternative to total artificial heart implants and ventricular assist devices. PVA hydrogels have also been investigated for replacement of damaged cartilage, due to their high water content, as well as their rubbery elastic and compressive mechanical properties, with tensile strengths in the cartilage range of 1–17 MPa. Applications of these PVA hydrogels on cartilage were found to have lower wear factor with increasing thickness and water content of the hydrogel [152, 153]. The overall morphology, microstructure and stability of freeze-thawed PVA hydrogels show that the stability of the hydrogels can be significantly enhanced by increasing the number of freeze thaw cycles and increase in chain length as well as free volume within the network together to allow for secondary crystallization to proceed as the material swells [154]. It is reported that PVA gels prepared by freeze thawing technique show increased mechanical strength over most hydrogels due to the presence of crystalline regions that serve as physical crosslinks [155]. PVA based scaffolds have been developed and studied for potential applications as artificial grafts, examples include but are not limited to, electrospun gellan-PVA based nanofibers as a hydrophilic scaffolding material for skin tissue regeneration [156], sterculia (an acid polysaccharide) crosslinked PVA and PVA-AAm hydrogel [157], savlon loaded PVA hydrogels[158] and PVA-alginate blends for wound dressing [159], as well as PVA composite matrix for artificial cornea [160]. PVA has very low acute oral toxicity and does not accumulate in the body when administered orally and it was approved by the Food and Drug Administration (FDA) and other regulatory organizations for embolization [161]

and a summary of current applications of PVA hydrogels in the biomedical field is presented in Table 3-1.

Application	Qualifying properties of PVA for application
Soft contact lenses	High water content, high oxygen permeability, high optical clarity and low protein adsorption [162, 163]
Artificial cartilage and meniscus tissues	Elastic and compressive mechanical properties, and high water content. Usually prepared from high concentration of high molecular weight polymers (30% PVA or higher) [164-166].
Artificial pancreas	Membrane permeability of the hydrogels, and adaptability of PVA hydrogel to be fabricated in various desired shapes [167, 168].
Haemodialysis	Membrane permeability in combination with drug loading and release within PVA hydrogels [169].
Hydrophilic coatings	Polymeric coating of catheters, leads
Vascular embolism treatment	PVA fabricated into particles used to induce contralateral lobar hypertrophy in patients with liver-only metastases and normal underlying liver function [170, 171]. Ability of PVA particles to adhere to the vessel wall, which were then covered by the thrombus and organized into a collagenous mass. However there have been contradicting reports on the efficacy of PVA applications in this manner [172].
Drug delivery	Excellent maintenance of drug within the hydrogel during the dry state, as well as minimal level absorption of PVA from the gastro intestinal tract into the blood stream. As well as elimination of the polymer reported to proceed via renal excretion and complete within 40 days [173, 174].

Table 3-1: Applications of PVA polymer hydrogels in the biomedical field, and related products in commercial use.

PVA based medical products in the market	
Product and detailed explanation of medical use	**Image of product**
COLDEX®Extra is an open cell PVA hydro foam with interlinked pores that are super absorbent with fluid retaining qualities, suitable for wound exudates removal hence optimized for the treatment of wounds by means of negative pressure. It can be used for a variety of wound applications such as traumatic, infected and surgical wounds as well as leg and diabetic ulcers and pressure sores [175].	 [175]
Ear, nasal, sinus, epistaxis and post operational tampons. Products include those by MONDOCEL® products, ideally used in otologic and rhinologic procedures. The products have small pore sizes minimizing tissue ingrowth thus facilitating atraumatic removal [176].	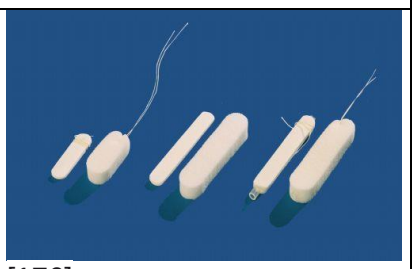 [176]
PVA RETRACTORPAD® and RETRACTORCOVER, were designed for abdominal and pelvic operations to cushion the intestines enhancing exposure of the surgical area. These pads possess antislip properties and possess excellent absorptive qualities. The retractocover was developed to cover the retractor and protect tissues and organs from the points and the blade of the retractor [177].	  [177]

RESOMED® is a femoral canal tampon used in total hip surgery. The femoral shaft can be plugged with the tampon until the prosthesis is ready for insertion as it is able to absorb body fluids and assist haemostasis [177].	 [177]
PVA sponge products are used during cataract and other refractive surgeries, such as PVA spears. These products are available in the market from companies such as EYETEC [178], Aion Co. Ltd [179] PL Medical Co.[180]	 [178]
PVA foam emobilization particles are used for embolization of the blood supply to hypervascular tumours, symptomatic uterine fibroids, and arteriovenous malformations, and for intracranial embolization [181].	 [181]

Table 3-2: PVA based products currently used and applied in the medical field. All images were adapted from the denoted reference next to the image.

Although freeze thawing has been shown to impact mechanical properties a systematic study that correlates concentration, molecular weight and comparable freeze-thaw process to make PVA gels is not available, and also despite the large number of studies on PVA for biomedical applications, there is a lack of dedicated and systematic study on the properties of physically crosslinked PVA hydrogels. PVA is an FDA approved synthetic biocompatible polymer, that can be modified through blending with other natural or synthetic polymers [182], as well as the ability to be incorporated with calcium phosphates to form bone composites with good structural and mechanical properties applicable for bone augmentation and regeneration. Based on the evidence from literature and the versatility of the properties of PVA, it was chosen as a base polymer towards the development of scaffolds for this study, thus a systematic evaluation of the

properties of PVA hydrogels with a known molecular weight crosslinked via facile physical crosslinking methods is reported in this chapter. The aim is to obtain a baseline understanding of the properties of PVA, in relation to different physical crosslinking methods, and was carried forward to analyse the effect freeze thaw cycles on PVA of a known concentration and molecular weight, which formed the basis for fabrication of interpenetrating dual networks of PVA and alginate subsequently. The specific focus related to the optimisation and development of these polymers to yield tough hydrogels with controllable water uptake properties that would allow for cell attachment infiltration and proliferation within the hydrogel. The physical characteristics of the hydrogels such as toughness, porosity and water uptake can be controlled by varying methods of fabrication.

Therefore the objective of this study was to:

- Fabricate 3D PVA hydrogels with varying concentrations of PVA, crosslinking via physical means such as air-drying and freeze thawing.
- Characterise the physical properties of the hydrogels.
- Study the effect of the different concentrations of PVA on the properties of the gels.
- Considering the importance of the method of physical crosslinking on the final properties of PVA, the effects of air-drying, freeze drying and both together on the properties of PVA hydrogels were investigated.

3.5 MATERIALS

Polymer	Chemical Structure
Poly(vinyl alcohol) (PVA), 145,000 mol. wt. hydrolysis≥98% (Merck)	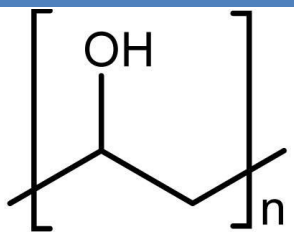 $[CH_2CH(OH)]_n$

Table 3-3: Polyvinyl alcohol used for fabrication of hydrogels.

PVA polymer stock solutions

PVA granules were weighed in appropriate amounts and dissolved in distilled water, and magnetically stirred at 350rpm at a temperature of 121°C until dissolved to form homogenous solutions of concentration 10, 20 and 30%. The aqueous polymer solutions were stored in Duran bottles. The viscosity of the PVA solutions was found to increase with increasing concentrations as expected. However it was found that a concentration higher than 30% led to a lumpy mass and the maximum workable concentration was found to be at 30% w/v, whilst 10% and 20%w/v polymer solutions were easier to handle as mentioned. Due to the high viscosity of the PVA 30% solution and difficulty in handling, a method was developed for preparing the of 30%w/v solution where:

- Polymer solution was prepared by dissolving 2/3rd of the weight of required PVA with 70% distilled water at 121°C until a homogenous solution was obtained. The remaining 1/3rd of PVA was mixed with cold water and later added to the homogenous polymer solution.
- Magnetic stirring was maintained between 150-250rmp depending on the varying viscosity as PVA granules were added. Once formed, the homogenous solutions were cast into desired moulds whilst it was warm at 40-50°C.

PVA hydrogels

In order to form the hydrogels, the PVA polymer solutions were cast into moulds, then rendered insoluble and physically crosslinked by 3 methods.

Method of crosslinking	Hydrogel fabrication
Freeze Thawing (FT)	The sample moulds were frozen to -80°C in a freezer for 1 hour before vacuum freeze drying (Vitris SP Scientific) at -59°C with vacuum of 17mT for 24hours. Samples in this study were placed in the condenser chamber for freeze drying. The xerogel were then allowed to thaw at room temperature for 12 hours before testing. This was considered as 1 freeze thaw cycle (1FT).
Air Drying (AD)	Air-dried hydrogel sheets of relatively uniform thickness were formed by leaving polymer solutions in moulds to air dry at room temperature for 7days. Care was taken to limit introduction of air bubbles.
Air Drying + Freeze Thawing (AD+FT)	The air-dried hydrogels were then hydrated in distilled water for 5 minutes before being frozen in a -80˚C freezer for an hour followed by vacuum freeze drying (Virtis SP Scientific) at -59.4°C with a vacuum of 17mT for a period of 24 hours before being thawed at room temperature for 24 hours before testing.

Table 3-4: A detailed description of the methods of crosslinking used in the fabrication of PVA hydrogels.

3.6 CHARACTERISATION

The hydrogels fabricated were characterised using FTIR, differential scanning calorimetry, equilibrium water content and ultimate tensile strength. Based on the results, a select group was taken for further characterisation by Raman micro-spectroscopy and scanning electron microscopy.

Viscosity

Viscosity measurements were carried out using a Brookfield viscometer. ~3.8ml of aqueous PVA solution was placed in a small chamber, after which a rotating spindle was placed inside the chamber allowing for determination of viscosity. The rotation speed of

the spindle were set to 100rpm and viscosity values were obtained from the viscometer were at 13%, 12.4 and 85% full range for PVA10, 20 and 30 respectively.

Attenuated Total Reflectance Fourier Transform Infrared spectroscopy (ATR – FTIR)

ATR/FTIR spectra of hydrogels were recorded on a Perkin Elmer Spectrum One spectrometer. The hydrogels prepared were placed in a desiccator for 24h prior to testing, and all spectra were obtained in the wavelength range of 4000-650 cm^{-1} with 4 cm^{-1} resolution. Spectrum software (Perkin Elmer) was used for analysis and processing with all spectra normalised.

Differential Scanning Calorimetry (DSC)

Perkin Elmer Jade DSC system was used to determine thermal properties of the hydrogels and Perkin Elmer Jade series software was used to process and analyse the raw data. The system was calibrated with zinc/indium, and all hydrogel samples were placed in a desiccator for a minimum of 24 hours prior to testing. 10-20mg samples were tested in crimpled aluminium pans, scans were carried out with reference pan calibrated using Indium[49] under a Nitrogen[7] atmosphere. Two cycles of heating and cooling were carried out, starting from 0 to 250˚C followed by a cooling cycle to 10˚C at a rate of 10˚C per minute. The glass transition temperature (T_g°C) and melting temperature (T_m°C) were determined. Tg is manifested by a change in the base line, indicating a change in the heat capacity of the polymer. The baselines before and after the transition are extrapolated from the linear portion of the phase transition and the intersections used to determine Tg.

Equilibrium Water Content (EWC)

Hydrogels were immersed in deionised water at 37°C and mass monitored using conventional gravimetric method until equilibrium was reached. The EWC and degree of swelling of the xerogels were determined using the following equation:

$$EWC = \frac{Ws - Wd}{Ws} \times 100$$

where Ws is hydrated weight and Wd the dry weight of xerogel prior to swelling.

Tensile Strength

Hydrogels were cut into dog bone shaped specimens (l=*24mm t=4mm)* and hydrated to equilibrium before tensile testing. Tensile test were carried out on a universal testing machine (Instron 5569A) at a rate of 5mm/min using a 50KN load cell. Bluehill (Instron) software was used to collect the mechanical data and measure: the tensile load (N), tensile stress (MPa), extension at tensile strength (mm) and Young's modulus (MPa).

Raman micro-spectroscopy

The Raman spectra were recorded using Renishaw In-Via Raman Microscope with a 785 nm diode laser, 1200 grating. Extended scans were carried out between 100-3500 cm^{-1} frequency of the Raman spectra.

Scanning electron microscopy (SEM)

Scanning electron microscopy was carried out on selected samples placed on aluminium stubs using conductive blue then coated in a thin layer of gold before being placed in a vacuum container of quanta field emission scanning electron microscope (Quanta 200F microscope (FEI), using 10-20kV and 10,000x Magnification.

3.7 RESULTS

Viscosity of PVA polymer solutions

A 98% hydrolysed PVA with an average molecular weight of 145,000 was used to prepare the aqueous solution of PVA. To obtain a homogenous solution even at high concentrations, the polymer was dissolved in water at 121°C with mechanical agitation to yield clear polymer solutions that did not require prolonged incubation in water.

Concentration (w/v) (%) of PVA	**Viscosity (Pa s)**
10	0.52
20	5.8
30	75

Table 3-5: Viscosity of PVA solutions at 10, 20 and 30% concentration (w/v).

The viscosity of the PVA polymer solutions are shown in Table 3-5 and as expected it was found to increase with increasing concentration. This indicated that an aqueous solution of PVA10 could be manipulated more easily in comparison to PVA30. An increase of 10% concentration led to an approximate 11-12 fold rise in viscosity of the solutions.

FTIR- infrared spectroscopy

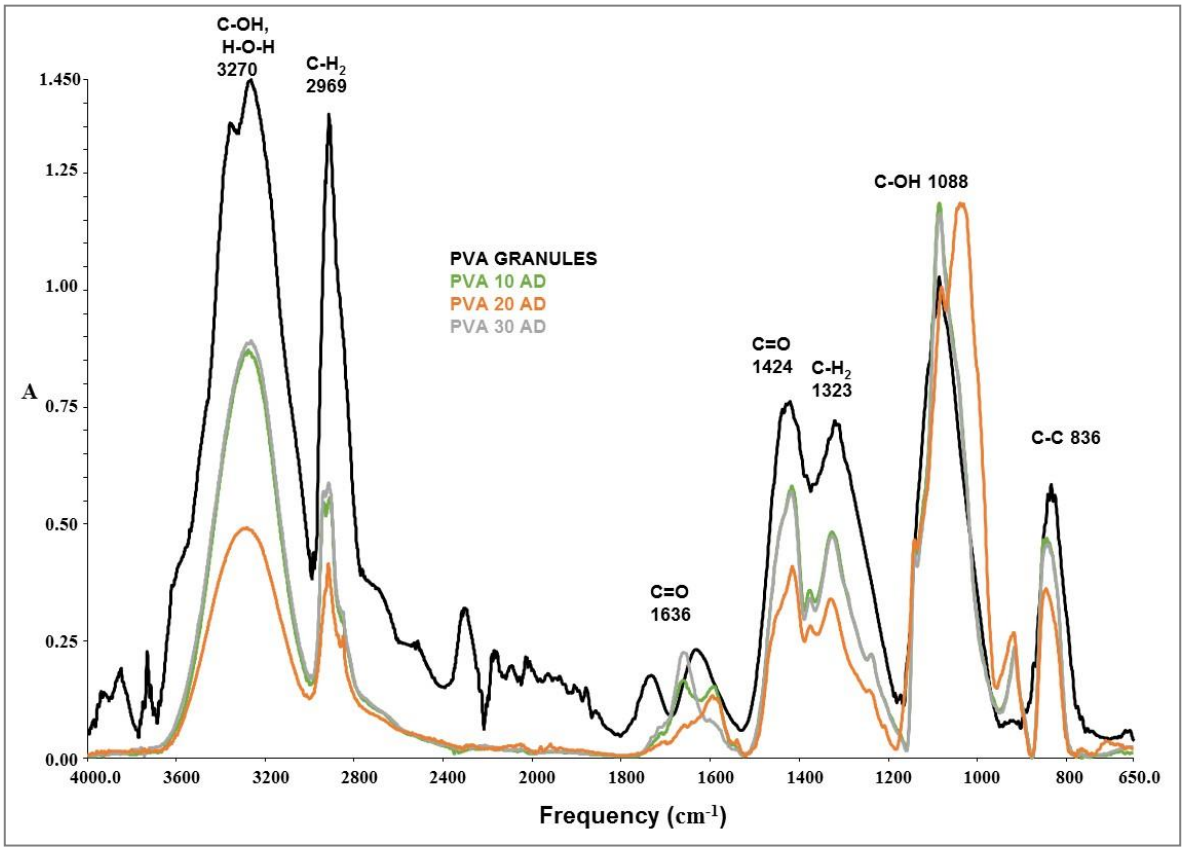

Figure 3-7: A comparison of the infrared absorbance peaks of air-dried only PVA10, 20 30%(w/v) hydrogel films.

Samples	PVA FTIR absorption band assignments								
	OH stretching	CH_2 asymmetric stretching	C-h symmetric stretching	C=O stretching	CH_2 bending vibration	C-H symmetric stretching	C-OH stretching vibrations	CH_2 rocking	C-C stretching
PVA granules	3270	2919		1636	1424	1323	1088		836
PVA air-dried	3276	2913	2960	1662	1417	1327	1087	916	840
PVA 1FT	3319	2941	2969	1707	1419	1329	1089	919	842

Table 3-6: The major FTIR absorption bands of the PVA granules and 10%(w/v) PVA hydrogels crosslinked by 1 freeze-thaw cycle and air-drying.

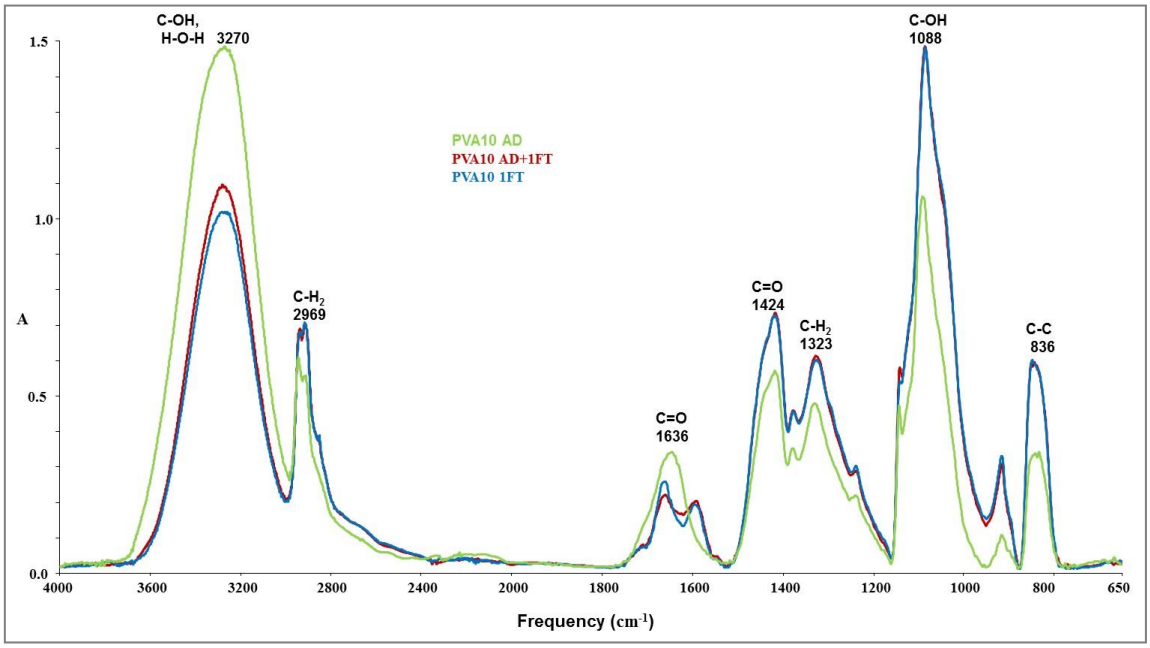

Figure 3-8: A comparison of the infrared absorbance peaks of 10%PVA (w/v) air-dried only (AD), air-dried +one cycle of freeze-thaw (AD+1FT), and one cycle of freeze-thaw only (1FT) hydrogel films.

A comparison of the FTIR spectra of all the PVA hydrogels with varying concentration and different methods of crosslinking is shown in Figure 3-7 and Figure 3-8. All showed characteristic absorption bands of PVA which can be assigned to the vibrations arising due to C=O, C-H, C-OH, C-O bonds, which are described in Table 3-6. A strong

characteristic feature of PVA is the O-H stretching band, indicating the presence of both the strong hydrogen bonding internally to OH or terminal vinyl OH groups, with broad peaks centred at 3265, 3285 and 3269 cm^{-1} [183, 184] which were observed for all hydrogels. Hydroxyl groups from residual water also contribute to the peak intensity [185]. Two strong peaks arising from the C-H stretching of the alkyl groups at 2916 cm^{-1} to 2969 cm^{-1}, are characteristic bands of the C-H symmetric (v_s) and CH_2 asymmetric(v_{as}) stretching vibration, with their position suggesting that the hydrocarbon chains of the polymer takes a trans zigzag conformation. The weak peak at 1595 cm^{-1} – 1636 cm^{-1} can be assigned to the C=O group from the residual acetate in PVA that result from manufacturing of PVA from hydrolysis of polyvinyl acetate.

The peaks at 1416-1424 cm^{-1} can be assigned to the -CH_2 bending with deformation bands of C-CH_3 appearing at 1377 cm^{-1}. The peaks at 1263 cm^{-1} and 1326 cm^{-1} are associated with CH_2 wagging and the C-C, C-O-C stretching vibrations respectively. The sharp absorption bands indicate that the film formed by this process resulted in a semi crystalline PVA. The peaks at 1038-1088 cm^{-1} are attributed to –C-O-H bending and C-O stretching vibration coupled with -OH bending vibration. The atactic form of PVA is shown by the peaks at 915 – 918 cm^{-1} (-CH_2 rocking) and 836 – 845 cm^{-1} (C-C stretching) [185-187].

Thermal analysis by differential scanning calorimetry (DSC)

PVA 10, 20, 30%(w/v) were subjected to different crosslinking methods and the glass transition (Tg) and melting temperature (Tm) of the hydrogels post different treatments are presented in Table 3-7. The 1st heating cycle of 1FT PVA displayed two endotherm melts that can be attributed to the loss of moisture or melting of crystallites due to the strong hydrogen bonding between PVA-water and PVA chains themselves [188]. Melting temperatures Tm for all remained relatively in a close range of 220.6 – 227°C. The literature value for the melting endotherm of PVA has been reported to be 230°C, which is slightly higher than the observed values [188]. The glass transition Tg, however showed that air dried (AD) gels had lower Tg (58.0 – 74.25 °C) than those of AD+1FT

and 1FT (61.1 -75.2°C, 69.4 – 73.4°C) respectively. Literature values for Tg of PVA have been reported to be ~80°C [189], but do range between 59°C to 74°C as noted in in previous studies [190].

Sample Name	Conc. Of PVA in water (%)	(T_g °C)	(T_m °C)
Commercial PVA granules		69.6	226.2
Air-dried (AD)	*10*	74.2	228.1
	20	61.1	220.6
	30	58.0	226.4
Air-dried and one cycle freeze thawed (AD + 1FT)	*10*	75.2	226.5
	20	67.3	225.0
	30	61.1	222.2
One cycle freeze thawed (1FT)	*10*	73.4	227.0
	20	72.4	226.8
	30	70.5	227.0

Table 3-7: Glass transition (Tg) and melting temperatures(Tm) of PVA 10,20,30%(w/v) crosslinked by air-drying, air-drying prior to freeze-thawing and one cycle of freeze-thawing, the T_g and T_m were obtained from the second cycle.

Raman spectroscopy

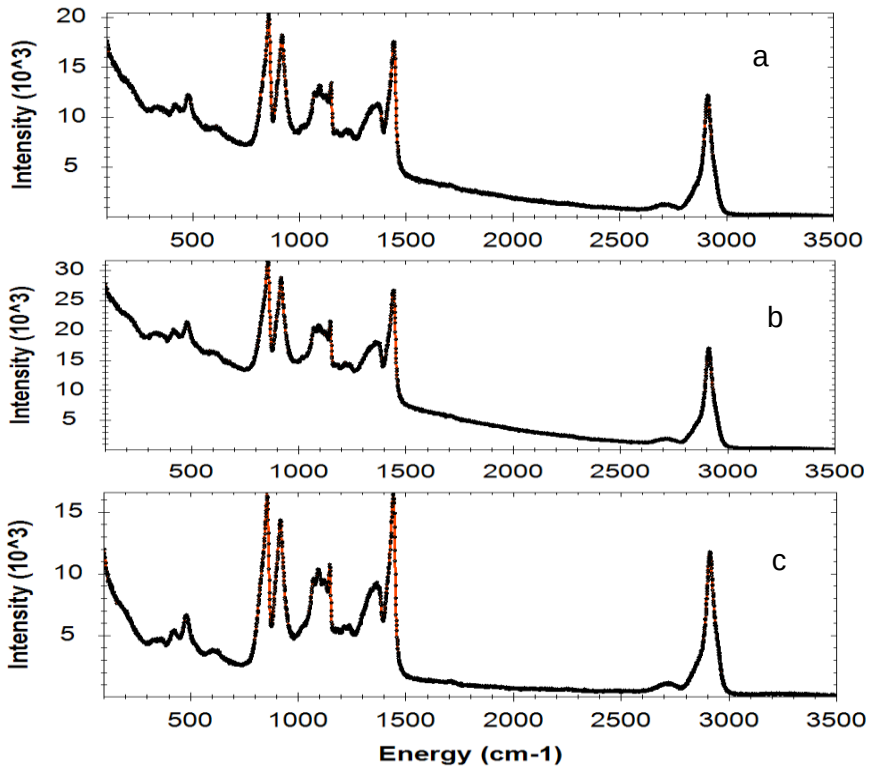

Figure 3-9: The Raman spectra scans of air-dried (a) PVA10, (b) PVA20 and (c) PVA30.

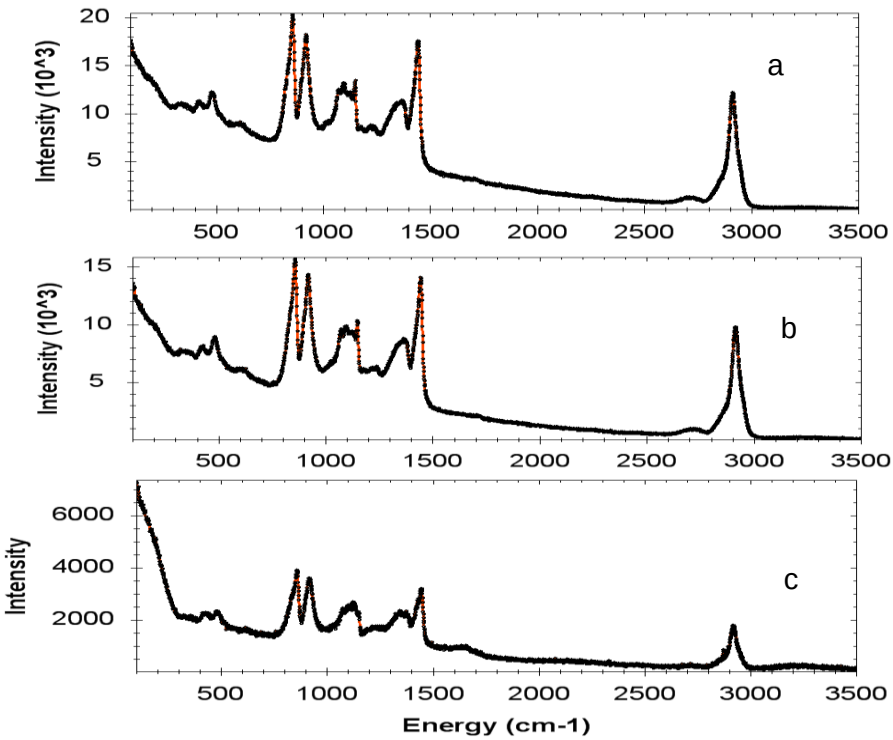

Figure 3-10: The Raman spectra of (a) PVA10 air dried (b) PVA10 air-dried and freeze thawing (c) and PVA10 freeze dried only.

	Raman Spectra (cm^{-1})		
Assignment	**PVA10 Freeze dried only**	**PVA10 Air-dried and Freeze dried**	**PVA10 Air-dried only**
Assym. CH_2 stretching	2920	2913	
C-H as stretching	2718	2709	2717
amide, C=O, C-N stretching	1651		
CH_2 bending/ scissors	1445	1443	1443
CH bend	1358	1369	1372
CH_2 twist	1123	1148	1147
C-C ring breathing	918	919	919
C-C ring	857	857	858

Table 3-8: The Raman peaks of each of the PVA hydrogel films cross-linked via three different methods along with its peak assignments.

Figure 3-9 and Figure 3-10 illustrates and compares the Raman spectra of representative PVA10, 20 and 30 hydrogels cross-linked via air-drying, and PVA10 hydrogels crosslinked via three different methods. The main differences between AD, AD+1FT, 1FT films, lie in the peaks between 1595-1661 cm^{-1} that corresponds to C=O stretching as well as the peaks at 916 cm^{-1} that correlates to out-of-plane bending of C-H

groups. With the C=O peaks at 1600 cm^{-1}, AD gels produced broader and multiple peaks at this frequency of the spectra compared to the sharper intense peaks of the AD+1FT and 1FT films. Individual absorption bands are described in Table 3-8 [191].

Equilibrium water uptake

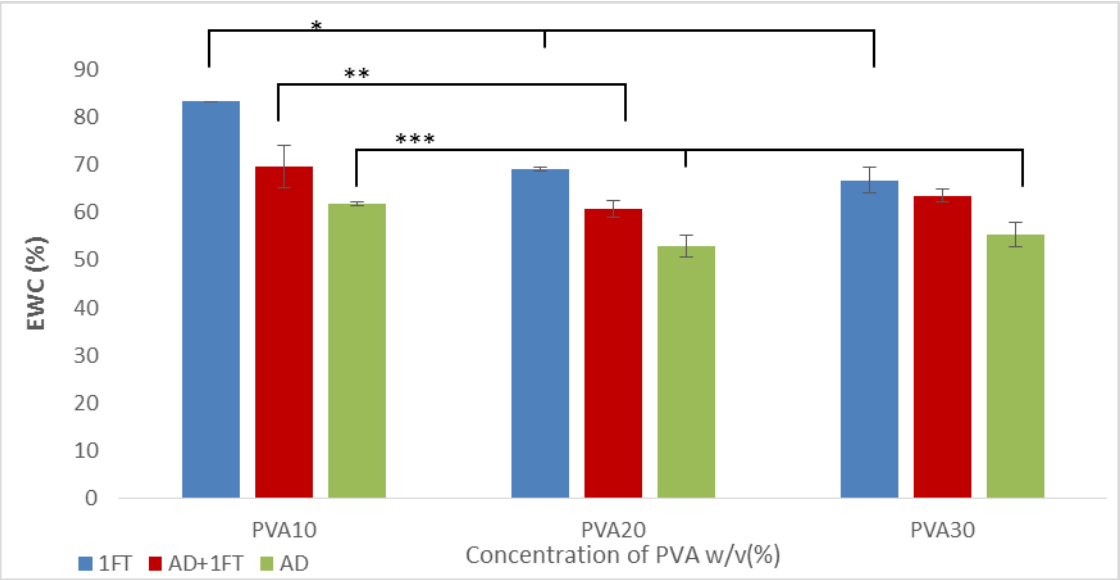

Figure 3-11: Equilibrium water uptake of the different hydrogel films of varying concentration prepared by one cycle freeze-thawing (1FT), air dried with one cycle freeze–thawing (AD+1FT) and air dried (AD). (n=3) (* P<0.0001, ** P=0.28 and *** P≤0.013); asterisk linked with lines indicate significant difference in values between the groups

Figure 3-11 shows the EWC attained from the different crosslinking methods with varying concentrations of PVA. The hydrogel films prepared by air drying (AD) exhibited the lowest EWC followed by air drying plus one cycle of freeze thawing (AD+1FT) and one cycle of freeze thawing (1FT) only. The EWC showed that with increasing concentration of PVA there was a decrease, irrespective of the method used to form the hydrogels, and that freeze thawing resulted in hydrogels with high water uptake as compared to all other methods of crosslinking.

Tensile strength

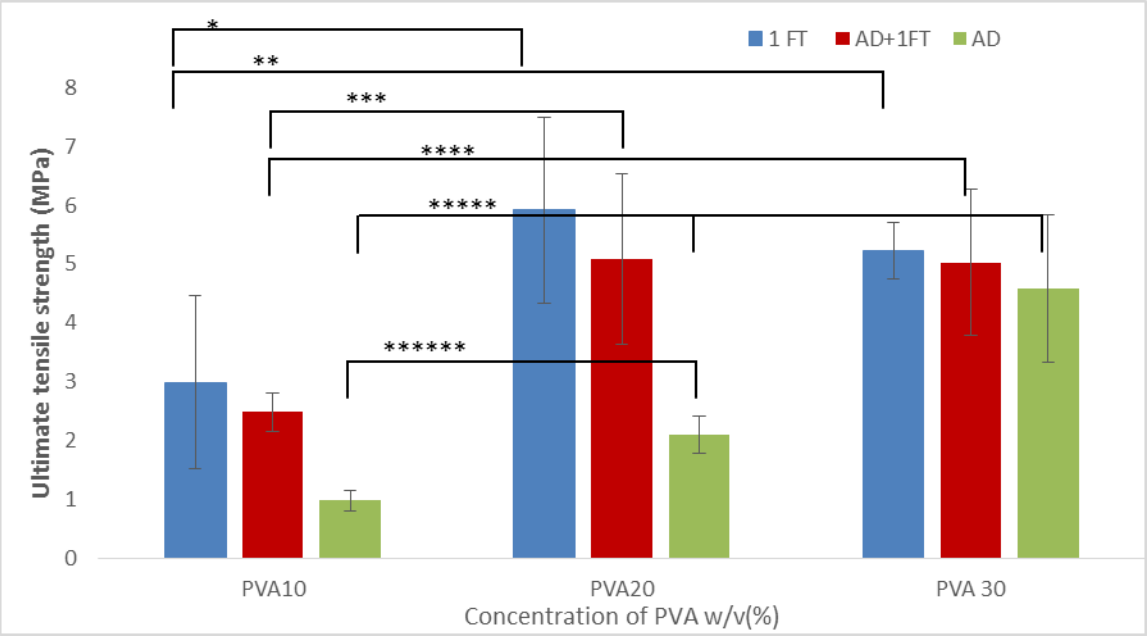

Figure 3-12: A comparison of the tensile strengths (uniaxial tensile tests) of PVA hydrogel films with varying concentrations crosslinked by one cycle freeze-thaw (1FT), air-dried and one cycle freeze–thaw (AD+1FT) and air-dried (AD) films, tests were carried out on fully hydrated hydrogel films. (n=6) (* P=0.004, **P=0.016, *** & **** P=0.003, ***** P<0.001 and ****** P=0.019); asterisk linked with lines indicate significant difference in values between the groups

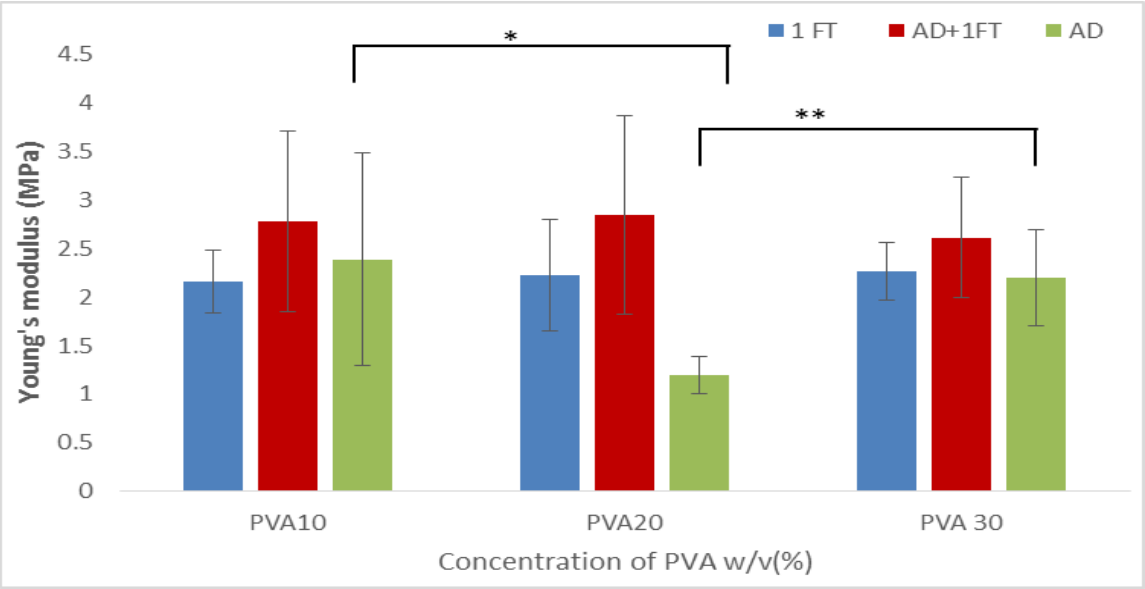

Figure 3-13: A comparison of the Young's modulus of PVA hydrogel films with varying concentration, carried out at equilibrium hydration after one cycle freeze-thaw (1FT), air-dried and one cycle freeze–thaw (AD+1FT) and air-dried (AD) films. (n=6) (* P=0.030 and ** P=0.049); asterisk linked with lines indicate significant difference in values between the groups

Results shown in Figure 3-12 indicated that, the tensile strength of all the hydrogels with different crosslinking methods increased with increasing concentration of PVA. The hydrogels subjected to freeze-thawing (FT) only, also exhibited the highest tensile strength, followed by AD+1FT and AD only hydrogels, in decreasing order. Stiffness of the hydrogels was variable (Figure 3-13), where with 1FT and AD+1FT there was no significant difference between the varying concentrations of PVA.

Scanning Electron Microscopy (SEM)

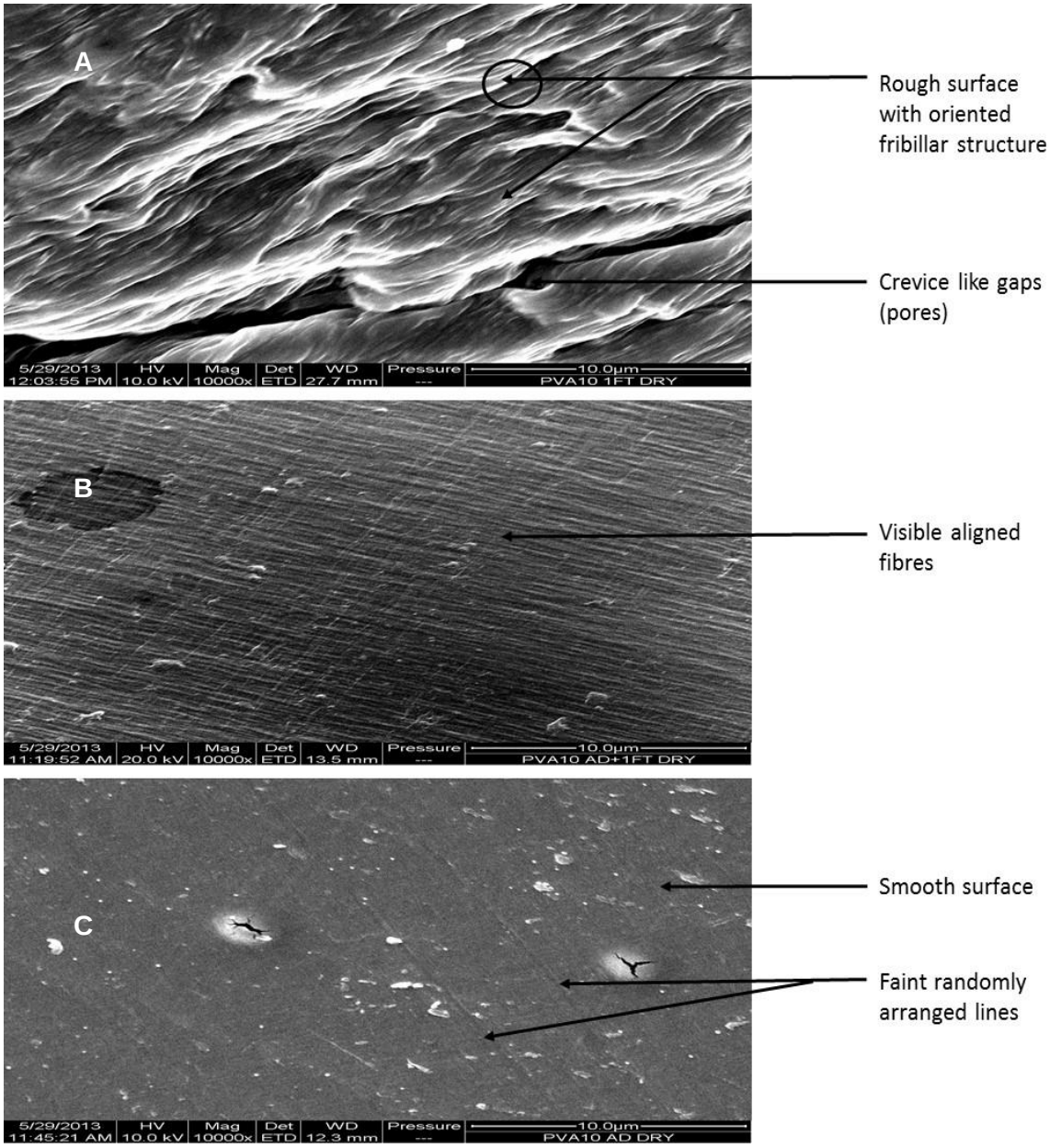

Figure 3-14: Scanning electron micrographs of the surface of, **[A]** freeze thawed PVA showing undulated striations of PVA, **[B]** air-dried plus freeze thawed, **[C]** and air-dried PVA10 hydrogels with no clear morphological features at 10,000X magnification.

The scanning electron micrographs of the AD, AD+1FT and FT only hydrogels of PVA10 hydrogels are shown in Figure 3-14. The micrograph elucidated the varying morphologies of the hydrogels, and a smooth and homogenous surface was observed for the AD only hydrogel with faint, randomly arranged lines whilst the AD+1FT hydrogel had visible and aligned fibres, and the FT only hydrogel had a rough surface, with more visible directionally orientated fribrillar structure. The presence of crevice like gaps on the surface of the material could be micro-pores that developed as a result of freeze-thawing.

3.8 DISCUSSION

PVA hydrogels derived from physical process of gelation occur due to the numerous interchain hydrogen bonds between the hydroxyl groups and Van der Waals interaction between the hydrocarbon polymer back-bone. The controlling parameters are the molecular weight, degree of hydrolysis and concentration of the polymer, however there is a lack of information on the correlation of these parameters.

The presence of the hydroxyl groups in each repeating unit, renders PVA with high hydrophilicity and ability to form hydrogen bonds enabling it to form crosslinked hydrogels. PVA hydrogels of concentrations 10, 20 and 30 (w/v %) were fabricated via physical crosslinking, the three techniques used were to just air dry (AD), air drying followed by freeze-thawing (AD-FT) and freeze thawing only (FT). The PVA hydrogels formed were characterised and dedicated to developing a systematic understanding of how the microstructure, water uptake, thermal and mechanical properties of the fabricated hydrogels were affected by varying the concentration of PVA polymer with a known molecular weight as well as the effects of different crosslinking methods on the aforementioned properties of the resultant hydrogels, as published literature does not provide understanding of these properties in a systematic manner.

The dissolution of PVA is essential to form physical hydrogels. The dissolution of PVA in water is dependent on the molecular weight and the degree of hydrolysis of the polymer.

It has been reported that high dissolution temperatures are required to dissolve PVA in water, especially if it has a high degree of hydrolysis [55, 56] due to the strong intra and intermolecular hydrogen bonds. However, PVA with a low degree of hydrolysis contains too many acetate groups, which renders the polymer too hydrophobic to dissolve in water. In this study, a 98% hydrolysed PVA of molecular weight of 145,000 was used and the dissolution was conducted in water at 121°C with mechanical agitation to yield clear polymer solutions with ease that did not require prolonged incubation in water. The viscosity of PVA aqueous polymer solutions was found to increase with increasing concentration of PVA (Table 3-5), and an eleven fold increase in viscosity was observed by doubling the concentration of PVA from 10 to 20 w/v% and a 12 fold increase from 20 to 30 % w/v. The higher viscosity solutions posed some difficulties in preparation of the polymer solution and fabrication of the hydrogels. The short range of action of both hydrogen bonding and Van der Waals interactions influences the interaction between the interacting chains and hydroxyl groups that dramatically affects the resultant gels.

The effect of concentration of PVA solution on the properties of the PVA hydrogel films

There are three basic models that explain the mechanism of gel formation via these physical means of crosslinking namely, i) hydrogen bonding, ii) polymer crystallite formation and iii) liquid-liquid phase separation [192], hence viscosity of the precursor solutions affect the three routes to gel formation.

FTIR spectra of the PVA hydrogels formed with different concentrations of PVA solutions

Infrared spectroscopy probes the molecular vibrations, and detects frequencies of infrared light that are absorbed by a molecule. Molecules absorb these frequencies of light because they correspond to the frequencies of vibrations of bonds in the molecule. Functional groups can be associated with characteristic infrared absorption bands, which correspond to the fundamental vibrations of the functional groups. For a molecule to

show infrared absorption it must possess a specific feature, which is an electric dipole moment which changes during vibration as the bond expands and contracts, strong IR absorptions are observed for groups with a permanent dipole such as the carbonyl groups. IR spectrometer records light absorbed from around 4000 cm^{-1} to 400 cm^{-1}, whereby frequencies with higher wavenumbers have more energy, while those with lower wavenumbers have less energy. Two types of vibration giving rise to absorption can involve either change in bond length (stretching) or bond angle (bending). With stretching bonds can stretch in-phase (symmetrical stretching) or out of phase (asymmetric stretching). Bending which is due to change in bond angle can either be in plane (rocking, scissoring) or out of plane (wagging, twisting) [193].

A comparison of the infrared absorbance peaks for air-dried PVA hydrogels of concentration 10, 20 and 30 are presented on Figure 3-7. No major distinct differences were observed in the spectra, however in general broad, high intensity peaks in PVA 30 were noted, arising due to the higher concentration of the polymer. Characteristics peaks at the 2850-2920, 1494-1427, 1280-1315 and 1160-1230 cm^{-1} frequencies associated with C-H vibrations of the PVA backbone (Table 3-6) were observed in the native PVA and the hydrogels. This was expected since the chemical composition of all the hydrogels remained unchanged. Compared to PVA granules, the OH peaks of 3000-3600 cm^{-1} frequency in the PVA hydrogels were shallower and broader indicating less hydroxyl groups in hydrogels especially at high PVA concentrations [194], this due to the loss of unbound H_2O in the hydrogels during the process of air-drying.

Thermal analysis of the films with different concentration of PVA solutions

Differential Scanning Calorimetry (DSC), is a thermal analysis technique that measures the energy changes that occur as a sample is heated, cooled or held isothermally, together with the temperature at which these changes occur. The energy changes enable measurement of the transitions that occur in the sample quantitatively, while noting the temperature where any changes occur, so as to allow for characterisation of

glass transition temperature, melting processes and phase changes [195]. The glass transition (Tg) is when a material transitions from a solid to a soft rubbery state due to independent movement of molecules in the structure. In non-crystalline and semi-crystalline polymer of any type, the Tg is the best indicator of material properties. As the Tg changes due to either different degrees of polymerization or modification by additives, the physical properties of the material change [196].

The melting temperature T_m of the hydrogels fabricated and formed as films using 10, 20 & 30% concentration of PVA in water was found to have values between 220-228°C, which was in close range with those reported in literature for PVA. PVA has been reported to exhibit a melting point of 230°C and 180-190°C for the fully hydrolysed and partially hydrolysed grades respectively.

The Tg values of the experimental hydrogels were between 58-70^{0}C, whilst literature values report them between ~60 to 80°C, after which PVA gels tend to lose their mechanical integrity [197]. The close agreement in the values with literature clearly showed that the heating regime used to dissolve the PVA initially to form the aqueous solutions did not have any effect on the polymers. However, it was expected that Tg would increase with increased polymer concentration because, the segmental mobility of polymer chains becomes restricted as the solution concentration is increased, possibly due to enhanced intermolecular hydrogen bonding but in fact Tg values were found to decrease with increasing concentration of PVA within each of the 1FT, AD+1FT and AD only groups. This indicated lower thermal stability in hydrogels with increasing concentration of PVA which, may be attributed to the presence of bound water within the gels. It has also been reported that glass transition can decrease significantly in the presence of water, thus this indicates that there may have been some residual water left over in the hydrogels during the drying process [192].

Raman spectra analysis

Raman scattering is a spectroscopic technique, where photons induce a change in polarizability of a molecule with respect to its vibrational motion. The interaction of polarizability with the incoming radiation creates an induced dipole moment in the molecule, and the radiation emitted by this induced dipole moment contains the observed Raman scattering. The light scattered by the induced dipole moment contains both Rayleigh scattering and Raman scattering. Rayleigh scattering corresponds to the light scattered at the frequency of incident radiation, whereas Raman radiation is shifted in frequency, and hence energy, from the frequency of the incident radiation by the vibrational energy that is gained or lost in the molecule.

This form of spectroscopy allows for the distinction of primary and secondary alcohols based on the location of the peaks assigned to the deformation of the hydroxyl group [198]. The medium intensity bands between 1140 and 1085 cm^{-1} are assigned to the C-O stretch of secondary alcohols on the PVA backbone, and the weak band at 1050 – 1000 cm^{-1} attributed to the C-O stretch of primary alcohols on the ends of the polymer chain, whilst the ~1085-1000 cm^{-1} region is also attributed to O-H bending. The bands at 1145 cm^{-1} and 1445-1475 cm^{-1} are associated with C-C stretching and CH_2 deformation respectively. The presence of high intensity broad peaks in the 1444, 1157 and 1094 cm^{-1} frequency in all three Raman spectra indicate PVA's crystallinity [191]. Differences in the spectra were observed in the intensity of the absorbance peaks, where low intensity was observed with PVA30 hydrogels whilst the highest was observed with PVA20 hydrogel.

Water uptake of hydrogels

When a biopolymer network is in contact with an aqueous solution or a biological fluid, the network starts to swell due to the thermodynamic compatibility of the polymer chains and water. The first water molecules entering the matrix will hydrate the most polar, hydrophilic groups, leading to 'primary bound water'. As the polar groups are hydrated, the network swells and exposes hydrophobic groups, which also interact with water

molecules, leading to hydrophobically-bound water, or 'secondary bound water'. Primary and secondary bound water are often combined and simply called the 'total bound water'. After the polar and hydrophobic sites have interacted with and bound water molecules, the network will imbibe additional water, due to the osmotic driving force of the network chains towards infinite dilution. The additional swelling water that is imbibed after the ionic, polar and hydrophobic groups become saturated with bound water is called 'free water' or 'bulk water', and is assumed to fill the space between the network chains, and/or the centre of larger pores, macropores or voids. The swelling force is counterbalanced by the retractive force induced by the cross-links of the network and the swelling equilibrium is reached when these two forces are equal. As the network swells, if the network chains or crosslinks are degradable, the gel begins to disintegrate and dissolve, at a rate depending on its composition. The character of the water in a hydrogel can determine the overall permeation of nutrients into and cellular products out of the gel [128, 199].

Hydration results are presented on Figure 3-11, and a comparison of the effect of increasing PVA concentration on EWC within the 3 different crosslinking groups was analysed. Results indicated that EWC decreased with increasing polymer concentration for all groups of crosslinking. For the freeze thawed groups, PVA10-1FT had a significantly higher EWC of 83.1% than PVA20 (69.1%) and 30-1FT (66.7%), at P values <0.001 respectively. PVA10-AD+1FT had a EWC of 69.6% which was significantly higher (P=0.028) than that of PVA20-AD+1FT (60.7%), however there was no difference in EWC comparison between PVA30 and 20 AD+1FT. Hydrogels crosslinked by air-drying only, showed that PVA10-AD had an EWC of 61.8% which was significantly higher than PVA20 (52.8%) and 30 (55.2%)

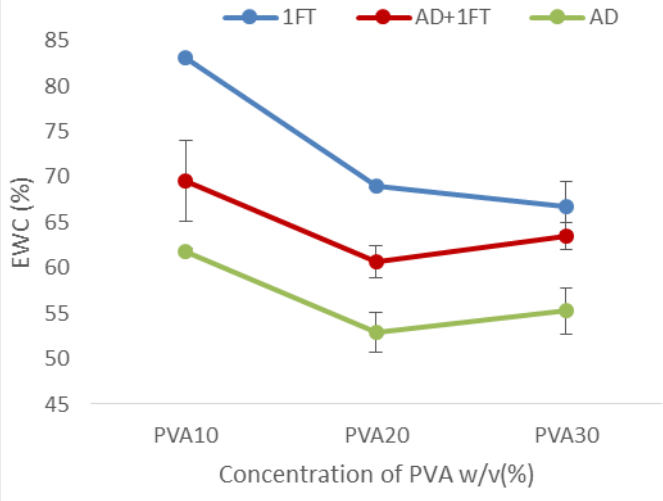

Figure 3-15: Effect of varying concentration of PVA on the EWC (%) of the hydrogel films.

AD (P= 0.04 and 0.013 respectively) with no significant difference between PVA 20 and 30 AD. This demonstrated that concentration of PVA does have a direct effect on the EWC of the hydrogels, implications were that lower concentration of PVA has a higher capacity for bulk and bonded water that make up the increase in weight. The decrease in EWC with increasing concentration demonstrated in this study was in agreement with results reported in literature where it was found that swelling ratio of their freeze thawed PVA hydrogels decreased with increase in PVA concentration using concentrations 6, 12 and 25%PVA [158, 200]. This was as a result of the increasing volume fraction of the polymer in the freeze dried gel, which effectively enhance the interaction between the PVA-PVA chains, thus an increased extent of crosslinking in the hydrogel results in a decrease in the swelling ratio.

Tensile strength of films formed with different concentrations of PVA solutions

Concentration of 10%PVA hydrogels exhibited the lowest tensile strength in comparison to PVA 20 and 30 hydrogels Figure 3-12. A comparison of the effect of varying PVA concentration within the individual groups of crosslinking showed that, in the case of hydrogels prepared by FT and AD+1FT, the tensile strength of PVA 20 and 30 hydrogels (5.9 and 5.2MPa)FT, (5.1 and 5.0MPa)AD+1FT respectively were found to be significantly higher than that of PVA10 hydrogels prepared by both methods (P<0.016). However there was no significant difference in tensile strength between the PVA20 and 30 hydrogels within each of the two FT and AD+1FT

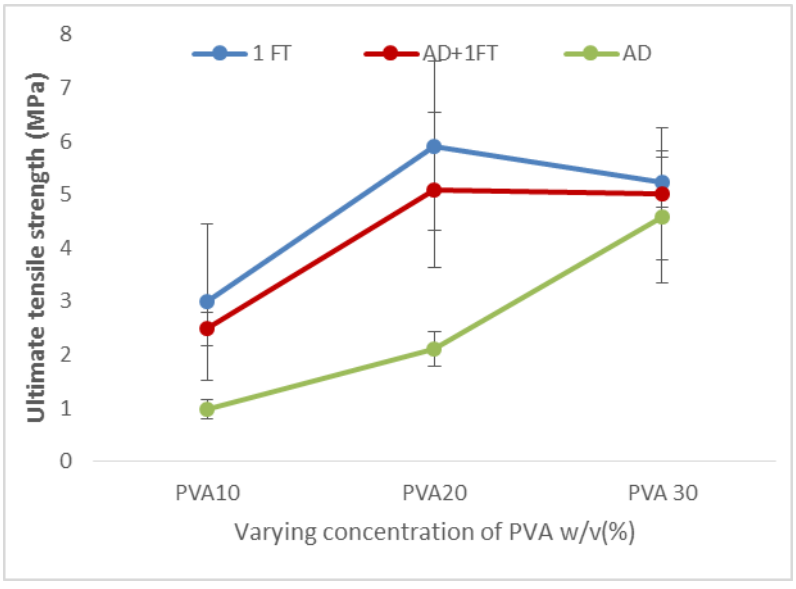

Figure 3-16: Effect of varying concentration of PVA on the ultimate tensile strength of the hydrogel films.

groups. With AD hydrogels there was a significant increase in the tensile strength of the hydrogels with increasing concentrations ($P < 0.019$). These results are in agreement with those obtained from the EWC, where the highest water uptake was obtained with PVA10 hydrogels. The explanation for this being that with a lower concentration of PVA there is less hydrogen bonding as compared to hydrogels with higher polymer concentration, therefore resulting in higher water up take for hydrogels of 10%PVA concentration. Also when water is removed from the aqueous polymer solutions of lower concentration i.e PVA10, by AD or FT this results in less crystallised and more amorphous regions within the hydrogel as compared to those formed in the presence of high polymer concentration. Results exhibited the highest tensile strength increase with PVA 20 hydrogels, which then decreased with increase in polymer concentration to PVA 30, with the exception of AD hydrogels, whose tensile strength was found to increase with increasing concentration of PVA. These results are in agreement with those from literature where, in a study on preparation of self-healable PVA hydrogels fabricated by freeze thawing the authors found tensile strength of PVA hydrogels to increase with increase in PVA content [200]. Another study on effect of freeze thaw cycles (15FT) and polymer concentration on tensile strength of PVA, reported that tensile strength of their hydrogels increased with increasing concentration of PVA [201].

Young's modulus of the hydrogels with varying concentration of PVA was found to provide results with no significant difference within the FT and AD+1FT crosslinked groups. However with AD hydrogels it was found that PVA10 and PVA30 hydrogels had a stiffness (2.4 and 2.2 MPa respectively), which was significantly higher than that of PVA20 hydrogels $P=0.030$ and 0.049 respectively. The trend of these results is contradictory to those in literature where PVA stiffness was found to increase with increasing concentration for freeze thawed hydrogels [201].

The effect of different crosslinking methods on the properties of the PVA hydrogel films

One of the main advantages of crosslinking of PVA solutions by repeated cycles of freezing and thawing is that no additional crosslinking agents are used. The air-drying prior to freeze thawing also has the same advantage, however forming homogenous films and imbibing porosity at a later stage on the formed film by eliminating water allows better control on maintaining shape and form. Crosslinking methods employed were reproducible cost effective with ease of fabrication.

FTIR- infrared spectroscopy films crosslinked by different methods

The FTIR spectra of AD, AD+1FT and 1FT are shown in Figure 3-8. The OH- stretching mode observed in the infra-red spectrum is a suitable band for monitoring the presence of hydrogen bonds that are involved in the crosslinking and gelation process of PVA hydrogels. The intensity of the peak at 1141 cm^{-1} in the IR spectrum depends on the degree of crystallinity, the band arises from a C-C stretching mode and increases with increase in the degree of crystallinity, which is determined by the method of fabrication. The spectra indicated that there is a higher degree of crosslinking in the FT and AD+FT groups as the peaks associated with the –OH are sharp with lower intensity in comparison to just air dried PVA hydrogel film. Stretching of the C-O bonds from primary alcohol groups in PVA can be observed through the peaks 1050-1095 cm^{-1} in crosslinked PVA, and this peak is associated more with the aliphatic ethers present in crosslinked polymers.

Thermal analysis of films crosslinked by different methods

Thermal analysis results of the hydrogels crosslinked by different methods showed that thermal stability is improved with freeze-thawing. A clear trend was observed (in the case of PVA20 and 30) across the different groups where Tg increased in value from AD to AD+1FT and 1FT presenting with the highest Tg, however with the exception of PVA10 even though there was no significant difference between the values. PVA20

(61.1-67.3-72.4)°C, PVA30 (58.0-61.1-70.5)°C for AD, AD+1FT and 1FT respectively. This result implied that there is greater thermal stability and formation of crystalline networks as a result of freeze thawing compared to air-drying alone.

Water uptake of hydrogels (EWC) crosslinked by different methods

A trend was observed on the EWC results obtained by the different methods of crosslinking, where EWC decreased in order with FT hydrogels exhibiting the highest EWC followed by AD+1FT and AD only hydrogels. PVA10-1FT exhibited the highest EWC (83.1%, P≤0.001) as compared to PVA10 AD and AD+1FT. EWC of PVA10-AD+1FT was significantly higher (P= 0.010) than that of PVA10-AD. For PVA20 hydrogels EWC of PVA20-1FT (69.1%, P≤0.002) hydrogels was significantly higher that of the PVA20 AD+1FT and AD only hydrogels, while comparison of PVA20-AD+1FT hydrogels showed a significantly (P=0.001) higher difference than the PVA20-AD hydrogel. Comparison of different crosslinking methods on PVA30 showed that FT resulted in significantly higher water uptake (66.7%) than AD and AD+1FT, P=0.003 and 0.009 respectively. Overall for all concentrations of PVA this indicated that water content of the hydrogels was higher for freeze-dried as compared to just air-dried hydrogels. This could be attributed to the micropores that result from the crystallising of bulk water molecules and its subsequent removal by vacuum suction from the hydrogel matrix as a result of freeze thawing. The presence of micropores could have facilitated the ingression of water and created more space within the matrix for storage of bulk

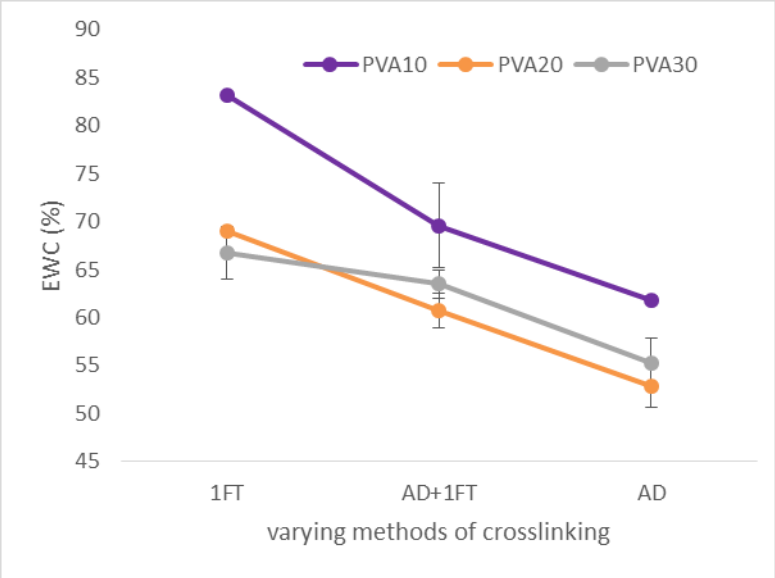

Figure 3-17: The effect of the crosslinking methods on the EWC (%) of the hydrogel films.

water thus the higher EWC. The subsequent exposure to distilled water during the hydration cycle allows for these spaces to be refilled through the pores created.

Tensile strength of hydrogels crosslinked by different methods

The effect of different methods of crosslinking on the resultant PVA hydrogels was analysed. Within the individual groups of PVA concentration, the tensile strength was found to decrease in order from FT hydrogels with the highest tensile strength, followed by AD+1FT and AD only hydrogels. Comparative analysis on the effect of crosslinking method for each individual concentration groups of the hydrogel films indicated that, for PVA 10 and 20 hydrogels tensile strength results of FT (3.0 and 5.9MPa) and AD+1FT (2.5 and 5.1MPa) hydrogels respectively was significantly higher than that of AD hydrogels at P (0.004 and 0.018) and P (<0.001 and 0.002) for PVA10 and 20 respectively. PVA30 hydrogels showed that the method of cross linking had no direct influence on the tensile strengths with only a slight lowering observed with the air drying method. The trend observed in this study where FT hydrogels exhibited higher tensile strengths than AD hydrogels is in agreement with reports on a study investigating the tensile strength of PVA films of freeze thawed cycled gels, where the tensile strength values from their cast PVA gels were lower than those from the freeze thawed gel [202]. This observation is simply explained by the fact that freeze thawed hydrogels undergo crystallite formation which can be reinforced by increasing cycles of FT, the presence of crystalline regions serve as the physical crosslink junctions along which mechanical load is distributed, hence resulting in higher tensile strength. The different methods of crosslinking between the PVA10 and 30

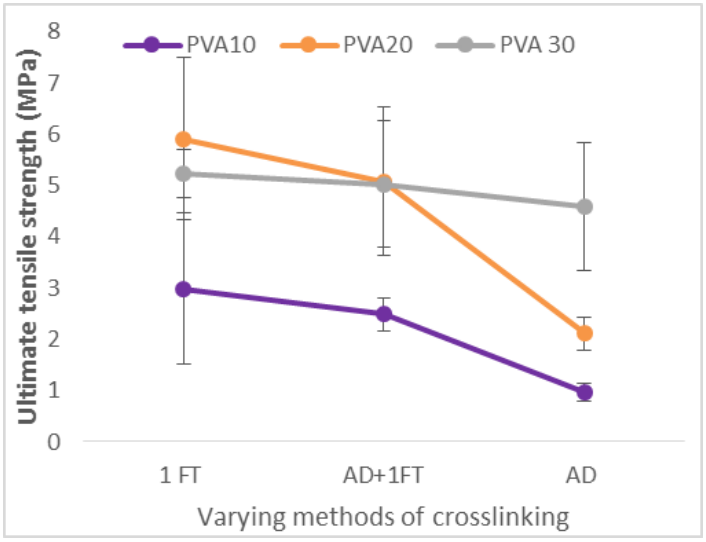

Figure 3-18: the effect of method of crosslinking on the final tensile strength of the hydrogel films.

hydrogels displayed no significant difference in stiffness, whilst with PVA20 hydrogels FT and AD+1FT hydrogels significantly higher stiffness as compared to the AD hydrogels P= 0.039 and 0.002 respectively. Stiffness values displayed by the PVA201FT and AD+1FT against the AD hydrogels, are in close agreement with those obtained in published literature where the authors observed FT hydrogels to have higher Young's modulus than cast PVA hydrogels [202].

SEM analysis

SEM micrographs of FT, AD+1FT and AD hydrogels are displayed in Figure 3-14 which show that the different methods of fabricating the hydrogels results in vividly contrasting microstructures of the resultant hydrogel. It was observed that with FT and AD+1FT hydrogels a fribrilar microstructure was present, which was more pronounced on the FT only hydrogels, this can be explained by the formation of crystallites on the hydrogels during the freeze thawing process. Also this fribrilar structure exhibited gross oriental order over macroscopic length resulting from abrupt dendritic growth of crystals during the first freezing of aqueous polymer solution at -80°C before subjecting the gels to freeze drying, similar observations have been reported [197] where the author went forward to state that "the basic scaffolding for this crystallisation is mechanically imprinted in the polymer network presumably occurring during the first quench, because the water structure is lost during the thaw portion of each cycle." Interpretation of this statement to observations from this study was that the imprinting of the crystal orientation on the hydrogels first occurs when they are subjected to freezing at -80°C as water is lost through sublimation during the freeze drying process. It was also observed that FT hydrogels were opaque, AD+FT hydrogels presented with a less opaque overall structure and AD only hydrogels looked translucent, a similar observation was observed in one study self-healable PVA hydrogels, however their observations were discussed with reference to PVA hydrogel morphologies fabricated from various concentrations on PVA. Briefly they stated that PVA crystallites formed at low concentrations of PVA form easily and are larger. The larger crystallites scatter more visible light which make the

hydrogels look opaque [200]. It can be inferred that for AD hydrogels the crystallite size is small hence resulting in hydrogels that look nearly transparent, the notion of small crystallites forming on AD hydrogels is deduced from a published discussion [197], which presented opinions from various published papers which argued that the driving force for spontaneous gelation of aqueous PVA solutions at room temperature is partly due to the role of crystallinity in polymer rich phases or liquid-liquid phase separation, which has been argued by other authors that crystallinity may be occurring from frustrated crystallisation kinetics instead of arising from polymer rich phases in the solution, whereas others argued all gelation possibilities to be true depending on gelation conditions.

3.9 CONCLUSION

3D hydrogels were obtained by facile methods of crosslinking and it was evident that both the concentration and method of crosslinking affected the physical and mechanical properties. Since the polydispersity, molecular weight and degree of hydrolysis of the PVA used in the study was identical for formulating the solutions to yield the hydrogels, it can be concluded that indeed an optimum concentration leads to optimised mechanical and physical properties. The high EWC results indicated that there is a high microporisity in the FT hydrogels in comparison to the AD+1FT and AD only hydrogels. The lack of a more pronounced crystalline structure is observed with AD hydrogels characterised by their low tensile strength, apart from the PVA30 hydrogels due to a high polymer-polymer chain interaction by virtue of the high concentration of PVA. These results have enabled the identification of base line properties of PVA with known molecular weight as follows.

- PVA of 10%(w/v) concentration had the lowest viscosity and was found to be easier to prepare and handle during fabrication of hydrogels. This implied that when moving forward to optimise studies for formation of dual networks, this concentration would be selected.
- Freeze thawing technique was found to yield hydrogels with higher tensile strength, indicating that for fabrication of mechanically tough hydrogels (dual

networks) this method would be selected as the 1st option for crosslinking. However due to the limited significant difference between FT and AD+1FT, dual networks developed by both methods would be studied to develop a clear distinct effect of the methods of crosslinking for further development of hydrogels.

Chapter 4
Combinatorial design of mechanically tough bone-like biocomposites

4.1 INTRODUCTION

Calcium phosphate based biomaterials have been recognised for the pivotal role they play in bone regeneration. Traditionally, biomaterials such as hydroxyapatite have been used as biomimetic supports to allow cell adhesion and maintain cell viability, however in the last two decades the importance of a porous interconnected network in a bone substitute has been established, and has been shown to play an important role in their performance. An interconnected porous network facilitates mass transfer and nutrient flow; a large surface area favours cell adhesion and proliferation whereas high pore volume allows the delivery of cell population for the regeneration process. Although a porous architecture is beneficial, it has an adverse bearing on the mechanical properties. Thus, the brittleness of the ceramic calcium phosphates combined with porosity leads to a fragile structure. It has also been highlighted that adequate wettability of the biomaterial has a direct correlation on protein adsorption and eventually the cell fate. Furthermore, the ability of a bone substitute to release biomolecules to enable rapid tissue formation is a consideration that is becoming apparent, whilst designing new biomaterials to function as efficacious bone substitutes.

Calcium phosphates (CaPs) are the major constituents of bone mineral and have received much attention as bone substitutes. The most extensively used CaP ceramic for bone replacement is hydroxyapatite (HA), because of its chemical similarities to the inorganic components of bone. It has been subsequently shown that these materials were able to enhance bone formation, guide bone ingrowth on their surface and undergo direct bonding with bone, without the formation of a fibrous capsule [203]. Hydroxyapatite is deemed to be the most stable phase and slight imbalances in the Ca/P ratio of HA

(1.67) can lead to the appearance of different phases. For example if Ca/P is lower than 1.67, β-tricalcium phosphate (β-TCP) and other phases such as tetracalcium phosphate (TTCP), is often seen with the HA phase. Tri calcium phosphate (TCP) is a biodegradable bioceramic that has four polymorphs, the most common being α and β; α-TCP is produced at temperatures in excess of 1125°C and β-TCP at lower temperatures 800-1000°C [204]. Both these phases are less stable than HA and hence more soluble in aqueous environments. The use of a tailor made mixture of HA and β-TCP known as biphasic calcium phosphate (BCP) has been used as bone substitute, which combines the low solubility and osteoconductivity of apatite with a more soluble phase such as TCP. Its resorption rate can be monitored and controlled by varying ceramic particle ratios, for example a higher ratio of TCP in BCP leads to a higher dissolution rate [205]. By mixing various calcium phosphates, setting cements be formed, called a calcium phosphate cement CPC, [206]. CPCs are hydraulic cements that undergo setting when one or more calcium orthophosphate powders and a liquid phase usually water or an aqueous solution is mixed under ambient conditions. The end results of this reaction only has two different end products i.e. precipitated HA at a pH >4.2 or brushite (DCPD) at a pH<4.2. The hydroxyapatite formed on the setting of CPC is similar to the biological apatites than the ceramic hydroxyapatite, which takes place at body temperature in a physiological environment [207]. The setting and solidification process of CPCs are based on two types of reactions which are hydrolysis and acid-base reactions [208, 209]. This mouldable or injectable paste can be adapted to bone defect sites due to their ability to set under ambient conditions hardening inside the damaged bone tissue and generating low heat transfer that avoids the premature death of surrounding cells [210]. Table 4-1 lists the common CaP materials with their stoichiometry used in bone engineering applications.

Type of calcium phosphate	Abbreviation	Formula	Ca/P ratio
Hydroxyapatite	HA	$Ca_{10}(PO_4)_6(OH)_2$	1.67
Tetracalcium phosphate	TTCP	$Ca_4O(PO_4)_2$	2.0
Tricalcium phosphate (α,β,γ)	TCP	$Ca_3(PO_4)_2$	1.5
Octacalcium phosphate	OCP	$Ca_8H_2(PO_4)_6.H_2O$	1.33
Dicalcium phosphate dihydrate (brushite)	DCPD	$CaHPO_{4.2}H_2O$	1.0
Dicalcium phosphate (monetite)	DCP	$CaHPO_4$	1.0
Monocalcium phosphate monohydrate	MCPM, CPM	$Ca(H_2PO_4)_2.H_2O$	0.5
Calcium metaphosphate	CMP	$Ca(PO_3)_2$	0.5

Table 4-1: Various calcium phosphates with the respective Ca/P ratios [205].

Traditionally, calcium phosphate ceramics have been processed by sintering at high temperatures, this type of process is restricted basically to obtaining stoichiometric HA and TCP. It can also be employed in the production of both dense, porous and mechanically stable grafts, as the fusion of crystals during sintering process reduces the porosity (obtained from compaction before sintering) while increasing the strength and density of the ceramic scaffold. Variation of pressure, temperature and the chemical composition of initial powders influences the final structure of the sintered CaP ceramic [211].

HA grafts are osteoconductive [212] and can induce a high rate of cellular activity, proliferation, differentiation and mineralisation in vivo [213, 214]. However HA is considered non resorbable as cellular resorption by macrophages is hardly seen, with the exception of small sized HA particle sizes (85nm to 3.2μm), which can be resorbed by phagocytes [215-217]. HA has also been used as surface coating material on implants such as titanium dental implants and hip and knee prostheses [218].

β-TCP bone graft substitutes in clinical use and animal studies [219, 220] show that both particle size as well as architectural design (pore size and interconnectivity) determine the resorption rate of β-TCP in vivo. TCP resorbs in the early phases making way for tissue invasion and bone formation whilst the graft resorbs. The osteoinductivity of CPCs in particular varies significantly depending on material properties. CPCs have perfect adaptability during implantation due to their minimally invasive injectable capability, self-setting ability in vivo and are bioactive leading to enhanced bone healing. The material is resorbed by two different mechanisms: - active resorption (regulated living cells like macrophages or osteoclasts) and passive resorption (which takes place via chemical dissolution or hydrolysis in the body fluids). However CPCs are dense with weak mechanical properties, and may incur microbial contamination during the synthesis process, which can lead to problems during implantation [207].

More recently, calcium metaphosphate (CMP) has been proposed as an alternative bone substitute material, due to its biocompatibility, degradability and osteoconductive properties, provoking specific responses at the interface of the materials resulting in the formation of a strong bonds between the tissue and material [221]. Lee & Seol et al 2001 reported that several authors [222-224] had proposed CMP as a bone implant material both in fibre and porous rod form, and could successfully be used as it was demonstrated that there was bone growth on calcium polyphosphate CPP structure in vitro and in vivo [175, 225]. There are four known crystalline forms (α, β, γ, δ) of CMP [226] with β-CMP reported to be the most stable, with high moisture resistance and the ability to maintain dimensional and mechanical integrity on exposure to moisture [1].

Buranawat et al [227] demonstrated the potential of a modified meta calcium phosphate construct with mixed porosity as a bone graft that resorbed in vivo within 8 weeks in a rabbit model showing new bone formation and complete healing across a critical sized defect in a rabbit model. The CMP discs in the study with mixed porosities showed a remarkable ability to resorb with rapid bone formation but essentially resulted in a brittle

material, not suited for surgical shaping in theatre to fit the anatomy of the bone defect or for load bearing applications.

PVA hydrogel has attracted attention in the development of articular cartilage replacement due to its high swelling ratio, easy processing [228] and cytocompatibility [229]. With the detailed study on the cross linking of PVA using freeze-thaw cycles, yielding a porous architecture and the ability to regulate the mechanical properties, combined with the bioactive properties of the modified meta calcium phosphate constructs and its degradability.

It was postulated that a composite hydrogel formed of a matrix derived from PVA with the dispersed phase as the meta-calcium phosphate would enhance the mechanical and osteoconductive competence. Employing a hydrogel as a matrix would also facilitate nutrient transport throughout the matrix, absorption of platelet rich plasma (PRP), localisation of bioactive molecules or growth factors and enable scaffolds with high permeability to support mass transfer requirements whilst providing a 3-D template for the cells generating highly compliant scaffolds.

The scaffolds fabricated in this study were evaluated for their potential use as a bone graft substitute, specifically to be employed as a bone plug.

4.2 MATERIALS AND METHODS

MATERIALS	CONCENTRATION
Poly(vinyl alcohol) (PVA), 145,000 mol. wt. hydrolysis ≥ 98% (Merck, Schuchardt OHG)	10, 20 and 30%wt./v
CMP (Calcium metaphosphate) (prepared in house, method by Deb et al)	60%wt with respect to PVA
MCPM (Monocalcium phosphate monohydrate) $Ca(H_2PO_4)_2.H_2O$ (M=252,07) Scharlab S.L	

Table 4-2: Materials used for fabrication of the hydrogel composites.

Filler phase: Monocalcium phosphate monohydrate (MCPM) powder was compressed into pellets and sintered using a temperature programme described in Figure 4-1. The resultant mass was cooled and milled to a fine powder using zirconia beads. Structural changes of conversion of MCPM to CMP were analysed by FTIR, XRD and the particle size was determined.

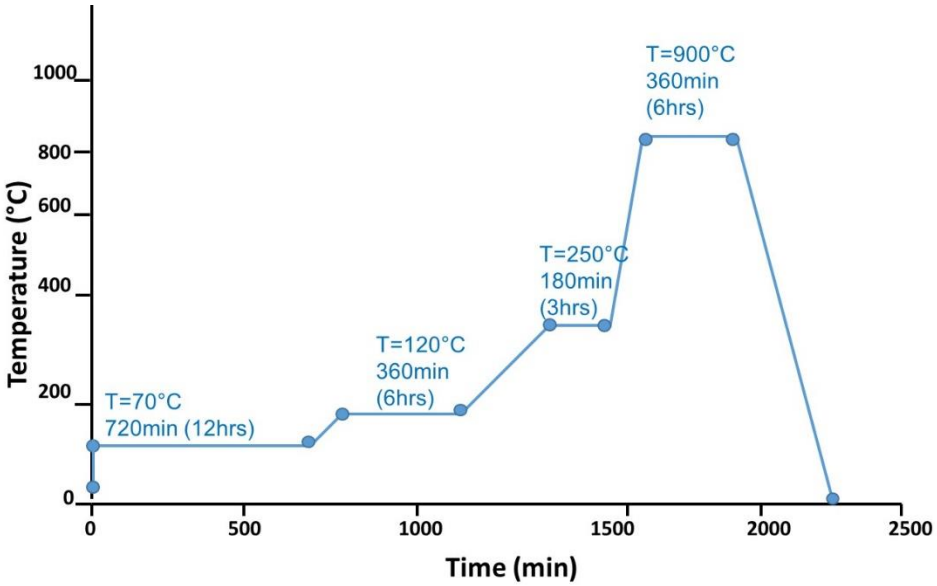

Figure 4-1: Temperature programme for sintering MCPM to CMP, time required by thermal process ~36h (including cooling step).

Matrix phase: PVA 10, 20 and 30 % w/v aqueous solutions were prepared by dissolution of the appropriate amount of PVA granules in distilled water and magnetically stirred at 121°C until all the PVA granules dissolved to form a homogenous solution.

Composite: The aqueous PVA solutions were mixed with CMP powder using ratio 1:1.5 (40%PVA:60%CMP) so as to obtain a paste like consistency. The amount of CMP was kept constant based on a pilot study that was designed to incorporate the highest amount of CMP yielding a mouldable paste. This mixture was subjected to centrifugation at 3400rpm for 15 minutes after which excess PVA was decanted. The paste was then subjected to freeze drying for 24h, and placed in desiccator immediately. All composites were prepared by 1 cycle of freeze drying and thawing (1FT). (**NB:** Hydrogels and composites were subjected to freeze drying in the upper chamber of the freeze dryer).

4.3 CHARACTERISATION

Particle size analysis

The particle size analysis was carried out using a CILAS 1180 laser diffraction particle analyser (Cilas, Orleans; France) operating at an 830nm central wavelength and 7mW energy power. The measurement was conducted by introducing approximately 200 mg of the powder into the tank of the analysing unit in an aqueous medium. The powders were sonicated (frequency 38 KHz for 60 sec) to aid dispersion in the media prior to the analysis. The system was cleaned and a background control reading was taken prior to each actual measurement. The results were analysed using the standard operating parameters by means of a software package provided (Particle Size Expert, Cilas, Orleans; France). The results are expressed numerically for the median particle size (d50), the 10th percentile particle size (d10) and the 90th percentile size (d90). In addition, a histogram is provided with particle size distribution as well as the curve of cumulative percentage.

FTIR spectroscopy

The infrared spectral analysis was performed to characterise the chemical interaction of PVA with CMP. The experimental procedure is detailed in the materials and method section of chapter 3.

Raman spectroscopy

The Raman spectra of the chemical structure of the hydrogel composites were recorded on a Renishaw Invia Raman microscope. The experimental procedure is detailed in the materials and method section of chapter 3.

DSC analysis

DSC thermograms of the composite samples were recorded on a PerkinElmer DSC Jade analyser, as detailed in the materials and method section of chapter 3.

Equilibrium Water Content (EWC)

The hydration studies were performed as detailed in the materials and method section of chapter 3.

The degree of swelling in water is defined as the ratio of the water mass of swollen gel to the dry gels mass. The swollen gel was measured by allowing gel samples to reach the equilibrium state in distilled water at the room temperature while the dry gel mass was determined by drying the gel samples to constant weight in a vacuum at 30°C.

$$\text{Weight swelling ratio (SR)} = \frac{\text{weight of the swollen hydrogel}}{\text{weight of the dry hydrogel}}$$

The gel fraction was defined as the ratio of the dried gel mass weight to the initial mass weight of the polymer.

$$\text{Gel \%} = \frac{\text{final weight of dry gel}}{\text{initial weight of dry gel}} * 100$$

Compression & diametral compression

A universal testing machine (Instron 5569A) with a cell load cell of 50KN and a crosshead rate of 0.5mm/min was used to determine the compression carried out on cylindrical specimens with dimensions (ϕ=4 mm, h=6 mm). Diametral compression was carried out on specimens with dimension d=12 mm and t=6 mm. The load to failure P obtained, was used to calculate strength using the formula $\sigma_T = 2P/\pi Dt$.

Where P is the indirect tensile load, d and t are the diameter and thickness of the specimens respectively.

Dynamic Amplitude Scan (DMA)

Rectangular bars with dimensions (L=34.6mm, W=10mm, and t=4.2mm) were tested with a dynamic mechanical analyser (DMA 8000 Perkin Elmer) in three point bending over a sweep of physiological frequencies (1–10Hz) at 25°C and displacement amplitude 0.3mm. To determine best amplitude or force to use when running a multi frequency scan, a dynamic amplitude scan was carried out at amplitude 0.001mm-1mm with frequency 1Hz at 25°C. Using the damping factor a suitable amplitude region was selected to run the multi frequency scans. Multi frequency scans were run at an amplitude 0.3mm which was selected to be suitable from dynamic amplitude scans. Prior to measurements, the samples were hydrated to equilibrium. The data measured were storage (*E'*) and loss (*E''*) moduli. Loss tangent was determined for each frequency as the ratio *E''/E'*.

SEM

The morphology of the hydrogel composites were determined using the methodology as detailed in the materials and method section of chapter 3.

EDAX

EDAX of the composites was determined using the methodology as detailed in the materials and method section of chapter 3.

CYTOCCOMPATIBILITY

The role of a biomaterial is one in which the properties of the material will facilitate tissue regeneration, the key function being their interaction and ability to support cell growth.

All hydrogels were sterilised by gamma radiation and hydrated for 24hrs before use in cell culture.

Human osteoblast (HOB) cell expansion

The primary HOB cells used were obtained from the femur of healthy patients undergoing surgery. The cells were expanded and used at passage 24, after full characterisation as previously described by Di Silvio and Gurav (2001)[230]. The growth medium was Dulbecco's Modified Eagle Medium (DMEM; D6046) (Sigma), containing : 10% Foetal calf serum (FCS) (Sigma), 5% of HEPES, 1% Minimal essential medium (MEM) (Sigma), 20 mM L-glutamines, 100 units/ml penicillin, 0.1 mg/ml streptomycin (Sigma). The cells were incubated in a humid atmosphere with 5% CO_2 at 37ºC.

Cell seeding and counting

Before seeding cells were counted and viability assessed using 0.1% Trypan blue solution in PBS with a haemocytometer. 10µl of cell suspension was added to 10µl of trypan blue stain; mixed and transferred to a haemocytometer and cells counted under the light microscope using a cell counter.

Cells were seed at $1x10^5$cells/ml for indirect (elution) studies. For direct studies, rolling method was used to seed hydrogels with $3.29x10^5$ cells for each sample, and $2x10^4$cells/well for the controls. Cells with hydrogels were placed on a rotating mixer for 1hour at room temperature to allow for cell attachment on either size of the hydrogels, after which hydrogels were placed in well plates with HOB media and incubated for designated tests. Prior to each test all hydrogel materials were moved to a new well plate so as to asses interaction between osteoblast cells and hydrogel material only.

Cytotoxicity testing (indirect MTT cytocompatibility assay)

MTT assay was used to determine in vitro cytotoxicity of biomaterials by assessing cell metabolic activity. The mitochondrial enzyme succinate-dehydrogenase within the viable cells is able to cleave the yellow tetrazolium salt MTT [3-(4,5-dimethylthiazol-2-yl)] and reduce it to form insoluble purple formazin crystals, which can be dissolved by addition of a detergent such as dimethyl sulfoxide (DMSO). The amount of formazin produced is directly proportional to the number of viable cells present, whose colour can be quantified by spectrophotometric means [231].

Material eluents were obtained by placing hydrogels in 3ml of HOB growth medium under sterile conditions in a 7ml bijou vial, then placed onto a rotating mixer at room temperature. The supernatants were collected at 24, 48 and 72hour time points and transferred into clean bijou vials.

HOB cells were seeded in 96 well-plates at a density of $1x10^5$cells/ml per well. The cells were incubated in HOB media for 24 hours to allow for cell to attach and acclimatisation prior to addition of the test eluents. The following elution times were tested: 24, 48 and 72 hours with cell exposure times: 24, 48 and 72 hours. At 24 hours post seeding under sterile conditions, the HOB media was removed from each well plate and replaced with 100µl of the leached eluents from the hydrogels, as well as the negative (non-toxic) and positive (Toxic) controls, which comprised of HOB media and HOB media with 10%v/v ethanol respectively. The cells were then incubated at 24, 48 and 72 hours and at selected exposure times, the elution medium was discarded and replaced with 100µl/well MTT solution.

MTT solution was prepared under sterile conditions with 5%w/v MTT powder (sigma UK), dissolved in PBS (Sigma, UK) and filtered using a 0.22milipore filter. The solution was added at 1:10 ratio with ascorbic free HOB media. The plates were incubated for 4hrs (37°C, 95%humidity and 5% CO_2), the solution was then removed and replaced with DMSO (Sigma) 100µl per well and placed on a shaker for 5mins to ensure dissolution of formazan crystals. The absorbance of the calorimetric assay was

measured at 570nm test wavelength with 630nm reference wavelength using a DYNEX Opsys technologies plate reader.

Live/Dead viability staining

Viability was analysed using a Live/dead viability/cytotoxicity kit (L-3224) from Invitrogen at time points 1, 3, 7, 14, 21 and 28 days. Hydrogels were removed and placed in new 24 well plates; cells were incubated with 1µM of calcein AM and 2µM of ethidium homodimer in phenol free media and placed in CO_2 incubator for 20mins. Calcein stains the live cells green due to intracellular esterase activity, and ethidium stains the cells red as it enters cells with damaged membranes and becomes fluorescent upon binding to nucleic acids in the dead cell. The cells were observed and imaged with a fluorescence microscope (Olympus IX51) between (x4-x20) magnifications. The live green signal was viewed/imaged using a 480nm band pass excitation filter with a 510nm bandpass emission filter. The dead (Red) signal was viewed with a 520nm bandpass with a 560nm bandpass filter for emission.

Alkaline phosphatase (ALP) concentration

Cell differentiation of the osteoblastic phenotype was determined by measuring the alkaline phosphatase (ALP) production of HOB cells. The activity of the ALP in cell culture media was determined by the release of p-nitrophenol from p-nitrophenol phosphate (PNPP). A standard curve was prepared from 200 µg/ml 4-nitrophenol stock solution to give a range from 0 to 100 µg/ml. 50 µl of cell culture media was transferred to a 96 well plate and 50 µl of substrate reagent (p-nitrophenol phosphate, magnesium chloride hexahydrate and triton X-100 in Glycine) was added. The plate was placed on a shaker for 2 minutes, absorbance was read immediately; measured spectrophotometrically (Dynex Technologies reader) at a test wavelength of 405 nm.

Protein concentration assay

The concentration of total protein was determined from culture media collected from wells of samples at known time points. A quick start Bradford protein assay was used in this study. Standard dilutions of bovine albumin serum were provided in the kit with ranges 0.125, 0.25, 0.5, 0.75, 1.0, 1.5, and 2.0mg/ml. 5µl of standards and samples were pipetted into 96-well microplate and 250µl of 1x dye provided in the kit was added to the 5µl of standards and samples. The plate was left to incubate at room temperature for 10 minutes, and the colour/absorbance changes were measured using a DYNEX Opsys technologies reader at test wavelength 590nm. All culture media samples gave absorbance readings within the range of the standard curve, and concentration of total protein of each sample was calculated.

Quantitative real time polymer chain reaction (qRT-PCR)

To investigate the cell phenotype mRNA was analysed using quantitative real time PCR. At each time point samples were suspended in 0.7ml TRIzol® LS reagent, cells were lysed by pipetting up and down several times, solution was transferred to an eppendorf and RNA extracted following the standard TRI reagent protocol [232].

RNA extraction-: 0.2 ml of chloroform was added to each sample, tubes were capped and shaken vigorously for 15 minutes, followed by 15minute incubation at room temperature. After incubation samples were centrifuged at 12,000xg for 15minutes at 4°C to enable phase separation (mixture separates into a lower red phenol-chloroform phase, an interphase and a colourless upper aqueous phase). The aqueous phase was collected and transferred to a fresh tube where RNA was precipitated by addition of 0.5ml 100%isopropanol and allowed to incubate at room temperature for 10minutes. The sample mixtures were centrifuged at 12,000xg for 10 minutes at 4°C. The precipitated RNA pellets were washed with 1ml of 75% ethanol and centrifuged at 9000xg for 8minutes at 4°C. The supernatant was discarded and the RNA pellet was allowed to dry for 10-20minutes, and resuspended in 40ul RNAse-free water. RNA concentration and

quality was quantified using Nano drop spectrophotometer and purity assessed using the 260/280nm ratio.

Preparation of cDNA-: single stranded cDNA was synthesized from total RNA using the High capacity cDNA reverse transcription kit and protocol provided (Applied Biosystems). Desired input of RNA was 1ug per 20ul reaction (RNA+master mix), volume of required RNA for 1ug was calculated with dilution RNAse free water determined for each RNA template to equal a total of 10µl. 10µl of the RNA template was combined with 10µl of the reverse transcription master mix to give a final volume of 20µl. The master mix was prepared with 10X RT buffer (2µl), 25X dNTP Mix(100mM)(0.8µl), 10X RT random primers (2µl) and nuclease-free H2O(3.2µl). A thermal cycler was used to perform the reverse transcription using optimised settings for High capacity cDNA reverse transcription kits [233].

	Step 1	**Step 2**	**Step 3**	**Step 4**
Temperature (°C)	25	37	85	4
Time (min)	10	120	5	∞

Table 4-3: Optimised thermal cycle conditions for performing reverse transcription.

qPCR-: PCR was achieved using the GoTaq® probe qPCR master mix kit (Promega). 2µl of CXR reference dye was added to the 1ml tube of GoTaq® probe qPCR master mix. 4µl cDNA template was combined with 10µl 2X TaqMan® Gene expression master mix, 5µl RNase-free water and 1µl 20X Gene expression assay to make a total volume of 20µl mixed into each well of a 96 well plate. The plate was sealed with the appropriate cover and centrifuged at 1000rpm for 1minute. The plate was loaded and analysed on a Rotor-Gene 6000 series sequence detection system (Corbett). The PCR reaction consisted of an initial enzyme activation step at 95°C for 2mins, followed by 40 cycles of 95°C for 15s and 60°C for 1min.

The gene expression assay consisted of the house keeping gene GAPD (X20) (applied biosystems), ALP (X60), RUNX2 (X60) (life technologies).

SEM cell morphology study

Cell morphology on hydrogels was carried out at time points 7, 14, 21 and 28 days, each sample was fixed with 1.5% glutaraldehyde buffered in 0.1 sodium cacodylate. The cells were stained in 1% osmium tetroxide and 1% tannic acid, and then dehydrated through a series of alcohol concentrations (20%, 30%, 40%, 50%, 60%, 70%, 90%, 96% and 100%). The final air-drying was in hexamethyl disilazane (HMDS). The samples were gold-palladium sputter coated for 2 minutes to reduce charging and viewed using a JOEL scanning electron microscope (SEM).

4.4 RESULTS

Particle size analysis of the CMP used as the filler phase

The particle size distribution percentiles (10, 50 and 90 %) of CMP powder are presented in Table 4-4, the histogram of particle size distribution and the cumulative percentage of the data are shown in Figure 4-2**.** The histogram of the tested powder exhibited a normal distribution with the mean particle size of 49.9µm.

	Diameter at 10%(µm)	**Diameter at 50%(µm)**	**Diameter at 90%(µm)**
CMP	6.2	24.1	49.9

Table 4-4: Particle size distribution of CMP.

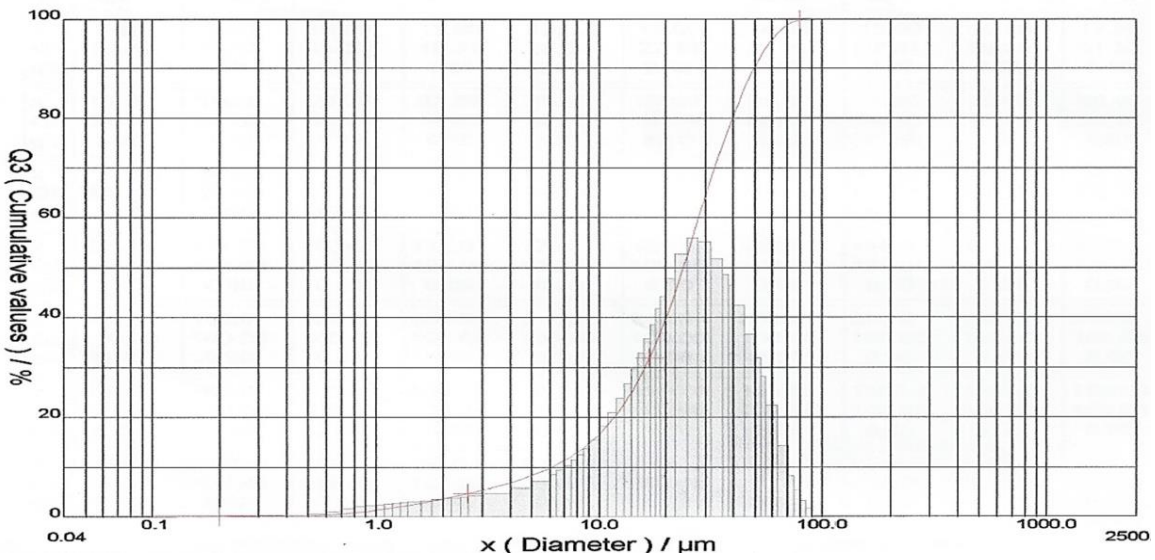

Figure 4-2: The particle size distribution of CMP powder in cumulative percentage (red line) and in frequency percentage (bars).

XRD analysis

The main peaks observed were at 26°, 29° and 32° 2θ angles, which indicated the presence of β-calcium metaphosphate. Other broader low intensity peaks characteristic of calcium phosphates were observed at 40°, 47° and 50°.

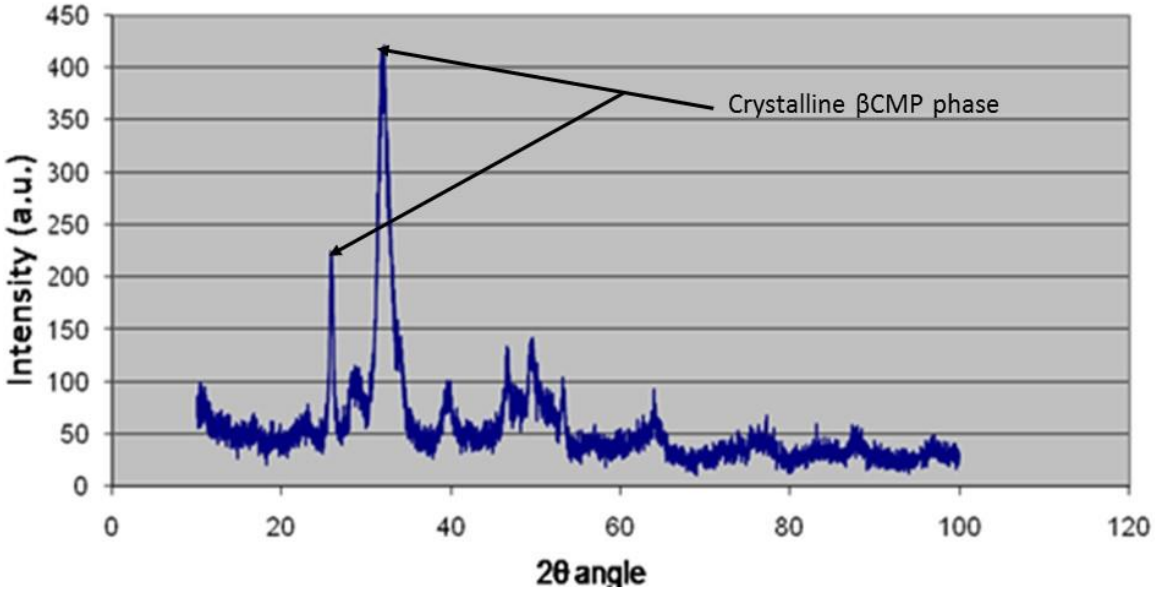

Figure 4-3: XRD pattern of CMP filler particles used in fabrication of the PVA-CMP particles.

FTIR analysis of PVA-CMP composites

The FTIR spectra of CMP (Figure 4-4) showed the characteristic absorption peaks of PO_3^- at 1061, 1115 and 1241 cm^{-1}. These results are in agreement with published studies which report PO_3^- absorption peaks to be in the ranges of (1100-1160 cm^{-1} and 1260-1320 cm^{-1}) [234] and (1080-1120 cm^{-1}) [235]. The shoulder at around 790 cm^{-1} and below on the spectrum can be assigned to the covalent bond between non-bridging oxygen and calcium ions as P–O–Ca stretching vibration. For PVA-CMP, the FT-IR spectra seem to be a superposition of the spectra of CMP and PVA.

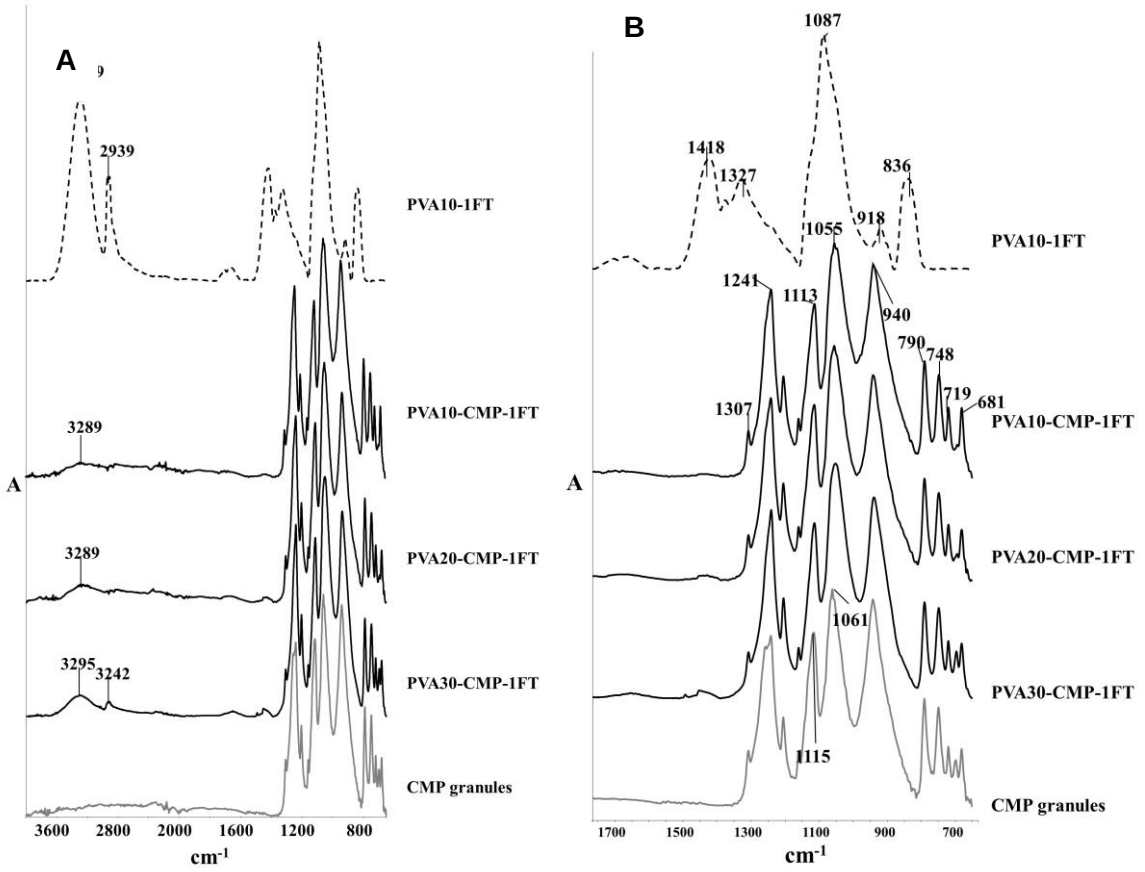

Figure 4-4: FTIR spectra of CMP granules, PVA10-1FT hydrogel and PVA-CMP composites fabricated by crosslinking using a single freeze thaw cycle. **[A]** Is a full range spectra and **[B]** is an expansion of the fingerprint region.

A slight shift of the PO_3^- peaks of PVA-CMP from CMP were observed at 1113 and 1055 cm^{-1} from 1115 and 1061 cm^{-1} on the composites. This minor shift was attributed to the presence of PVA in the composite specifically the C-OH bending vibration at 1087 cm^{-1}. This may be evidence of intermolecular interaction between PVA and CMP. The prominent hydroxyl stretching band (3289 cm^{-1}) and C-H stretching of alkyl groups (2939 cm^{-1}) of PVA were not observed on the PVA-CMP composites. However absorption bands with weaker intensity were observed on the PVA(10 & 20)-CMP composites at 3289 cm^{-1}, which increased in intensity for PVA30-CMP to 3295 cm^{-1} with a minor C-H stretching alkyl group also observed at 3242 cm^{-1}. This observation was attributed to the fact that due to the lower viscosity of PVA10 & 20 fluid phase used in fabrication of the composite, more PVA aqueous solution was decanted after the centrifugation phase during formulation, whereas the viscous PVA30 had more binding capacity with the CMP

filler particles resulting in a reduced amount that was decanted. However FT-IR spectra does not indicate chemical reactions having taken place.

Raman spectra analysis

No differences were observed between the spectra of the PVA-CMP composites (Figure 4-5), however prominent peaks attributed CMP were observed in the composites. The peaks observed at 681 cm^{-1} and 1168 cm^{-1} correlate to the P-O-P and PO_3^- vibrations respectively, which are in agreement with other studies [236, 237]. The peaks at 1000 cm^{-1} correlate to the out of plane bending of C-H groups in PVA.

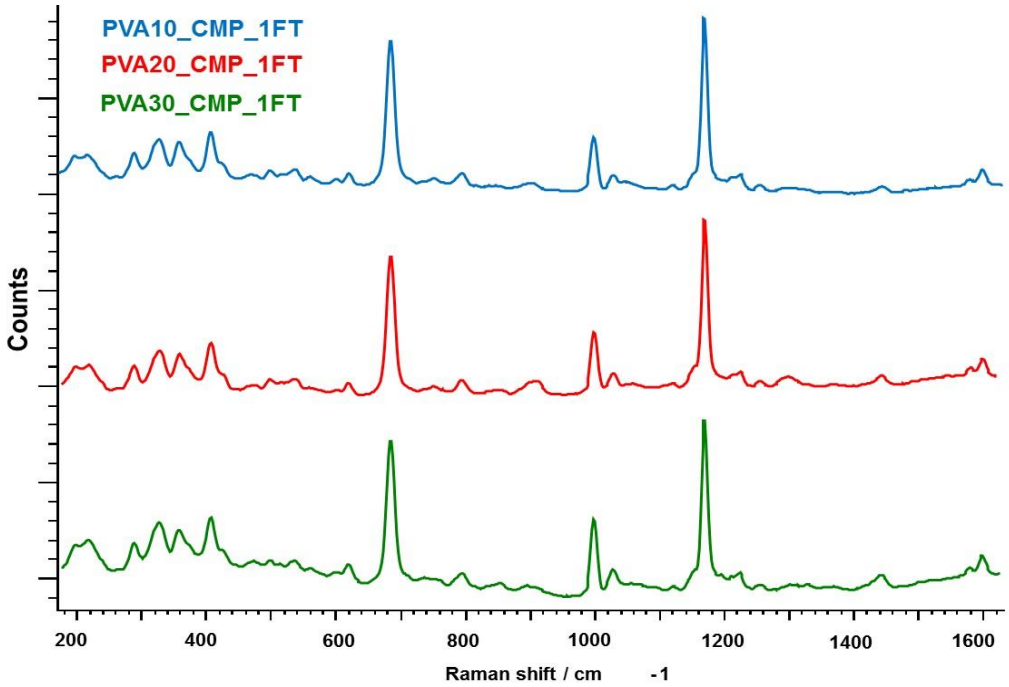

Figure 4-5: Raman spectra of PVA-CMP composites fabricated from 10, 20 and 30% PVA, all subjected to one cycle of freeze thawing.

Thermal analysis (DSC)

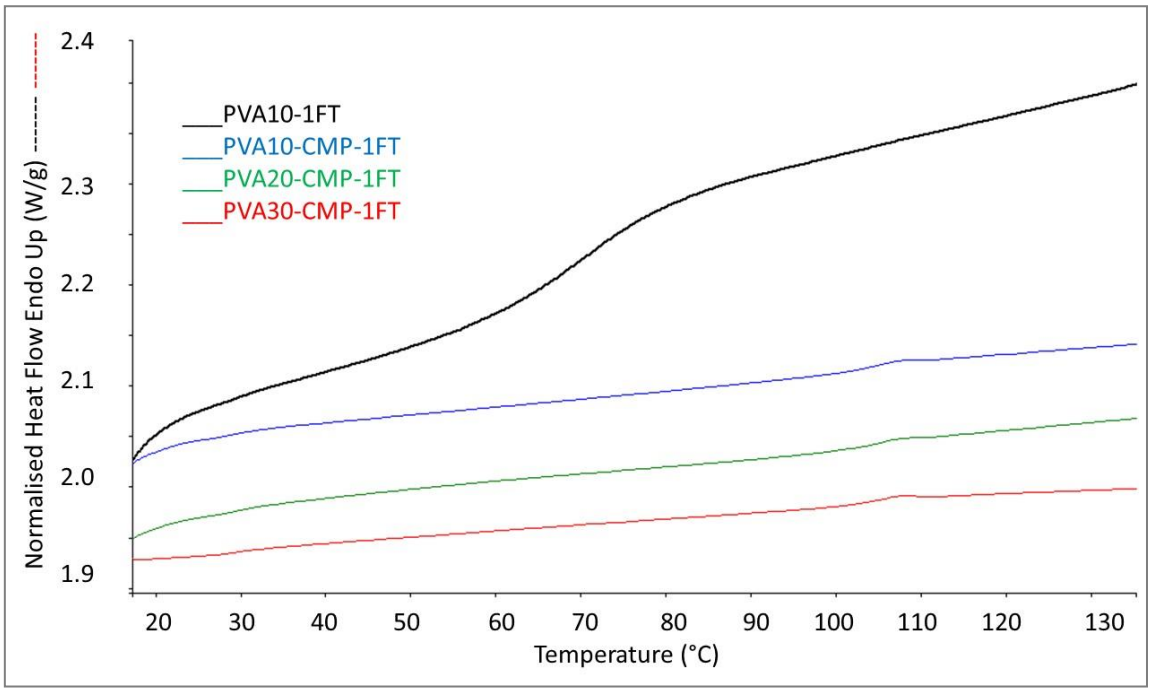

Figure 4-6: Normalised thermogram of PVA10-1FT, PVA10, 20 and 30-CMP composites, crosslinked by 1 freeze thaw cycle.

Hydrogel composites fabricated by 1FT cycle	**Glass transition Tg(°C)**
PVA10-CMP	104.7
PVA20-CMP	105.3
PVA30-CMP	105.4

Table 4-5: Glass transition temperatures (Tg°C) of the PVA 10-CMP, PVA20 & PVA30-CMP composites fabricated by one cycle of freeze thawing.

The glass transition temperature of the composites of PVA-CMP has not been affected by the variation in concentration of the PVA (Table 4-5). The Tg was also found to be higher than those of PVA matrix hydrogels (70.5 – 73.4°C) obtained by one cycle of freeze thawing as reported in (Chapter 3).

Water uptake of the composites

The EWC of the PVA-CMP composites in SBF, 100% humidity and distilled water in Figure 4-7 showed that the EWC decreased with increasing concentration of PVA regardless of the immersion medium.

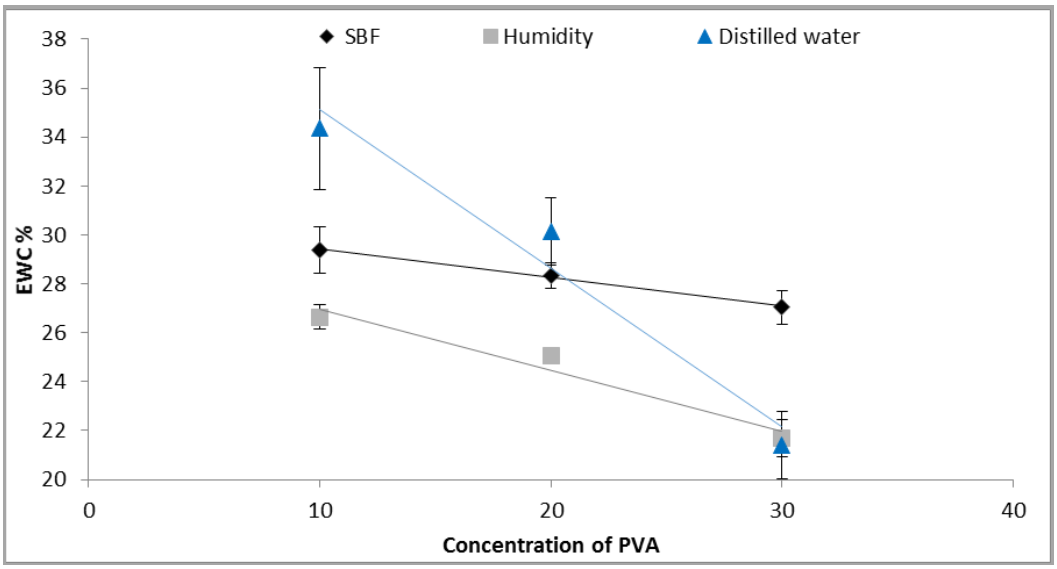

Figure 4-7: EWC of the PVA-CMP-1FT composites fabricated with PVA of concentrations 10, 20 and 30%. The scatter plot presents EWC of composites in SBF, 100%humidity and distilled water. (n=3)

The lowest concentration of PVA at 10% used to formulate the composites exhibited the highest EWC whilst storing the composites at 100% humidity led to lower EWC's as expected.

Hydrogel network obtained by 1-FT	EWC (%)	Swelling ratio (SR)	Gel fraction, GF (%)
PVA10-CMP	34.3 ± 2.5	1.5 ± 0.1	97.7 ± 0.2
PVA20-CMP	30.2 ± 1.4	1.4 ± 0.03	96.9 ± 0.9
PVA30-CMP	21.4 ± 1.4	1.3 ± 0.02	90.9 ± 4.1

Table 4-6: Equilibrium water content, swelling ratio and gel fraction of PVA-CMP composites prepared by one cycle of freeze thawing. Tests carried out in distilled water (n=3).

EWC and swelling ratio (Table 4-6) in distilled water decreased with increasing concentration of PVA in the composite network. This due to the tighter dense network obtained with higher concentration of PVA which in turn limits the amount of water absorbed in the network. The gel fraction of the composites was also found to decrease with increasing concentration of PVA in the network. This could be attributed to the loss

of unbound CMP filler particles, incurred during fabrication stage with PVA solutions of higher viscosity.

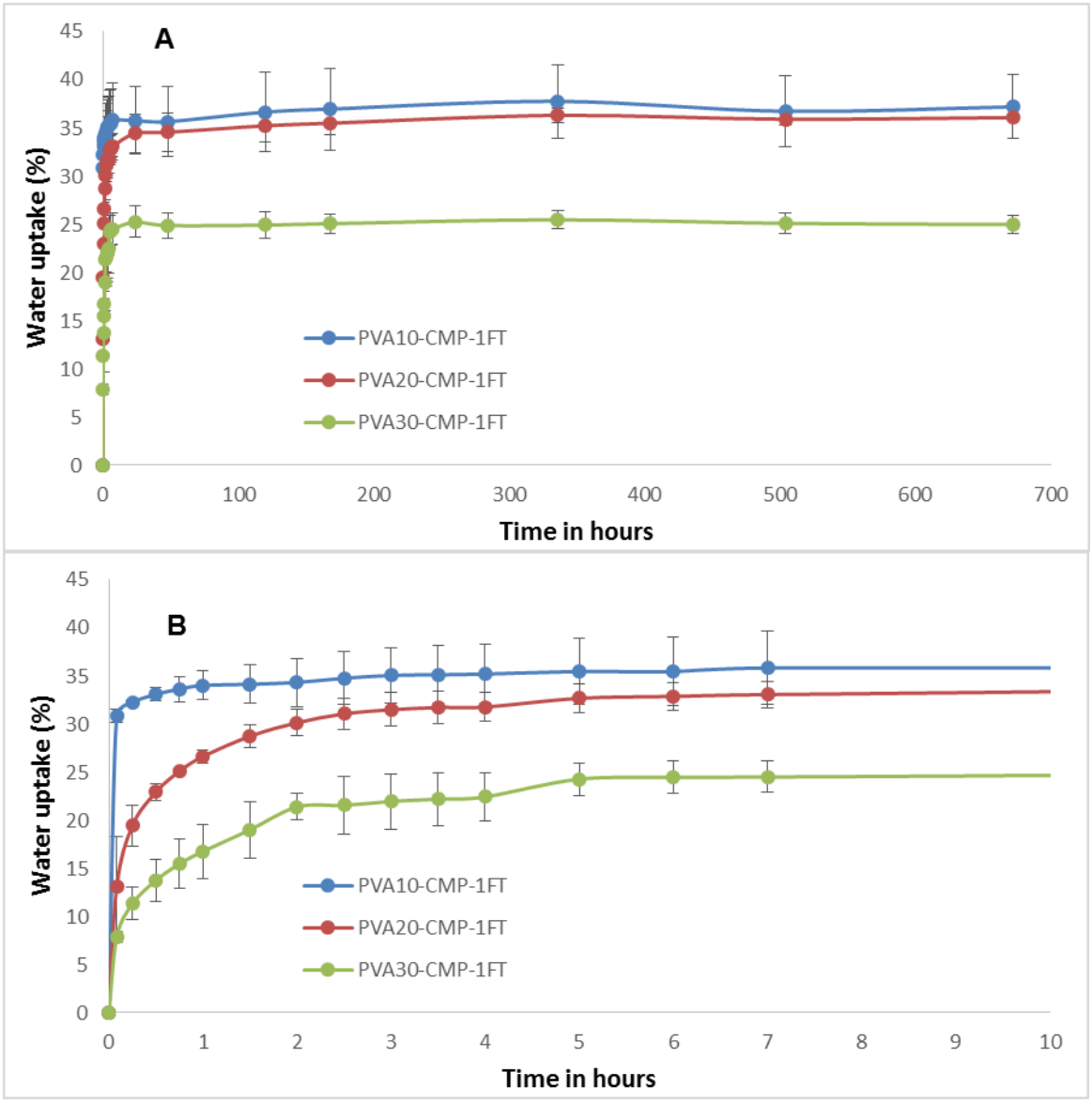

Figure 4-8: Water uptake of the PVA-CMP composites fabricated with PVA of concentrations 10, 20 and 30% and crosslinked via one cycle of freeze thawing. **[A]** Represents a full scale plot of water uptake from the initial time point to the final 4weeks time point. **[B]** Represents an expanded version of water uptake within the first 10 hours, to highlight the differences in the rate of uptake. (n=3)

Water uptake of the composites (Figure 4-8) indicates a linear trend within the first 2hrs after immersion in water. The rapid water uptake of the composites reached equilibrium within 8hours and remained relatively constant over the 4 week duration of the test. Water uptake values were found to decrease with increasing concentration of PVA with the most rapid uptake for the PVA10 composite followed by the 20 and 30% PVA composites.

Compression tests

Compressive strength and modulus of the hydrogel composites are presented in Figure 4-9 and Figure 4-10 respectively, which were carried for both dry and hydrated specimens in distilled water and SBF.

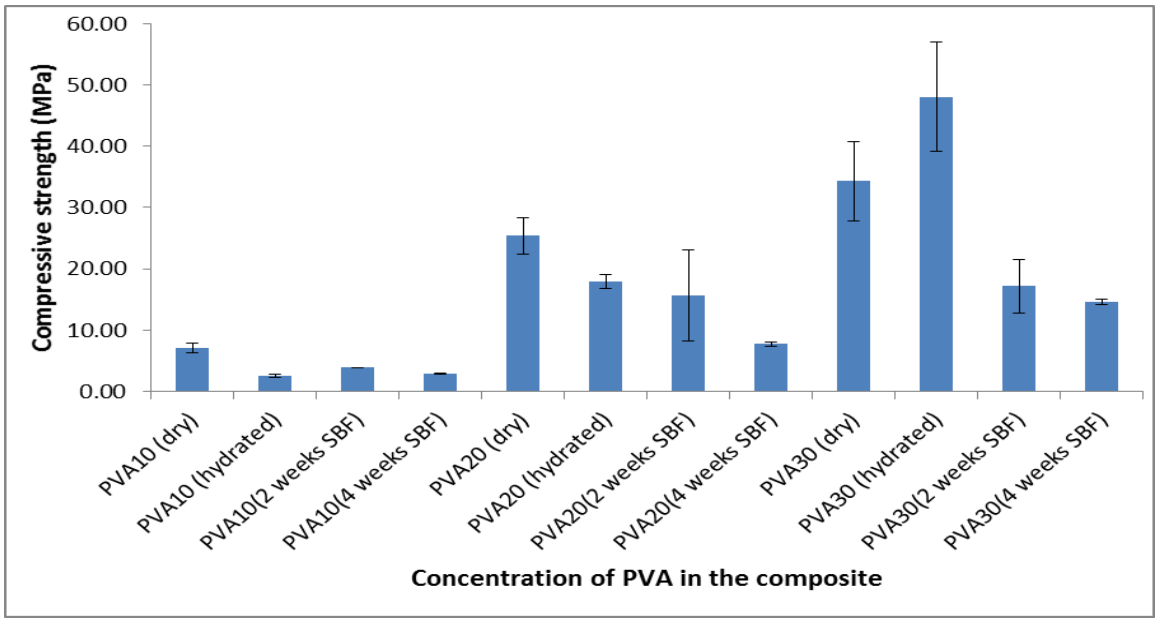

Figure 4-9: Compressive strength of PVA-CMP composites fabricated with PVA of concentrations 10, 20 and 30% and crosslinked via one cycle of freeze thawing. Tests were carried out under dry and hydrated specimens (n=6), as well as after 2 and 4 weeks immersion in SBF (n=4). As the materials are not brittle it should be noted that the values are comparative within the group.

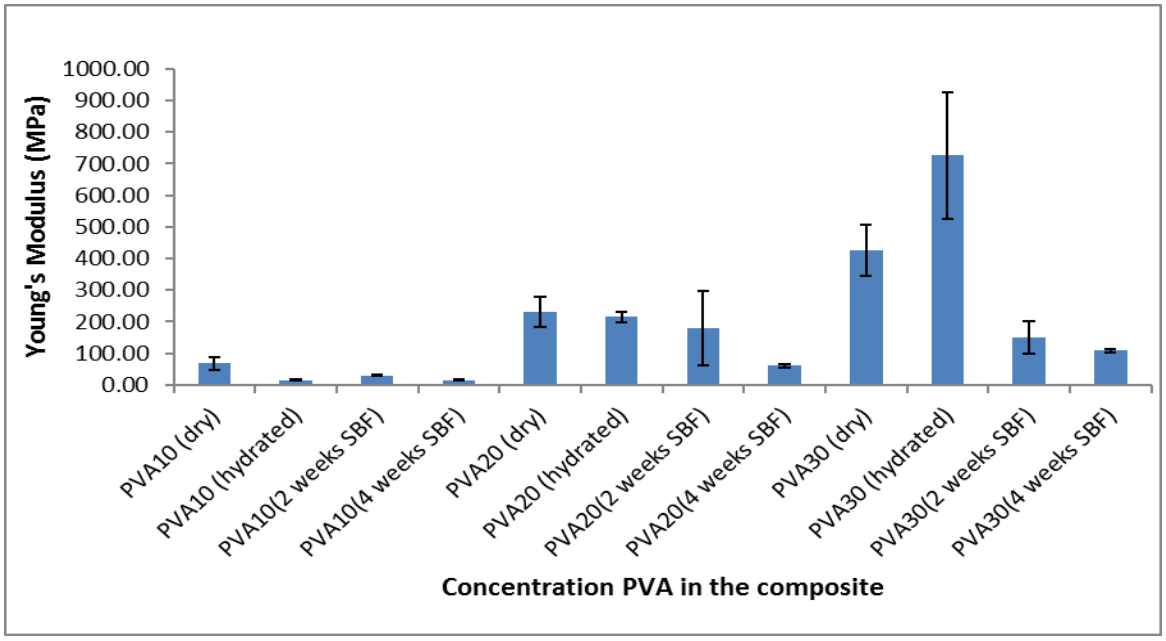

Figure 4-10: Young's Modulus of PVA-CMP composites fabricated with PVA of concentrations 10, 20 and 30% and crosslinked via one cycle of freeze thawing. Tests were carried out for dry and fully hydrated specimens (n=6), as well as after 2 and 4 weeks immersion time in SBF (n=4). As the materials are not brittle it should be noted that the values are comparative within the group.

The compressive strength of the PVA-CMP composites were found to increase with increasing concentration of PVA. The compressive strength values ranged between 7-25MPa, 2.5-48MPa and 2.9-17MPa, for the dry, hydrated in water as well as after immersion in SBF respectively for the composites respectively. All the composites exhibited higher compressive strengths in the dry state, as expected, with the exception of PVA30-CMP composite, which exhibited the highest compressive strength even for the hydrated specimens. Compressive strength after immersion in SBF was found to decrease with increased immersion time for all the composites. The compressive modulus of the composites also increased with increasing concentration of PVA and the values ranged between 68.3-425.4, 16-725 and 16-180MPa, for the dry, hydrated conditions, as well as after immersion in SBF respectively. The modulus of the composites after immersion in SBF were found to decrease with increasing immersion time.

Diametral compression test

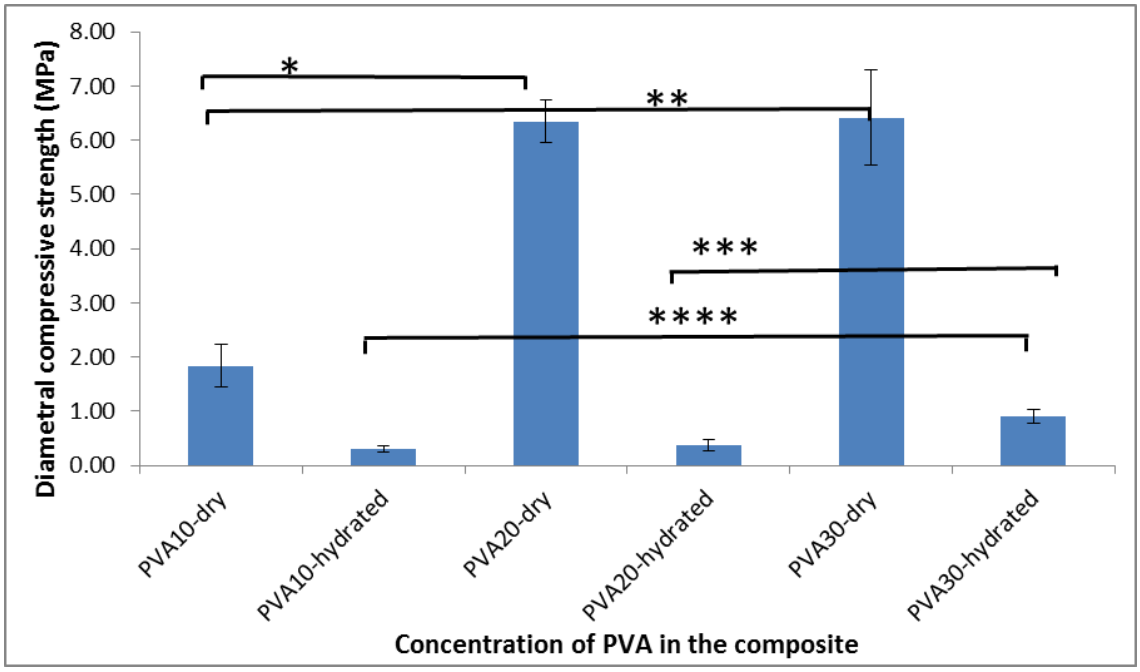

Figure 4-11: Diametral compressive strength of PVA-CMP composites fabricated with PVA of concentrations 10, 20 and 30% and crosslinked via one cycle of freeze thawing. Tests were carried out under dry and hydrated to equilibrium conditions. (n=6) (*, **, *** and **** P<0.001); asterisk linked with lines indicate significant difference in values between the groups. As the materials are not brittle it should be noted that the values are comparative within the group.

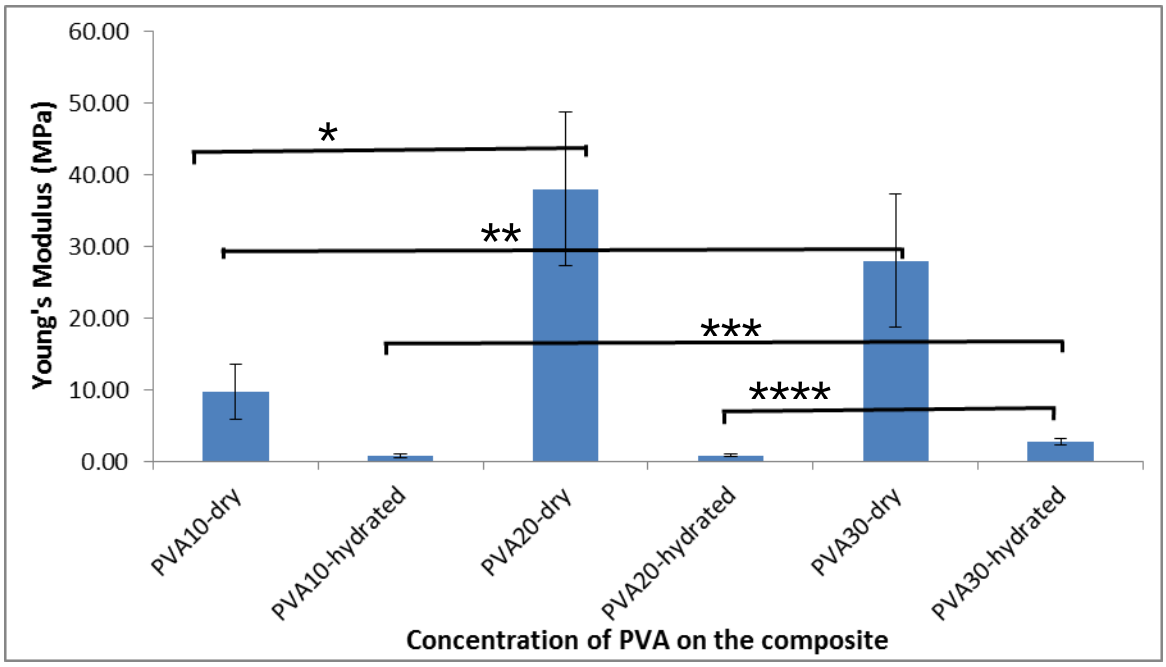

Figure 4-12: Diametral stiffness of PVA-CMP composites fabricated with PVA of concentrations 10, 20 and 30% and crosslinked via one cycle of freeze thawing. Tests were carried out under dry and hydrated to equilibrium conditions. (n=6), (*, ***, **** P<0.001 and ** P=0.004); asterisk linked with lines indicate significant difference in values between the groups. As the materials are not brittle it should be noted that the values are comparative within the group.

The diametral compressive strength of the dry composite hydrogels ranged between 1.8-6.4MPa with concentration of PVA influencing the strength but no significant differences (P=0.160 & 0.856 for hydrated and dry composites respectively) were found between the 20 & 30% concentration of PVA. There were significant differences in the stiffness values obtained in this mode that ranged between 9.8-38.0MPa. Both diametral compressive strength and stiffness values of the hydrated gels were lower in comparison to the dry composites. There was no significant difference (P=0.059) between the stiffness values of PVA20 and 30 dry composites.

Dynamic mechanical analysis (DMA)

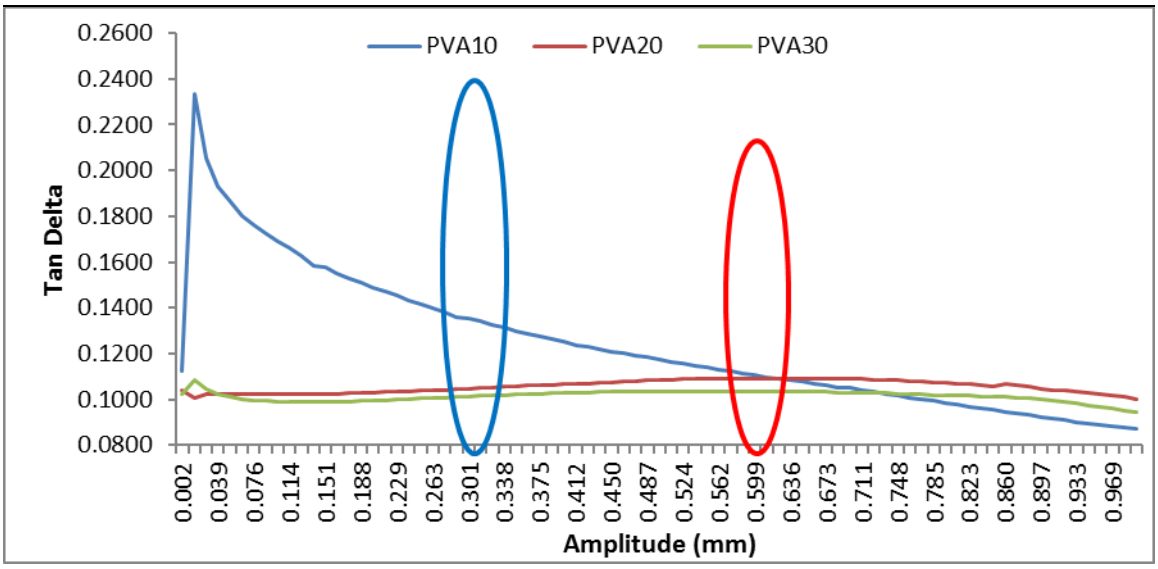

Figure 4-13: Dynamic amplitude scan of PVA-CMP composites fabricated with PVA of concentrations 10, 20 and 30% and crosslinked via one cycle of freeze thawing. Tests were carried out on specimens that were hydrated to equilibrium.

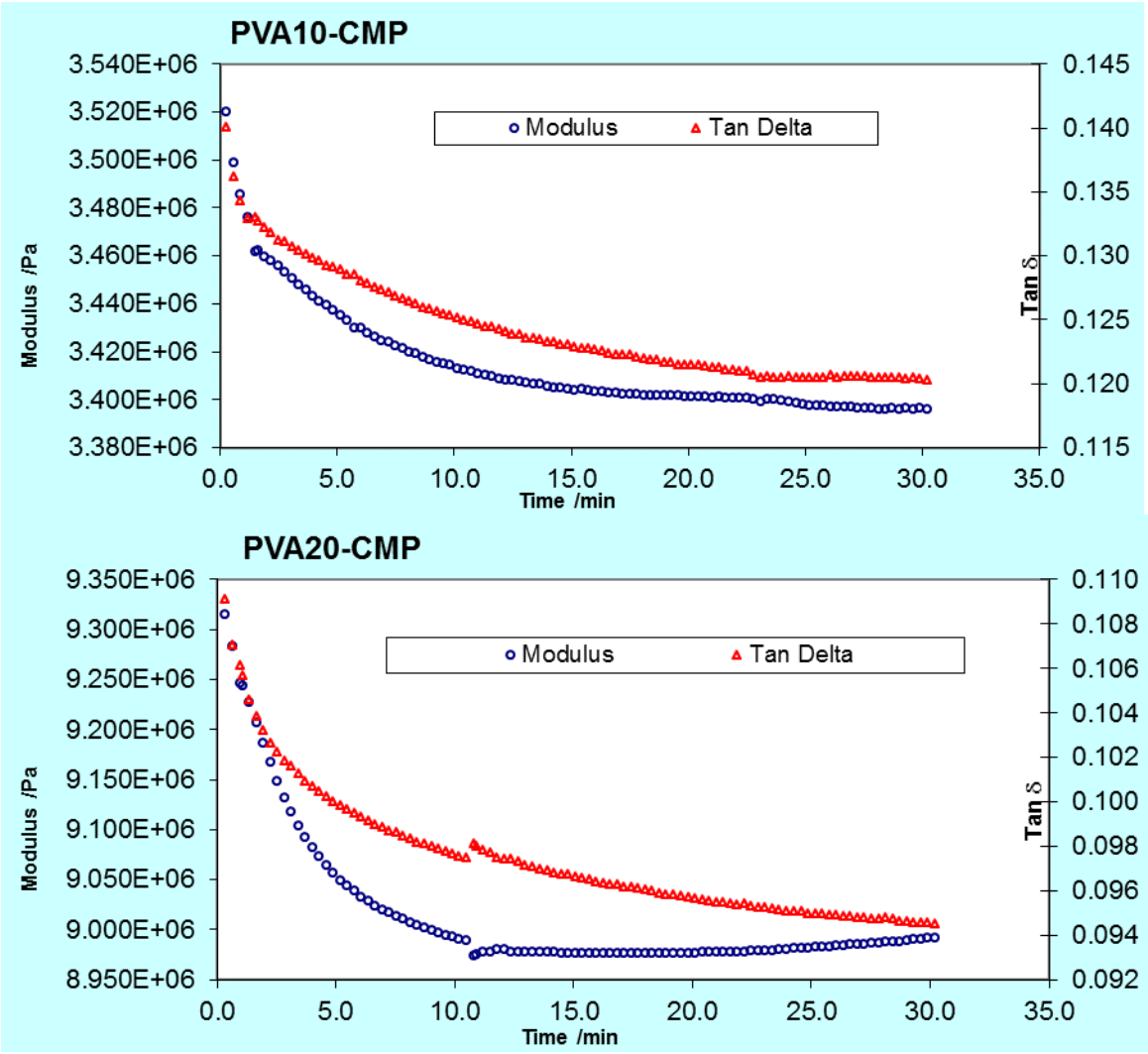

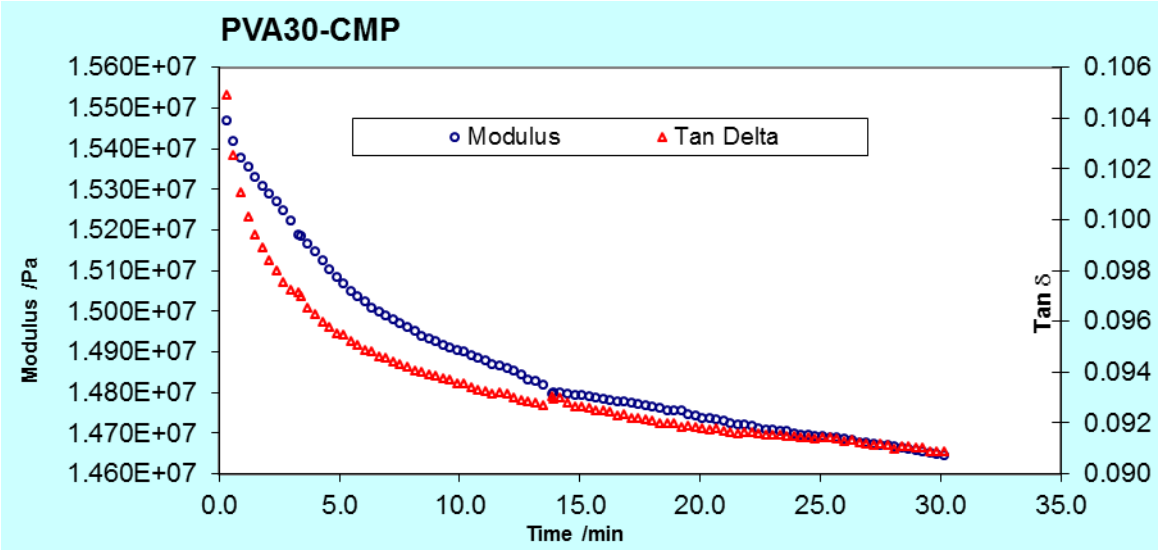

Figure 4-14: Dynamic properties of the PVA-CMP composites vs time. Specimens were tested at frequency 1Hz and under hydrated conditions at 25°C for 30minutes.

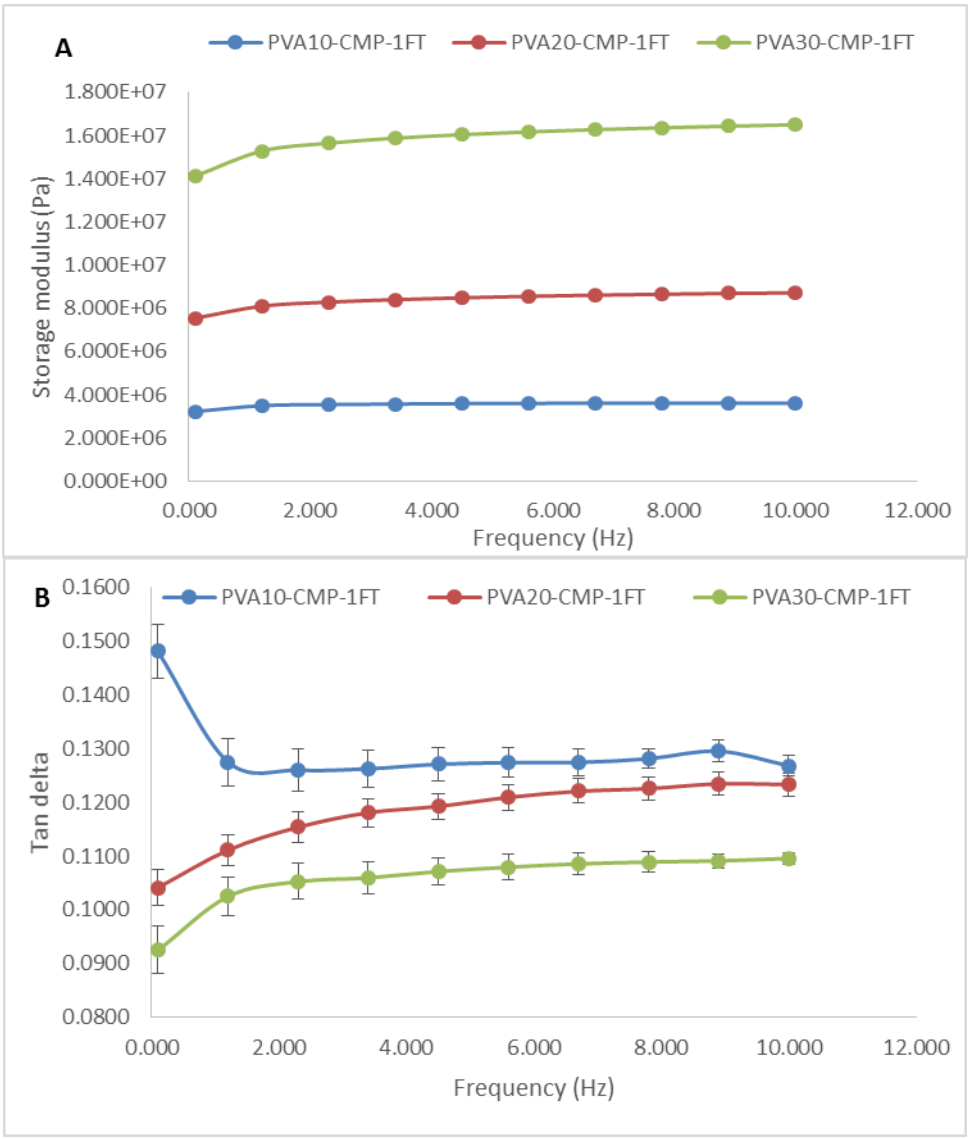

Figure 4-15: Modulus **[A]** and energy absorbing potential **[B]**, of PVA10,20,30-CMP composites at static temperature 25°C and multi-frequency 1- 10Hz. Multifrequency scans were run at amplitude 0.3mm which was selected to be suitable from dynamic amplitude scans. (n=3)

Storage modulus results indicated a clear trend, with PVA10 exhibiting the lowest modulus followed by PVA20 and PVA30. This result is within expectation as stiffness of the composites increases with increasing concentration of PVA. Results showing the energy absorbing potential of the composites are in agreement with those of loss modulus as they indicate that PVA10 has the highest energy absorbing potential which reduces with increasing concentration of PVA. This would be expected as low amount of energy lost or irrecoverable would directly translate to high absorbing potential.

SEM analysis

	PVA10-CMP-1FT		
Mag	**100X**	**500X**	**2500X**

PVA10-CMP-1FT

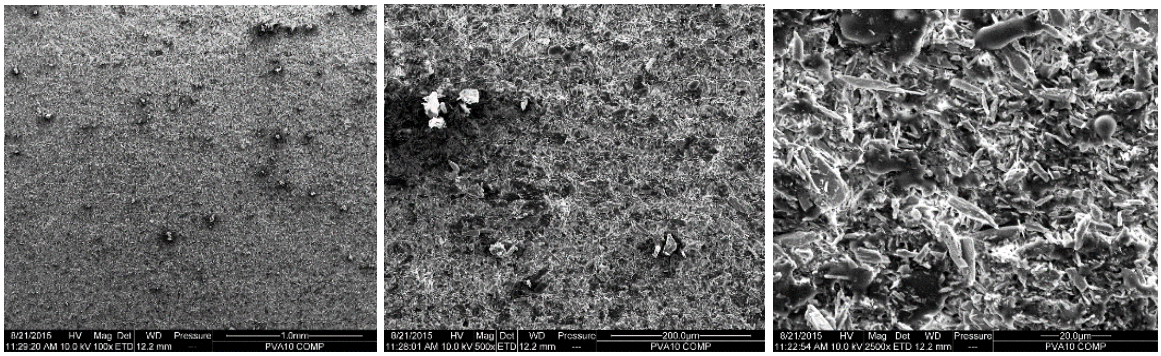

PVA20-CMP-1FT

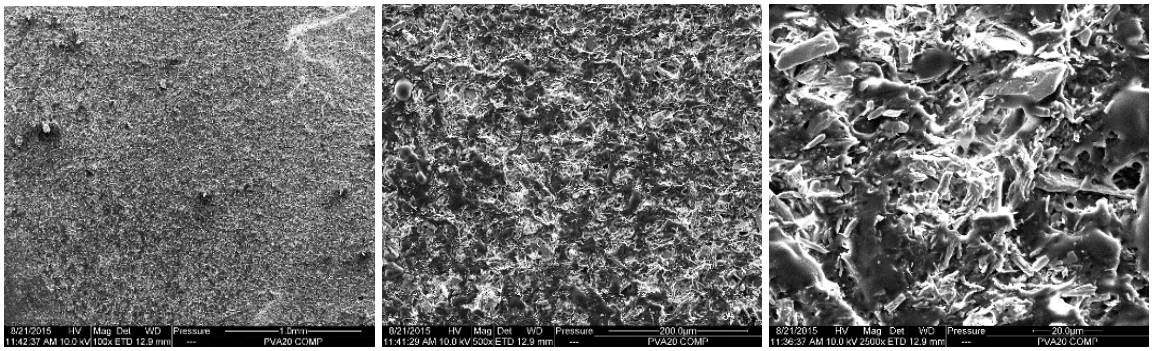

PVA30-CMP-1FT

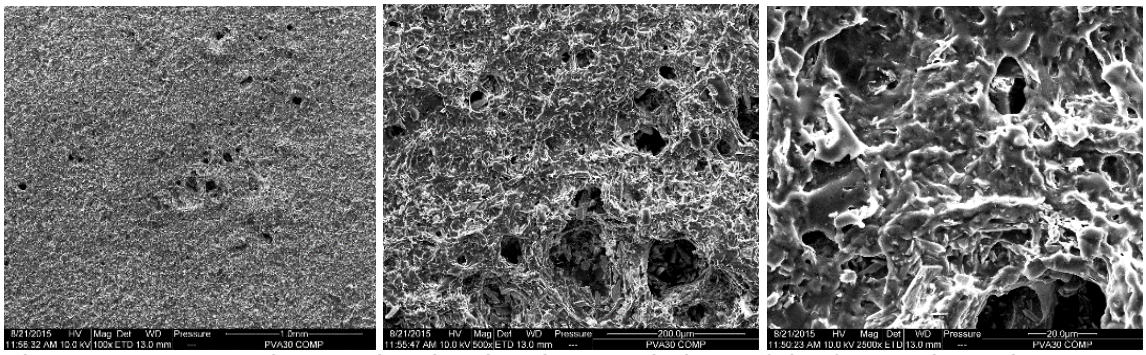

Figure 4-16: SEM micrographs showing the morphology of the freeze-thawed PVA-CMP composites starting with PVA10, 20 then 30 from top to bottom respectively, at magnifications 100X, 500X and 2500X from left to right respectively.

SEM micrographs of the PVA-CMP composites shown in Figure 4-16 clearly demonstrated the variation of microstructure of the composites, with visible micro-pores and in some cases randomly scattered macro-pores.

EDAX analysis

PVA-COMPOSITES Wt.% ELEMENT VALUES

Polymer enriched zone			**Inorganic enriched zone**			
C	**O**		**C**	**O**	**P**	**Ca**
51.8 ± 10.1	46.8 ± 8.7		3.1 ± 0.8	64.2 ± 2.5	25.2± 1.4	7.6 ± 0.6

Table 4-7: Wt. % of elemental values in the composites, taken from identified polymer areas and spindle crystals.

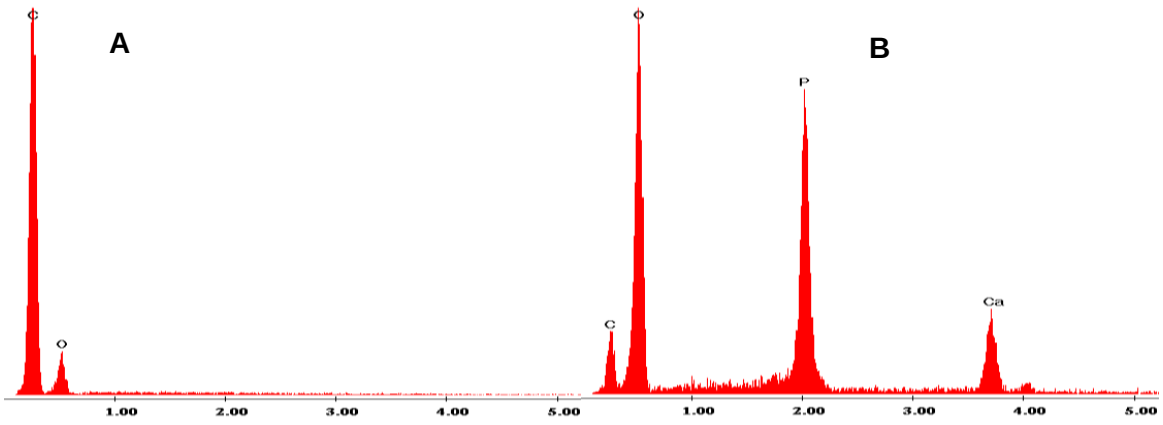

Figure 4-17: EDAX of PVA-CMP composite, **[A]** represents spectra obtained from the polymer like area and **[B]** represents spectra obtained from spindle like CMP crystal area.

X ray micro-analysis of elements present in the PVA-CMP composite networks are presented on Table 4-7 and Figure 4-17. EDAX confirmed the presence of both the polymer and ceramic phase in the composites, indicating the presence of polymer rich and polymer poor phases/areas.

CYTOCOMPATIBILITY

Cell viability study using MTT assay

Figure 4-18 shows the viability of HOB cells seeded on the elusion extracts of the VA-CMP composites, tested by MTT assay at 24, 48 and 72 hour exposure time of eluents collected after 24, 48 and 72 hours. Results indicated that the PVA-CMP composite eluents were not toxic to the HOB cells.

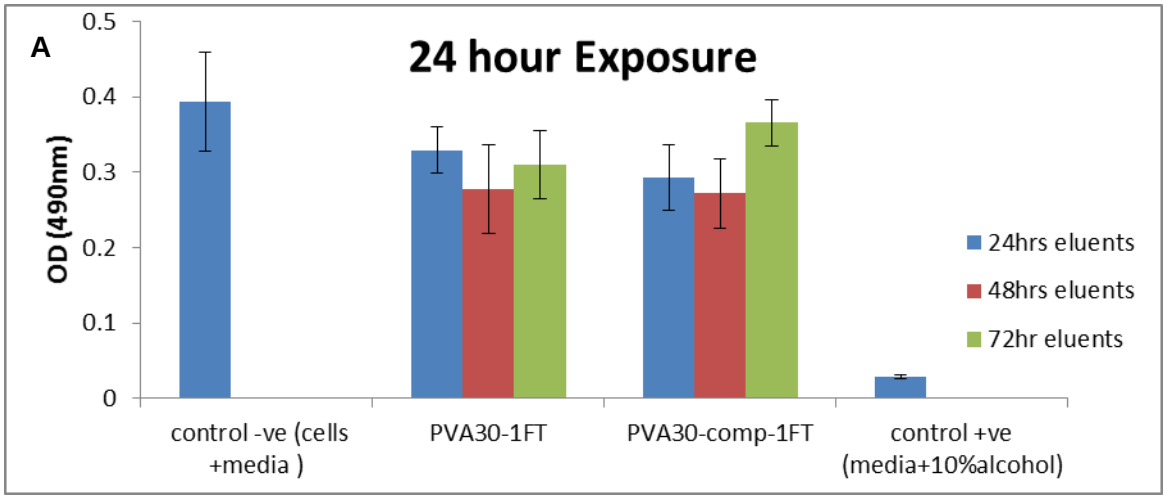

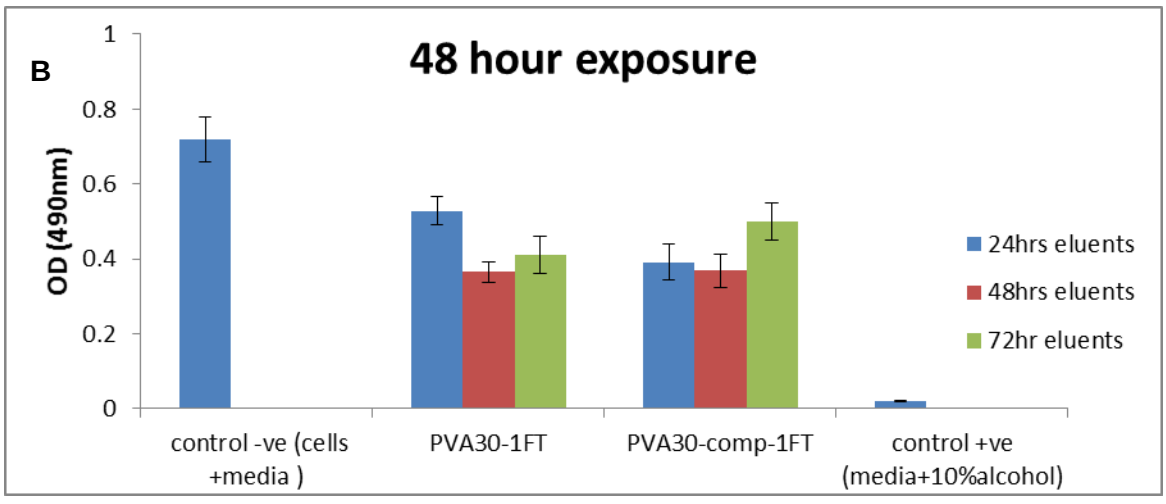

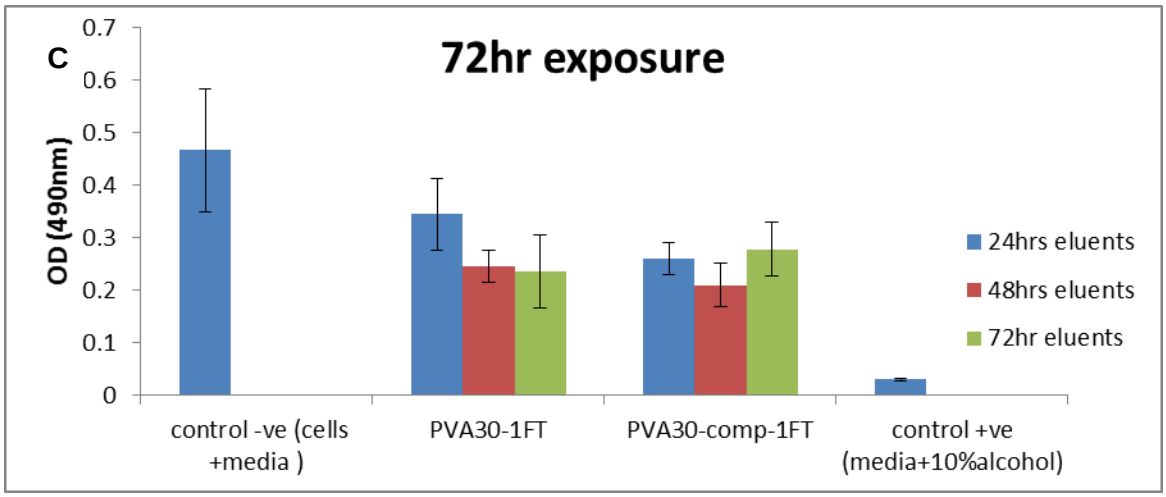

Figure 4-18: MTT assay test showing the response of human osteoblast cells following exposure to eluents from PVA30 hydrogel and PVA30-CMP composite. Cells were exposed for 24, 48 and 72hrs to a **[A]**. 24hr elusion wash time **[B]**. 48hr elusion wash time and **[C]** 72hr elusion wash time. (n=4)

Live/dead cell analysis

Live cells were observed on all the hydrogel composites over a period of 28 days, indicating good cell attachment, proliferation and migration on the surface as well as within the micropores of the composites.

PVA30-1FT hydrogel

Day 3

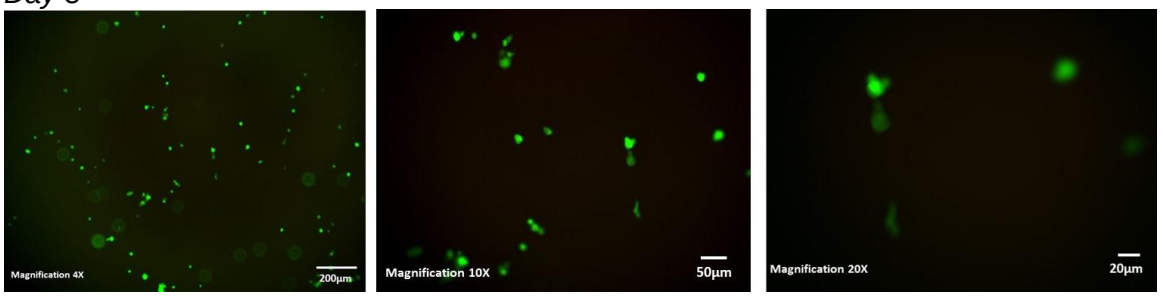

Day 7

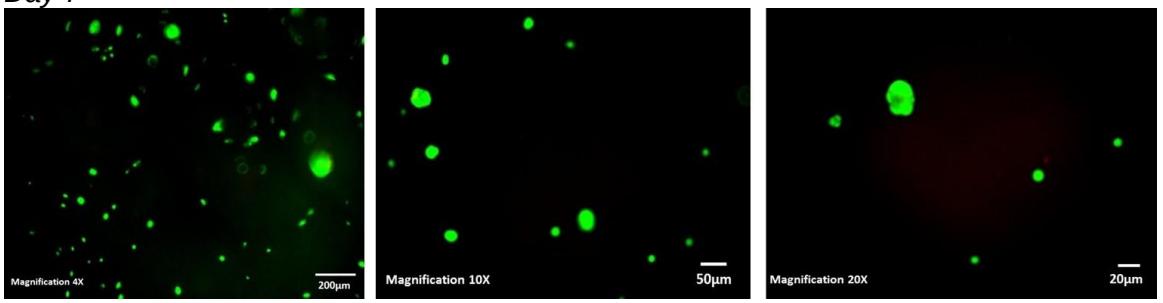

Day14

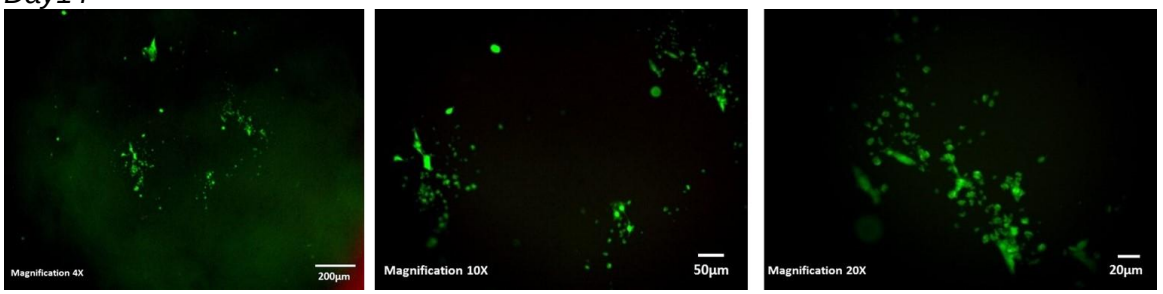

Day 21

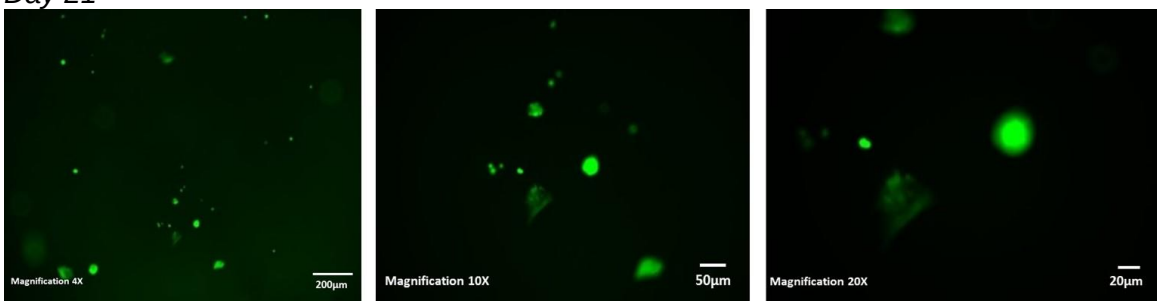

Day 28

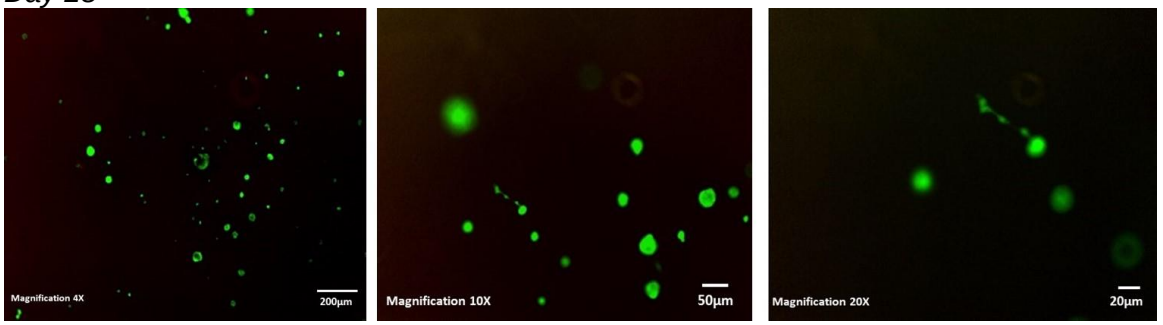

PVA30-CMP-1FT hydrogel composite

Day 3

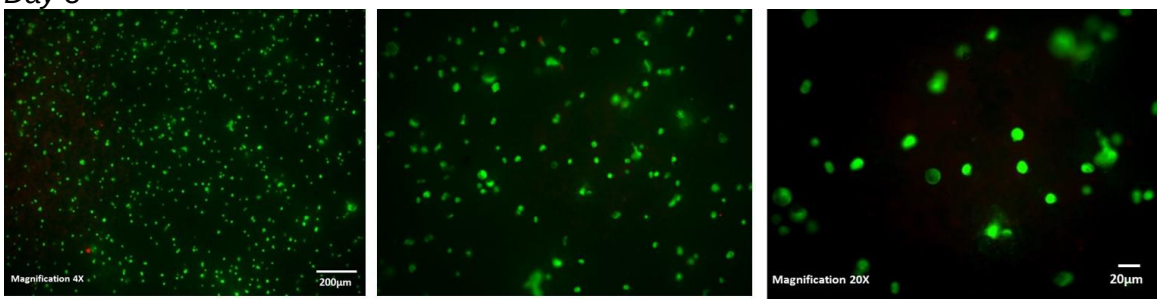

Day 7

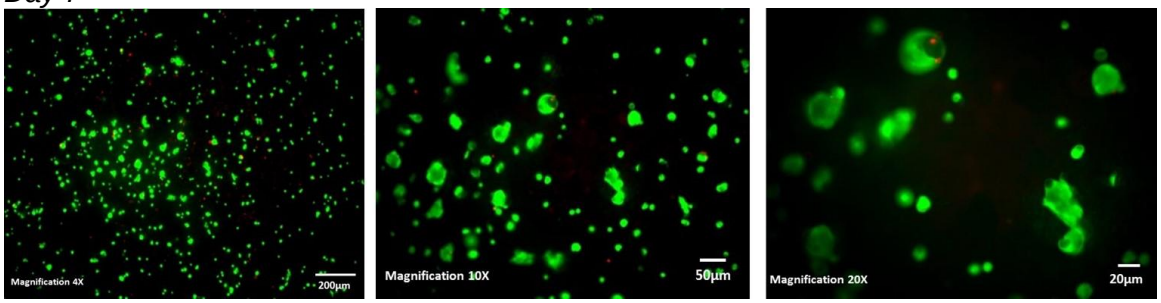

Day 14

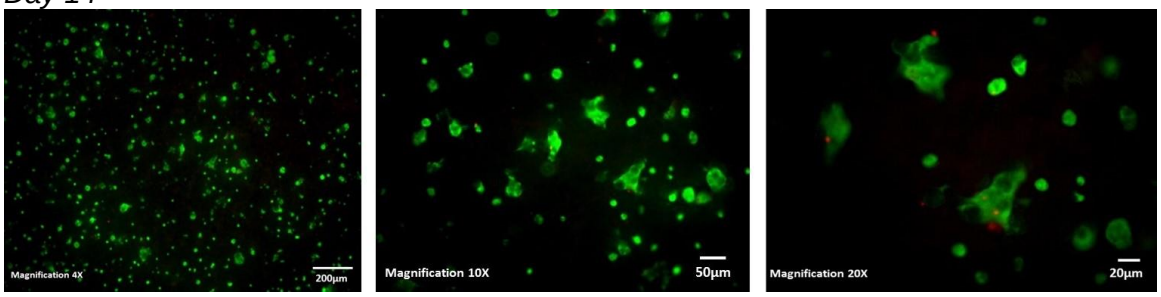

Day 21

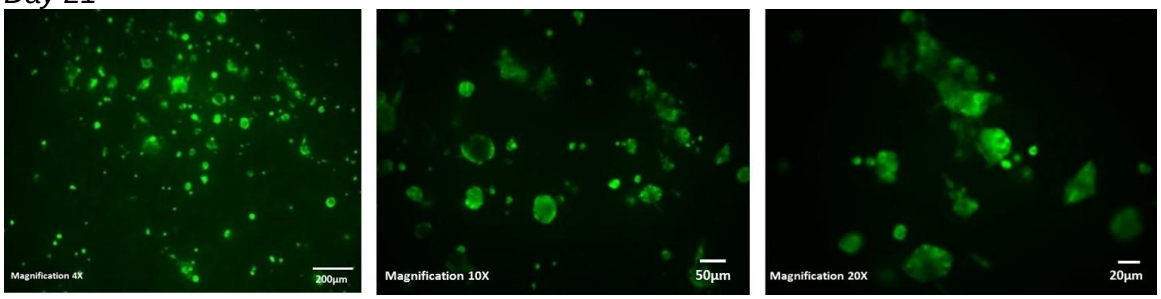

Day 28

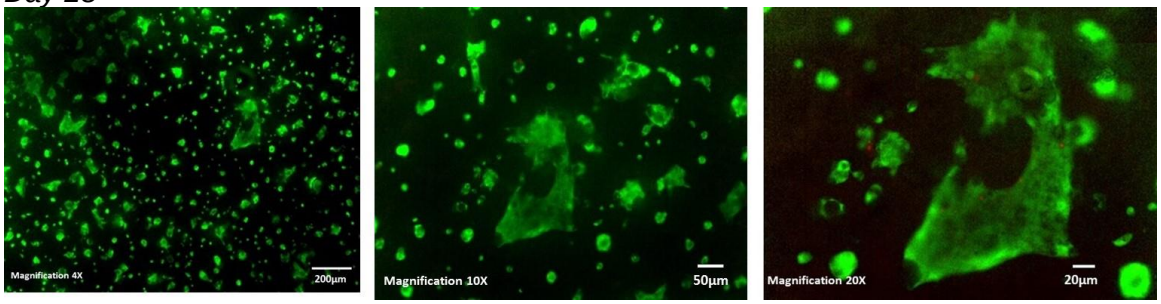

Figure 4-19: Images of live/dead staining of HOB cells (x4, 10 and 20 magnification) on the PVA30 hydrogel and PVA30-CMP composite at day 3, 7, 14 and 28.

Cell morphology analysis by SEM

Mag	500X	2000X	5000X

PVA30-1FT hydrogel – Day 7

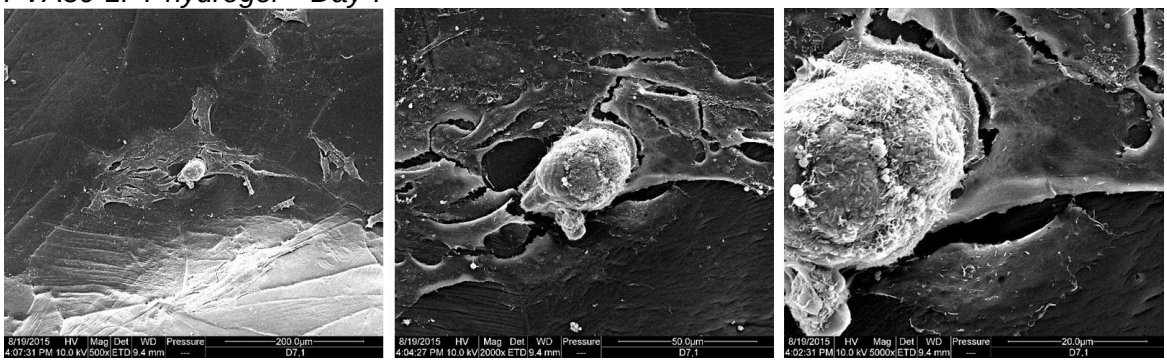

PVA30-CMP-1FT composite – Day7

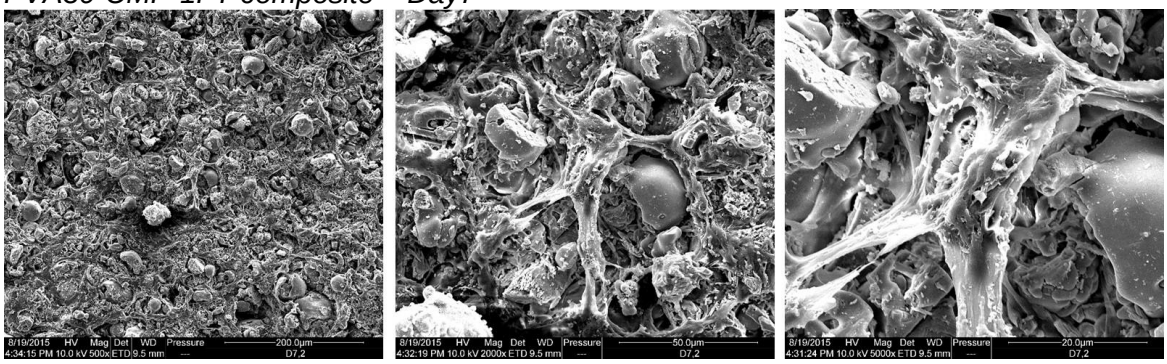

PVA30-1FT hydrogel – Day 14

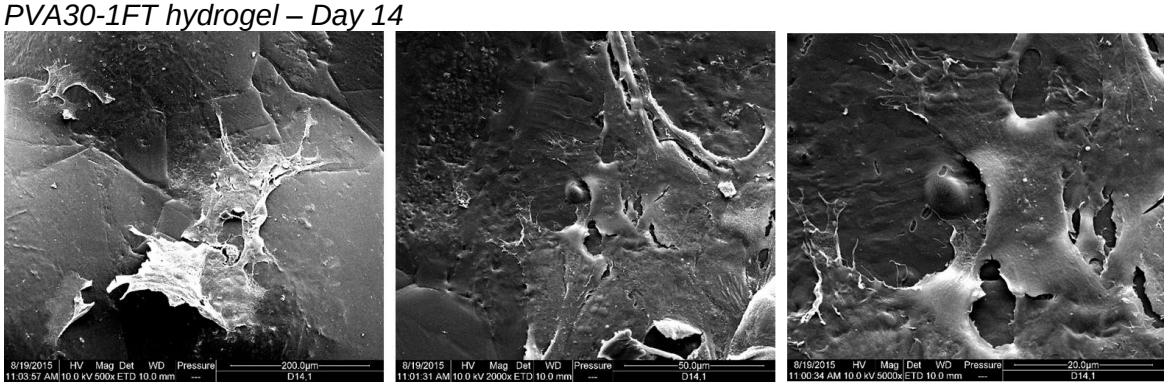

PVA30-CMP-1FT composite – Day 14

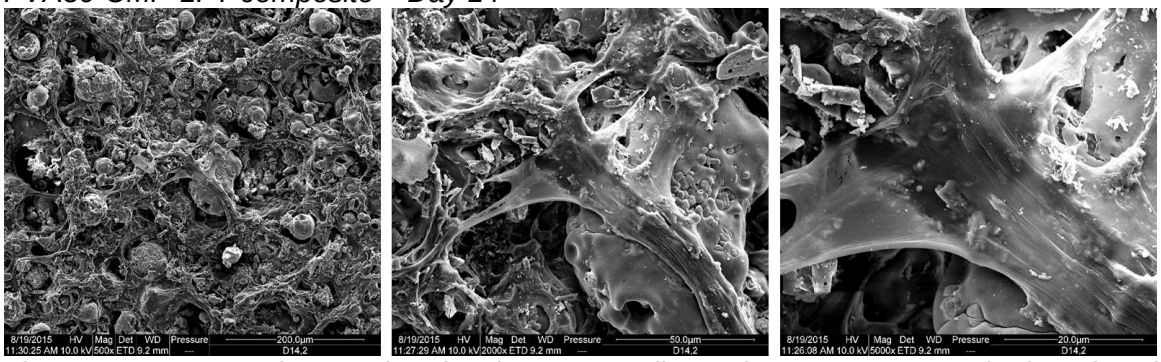

Figure 4-20: SEM micrographs showing HOB cell attachment on PVA30 hydrogel and PVA30-CMP composite after 7 and 14 days in culture.

The results showed that the cells adhered well to the surface of the scaffolds, confirmed by the flat stretched morphology of the cells. It was also observed that on the PVA-CMP composites the cells were able to spread across the pores of the composites, eventually entirely covering the pores.

HOB cell differentiation by alkaline phosphatase activity and protein concentration

The ALP/Protein concentration production of cells seeded on the hydrogels is shown in Figure 4-21. A peak in alkaline phosphotase activity was observed after 14 days in culture.

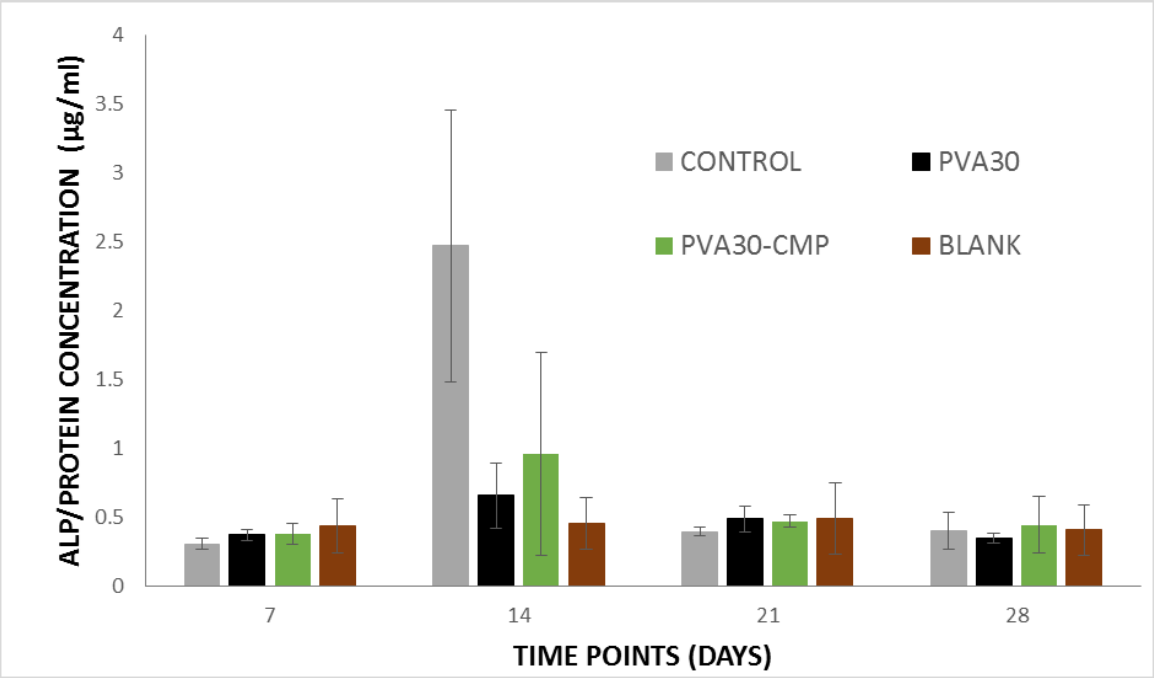

Figure 4-21: The alkaline phosphatase activity in balance with the protein concentration of human osteoblast cells (HOB) on the PVA30 hydrogel and PVA-CMP composite, with the tissue culture plate as the control. Tests were carried out on culture media supernatant of hydrogels composites at different time points day (7, 14, 21 and 28). Data represents as mean±SD. (n=4)

Real time quantitative PCR: Molecular quantification of osteoblastic phenotype

RUNX2 & ALP

Relative expression of RUNX2 and ALP of HOB cells on the PVA30 hydrogel and PVA-CMP composite is shown in Figure 4-22 and Figure 4-23. RUNX2 results indicate an increase in expression from day 7 to day 14 followed by a decrease on the control, whilst the PVA-CMP composite showed down regulation at day 21 followed by and up

regulation at day 28. ALP results showed a peak in expression at day 14 for the control and PVA-CMP composite. The results indicate differentiation of HOB cells towards mature osteoblasts.

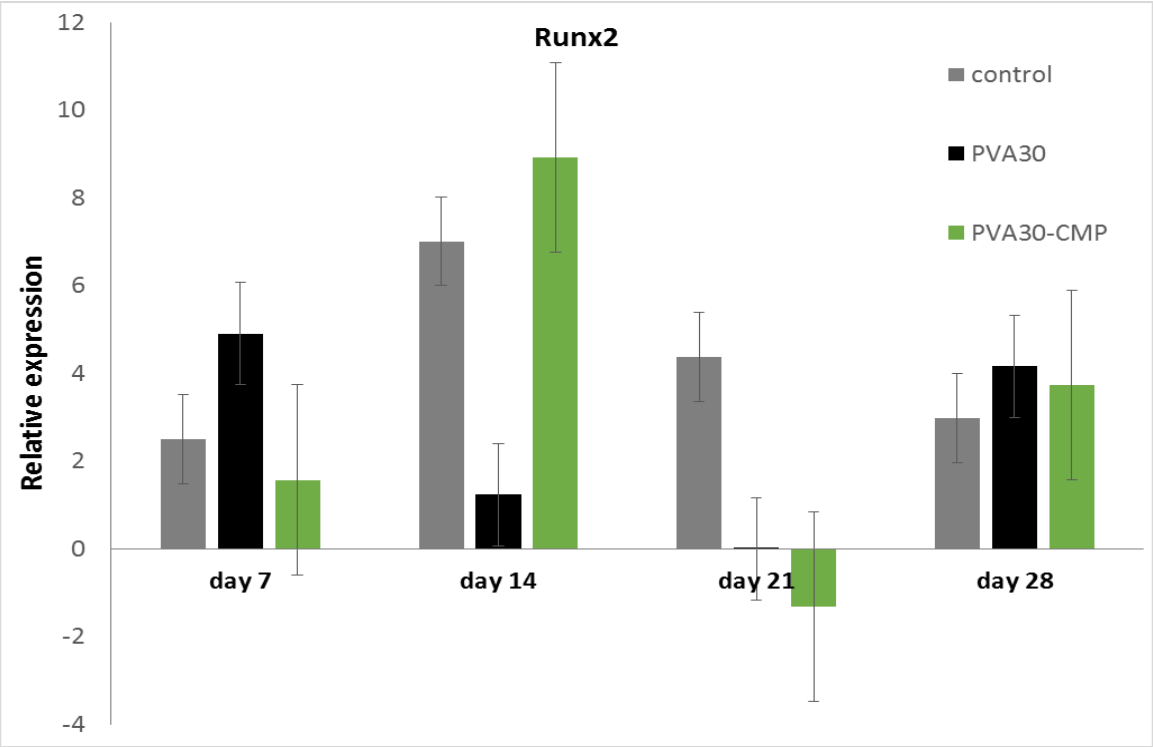

Figure 4-22: Relative expression of Runx2 of the HOB cells cultured on the PVA30 hydrogel and PVA-CMP composite, analysis was carried out at time points (7,14, and 28 days). (n=3). NB: data presented is relative to day 7.

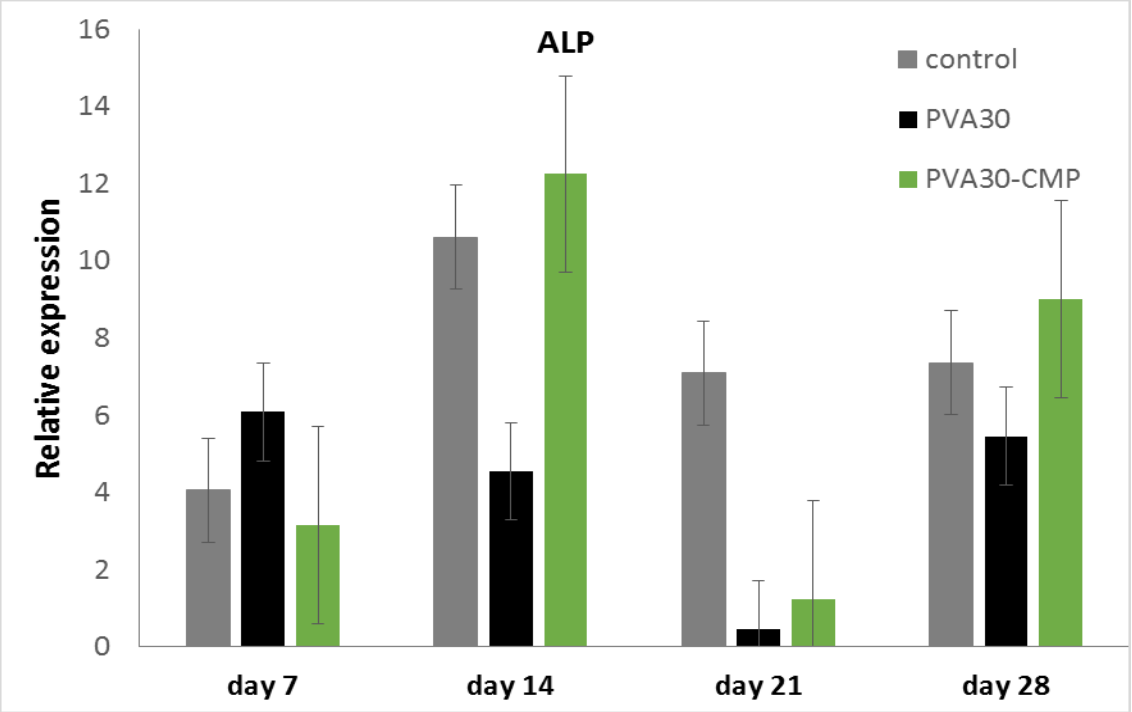

Figure 4-23: Relative expression of ALP of the HOB cells cultured on the PVA30 hydrogel and PVA-CMP composite, analysis was carried out at (7,14,21 and 28 days). (n=3). NB: data presented is relative to day 7.

4.5 DISCUSSION

In designing bone substitutes, one of the main strategies is to create a 3D environment that enables osteogenesis. A 3D matrix mimicking the extracellular matrix, which allows the attachment of osteoprogenitor cells to proliferate and differentiate into osteoblasts whilst simultaneously providing the requisite mechanical integrity which is key in bone regeneration. Calcium phosphate based biomaterials promote osteogenic differentiation through several mechanisms. The ability to sequester osteoinductive factors such as bone morphogenetic proteins and regulate calcium and phosphate ions imbibes an osteoinductive effect. However, calcium phosphate scaffolds are limited by their brittleness thereby limiting their clinical use. Three-dimensional (3D) porous PVA-CMP hydrogel composite scaffolds were successfully developed to overcome the weak mechanical properties, poor cell adhesion and low osteogenic ability of hydrogels that limit their capability for bone regeneration in vivo.

In this study the filler phase was obtained by milling CMP with a mean particle size of ~50µm. The filler phase was selected on the basis of a previous study [227] which confirmed that porous blocks of CMP when placed in critical sized defects in a rabbit model were able to completely close the defect site. The histological findings suggested a natural healing process with no signs of inflammation, and also showed that a significant amount of graft resorption occurred within four weeks, which is in contrast to other xenografts used in the same model [238]. The porous block of CMP was seen to resorb totally at 8 weeks and vascularised bone was formed within the defect. The addition of osteogenic protein-1 (OP-1) within these scaffolds showed that bone formation occurred earlier, however even without the inclusion of OP-1, there was excellent bone growth and full coverage of the defect. With the resorbability of the CMP and cytocompatibility established, it was incorporated as the filler phase in aqueous PVA polymer solutions to create bone plugs suited for use in maxillofacial and other bone defects. Three different concentrations of PVA (10, 20 and 30 %) were used to prepare the precursor paste because the resultant viscosities varied and the degree of crosslinking would vary due to the different concentration of the hydroxyl groups in the

mileu thereby influencing the resultant properties. With an aim to incorporate a high concentration of the filler, a pilot study indicated that a maximum of 60% by weight of CMP could be incorporated as higher concentrations led to only partial wetting of the filler phase by the aqueous PVA solutions due to increased viscosity of the mix. Although higher concentration could be included in 10% PVA solutions, results on the study of the matrices showed that the lower concentration of PVA yielded fragile matrices. Hence a concentration of 60% of CMP was used for all the PVA concentrations. These composites were designed to be able to act as a bone plug, having the ability to absorb bodily fluids and retain them and the inclusion of PVA in the network was postulated inherently reduce the degradation and resorption rate of the CMP filler phase in the composite. The composites obtained were characterised to understand the effect of incorporation of CMP filler particle as well as the effect of variation of PVA concentration on the properties of the composites, whilst surgical handling was a parameter of influence that was based more on the opinion of the surgeon's handling and the ability to insert in a bone defect.

FTIR and Raman analysis of the PVA-CMP composite scaffolds

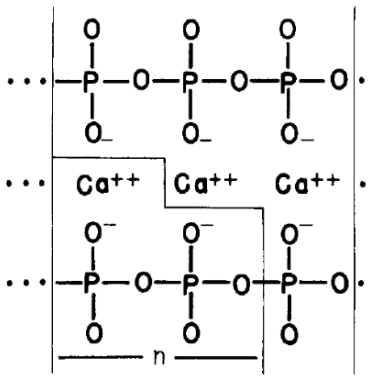

Figure 4-24: Schematic structural representation of CMP, depicting its polymeric structure with covalently bound PO_3 units whose chains are ionically bound to Ca between the chains. Adapted from Antonucci et al [1]

FTIR and Raman analysis results presented in Figure 4-4 and Figure 4-5 respectively indicated that CMP was successfully incorporated within the PVA polymer phase. This was demonstrated by the characteristic peaks of PO_3^- at 1061 and 1241 cm^{-1} in the FTIR spectra, and 681 cm^{-1} and 1168 cm^{-1} on the Raman spectra, which are in agreement with those obtained from other studies [234, 236]. The PO_3 units in CMP ($Ca(PO_3)_2$) are structurally linked through the -P-O-P- bonds to form chains that have lengths of about 10,000 units i.e. in the beta form of CMP [1]. The FTIR spectra of

the composites showed the main characteristic peaks associated with PVA and calcium meta phosphate. The strong absorption peak arising due to hydroxyl groups (3289 cm^{-1}) and C-H stretching of alkyl groups (2939 cm^{-1}) of PVA (observed on the PVA-1FT spectra) were not as prominent and much weaker in the PVA-CMP composites. This was attributed to the low ratio content of PVA (6:4) in the composite network, combined with the fact that excess PVA was decanted after the centrifugation process, during fabrication of the composites. However, the absorption peak for the hydroxyl group had an increased intensity with the PVA30-CMP composites, this difference could be attributed to the highly viscous nature of aqueous PVA30 which directly impacted the binding ability between PVA and CMP filler particles, resulting in a lower amount of PVA decanted after centrifugation and hence observation of higher intensity of hydroxyl bands as compared to PVA (10&20)-CMP composites. The fingerprint region of the composites fabricated from the varying concentrations of PVA displayed no changes or shifts in the spectra, this was expected as all composites were crosslinked through the PVA when it was subjected to one cycle of freeze thawing.

Thermal analysis of composites

A vast difference was observed between the DSC thermograms (Figure 4-6) of PVA and PVA-CMP composites. The Tg area of PVA can be clearly observed whereas that of the PVA-CMP can hardly be seen, however when zoomed in it is clear that the Tg of the PVA-CMP composite have shifted. The Tg (Table 4-5) values obtained were found to be between 104-105.5°C for all composites. The increase from Tg of PVA reported in chapter 3 (observed ~70°C) to that of the composites can be accounted by the incorporation of CMP particles within the polymeric structure, reinforcing the resultant composite. The limited variation in Tg indicates that the formed composites incurred the same level of crosslinking. This observation is accurate and is in agreement with observations reported in the FTIR and Raman analysis, as all composites were crosslinked in the same manner which was by subjecting it to one cycle of freeze

thawing. The loss of the prominent melting peak of PVA in the composites indicated incorporation and interaction of PVA with the CMP filler particles.

Water uptake of composites

Although in vitro simulation of water uptake is essential for an understanding of the anticipated in vivo behaviour of bone substitutes and their long term performance, it is difficult to draw a direct correlation. However, the in vitro behaviour of biomaterials is beneficial to understand the in vivo swelling and interaction with fluids, which can provide some useful information for guidance for the design of biomaterials. Hence three different biologically relevant environments were selected.

EWC of the composites were determined in distilled water, simulated body fluid and 100% humidity as shown in Figure 4-7. Swelling behaviour of the composite network is a process that is mainly related to the amorphous region and the free hydroxyl (OH) groups of the compound, therefore incorporation of CMP should improve network stability of the composites.

The decrease in water content with the increasing concentration of PVA in the composites is caused by two factors; the interaction between Ca^{2+} ion and the matrix of PVA gel leading the matrix to become denser, and the CMP particles occupy the space to squeeze out water from the hydrogel. Therefore the higher the concentration of PVA the denser the network and the smaller the space to support water. For all PVA10-CMP had significantly ($P \leq 0.032$) the highest EWC (29.4, 34.3 and 26.6%) as compared to PVA20-CMP (30.5 and 25.1%) and PVA30-CMP (27.0, 21.4 and 21.7%) respectively for SBF, DW and humidity, with the exception of PVA20-CMP in SBF. This trend was due to the dense nature (increase in viscosity) of PVA formed at higher concentrations, which results in hindered mobility of the polymer chains, when expanding during hydration, resulting in a limit to the amount of fluids that can be absorbed by the hydrogel network. This results was found to be in agreement with results obtained earlier and reported in Chapter 3 on PVA polymers hydrogels formed from different concentrations. Comparison of results also indicated that EWC in DW was significantly higher than in 100% humidity

and SBF for PVA10-CMP (P=0.003 and 0.017), and PVA20-CMP (P=0.001 and 0.042) respectively, with the exception of PVA30-CMP where the highest EWC was in SBF (P=0.001). Therefore for all PVA concentrations, overall EWC under humid conditions was significantly lower than in SBF and distilled water. These observations were justified by the fact that under humid conditions the composites are not immersed in aqueous solution, but are placed on moist cotton in a sealed glass vial, thus there is no direct diffusion via the surface initially, resulting in reduced overall amount of water molecules absorbed. The EWC in distilled water was higher than in SBF due to the fact that, SBF contains an ion concentration similar to that of human plasma, while DW in essence has been purified of ionic salts and molecules. The osmolarity of the medium in which the hydrogel is hydrated can affect the overall EWC of the hydrogel in a transient manner, thus a shift in the hydration of the hydrogel with changes in osmolarity of hydrating solution can be expected. When soaked in water, because of the lower osmotic pressure inside and outside of the gel, a large number of water molecules spread into the gels and therefore the quality and volumes of the hydrogel and water are both increased. A higher salt concentration Na+ in SBF would tend to promote hydrogel de-swelling. A high salt concentration implies that more Na+ ions are available to bind with the gel, thereby resulting in increased osmotic pressure which results in deswelling of the hydrogel.

Water uptake plots presented in Figure 4-8 indicate that the composites reached equilibrium had a linear uptake profile and was reached within the first 8hours, and remained at a steady point for 4 weeks. This result indicated that the composites do not undergo hydrolysis and disintegration over prolonged periods of time in water. Contrastingly studies from literature have reported relatively high water uptake values for three-dimensional polymer/ceramic composites. Examples include a study on PVA/HA cryogels fabricated by three cycles of freezing and thawing which reported that they found similar values between the water content of the PVA/HA composites (215.5-234.8%) as compared to the PVA hydrogel (229.1%) [239]. Another study on poly(lactic acid)(PLA)/HA 3D porous scaffolds, reported that in comparison with their pure PLA scaffolds the mean water absorption rate of PLA/HA scaffolds increased significantly

from 65.2 to 159.3%, and scaffolds did not undergo hydrolysis. The authors went further to justify their results by stating “Existence of HA can drastically improve the hydroscopicity of PLA scaffolds; however, because HA is enshrouded in PLA matrix, this improvement of water absorption ability is not evidently varied within the certain range [240].” It should also be noted that the PLA/HA scaffolds had a higher level of porosity as compared to the composites reported in this study. However the bone plugs in this study were designed with the aim of having lower swelling ratios as excessive fluid uptake can lead to excessive swelling, thus compromising the bone plug, which in turn would exert pressure on the wound defect edges resulting in cell death and necrosis of the tissue. However a small amount of swelling assists in fitting of the bone plug within the wound without exerting too much pressure on the edges.

Compression analysis

Biomechanical properties help to guide surgeons in use of bone plugs and guide the rehabilitation programmes of those patients who have had augmentation procedures with bone plugs. TruFit CB plugs (Smith and Nephew) are resorbable material composed of polylactide-co-glycolide (PLG) copolymer, calcium-sulfate, polyglycolide (PGA) fibres and surfactant. A study was carried out by JTK Melton et al (2010) to evaluate the material properties of the new cylindrical scaffold plug licensed for the treatment of osteochondral defects. It was found that the maximum compressive stresses at failure for the dual layer implants occurred at 5.5MPa (7mm), 5.8MPa (9mm) and at 8.5MPa (11mm) plugs of different diameter. The modulus of elasticity was calculated at 50 MPa (7mm), 60 MPa (9mm) and 80 MPa (11mm). The larger the plug size, the higher the strength shown under test conditions at all strain rates. The Young’s moduli of the implants were reported to be in keeping with previous estimated values for successful regeneration of cartilage within a synthetic scaffold [241].

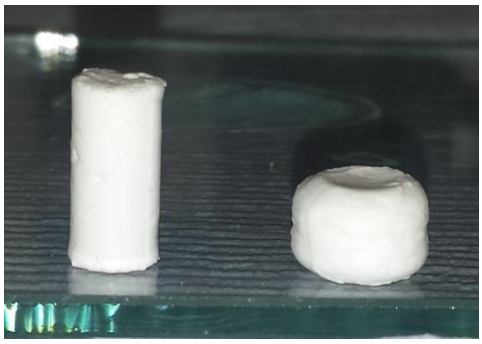

Figure 4-25: Image of PVA-CMP composite before compression (left) and after compression (right).

In this study the compressive strength of the dry and hydrated PVA-CMP composites was found to increase with increasing concentration of PVA, which was expected as previous studies (Chapter 3) showed that strength of PVA single network hydrogels increases with increase in concentration. The dry composites had significantly higher (P≤0.006) compressive strength than the hydrated composites of PVA10&20-CMP (7.0 and 25.4MPa respectively), with the exception of PVA30-CMP. The hydrated PVA30-CMP composite was found to have a significantly higher (P≤0.005) compressive strength of 48.0MPa than all the groups tested. This was due to the fact that the higher concentration of PVA results in a dense elastic network which provides enhanced reinforcement in combination with CMP filler. This network when hydrated results in a higher resistance to larger loads of compression as compared to PVA10 and 20 concentration which are less dense. The elastomeric nature of the composite means that the composites do not shatter or break down completely when compressed under hydrated conditions, but they undergo compaction as the pores collapse and the moisture is released, this is demonstrated in Figure 4-25. The compressive stiffness of the composites was also found to increase with increasing concentration of PVA, with PVA30-CMP displaying the highest stiffness values of 425.4 and 725.8MPa (P=0.003) under dry and hydrated conditions respectively. Composites tested under dry conditions were found to have higher modulus values than those tested under hydrated conditions with exception of PVA30-CMP. However only PVA10-CMP was found to have a significant difference P≤0.001. These values are higher than those of the commercially available TruFit CB plugs (Smith and Nephew) by a factor of over 5 (comparison of PVA30-CMP vs TruFit 11mm) indicating that the PVA-CMP bone plug composites are in keeping with previous estimated values for successful regeneration of cartilage within a synthetic scaffold as reported by JTK Melton et al (2010). Other comparisons (non-commercial) include a study on fabrication of three-level hierarchical CaP/Collagen/HA

reported compressive strength values of 6.2MPa with stiffness of 352MPa, these values are relatively comparable to the PVA10 and 20-CMP composites which had stiffness values of 16.0 and 215.9MPa respectively. They were however not comparable to the PVA30-CMP composite which had strength and stiffness which was 7 and 2 times higher respectively [242]. Another study by Gonzalez et al, (2014) reported their PVA/HA composite's highest compressive properties to be 16.3MPa and 120MPa for strength and stiffness respectively, for 15%wt concentration of PVA and 6%wt HA content in the composite [239].

The compressive strength after immersion in SBF was found to decrease with increasing immersion time in SBF, for all the composites. These values were found to be significantly lower ($P \leq 0.037$) than the strength obtained under hydrated conditions. This decrease in strength indicated that the composites undergo some level of polymer degradation and/or CMP dissolution resulting in the weakening of the interaction link between the polymer and ceramic phase, this due to the interaction of the composite with ions in SBF. This notion was reinforced by further reduction in strength and stiffness of the composites after 4weeks immersion in SBF. Bohner et al, (2012) reported that a potential approach to understand the mechanism of degradation or resorption in vivo is to look at the materials solubility in vitro in physiological fluids. The authors went further to state that " The material should not be soluble in physiological fluids at pH 7.4, because spontaneous rather than osteoclastic dissolution would occur, but should be soluble at a slightly lower pH value, typically between the pH value present at the osteoclast interface (pH 4–5) and pH 7.4. [217]". This statement is agreement with the fact that the composites do undergo some dissolution but do not undergo complete dissolution as the polymer phase acts as a binder and protective barrier to the CMP particles. The reduction in strength and stiffness also indicates that there is no deposition of minerals on the composites during immersion in SBF, as would occur in the case of bioglass, this notion is in agreement with results obtained from a study on surface

modification of CMP fibres, where they found that no products were formed on the surface of CMP fibres that were soaked in SBF for 30 days at 37°C [236].

Diametral compression analysis

Diametral compression tests (Figure 4-11 and Figure 4-12) were carried out on the composites, using the same bone plug shape that would be used clinically such as in tooth extraction cases. This is an indirect tensile test via induction of the local tensile stress in the transverse direction of the applied compressive stress, estimating the strength of materials as they undergo elastic deformation. Results indicated that diametral compressive strength ($P<0.001$) and elastic modulus ($P\leq0.004$) under dry conditions were found to be highest with PVA20 (6.3 and 38.0MPa) and 30-CMP (6.4 and 28.0MPa) respectively. Under hydrated conditions strength and stiffness increased with increasing concentration of PVA, where PVA30-CMP had significantly ($P\leq0.001$) the highest strength and stiffness (0.9 and 2.8MPa) compared to PVA10-CMP (0.3 and 0.8MPa) and PVA20-CMP (0.4 and 0.9MPa) respectively. Deformation of the hydrated specimens resulted in a barrel shape without rupture whereas dry specimens showed a typical brittle fracture however without total failure of the composite. Results obtained were significantly higher under dry conditions as compared to hydrated conditions. However these values were not as high as those reported by Gay et al, 2009 whose PLLA synthetic bone graft substitutes incorporated with 50% nHA had an elastic modulus of close to 6GPa [243]. These values were significantly higher than those obtained in this study, due to the variance in particle size, polymer and ceramics used. Bone Plugs have been used clinically as bone grafts for ridge maintenance and socket preservation after tooth extractions, examples include; EZ Cure™ plug composed of MBCP™ a biphasic calcium and phosphate with collagen

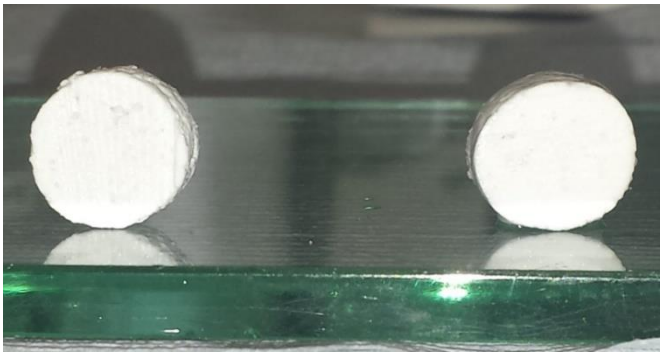

Figure 4-26: Image of hydrated PVA-CMP composite before compression (left) and after diametral compression (right).

[244], OsteoGen® Bone Grafting Plug composed of bovine collage and calcium apatite [245]. Other applications of bone plugs include clinical applications for cartilage repair, filling of bony voids or gaps caused by trauma or surgery that are not intrinsic to the stability of the bony structure e.g TRUFIT™ CB Plug synthetic osteochondral graft [246, 247]. However diametral compression properties of these bone plugs have not been published and therefore cannot be compared with those of this study.

DMA analysis

Dynamic mechanical analysis was used to explore the viscoelastic properties of the composites. Time dependant plots of tanδ and E' (Figure 4-14) carried out at 1Hz showed no apparent differences between the 3 groups with the exception of the change in moduli values. A steep decline in both tanδ and E' was observed within the first 5 minutes and remained relatively constant by 30 minutes. These results are contradictory to those obtained in a study on DMA analysis to assess the viscoelastic properties of bone where changes in *E'* were opposite to the trends exhibited by tanδ where for *E'* a steep increase was detected in the first 20 minutes, followed by a slower rise [248]. Testing was also performed over a frequency sweep covering the normal physiological frequencies from 1 to 10Hz simulating the walk to fast running. Results displayed on Figure 4-15 indicated that storage modulus increased with increasing PVA concentration in the composites with 3.6, 8.7 and 16.5MPa for PVA(10, 20 and 30)-CMP respectively which is significantly lower than the 9.4GPa obtained on cortical bone [248]. The storage modulus in this case referred to the measurement of how a material resists stress (the measure of elastic moduli). The loss tangent i.e. damping factor gives a measure of viscous energy loss within a material under conditions of dynamic loading. In this study the loss tangent was found to decrease with increasing concentration of PVA. This result was within expectation as low amount of energy lost or irrecoverable would directly translate to high absorbing potential. Values were in the ranges 0.13, 0.12, and 0.11 for PVA(10, 20 and 30)-CMP composites respectively, values reported in literature range from 0.04 for wet cortical bone [248], the same study also reported values from other

studies to be 0.01 for human tibial bone (Lakes et al.) and 0,02 for bovine bone (Ramaekers et al.), a variation which may have been due to the analytical techniques employed (studies were conducted under shear loading). A study on composites comprised of CaP and L-lactide/D-lactide copolymers, which conducted DMA analysis on their hydrated scaffolds under similar conditions as in this study reported values of *E*' at ~2GPa and tanδ at ~0.1 [249], while the PVA/HA study reported their highest E' to be 5.2MPa [239].

SEM and EDAX analysis

SEM micrographs displayed in Figure 4-16 highlight the morphology of the PVA-CMP composites. The composites were characterised by a dense network structure with micropores. It was observed, exposed crystal spindles of CMP as well as polymer like areas. EDS micro-analysis confirmed the elements on the crystal and polymer areas and, the Ca/P ratio of the CMP in the composite was found to be 0.3, similar observations on the EDS of CMP were reported elsewhere [236]. It was noted that the Ca/P ratio measured in human mineral for cortical bone is 1.71. The dense polymer phase was observed to increase more with increasing PVA concentration, where on PVA30-CMP spindle crystals of CMP were not clearly observed as in PVA10 and 20-CMP composite. This explained the water uptake behaviour of the composites reported, where EWC decreased with increasing PVA concentration due to the dense nature of the PVA30 polymer resulting in a tight network structure. It was expected that the dense PVA30-CMP composite observed on the micrograph would result in higher mechanical properties, due to the tightly bound link between the CMP filler particles and polymer phase, this notion was confirmed by the compression and diametral compression results obtained.

Cytocompatibility

Ideally, a bone graft should possess properties similar to natural bone and have clinically relevant structure to remodelling and regeneration of the native tissue. CMP is a novel

scaffold material for tissue engineering and has been demonstrated to possess excellent biocompatibility, osteoconductivity, osteoinductivity and degradability in vitro and in vivo, features of which are detrimental to the process of new bone formation. Biocompatibility and functionality tests were carried out to enable an understanding of how osteoblasts cells would behave in vitro on the formed PVA-CMP composites.

MTT assay is based on the reductive capacity of living cells to metabolize the tetrazolium salt, 3-(4,5-dimeththizaol-2yl)2,5-diphenyl tetrazolium bromide to a blue formazin product. Results displayed on Figure 4-18 indicated that there was a decrease in cell proliferation with increased exposure time to eluents. Calculations of the RGR confirmed that the degradation products of the PVA and PVA-CMP composite became moderately cytotoxic at increased osteoblast cell exposure times on eluents obtained after 48 and 72 hours sample wash time periods.

Hydrogel System	Eluents (hr)	Relative growth rate (RGR) (%)		
		24 exposure	48 exposure	72 exposure
PVA30-1FT	24	82.3	68.2	76.8
	48	72.7	49.3	55.8
	72	72.0	49.2	47.0
PVA30-CMP-1FT	24	72.5	66.6	92.4
	48	53.0	49.8	68.6
	72	52.7	41.2	56.8

Figure 4-27: Relative growth rate percentage of PVA30-1FT hydrogel and PVA30-CMP-1FT composite demonstrating viability of HOB cells within the hydrogels. Eluents were obtained after 24,48 and 72hr sample wash times, osteoblast cells were exposed (cultured) to the eluents for 24, 48 and 72 hours each.

CMP has been reported in a previous study by Buranawat et al, 2013 to be relatively nontoxic [227], the toxicity levels observed in this study could therefore be attributed to the presence of high concentration of PVA in the composite, reflected by the osteoblast RGR of 48 and 72hr eluents at 48 and 72 hour exposure or culture periods with osteoblast cells.

Live/Dead Staining of the HOB cells cultured on the hydrogel and composite for up to 28 days (Figure 4-19) showed cell attachment and proliferation on all the scaffolds. Cell attachment was observed on the PVA30 hydrogels, difficulties were encountered when imaging cells on the hydrogels as it was observed that some cells had penetrated and migrated into the internal structure of the hydrogel. When observed at low magnification of x4 cells appear to be at the same dimension however at high magnifications of x20 and even x10 it was difficult to image cells at different depths as most of the cells would go out of focus depending on the depth level being imaged. In all cell attachment proliferation and migration within the PVA30-1FT hydrogel was observed throughout 28 days of culture.

A large volume of cells was observed on the PVA-CMP composites from day 3. Cells were observed to have lodged within the micropores of the scaffolds. From 7 to 28 days in culture, the HOB cells were observed to grow and proliferate within the pores of the composites, this growth and expansion within the pores is observed to become interconnected with cells in the surrounding pores at 21 days in culture, and finally forming what resembles a sheet layer of cells on the outer surface of the composite (this is clearly observed after 28days in culture). These observations indicate that the PVA-CMP composite is not only biocompatible, but allows for excellent cell proliferation and migration on the composite with minimal cell death they can be accounted to the micropores and lack of interconnected porosity.

SEM HOB cell morphology on the hydrogels and composites was observed after 7 and 14 days in culture. Cell attachment was observed on both the hydrogel and composite, results displayed in Figure 4-20. On the PVA30 hydrogel, the osteoblast cells appeared to have fully spread with a flattened morphology, with visible large extensions and a raised nucleus. After 14 days in culture, very thin capillary like filopodia extensions were observed and the cells appeared to have been scattered on the surface with no regular orientation. On the PVA30-CMP composites, cells were observed to have spread all over the surface of the composite with no oriental direction, cells also appeared to be three dimensional and connected to each other, bridging micropores around them forming a

three dimensional web. The surface of the composite seemed to be undergoing some early degradation, as granular particles that were assumed to be CMP were observed, exposed on the surface of the composite. It has been reported that on a cellular level, it could be possible that roughened surfaces promote the differentiation of osteoblasts and provides the possibility to form a three-dimensional cellular network [250], this explaining the 3D appearance of the HOB cells. A review on failures and hopes of calcium phosphate bone grafts stated that " The presence of dissolution pits or etched crystals are indicative of cell mediated resorption, and when a ceramic is dissolved in vitro or in vivo, resorption takes place preferentially at the grain boundaries [217]." In this study dissolution could account for the granular particles observed on the composite indicating that PVA-CMP scaffold underwent some degradation in vitro.

ALP assay showed peak levels at 14days in culture, indicating bone formation activity, with PVA-CMP composite showing a higher concentration than the PVA30 hydrogel. ALP results obtained via **qPCR** analysis confirmed results obtained for PVA-CMP composite indicating peak expression at 14 days in culture.

Runx2 transcription factors contribute to regulatory mechanisms that are operative throughout osteoblast differentiation and are required to modulate expression of target genes at key developmental transitions. This protein is first detected in pre-osteoblasts. The expression is upregulated in immature osteoblasts, but down regulated in mature osteoblasts. Runx2 regulates the expression of major bone matrix genes during the early stage of osteoblast differentiation, but it is not essential to maintaining these gene expressions in mature osteoblasts. Runx2 is downregulated in mature osteoblasts during bone development. Therefore Runx2 expression increases during osteoblast differentiation validating involvement in maturation of osteoblasts. Expression of RUNX2 showed an increase at 7 and 14 days in culture indicating osteoblast differentiation, showing maturation of osteoblast. A decrease from 21 to 28 days in culture on the PVA-CMP composite, with a down regulation at 21 days indicated bone development and maturation of osteoblasts.

These results together with data reported by Buranawat et al, 2014 indicate that CMP grafts developed in this study are biocompatible with good potential to allow for resorption at a reduced rate than that previously reported by Burnawat, as well as improved hydration and mechanical properties.

4.6 CONCLUSION

The key to successful bone regeneration is to provide the wound site with suitable delivery vehicle that allows for sufficient cell infiltration and attachment to ensure osteoblastic differentiation and optimal cellular functions.

3D PVA-CMP composite scaffolds were successfully fabricated and obtained by crosslinking via freeze drying technique. The composites demonstrated mechanical properties suitable for bone tissue engineering applications, where they can be applied in medium to low load bearing bone defects. Mechanical properties of the composites can also be varied to meet desired needs by simply changing the concentration of polymer content used in fabrication.

The present results also indicated that the PVA-CMP matrices provide excellent osteoconductivity and biocompatibility. Live/dead staining as well as SEM cell morphology results showed that the osteoblast cells attached well and proliferated on the surface of the composite displaying the characteristic cell morphology. The efficacy of these scaffolds can be improved by entrapping growth factors within the scaffolds, which could be achieved either exogenously by swelling the scaffold in the patient's own PRP during surgery before implantation or endogenously whereby the scaffold would absorb and retain the patient's blood which contains growth factors after implantation.

Chapter 5
Fabrication and optimisation of dual networks as potential biomaterials

5.1 BIOMATERIALS BASED ON HYDROGELS

Synthetic hydrogels form the basis of several soft tissue and wound healing products and are increasingly being researched for tissue engineering applications due to their similarity to natural tissues. The ability to tune their chemical properties to respond to environmental cues, e.g. temperature, pH and light and diffusion of not only low molecular solutes but also macromolecules and cells, allows the potential to impart biochemical and biophysical cues into the biomaterial for regenerative medicine, to achieve optimal clinical outcomes.

There are currently a variety of hydrogel based products commercially available for soft tissue grafting and wound treatment. These products differ in species source (e.g., human cadaveric, synthetic, bovine, porcine, equine, a combination of several types, etc.), tissue source (e.g., dermis, pericardium, intestinal mucosa, etc.), additives (e.g., antibiotics, surfactants), delivery formats (e.g., wet packaged, freeze-dried), and preparation requirements (e.g., multiple rinses, rehydration), and a summary is shown in Table 5-1.

Description and applications of soft tissue hydrogel products currently available in the market	Image of the Hydrogel products
Mucoderm® is a collagen 3D porous tissue matrix derived from porcine dermis, supports revascularization and fast soft tissue integration and is a valid alternative to patients own connective tissue. Others include Mem-Lok® Pliable, Bio-Gide® which are collagen barrier membrane manufactured from highly purified porcine tissue[251]. Collagen fleeces are natural collagen products with a hemostatic effect with a short-term barrier function which are used for wound dressing. Zimmer alongside Botiss produce collagen products as tapes, patches and plugs [252].	 [253]  [254]
Botiss soft tissue biomaterials derived from porcine, acellular pericardium, include: Duraheal® is a dura substitute, adhesion prophylaxis (neuro, gastro, intestinal, cardio), scaffold for cellular guidance. Xenogaurd® used in orbital floor reconstruction, ENT e.g. tympanum substitute & rhinoplasty, as well as reconstruction of smaller defects e.g. paediatrics, covering of bone fillers.	 duraheal® 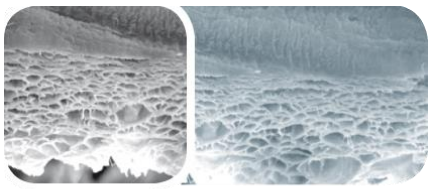 xenoguard® [255]
TransCyte™ a temporary burn wound covering made of human cells and a silicon mesh-like material. It is typically used to treat second degree burns that are not expected to heal on their own. ALGISITE a calcium alginate dressing, (Smith and Nephew) intended for use in wounds where there is a moderate to heavy level of exudate such as pressure sores, post-operative wounds, partial thickness and	 [256]

full thickness wounds, arterial, venous and diabetic leg ulcers, pressure sores, post-operative wounds and fungating lesions. Hydrocolloid dressings such as, Tegasorb, Tegadem etc. combine moisture vapour permeability with absorbency and conformability, and its transparency allows for wound observation.	 [257]  [258]
Apligraf® from Organogenesis, the graft is a living cell based product for chronic venous leg ulcers and diabetic foot ulcers it is supplied as a living, bi-layered skin substitute. The lower dermal layer combines bovine type 1 collagen and human fibroblasts (dermal cells), which produce additional matrix proteins. The upper epidermal layer is formed by promoting human keratinocytes (epidermal cells) first to multiply and then to differentiate to replicate the architecture of the human epidermis.	 [259]
Dermagraft®, Composed of human fibroblasts, an extracellular matrix, and a bio-absorbable polyglactin mesh scaffold. It is used in treatment of ulcers such as diabetic foot ulcers.	 [260]

GORE-TEX® Soft Tissue Patch has a material strength of ~1MPa. It is a soft and conformable microporous sheet material. It is made from solid nodes, connected by thin fibrils of expanded polytetrafluoroethylene (ePTFE). Its applications are varied ranging from Chest Wall Reconstruction, Diaphragmatic Hernia, Ventral Hernia, Gastroschisis and Omphalocele.	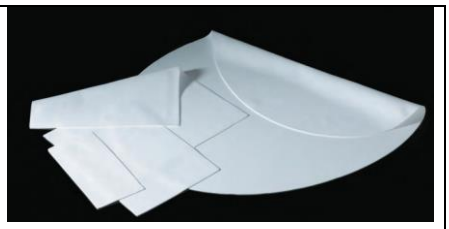 [261]
GORE® BIO-A® Tissue Reinforcement is a synthetic product is composed of [co]polymer (polyglycolic acid: trimethylene carbonate [PGA:TMC]) that is gradually absorbed by the body. The device has a three-dimensional matrix consisting of open, interconnected pores and like ECM, the matrix serves as a scaffold for tissue regeneration, but consists of polymer fibres instead of decellularized tissue [262].	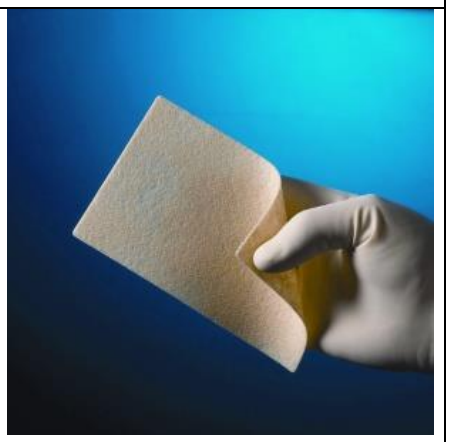 [262]

Table 5-1: A variety of soft tissue grafts commercially available for tissue augmentation and wound healing. All images were adapted from the denoted references provided next to the images.

The grafts listed in the Table 5-1 have certain limitations both in terms of their biological and mechanical performance and often lead to rejection, due to limited of resorbability and inadequate mechanical properties required for the applications. To overcome the shortcomings of the current materials used mainly in soft tissue applications, advances in material design and polymer chemistry have allowed for incorporation of advanced dynamic features in biomaterials such as controllable degradability and stimuli responsiveness. Hydrogels, are particularly useful in soft tissue applications, however have been limited by weak mechanical properties. Structural and mechanical load of tissues vary as behaviour is optimised for their respective physiological functions, thus engineered tissue constructs should exhibit stress–strain responses comparable to the tissues they are intended to replace or provide structural support [263, 264]. Thus strategies to toughen hydrogels, which include formation of hydrogels from a combination of synthetic and natural polymers, development of inter penetrating

networks (IPN) networks and double networks (DbN) are being explored for biomedical applications.

Inter Penetrating Networks (IPN)

The International Union of Pure and Applied Chemistry (IUPAC) has defined IPNs as; polymers comprising of two or more networks that are at least partially interlaced on a molecular scale but not covalently bonded to each other and cannot be separated unless chemical bonds are broken (Figure 5-1) whilst semi IPNs are; polymer comprising of one or more polymer networks and one or more linear or branched polymers characterized by the penetration on a molecular scale of at least one of the networks by at least some of the linear or branched macromolecules (Figure 5-1). This means semi IPNs consists of only one crosslinked component within the network structure and one of the linear or branched macromolecules can in principle be separated from the integral/elemental polymer network without breaking the chemical bonds [138].

Preparation and formation of IPNs can be classified as simultaneous or sequential, where with simultaneous reactions, the polymers or monomers of both networks are mixed together and the two networks are synthesized together at the same time by independent, noninterfering routes such as chain or stepwise polymerisation. Sequential reactions are formed by swelling a 1st single polymer network hydrogel in a solution of the second polymer, forming a semi IPN and if the 2nd polymer is crosslinked then this forms a full IPN [139, 140].

The combination of favourable properties of each composing polymer used to prepare the IPNs often leads to a new system with improved properties considerably divergent from those of the individual polymer, that have resulted in the successful use of IPNs in pharmaceutical and biomedical applications [141]. Smart hydrogels that are stimuli responsive i.e. temperature, pH and a combination of both temperature/pH responsive hydrogels, which achieve their properties by exploiting the properties of at least one of if not both polymeric component of the network. The network structures have led to

improvements in bioadhesion recently shown by formulation of photocrosslinkable acrylated β-cyclodextrins [265].

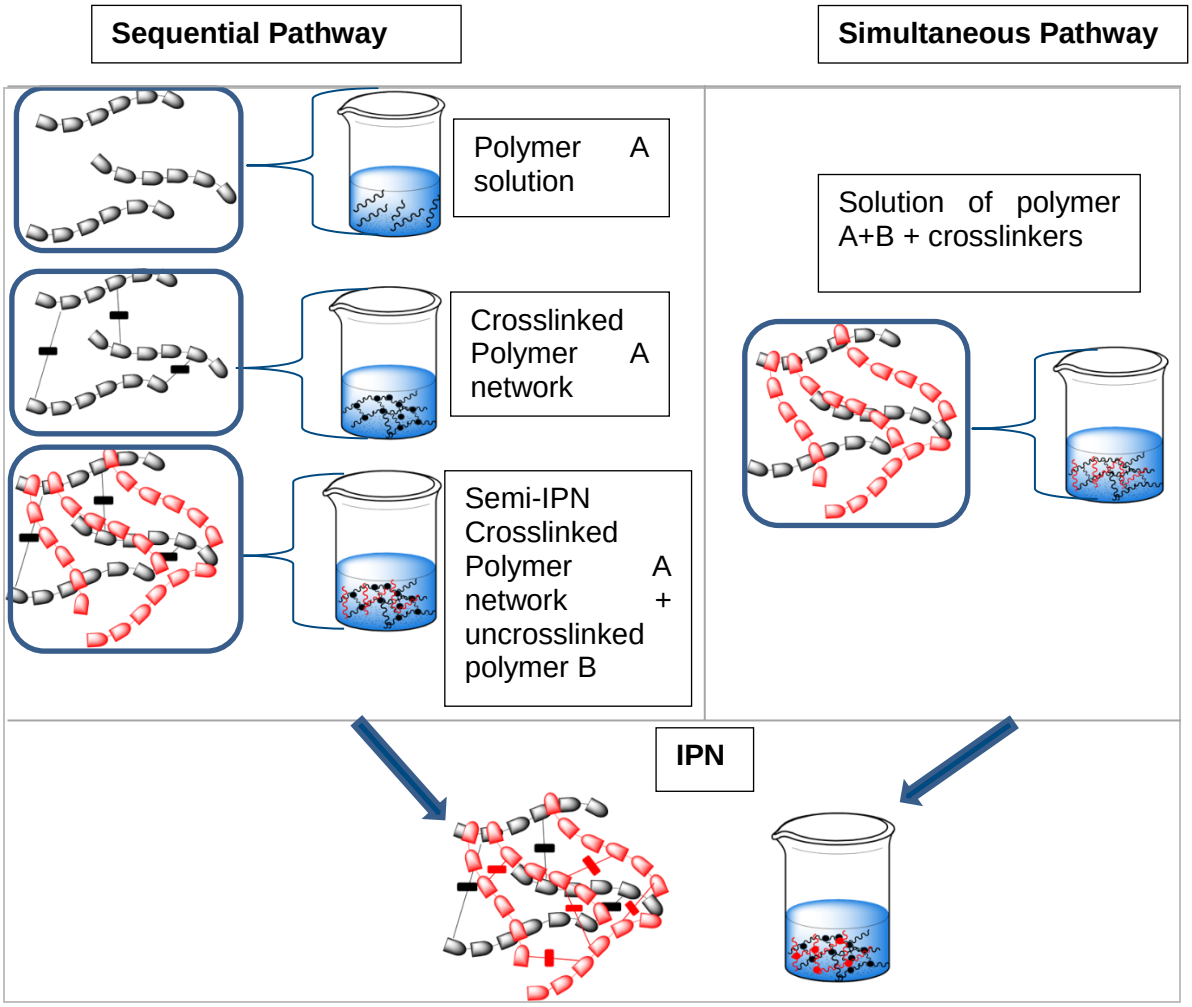

Figure 5-1: Schematic representation of the semi-IPN and IPN formation. Polymer A and Polymer B are generic polymers (such as linear, comb or grafted).

Double networks (DbN)

Double network were first reported by Gong laboratories [68], that are characterised as tough IPN matrices in which a relatively high molecular mass neutral polymer network is incorporated within a swollen heterogeneous polyelectrolyte network. The difference between the DbN and conventional IPN are based on the contrasting structures of the polymers in use, the following principles are essential features/parameters used to attain DbN hydrogels and can be adjusted and varied to achieve a wide range of mechanical performance of the final networks:

- A first network, being a brittle polymer such as a polyelectrolyte; a second network, being a soft and ductile polymer such as a neutral polymer.

- The molar concentration of the second network is 20 – 30 times the first network.

- The first network is tightly crosslinked, whilst the second network is loosely crosslinked, which requires a high molecular weight second polymer.

DbN are reported to contain up to 90% by weight of water, with tensile strengths of 1~10MPa at 1000 – 2000% strain, compressive stress of 20-60MPa at 90 – 95% strain, elastic modulus of 0.1 – 1.0MPa and toughness (tearing fracture energy) of 100 – 1000Jm^{-2}. The toughness of the hydrogels and its large fracture energies has been described to be attributed to the necking phenomenon, where polyelectrolyte polymer (first network) breaks into small clusters that efficiently disperse the stress around the crack tip into the surrounding damage zone, thus serving as sacrificial bonds, the ductile polymer (second network) is believed to extend extensively thereby sustaining the large deformation [69, 266, 267]. However it has been reported that fragmentation of the first network is accumulative and irreversible. Following the work by J. Gong on the development of poly(2acrylamido-2methylpropanesulfonic acid) (PAMPS) and poly(acrylamide) (PAAm) [68], further novel DbN were developed by other groups examples include; bacterial cellulose/polyacrylamide (BC/PAAm) [268], poly(ethylene oxide) (PEO) and poly(acrylic acid) (PAA) [269], thermoresponsive DbN of poly(N-isopropylacrylamide) (PNIPAAm) and N-isopropylacrylamide (NIPAAm)[270], a review of other DbN hydrogels has been reported by Haque et., al 2012 [266]. Some of these DbN hydrogels exhibit good biocompatibility and low friction resistance, making them desirable with a promising perspective in a wide range of biomedical applications such as load bearing applications in ligament and artificial cartilage regeneration [268, 271, 272].

Sodium Alginate

Sodium alginate (SA) is a naturally occurring polysaccharide widely used as a biomaterial for tissue engineering due to its biocompatibility, ability to undergo gelation under physiological conditions and non-thrombogenic nature. It is also a naturally abundant material and can be used solo or in combination with other bio or synthetic

polymers in formation of hydrogels [232]. SA is derived mainly from brown seaweed through treatment with aqueous alkali solutions typically with NaOH, thereby after which the extract is filtered and mixed with calcium chloride so as to precipitate the alginate. Treatment with dilute hydrochloric acid (HCl) can convert the alginate salt to alginic acid [232]. Alginates are composed of β-D- mannuronic acid units (M units) and α-L-guluronic acid (G units) monomers linked together by -β(1,4) and –α(1,4) glycosidic bonds, which vary in amount and sequential distribution along the polymer chain (MM, GG OR MG) depending on the source of the alginate [233]. Due to their physical and chemical properties alginates have been widely used in food, textile, medical and pharmaceutical industries. Even though alginates are readily dissolved in water, they can be rendered insoluble by allowing them to gelate in the presence of divalent cations, where these ions interact ionically with blocks of guluronic acid residues. An example on how the gelation occurs is by the interaction of Ca^{2+} ions with the G block units leading to the formation of an egg box structure, where CaAlg is formed by the G components enclosing the calcium ions; resulting in the formation of a three-dimensional network structure shown in Figure 5-2. Alternative di- as well as tri-valent cations may also be used in gelation of alginates such as Fe^{2+}, Cu^{2+} and Al^{3+} [273, 274]. Ionically crosslinked alginates are weak and lose mechanical properties and stability over time in vitro, therefore stable covalent cross-links may be introduced to the alginate hydrogels using bifunctional crosslinkers allowing for greater control over the mechanical and swelling properties of these gels [233].

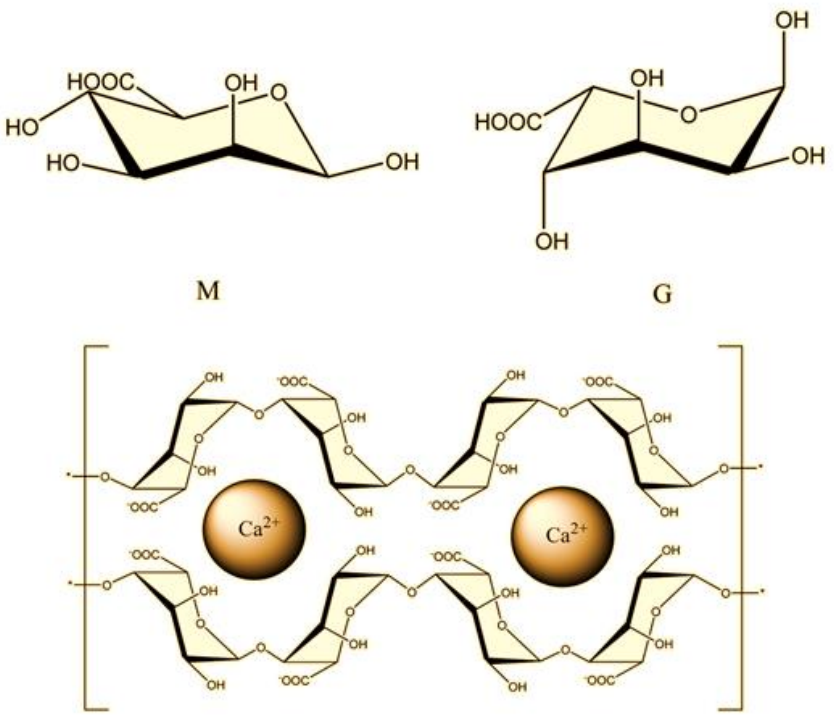

Figure 5-2: Egg box structure demonstrating G units enclosing calcium ions during gelation. Adapted from Marriott et al. [275].

The biocompatibility and facile crosslinking to gelate alginate make them versatile biomaterials for drug delivery, cell encapsulation, cardiac tissue engineering [276] and bone tissue engineering [232]. Alginates are considered not to degrade but on gelation the process can reverse with time to allow an erodible matrix via dissolution.

The aim of this study was to develop tough interpenetrating (IPN) dual network hydrogel system by adopting the concepts and principles of double network hydrogels, where the 1st network is a dense tightly structured poly electrolyte, which is swollen in a second ductile loosely crosslinked monomer. However, in this study a neutral base polymer of PVA was selected to form the 1st dense network mesh and 2nd polyelectrolyte polymer network of sodium alginate was selected to form the interpenetrating network within the 1st mesh and the first network of PVA was also obtained by a physical process of crosslinking. Hydrogel blends of PVA and alginate [182], and IPN's of PVA and alginate have been reported all developed by various methods, but none fabricated via techniques proposed in this study. This unique, simple and nontoxic method of fabricating hydrogels gives rise to prospects of developing tough hydrogels with ability to

be tailored for various applications of interest and further to utilize these systems as matrices for elastomeric biocomposite formulation. In this study the following steps were implemented as to optimise the study and determine the levels of crosslinking required to yield tough hydrogels.

- Due to the mechanism of PVA gelation via physical crosslinking it was critical to analyse the effect of freeze thawing cycles on the 1st network.
- The effect of incorporation of alginate in the network structure was determined by analysing the physico-chemical properties of the hydrogels.
- The biocompatibility of the optimised hydrogels was assessed.
- Drug release from dual network hydrogels.

5.2 MATERIALS AND METHODS

	Chemical structure
PVA as described in chapter 3 was used	
Sodium Alginate (SA), Fisher scientific	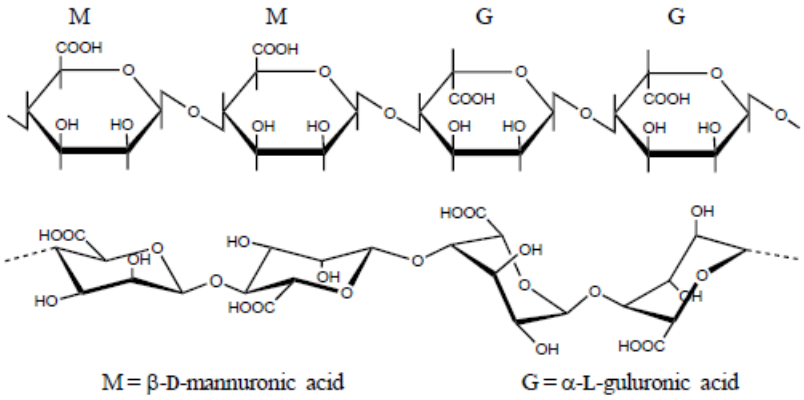 [277]
Calcium chloride, Merck, UK	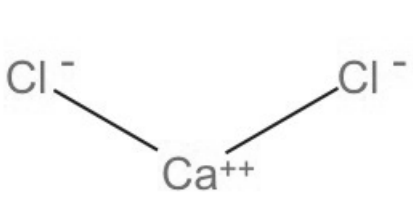

Table 5-2: Materials used in the synthesis of dual network hydrogels.

Based on the results detailed in Chapter 3, a 10% wt./vol concentration was used to make the solutions of PVA in water(PVA10), which exhibited good handling properties, hence used in the synthesis of dual network hydrogels.

PVA hydrogel films

PVA10 solutions were prepared as previously reported in chapter 3. Polymer solutions were cast into moulds to form thin hydrogel sheets and subjected to different (1, 2 and 3) cycles of freeze drying for 24 hours and allowed to thaw for 12 hours before repeating the next freeze drying process to obtain PVA1FT, PVA2FT and PVA3FT gel films, (**NB:** All xerogels fabricated from here on were subjected to freeze drying in the upper chamber of the freeze dryer). The PVA xerogels were characterised to identify the effects of different cycles of freeze thawing on the formed networks before the xerogels were further used to form interpenetrating dual networks with SA.

Synthesis of PVA/SA interpenetrating dual hydrogel networks

The PVA10 xerogels films were immersed in 2%wt./vol. SA till equilibrium uptake, to allow for penetration of SA into the PVA gel. The PVA gels swollen in sodium alginate were then immersed in 10% $CaCl_2$ to allow for chelation to occur. The hydrogels were then separated into two groups for further crosslinking by (a) 1 freeze-thaw cycle and (b) air-drying (AD) + 1 cycle of freeze thawing (1FT). All xerogels formed were placed in a desiccator until physiochemical characterisation.

5.3 CHARACTERISATION

Attenuated Total Reflectance- Fourier Transform Infrared spectroscopy (ATR – FTIR)

The infrared spectral analysis was performed to characterise the chemical structure of the network formed. The experimental procedure is in chapter 3.

Differential Scanning Calorimetry

The experimental procedure is detailed in chapter 3.

The crystallinity of PVA10 xerogels were determined by calculations from the thermal curves of the freeze-thawed hydrogel films. The heat required for melting the sample ΔH was determined by integrating the area under the peak over ranges 180 – 250°C. The peak representing heat required for the evaporation of water at around 100°C was analysed and used to obtain the corrected value of ΔH [154, 278].

%Crystallinity= [(ΔHm – ΔHw) / ΔHm°] x 100%

ΔHm = heat of melting

ΔHw = heat of vaporisation of water

ΔHm° = heat of melting polymer at 100% crystallinity

ΔHm° PVA = 138.6J/g [154]

Water uptake

Hydration studies to obtain EWC were performed as detailed in the material and method section of chapter 3 and 4.

The following equations were used to determine the nature of diffusion of water into the hydrogels.

$$\frac{\mathrm{Mt}}{\mathrm{M}_\infty} = 2\left(\frac{Dt}{\pi l 2}\right)^{1/2}$$

Where Mt and M∞ denote the amount of solvent diffused into the gel at time t and an infinite time (equilibrium) respectively. The slope s is obtained from the slope of a straight line of the plot M_t/M_∞ against $t^{1/2}$ where *l* is the thickness and D is the diffusion coefficient.

$$\mathrm{s} = 2\left(\frac{\mathrm{D}}{\pi l^2}\right)^{1/2}$$

$$\mathrm{D} = \frac{s^2 \pi l^2}{4}$$

For absorption $Mt = W_t - W_i$ and $M_\infty = W_s - W_i$

For desorption $Mt = W_s - W_t$ and $M_\infty = W_s - W_d$

Where weight of hydrogels W_t = at time during swelling, W_i =initial weight, W_s =weight at equilibrium, W_d = dry weight after dehydration.

Ultimate Tensile Strength

Tensile strength measurements were performed as detailed in the material and method section of chapter 3.

Trouser tear test

This test method covers the determination of the force necessary to propagate a tear in the hydrogel films. Fracture energies were obtained using the trouser tear test on a rectangular shaped specimens (50mm x 17mm) with a 33mm long initial notch. The fracture energies of the hydrogels were calculated as

$G=2F_{ave}/w$

Where F_{ave} is the average tearing force and w is the thickness of the tested samples.

Hydrolytic degradation

Hydrogels were fabricated as previously described and solutions of phosphate buffered saline (PBS) of concentration 0.1M with pH 7.4 was used as the immersion medium. Samples were weighed and their dimensions taken before immersing them in 3ml of the PBS solution at 37ºC. The samples were removed at timed intervals and then wiped gently with soft paper to remove surface water. The samples were dried under vacuum at room temperature and weighed after complete drying. All experiments were done in triplicates.

Drug release studies

Hydrogels were loaded with a total of 1% vancomycin hydrochloride (Sigma Aldrich): to fabricate the drug loaded hydrogels, a solution of PVA was mixed with 1% vancomycin at 300rpm until the drug was homogenously incorporated in the solution. The PVA solution was allowed to settle to allow the release of all bubbles before casting onto moulds and

subjecting to cycles of freeze thawing as previously described. For formation of the dual network hydrogels, 1% vancomycin was added to the 2%sodium alginate solution to prevent diffusion of the drug from PVA to sodium alginate. Once fully swollen with alginate the hydrogels were chelated with $CaCl_2$ before subjecting to one more cycle of freeze drying.

Drug release studies were conducted in phosphate buffered saline solution (PBS), pH 7 at 37ºC. Dimensions of the specimens and weights were recorded before immersing in 2ml PBS. 200µl solution of samples was withdrawn at recorded time points and diluted with 500µl distilled before reading on a UV spectrophotometer (Cecil 9000 series) at wavelengths 281nm, the extracted 200µl was replenished with exactly 200µl at each time point. Tests were carried out in triplicates. The calibration curve was constructed using vancomycin solutions in PBS with concentrations of 5-100µg/ml. To determine if the absorbance of vancomycin changed with each day an intra-day precision on the assay was carried out by processing and analysing three individual vancomycin standards at concentrations of 40, 50 and 60µg/ml respectively, for the duration of the study.

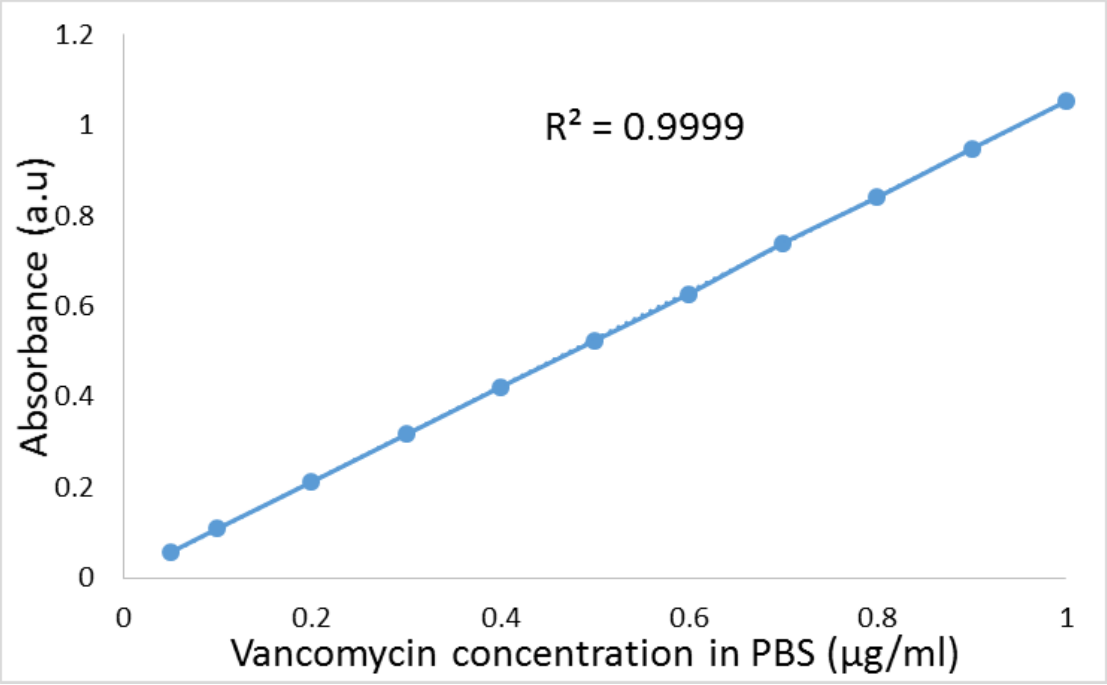

Figure 5-3: Relationship between optical density and concentration of vancomycin in the PBS solution.

Scanning electron microscopy (SEM)

The experimental procedure is detailed in chapter 3.

CYTOCOMPATIBILITY

MTT, Live/Dead Staining, Cell morphology (SEM), Protein concentration, qPCR

Cytocompatibility of the hydrogels were determined using the methodology as detailed in the materials and method section of chapter 4.

5.4 RESULTS

Effect of different freeze thaw cycles on PVA10

PVA subjected to freeze thawing induces crosslinking of the PVA chains by hydrogen bonding and crystallite formation. In this study the effect of different freeze thaw cycles on PVA10 were investigated. PVA xerogels were fabricated by subjecting a PVA10 aqueous solution which was cast onto a mould, to consecutive 24hr cycles of freeze-drying; 1, 2 and 3 freeze thaw cycles. These xerogels were characterised to determine the effect of freeze drying on the hydrogels under the same processing conditions prior to formation of interpenetrating dual networks.

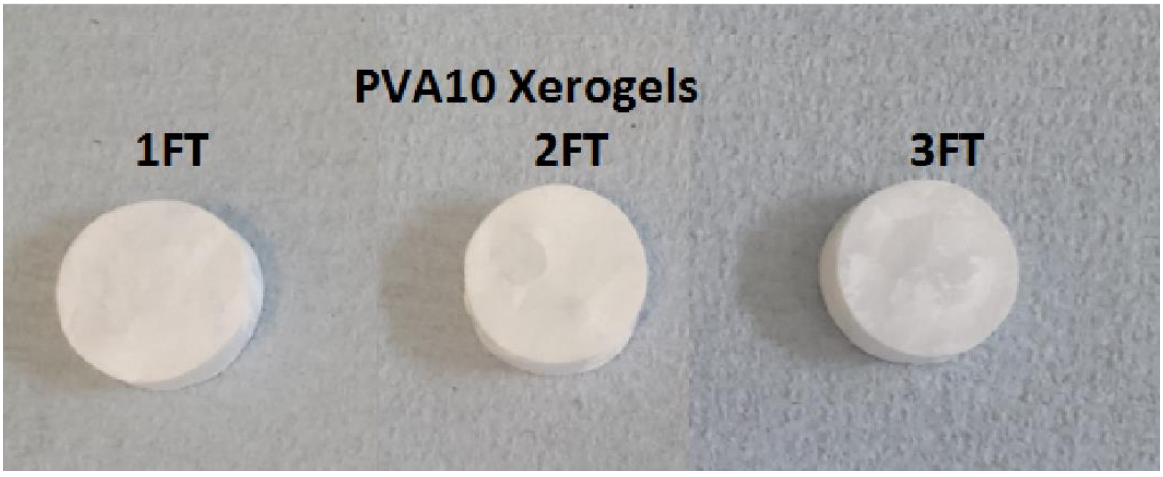

Figure 5-4: Images of the dry PVA10 xerogels subjected to different cycles of freeze thawing showing that intact discs could be obtained that retained their shape post processing.

ATR-FTIR spectra of PVA10-FT xerogels

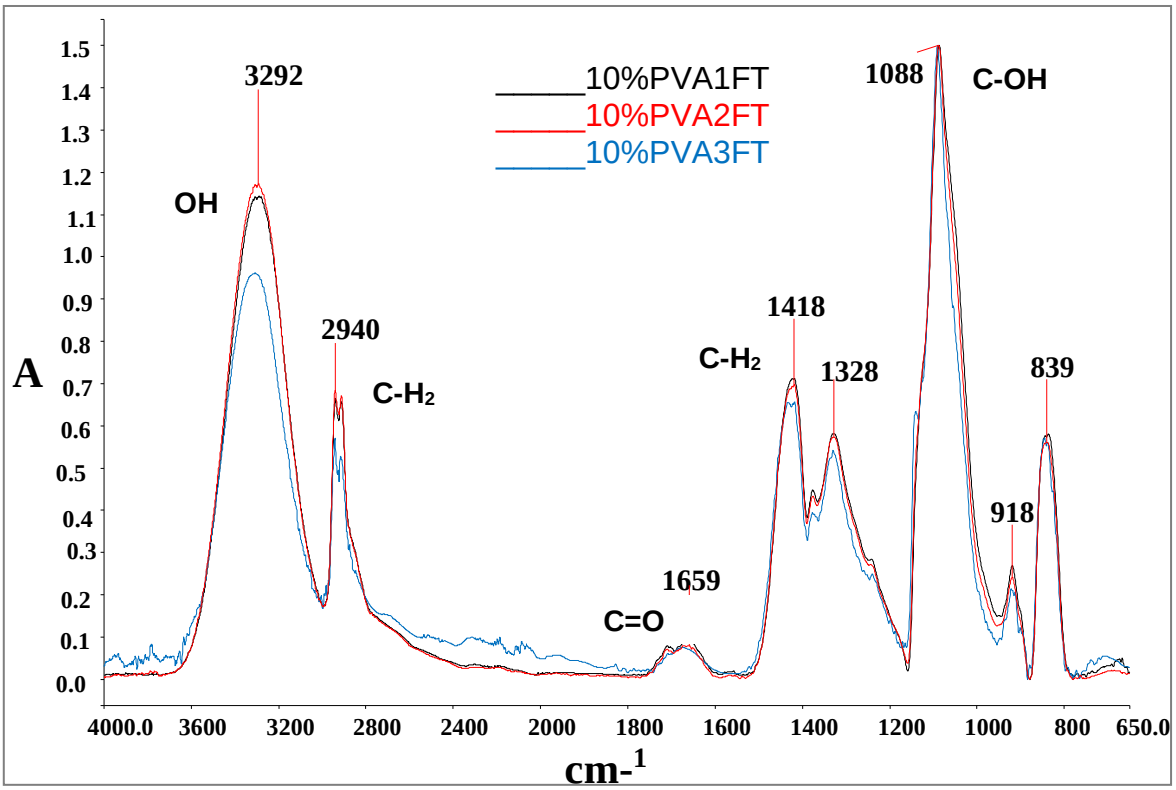

Figure 5-5: A comparison of the FTIR spectra of 10%(w/v)PVA hydrogel films after 1,2 and 3 freeze thaw cycles respectively. All three spectra were normalised to allow for comparison.

The characteristic peaks of PVA were observed with vibrations corresponding to the OH groups (~3292 cm^{-1}) due to the intermolecular and intramolecular hydrogen bonds, C-H stretching (~2940 cm^{-1}) from the alkyl groups, C-OH(~1088 cm^{-1}) related to the symmetric C-C stretching mode or C-O stretching where an intramolecular hydrogen bond is formed between two neighbouring OH groups on the same side of the plane of the carbon chain. The weak vibration at 1659 cm^{-1} assigned to C=O is due to acetal residual in PVA [182, 279].

Thermal analysis and degree of crystallinity

The crystalline structure of PVA10 hydrogels subjected to different cycles of freeze thawing were examined in terms of the overall degree of crystallinity as obtained from DSC thermograms.

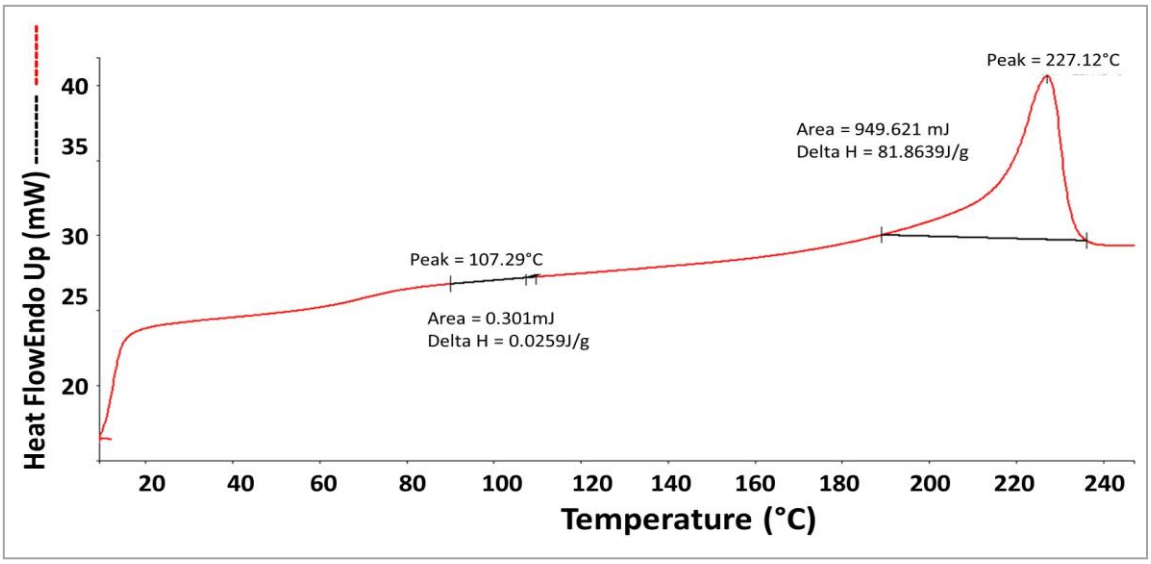

Figure 5-6: DSC thermogram for PVA10 hydrogel prepared by one cycle of freeze thawing.

A typical DSC thermogram for PVA10 subjected to consecutive cycles of freeze thawing is shown in Figure 5-6. The sharp peak at 227°C corresponds to the melting of PVA10 and at approximately 100°C there is the change due to the evaporation of residual water present in the hydrogel. The degrees of crystallinity were calculated by analyzing the DSC thermograms for each of the PVA10 hydrogels subjected to different cycles of freeze thawing. A known mass of each of the hydrogels was subjected to a constant rate of heating. The heat required for melting the sample, Δ*H,* was determined by integrating the area under the melting peak over a range of 190-240°C. The residual water present in the sample was calculated by analysing the heat required for evaporation of water on an area approximately at 100°C, this was used to correct the Δ*H* value. The degree of crystallinity was calculated by dividing the corrected Δ*H* with the heat required for melting 100% crystalline PVA sample Δ*Hm*°= 138.6J/g.

Cycles of freeze thawing	% Crystallinity	Glass transition Tg(°C)
1	67.4	70.9
2	69.0	73.4
3	68.9	72.5

Table 5-3: Shift in the crystallinity and glass transition (Tg) of the PVA10 hydrogel films as a function of freeze thaw cycles.

Table 5-3 shows the crystallinity and glass transition values obtained from analysis of thermal scans of PVA10 hydrogels after different cycles of freeze thawing. Results indicated that 2 cycles of freeze thawing led to a higher Tg and degree of crystallinity than 1 and 3 freeze thaw cycles. No further increase in either Tg or crystallinity was observed with 3 freeze thaw cycles, an increased number of freeze thaw cycles does not necessarily increase the overall initial degree of crystallinity in the PVA sample, it is apparent that repeated cycles of freeze thaw only reinforce the crystals that already exist [154].

Interaction with water

Hydrogels have the ability to take up and retain water as well as biological fluids, this behaviour is highly dependent on the composition of crosslinking. To investigate the effect of different cycles of freeze thawing on the hydration dynamics of the PVA10 hydrogels, equilibrium water content, swelling ratio, gel fraction and diffusion coefficient of hydrogel were calculated.

Cycles of freeze thawing	**EWC (%)**	**Swelling ratio (SR)**	**Gel fraction, GF (%)**	**Diffusion coefficient, D, ($10^{-6}cm^2s^{-1}$)**
1	83.2 ± 0.1	7.3 ± 0.2	82.0 ± 3.0	1.9
2	81.3 ± 0.4	6.0 ± 0.1	89.0 ± 3.4	1.6
3	79.2 ± 0.7	5.5 ± 0.1	87.2 ± 1.5	2.0

Table 5-4: Equilibrium water content, swelling ratio, gel fraction and diffusion coefficient of PVA10 hydrogels prepared by different cycles of freeze thawing (n=3).

Table 5-4 displays the effect of different cycles of freeze thawing PVA10 hydrogels on the EWC, swelling ratio and gel fraction obtained from the hydration study. Both EWC and SR were found to decrease with increasing number of freeze thaw cycles, and no significant difference were found between different cycles of freeze thawing.

The solubility or remaining hydrogels content after initial hydration (Gel fraction) was determined by dividing the dry insoluble part of the hydrogel with the initial dry weight of

the sample, the gel fraction was found to increase with increasing cycles of freeze thawing. There was no significant difference between the diffusion coefficient of the PVA10 hydrogels subjected to different cycles of freeze thawing, however the diffusion coefficient was found to be lowest for the PVA10 hydrogel subjected to 2 cycles of freeze thawing.

Tensile strength

The ultimate tensile strength (σ_T) and Young's modulus (*E*, tensile modulus) of PVA10 freeze thawed hydrogels shown in Table 5-5 ranged between 0.3 – 0.4MPa and 0.5 - 0.8MPa respectively for the hydrated gels.

Cycles of freeze thawing	**σ_T (MPa)**	***E* (MPa)**
1	0.3 ± 0.1	0.5 ± 0.1
2	0.4 ± 0.1	0.5 ± 0.1
3	0.4 ± 0.1	0.8 ± 0.3

Table 5-5: Tensile strength and modulus of the hydrated to EWC, PVA10 hydrogels subjected to different cycles of freeze thawing, (mean ± standard deviation) n=6.

Tensile strength of the hydrogels were found to increase with increasing number of freeze thaw cycles, but was not statistically significant (p=0.161). The Young's modulus of PVA10-3FT was found to be the highest and statistical analysis showed that PVA10-3FT was only significantly higher ($p<0.05$) than PVA10-2FT, and no difference was found between PVA10-1 and 2FT.

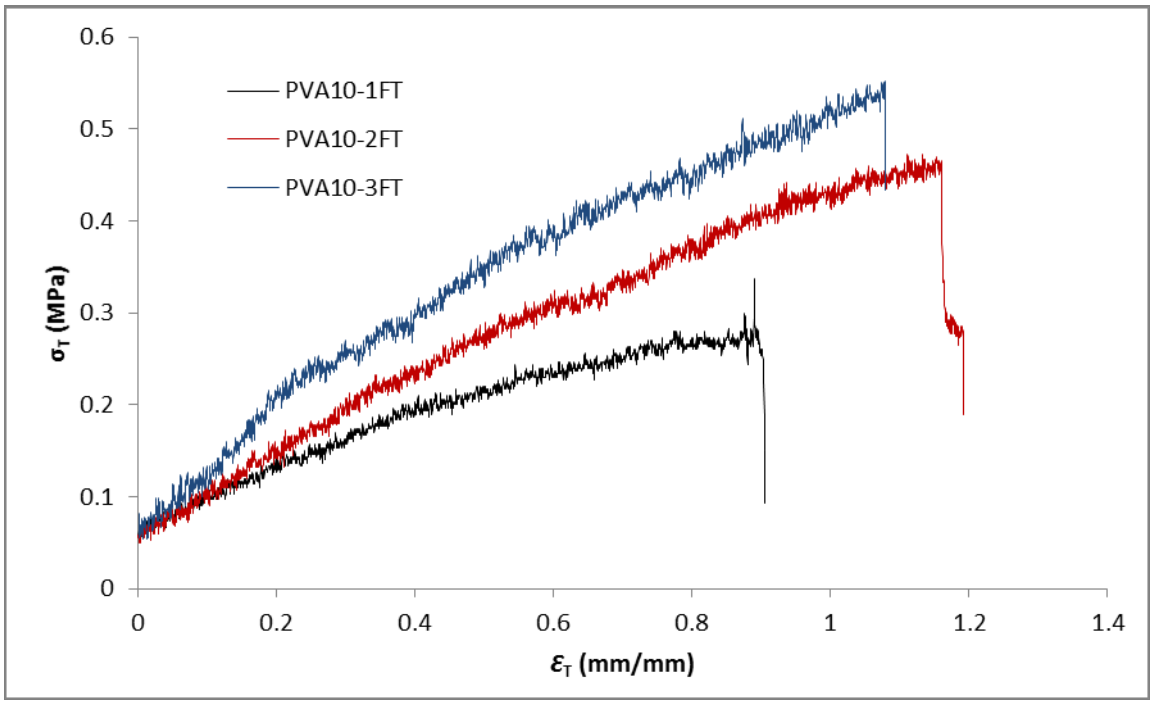

Figure 5-7: Stress strain curve of hydrated PVA10 hydrogels prepared by different cycles of freeze thawing.

The typical stress strain curve in tensile mode of the hydrated PVA10 hydrogels in Figure 5-7 indicate that there is an effect of the freeze-thawing cycles. The stress strain curves also highlight the ductile behaviour of the PVA hydrogels, with a high capacity for deformation however with the ability to withstand relatively low stresses.

Dual network hydrogels of PVA-Alginate

With the optimization and characterisation of the effect of freeze thaw cycles on PVA10 hydrogels; the hydrogel systems were taken further to develop interpenetrating dual networks of PVA with sodium alginate (SA). The objective being to create a network system that constitutes of a robust synthetic 1st polymer network in conjunction with a weak natural polymer, interpenetrating within the 1st network to form a 2nd network, forging the creation of biocompatible mechanically enhanced network system.

The dual network (DN) hydrogels were prepared via:

I. 1st crosslinking by freeze thaw cycles previously reported for PVA10
II. Allowing SA to penetrate the PVA10 hydrogel by swelling them to equilibrium in SA
III. Chelation of the SA in a solution of calcium chloride

IV. 2nd crosslinking by either subjecting the interpenetrating network (IPN) hydrogels to 1 cycle of freeze thawing or air-drying prior to freeze thawing (AD+1FT).

The two different final crosslinking methods used for the 2nd crosslink were undertaken to determine or identify if AD+1FT could have a significant improvement on the strength of the hydrogels.

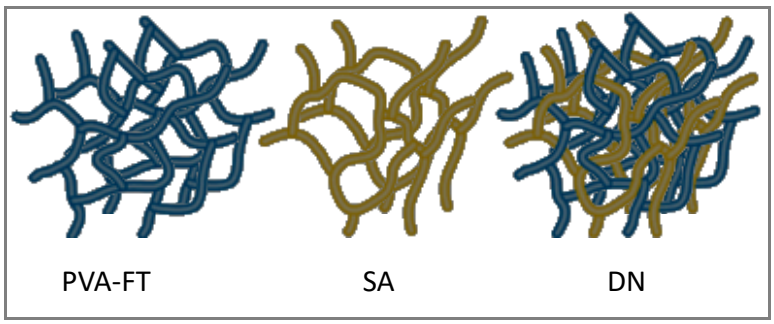

Figure 5-8: Schematic representation of the formation of a dual network formed from a 1st network of PVA crosslinked by freeze thawing, which is allowed to swell in a 2nd network of alginate and chelated with Ca^{2+} followed by a second crosslinking by freeze thawing.

Development of the dual network hydrogels

Dual network hydrogels were synthesized by swelling the 1st PVA xerogel network in a solution of sodium alginate until equilibrium was reached. Table 5-6 presents values of the calculated percentage of sodium alginate absorbed before chelation and after chelation + one freeze thaw cycle.

Concentration of PVA	Cycles of Freeze thawing	% Sodium alginate absorbed in PVA Hydrogel at equilibrium	% of alginate in the Hydrogel after one cycle freeze thawing
10	1	76.3 ± 1.5	39.6 ± 0.6
	2	75.4 ± 0.4	34.9 ± 0.2
	3	74.7 ± 1.6	33.9 ± 2.3
20	2	63.6 ± 1.1	23.3 ± 0.4

Table 5-6: Percentage of sodium alginate absorbed by the PVA hydrogels formed by different numbers of freeze-thawing cycles (n=3). Mass of PVA xerogels was measured before and after swelling to equilibrium in SA as well as after freeze drying, values of which were used to calculate percentage of alginate in the networks.

Determination of concentration of calcium chloride ($CaCl_2$)

When sodium alginate solution is immersed in a solution of calcium chloride a rapid ion exchange process takes place. Sartori et al. 1996 reported that more than half the ion conversion between sodium and calcium occurs within the first 30 seconds, where there is an exchange of approximately two Na^+ by one Ca^{2+}; the expected ion exchange between a monovalent and a divalent cation. When left for longer immersion times in $CaCl_2$ there is a greater ion exchange and it is reported that full ion conversion is obtained after ~300 minutes, when 1%wt sodium alginate and 0.8%wt $CaCl_2$ [280] was used.

A sodium alginate solution of 2%(w/v) was used, and from calculations only 1.8%(w/v) concentration $CaCl_2$ would be required for full ion conversion in 5 hours. However considering the sodium alginate solution will require to penetrate within the PVA hydrogel and as well as considering reducing the immersion time of SA in $CaCl_2$ to obtain maximum ion conversion; interpenetrating hydrogel networks of PVA and SA were formed by immersing in 10% $CaCl_2$ for 3 hours to allow for maximum ion conversion throughout the depths of the hydrogel network.

Optimisation of freeze thaw cycles to be used for 2nd crosslinking

Thermal analysis was used to determine the number of freeze thaw cycles required/necessary to form the 2nd crosslinking that would provide sufficient crosslink density in the hydrogels, yielding superior mechanical properties and stability.

Hydrogel Network system	Number of freeze-thaw cycles for dual networks	Glass transition (Tg)
DN10-2FT-1FT	1	163.6 ± 2.8
DN10-2FT-2FT	2	167.1 ± 3.1
DN10-2FT-3FT	3	167.5 ± 0.2

Table 5-7: Variation of Tg from the effect of different cycles of freeze thawing to form a 2nd crosslinking on the PVA10-2FT hydrogels.

The glass transitions (Tg) reveal that there was no significant increase in Tg of the hydrogels when subjected to a further 2nd crosslinking of more than two freeze thaw cycles. The data in Table 5-7, made it evident that the second crosslinking of only 1 freeze thaw cycle after swelling of PVA10 hydrogels in SA provided sufficient crosslinking density present in the final hydrogel network. The Tg values of the three dual networks formed via different cycles of crosslinking showed no significant differences, hence only cycle of freeze-thawing was taken forward for forming the dual networks.

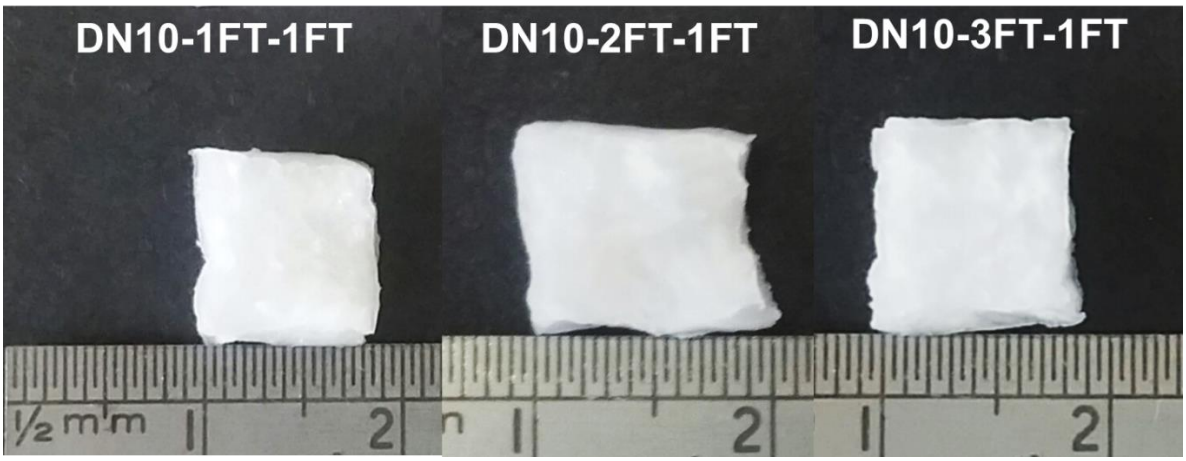

Figure 5-9 : Photographs of dual network hydrogels, hydrated to equilibrium prepared via a second crosslink of 1 freeze thaw cycle.

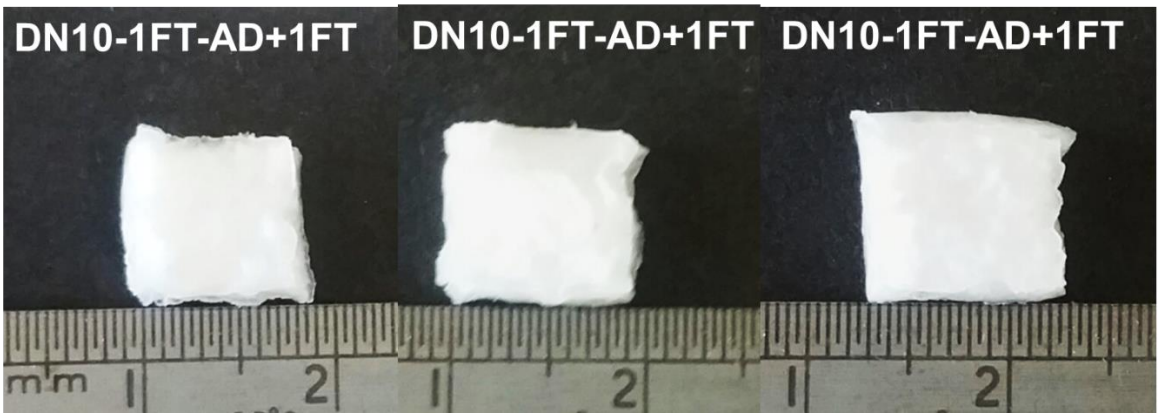

Figure 5-10 : Photographs of dual network hydrogels, hydrated to equilibrium prepared via a second crosslink of air drying and 1 freeze thaw cycle.

FTIR spectra

Assignments of Sodium alginate	Frequency cm^{-1}
-OH stretching	3258
-C-H stretching	2133-2377
$-COO^-$ asymmetric	1594
-COO- symmetric	1403
-C-O-C stretching	1027

Table 5-8: Peak assignments for the FTIR spectra of sodium alginate granules.

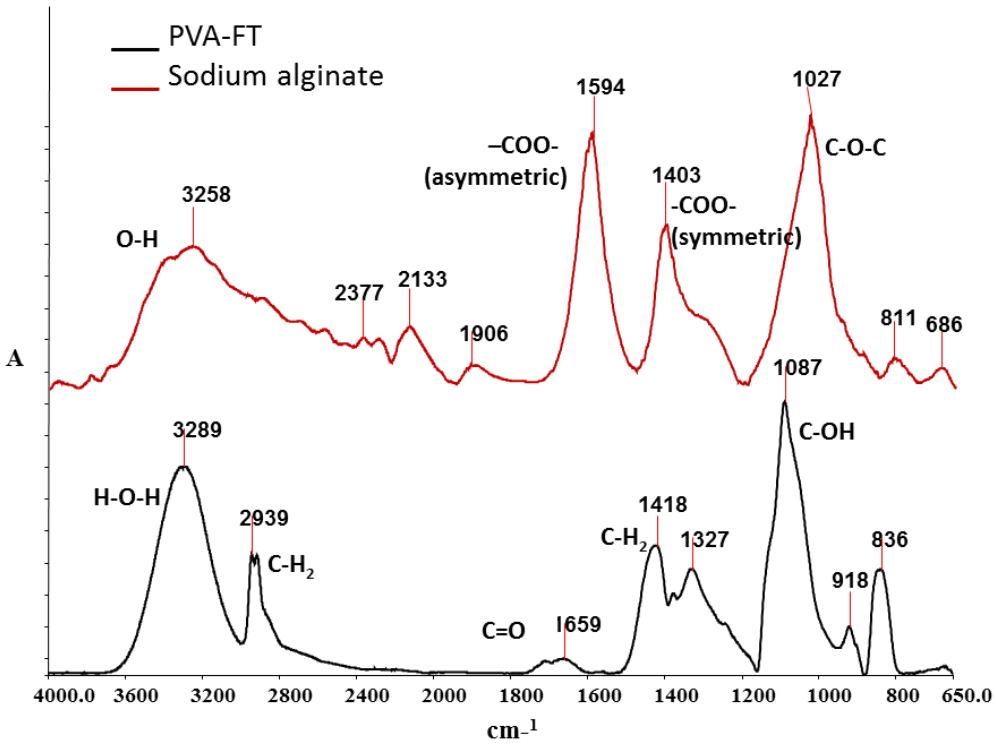

Figure 5-11: A split layer FTIR spectra of PVA10 after 1 cycle of freeze thawing and sodium alginate granules.

A comparison of the FTIR spectra of sodium alginate and PVA10-1FT is shown in Figure 5-11, with the peak assignments of raw sodium alginate summarised in Table 5-8. A broad band centred peak at 3258 cm^{-1} is assigned to O-H stretching and a weak signal 2377-2133 cm^{-1} due to the C-H stretching vibrations. The asymmetric stretch of the carboxylate COO^- vibrational peak arises at 1594 cm^{-1} and the band at 1403 cm^{-1} is assigned to C-OH deformation vibration with contribution of the COO^- symmetric stretching vibration of the free carboxyl group. The C-O stretching vibrations were seen at 1027 cm^{-1} [281]. The fingerprint region is represented by the mannuronic acid residues at 811 cm^{-1} and the guluronic acid residues at 686 cm^{-1} [281, 282]. Studies have shown that when sodium alginate contains high guluronic units, the bands or shoulders around the 1027 cm^{-1} absorbance peak would have a greater intensity than those of alginates with medium or low guluronic units. From Figure 5-11 it is evident that the sodium alginate used in this study is of low guluronic unit content as the shoulder peak reported to appear (in literature) on the C-O-C peak are not visible [280].

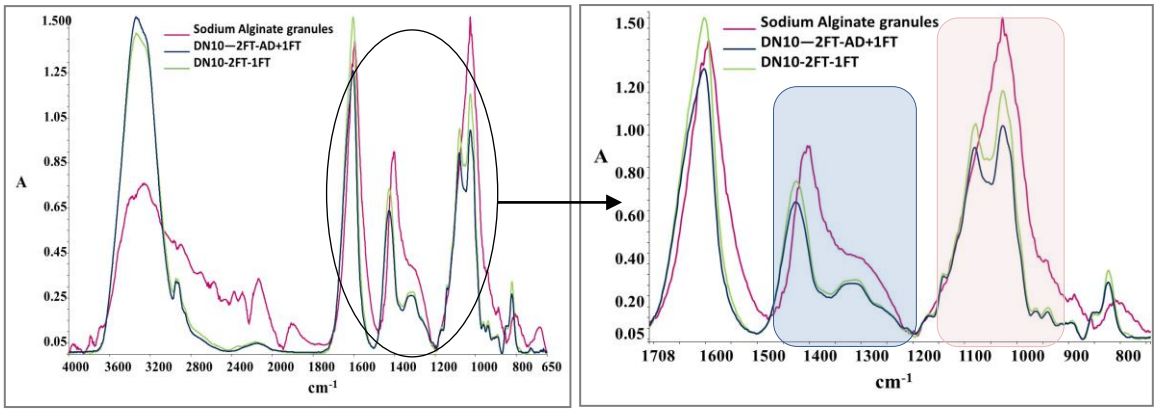

Figure 5-12: An overlay of the FTIR spectra of sodium alginate granules, and dual network hydrogels chelated with calcium chloride and subjected to further crosslinking.

A comparison of the FTIR spectra of the dual networks with sodium alginate (Figure 5-12) showed that a sharp O-H stretching peak (~3290 cm^{-1}), which increased in intensity as compared to the low broad peak of the SA granules, which is due to the intramolecular bonding in the dual network hydrogel. The C-H (~2940 cm^{-1}) corresponding to intermolecular binding is more defined on the dual network hydrogels and does not change with the different second crosslinking of the dual network

hydrogels. The COO- symmetrical peak (~1400 cm^{-1} highlighted in blue) in SA granules shifts to higher wavenumbers (~1420 cm^{-1}) in the DN with a decrease in intensity due to the ionic binding, as the calcium ions replace sodium ions in the alginate blocks, therefore the charge density, radius and atomic weight of the cation are changed, creating a new environment around the carbonyl group. The blue highlighted area shows the change in the peak arising at ~1300 cm^{-1}, which becomes more pronounced in the DN as compared to the granules, suggesting a strong binding of the calcium to the G blocks. Within the red highlighted region, a new peak arises at around 1150 cm^{-1}, which corresponds to a partial covalent bonding between calcium and oxygen atoms. New peaks at ~1070 and ~1026 $cm^{-1}$are associated with the guluronic blocks and indicate a change in the binding within these blocks as calcium is introduced [280].

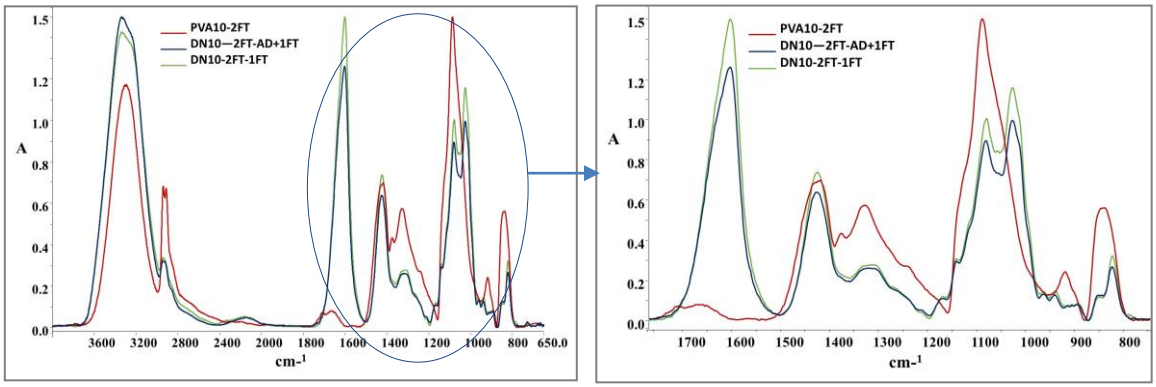

Figure 5-13: A comparison of infrared spectra (overlay) of PVA10-2FT, PVA10-2FT dual network hydrogels subjected to a further crosslinking of one freeze thaw cycle and air-drying prior to freeze thawing.

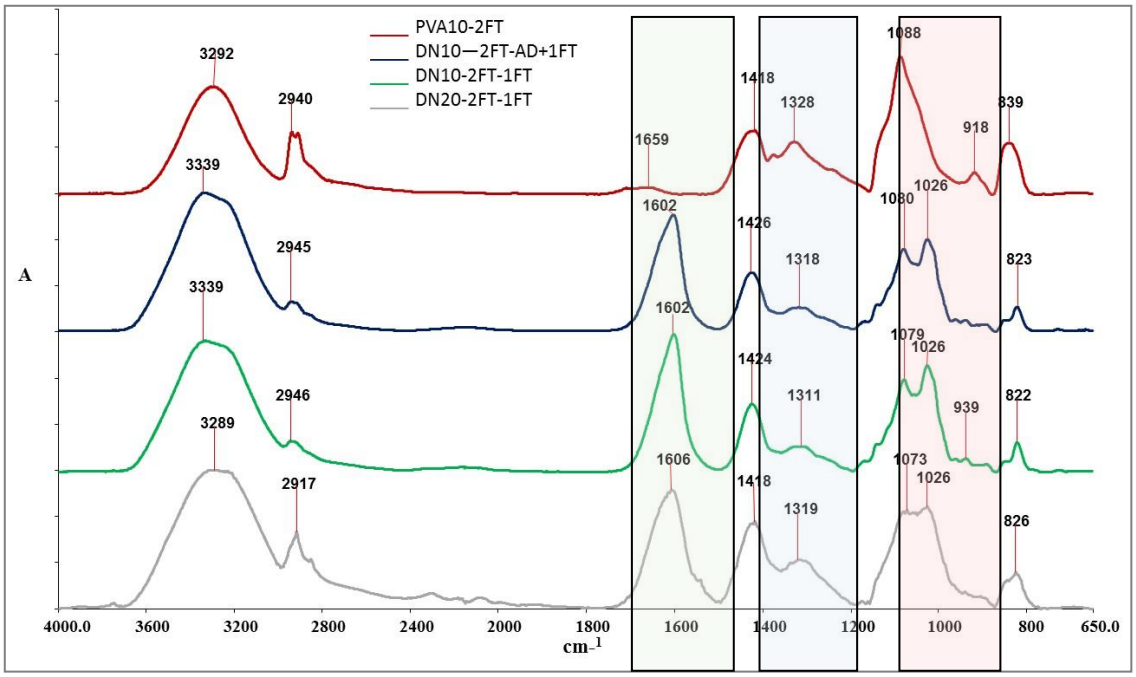

Figure 5-14: A split layer FTIR spectra comparing PVA10-1FT, PVA10-2FT dual network hydrogels subjected to a further crosslinking of one freeze thaw cycle and air-drying prior to freeze thawing, and PVA20-2FT dual network subjected to a further crosslinking of 1 freeze thaw cycle.

Figure 5-13 and Figure 5-14 show the comparison of the FTIR spectra of the dual network hydrogels and PVA-2FT only hydrogel. The peak arising at 1600 cm^{-1} (green block) is assigned to the carboxylate groups present in both guluronic and munnoronic acids units in alginate, which confirms the incorporation of the alginate in the dual network. A slight shift in the carboxylate peak highlighted in the blue region indicates an interaction between PVA and sodium alginate. The C-O stretching at 1027 cm^{-1} (pink) in PVA, is replaced by a double peak in the dual networks (at 1058-1081 and 1023-1026 cm^{-1}) which can be attributed to the ether (C-O) and acetal ring (C-O-C) formed due to a crosslinking between PVA and SA (or due to the antisymmetric stretch of C-O-C revealing the presence of alginate) [283, 284].

Differential scanning calorimetry – Thermal analysis

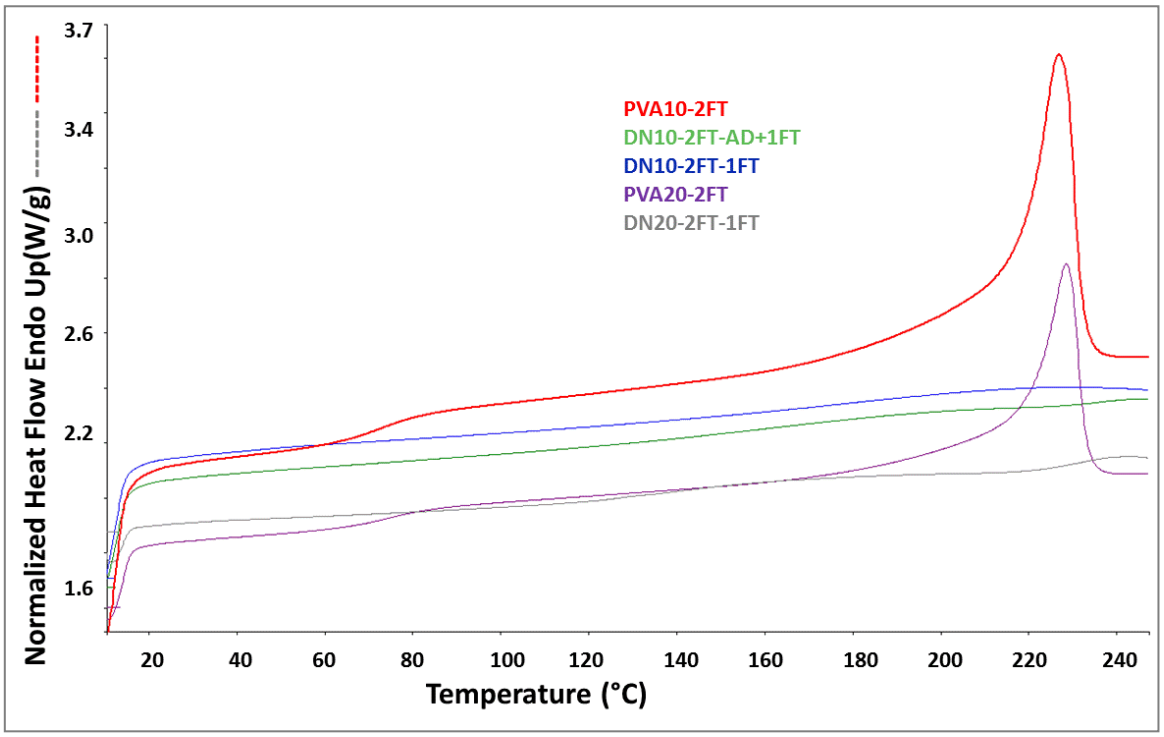

Figure 5-15: Normalised thermograms of PVA10-2FT, PVA20-2FT, PVA10-2FT dual network hydrogels subjected to a further crosslinking of one freeze thaw cycle and air-drying prior to freeze thawing, and PVA20-2FT dual network subjected to a further crosslinking of 1 freeze thaw cycle.

Hydrogel network	Cycles of PVA10 freeze thawing	Glass transition, Tg (°C)
DN10-(x)-1FT	1	155.2 ± 3.0
	2	163.6 ± 2.8
	3	169.1 ± 3.2
DN10-(x)-AD+1FT	1	169.3 ± 2.2
	2	176.6 ± 2.6
	3	177.4 ± 2.3
PVA20-(x)-1FT	2	75.9
DN20-(x)-1FT	2	139.0

Table 5-9: Glass transition of PVA10 and PVA20 dual network hydrogels prepared by different cycles of freeze thawing. (x=1, 2 or 3 FT as shown in column 2).

The Tg values of the dual networks ranged from 139-177^{0}C and were found to show a correlation to the number of FT cycles as expected. The single network of PVA exhibited

a Tg at ~75^{0}C (Table 5-3) and this large difference also confirms the formation of a new network that reinforces the matrix. The Tg values of the dual networks also showed a relationship with the concentration of the PVA used with the higher concentration of 20% PVA yielding a lower Tg, which may be attributed to the reduced uptake of the alginate phase due to the higher crosslinking in the PVA 20% network.

Hydration

Hydrogel network	Cycles of freeze thawing	EWC (%)	Swelling ratio (SR)	Gel fraction, GF (%)	Diffusion coefficient, D, ($10^{-6}cm^2s^{-1}$)
DN10-(x)-1FT	1	69.1 ± 0.9	4.6 ± 0.1	70.6 ± 2.2	0.3
	2	69.8 ± 0.5	4.7 ± 0.1	71.0 ± 1.3	0.1
	3	71.8 ± 0.8	4.5 ± 0.1	78.4 ± 3.2	1.0
DN10-(x)-AD+1FT	1	70.7 ± 1.4	4.7 ± 0.1	70.2 ± 1.2	0.4
	2	72.6 ± 0.7	5.1 ± 0.1	72.1 ± 0.7	0.9
	3	72.4 ± 0.7	4.7 ± 0.1	76.3 ± 1.0	0.8
PVA20-(x)-1FT	2	66.3 ± 0.7	3.0 ± 0.1	99.0 ± 1.7	1.0
DN20-(x)-1FT	2	55.0 ± 0.5	2.7 ± 0.01	83.4	1.3

Table 5-10: Equilibrium water content, swelling ratio and gel fraction of PVA10 and PVA20 dual network hydrogels prepared by different cycles of freeze thawing (n=3). (x=1, 2 or 3 FT as shown in column 2).

The results of EWC, SR, GF and diffusion coefficients of the different hydrogel groups are summarised in Table 5-10. EWC and SR of dual networks subjected to a 2nd crosslinking of 1 FT cycle exhibited lower values than those subjected to a 2nd crosslinking of AD+1FT, both networks of which were found to be significantly lower ($p<0.001$) that of the PVA only hydrogels. This indicates the formation of a tighter more compact and rigid network structure. The concentration of PVA to form the dual networks

had a significant effect on both EWC and SR with the higher concentration of 20% yielding lowest values. The variation of the diffusion coefficient of water on the hydrogels showed a similar trend, where the average water diffusion into hydrogels decreased as crosslinking density increased, with the exception of the DN20 dual network hydrogel.

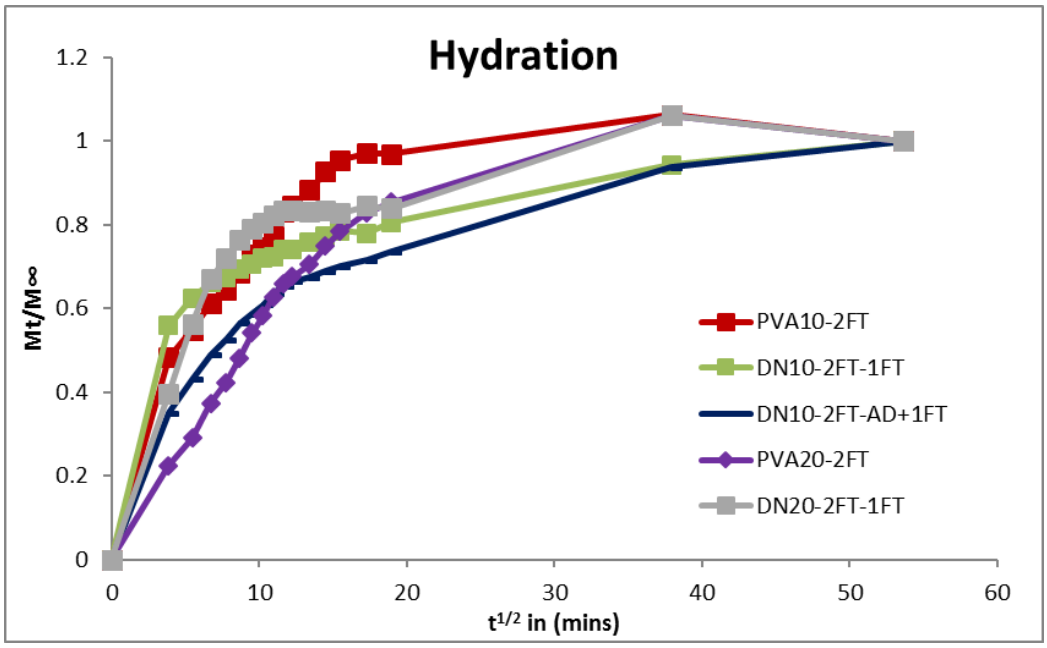

Figure 5-16: A comparison of the hydration of PVA10 and 20 subjected to 2 freeze thaw cycles, as well as their dual network hydrogels.

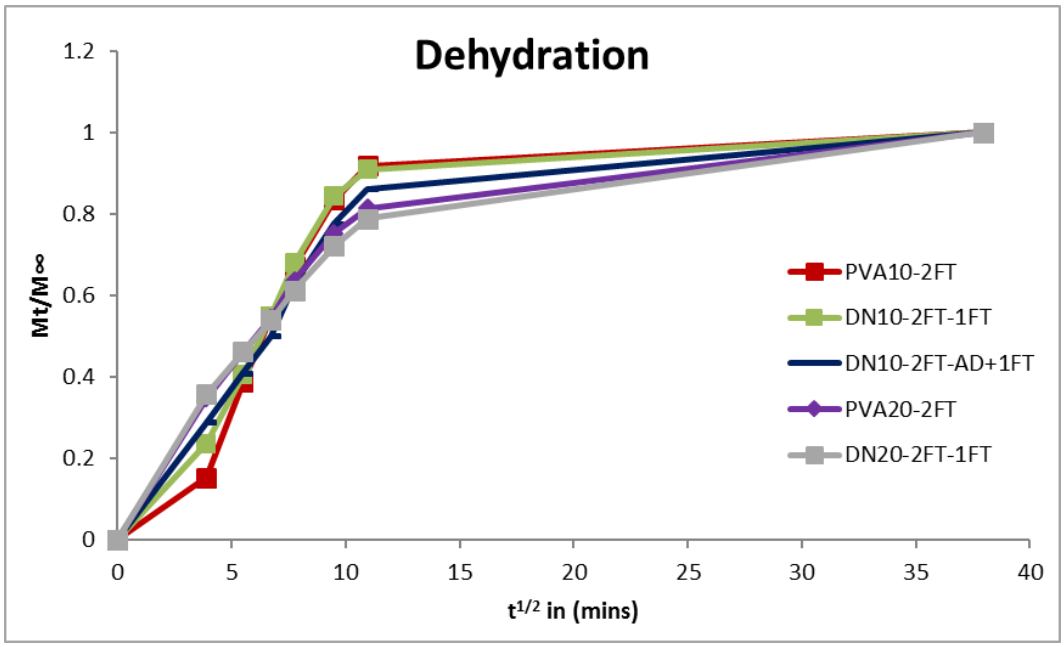

Figure 5-17: A comparison of the dehydration curve of PVA10 and 20 subjected to 2 freeze thaw cycles, as well as their dual network hydrogels.

Figure 5-16 and Figure 5-17 are typical plots of the behaviour of water absorption and desorption versus $t^{1/2}$ for the different PVA10 and 20 hydrogel groups and their

respective dual networks. The hydrogels all present with similar hydration and desorption curves.

Hydrolytic degradation

Degradation studies on hydrogels bring to view the rate at which structural integrity of hydrogels is compromised / lost in time whilst immersed in a solution of known pH and temperature.

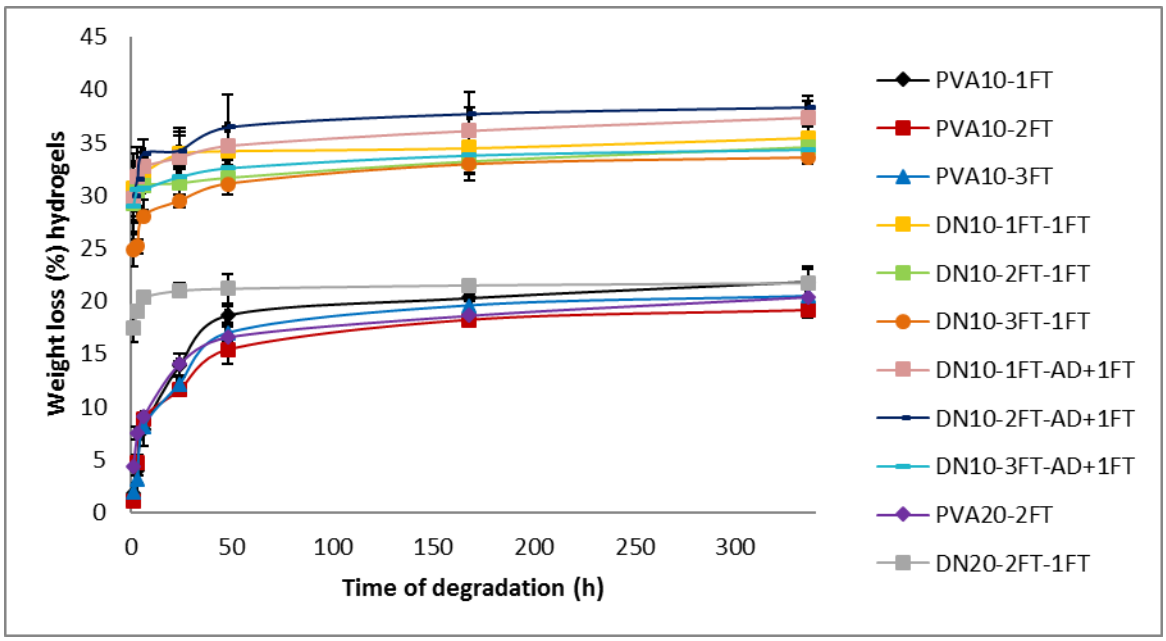

Figure 5-18: A comparison of degradation curves for PVA only hydrogels and their dual networks. (n=3)

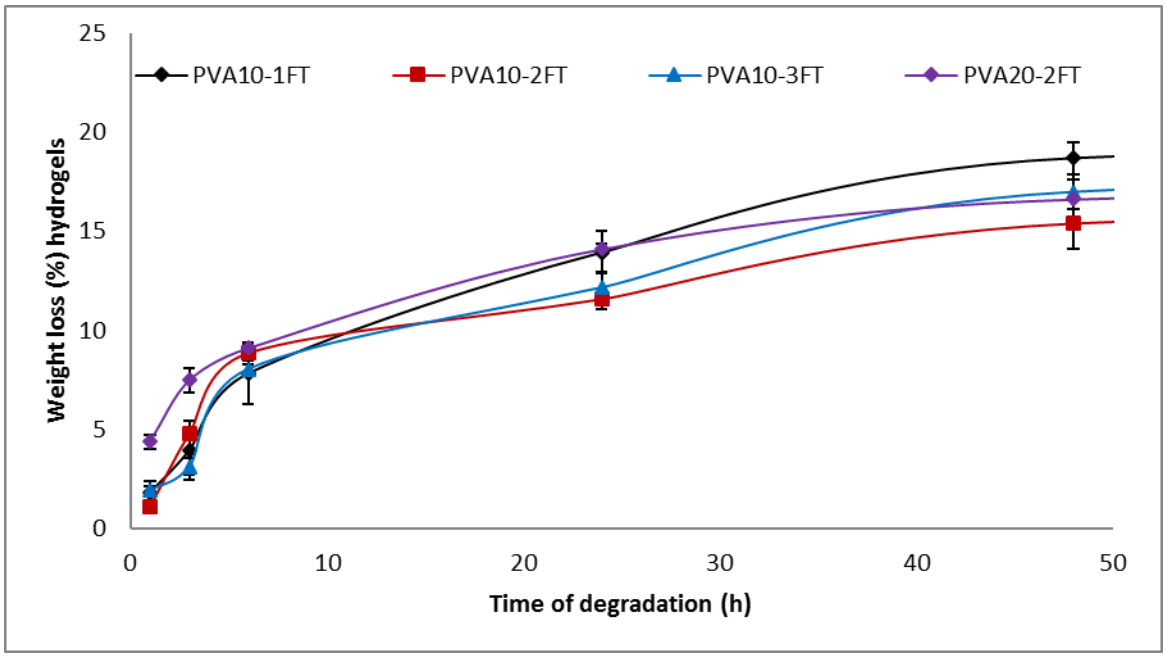

Figure 5-19: Expanded plot representing a comparison of the degradation curves for the PVA only hydrogels subjected to different cycles of freeze thawing in the 1st 50h. (n=3)

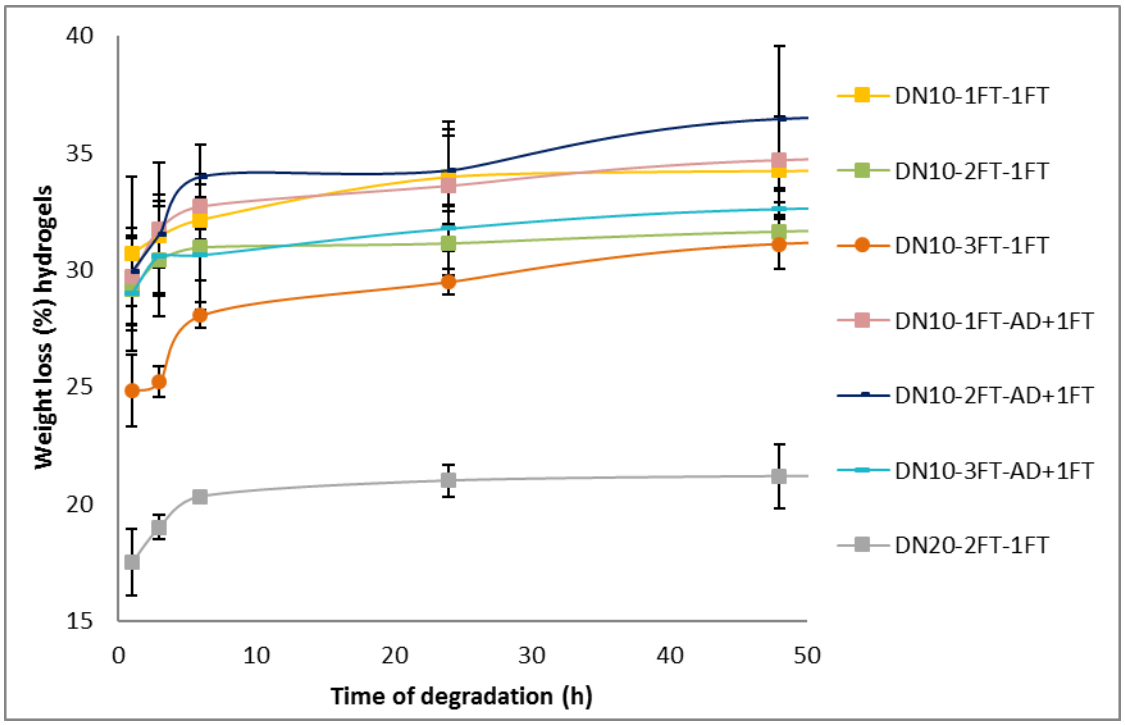

Figure 5-20: Expanded plot representing a comparison of the degradation curves for the the dual networks subjected to different methods of crosslinking in the 1st 50h. (n=3)

Figure 5-18, Figure 5-19 and Figure 5-20 show a comparison between the degradation of the PVA only hydrogels and their respective dual network gels. The plots are presented as %weight loss from hydrogels as a function of time. The results that dual network hydrogels undergo a higher weight loss percentage as compared to the parent PVA only hydrogels.

Tensile strength

Tensile strength tests were carried out to elucidate the effect of the different forms of crosslinking as well as the integration of SA into the PVA network, on the mechanical properties of the hydrogels.

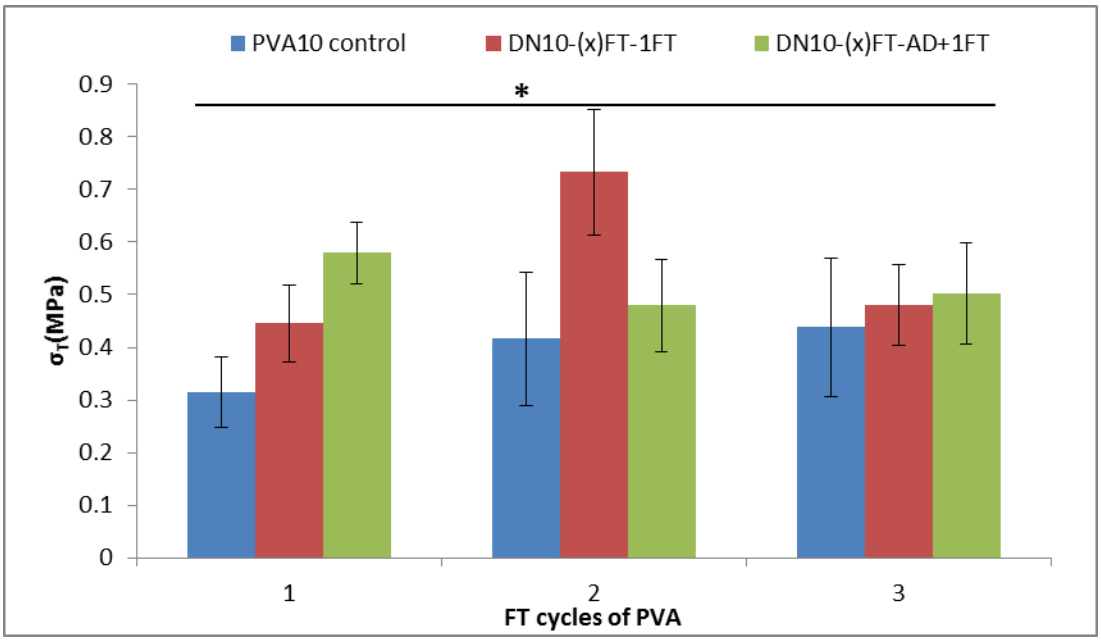

Figure 5-21: A comparison of tensile strength of the freeze-thawed PVA hydrogels with PVA/alginate dual network hydrogels prepared via various methods. (n=6) (* P<0.001); asterisk linked with lines indicate significant difference in values between the groups

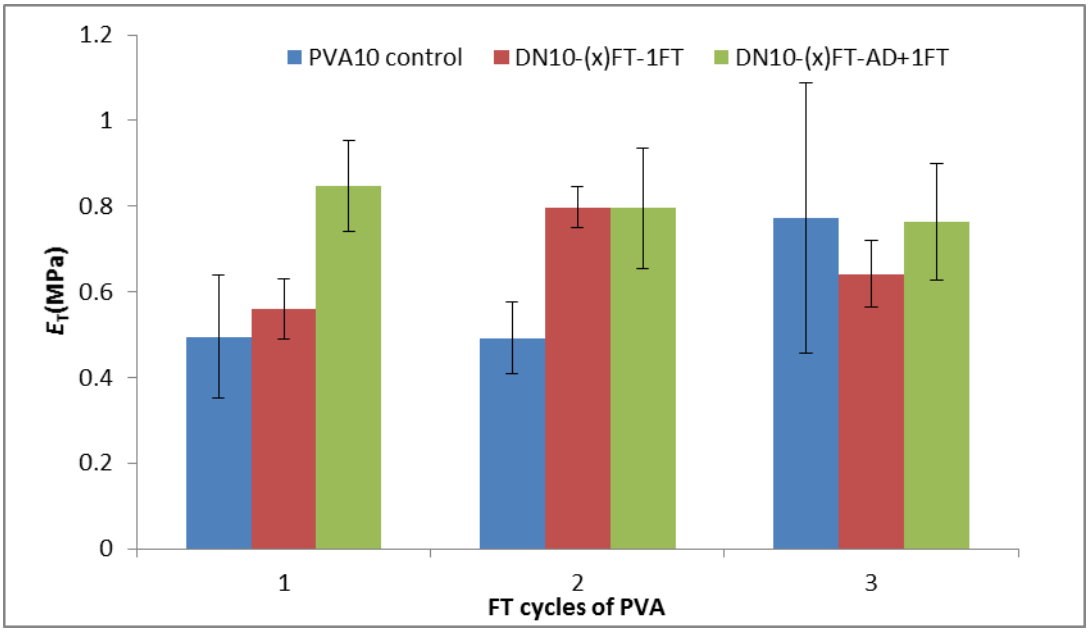

Figure 5-22: A comparison of the Young's modulus of the of the freeze-thawed PVA hydrogels with PVA/alginate dual network hydrogels prepared via various methods. (n=6)

Fully hydrated hydrogels were used to determine the tensile strength and modulus, shown in Figure 5-21 and Figure 5-22. The PVA only hydrogel exhibited lower tensile strengths compared to dual network hydrogels, whilst DN10-2FT-1FT exhibited a significantly higher ultimate tensile strength of 0.7Mpa as compared to the other dual network hydrogels subjected to 1 and 3 cycles of freeze-thawing.

.

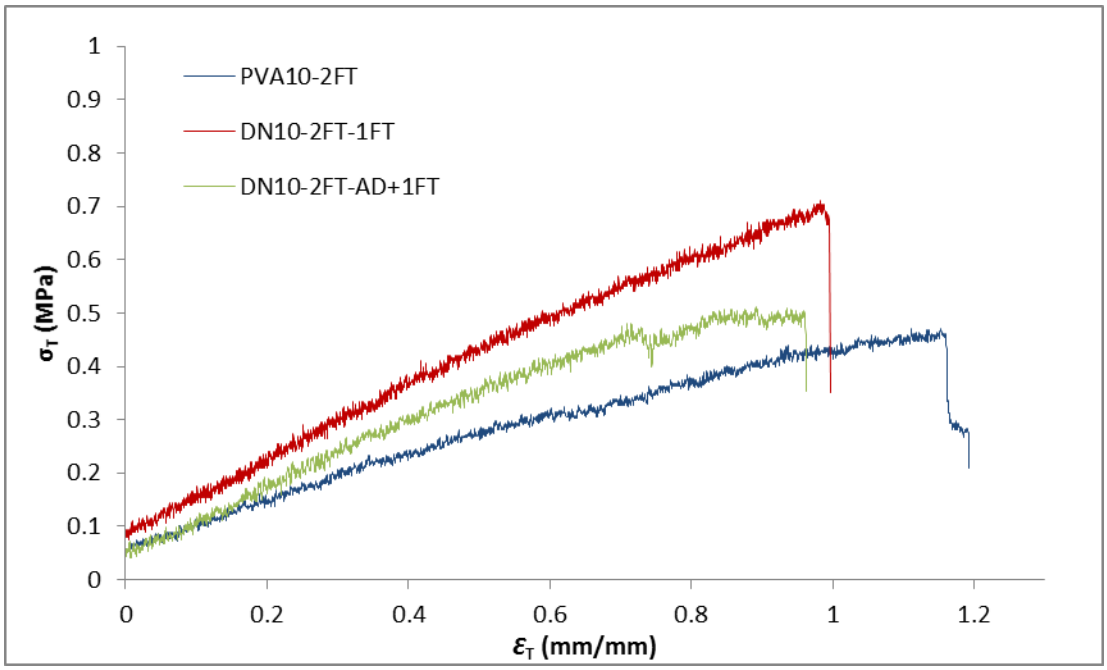

Figure 5-23: A comparison between stress strain curves of PVA10 and dual network hydrogels subjeccted to two freeze thaw cycles before a further crosslinking by either 1 freeze thaw cycle or air drying prior to freeze thawing.

The modulus values of the hydrogelas showed that the dual networks exhibited higher values in comparison to the PVA only networks with the exception of the PVA 10 that was subjected to three cycles of freeze-thaw. Typical strees-strain curves shown in Figure 5-23, indicates the ductile nature of the ductility of the hydrogels hydrogels.

From the optimisation study it was apparent that PVA10-2FT hydrogels yielded dual network hydrogels with superior mechanical properties only with a second crosslinking of 1FT. To obtain dual network hydrogels with tensile strength greater than 1MPa, PVA of concentration 20%(w/v) was used for 2FT cycles of freeze thawing to form DN20-2FT-1FT.

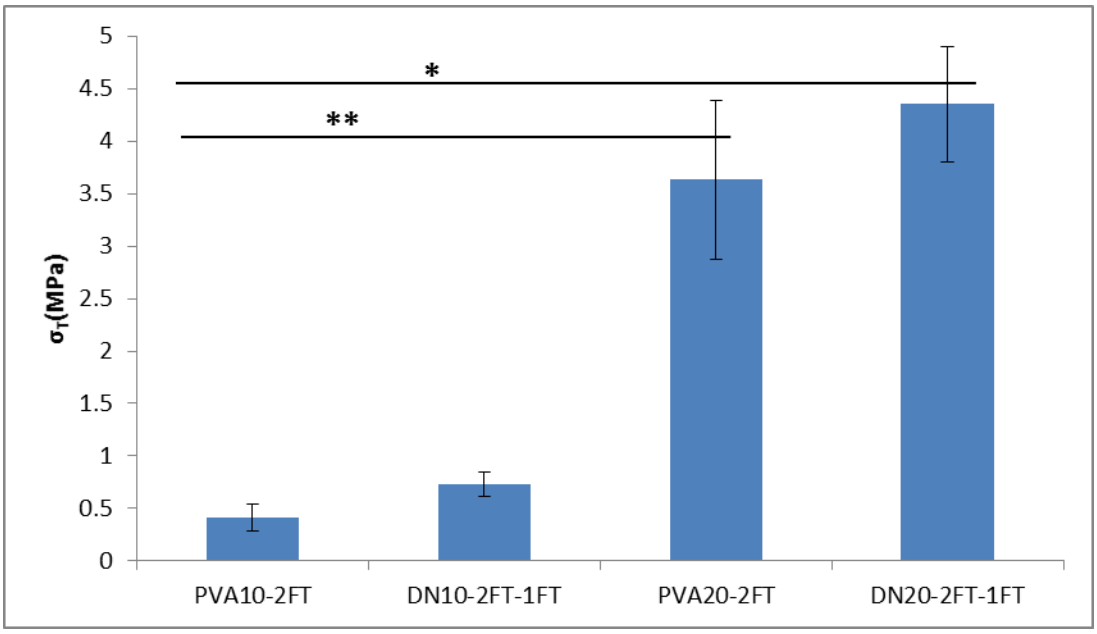

Figure 5-24: A comparison of tensile strength of the PVA (10, 20)-2FT and DN (10, 20)-2FT-1FT hydrogels. (n=6) (* P≤0.033 and ** P<0.001); asterisk linked with lines indicate significant difference in values between the groups

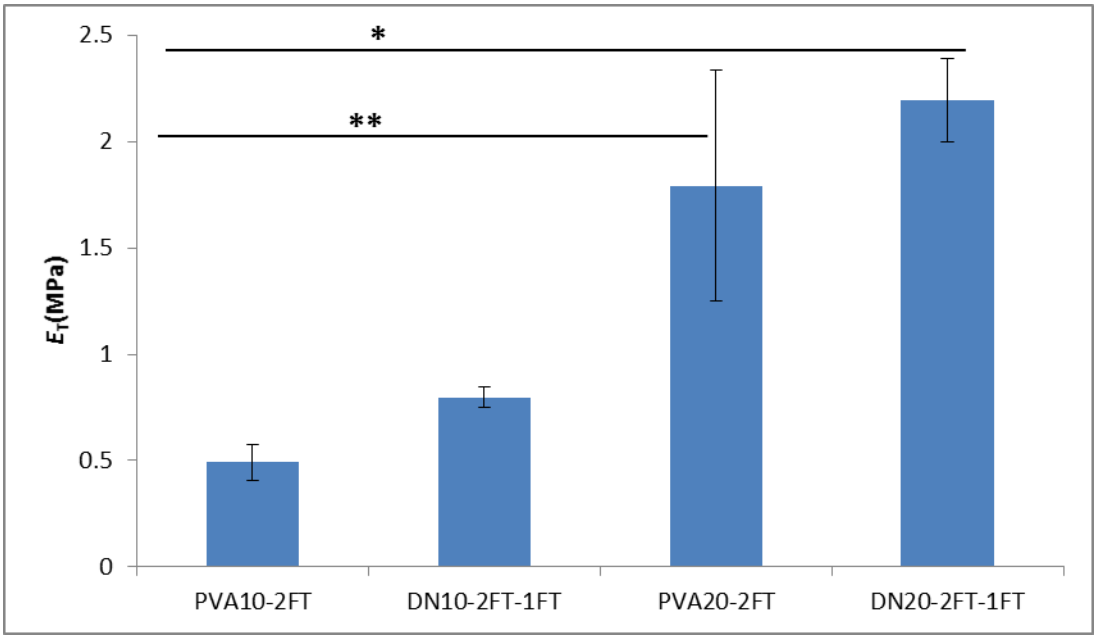

Figure 5-25: A comparison of Young's modulus of the PVA (10, 20)-2FT and DN (10, 20)-2FT-1FT hydrogels. (n=6) (* and ** P<0.001); asterisk linked with lines indicate significant difference in values between the groups

Tensile strength and Young's modulus PVA 10, 20 only and their respective dual network hydrogels formed from two cycles of freeze thawing are presented on Figure 5-24 and Figure 5-25 respectively. The results showed that tensile strengths of the dual network hydrogels could be increased by increasing the concentration of PVA to 20%, which were three orders of magnitude higher than most hydrogels.

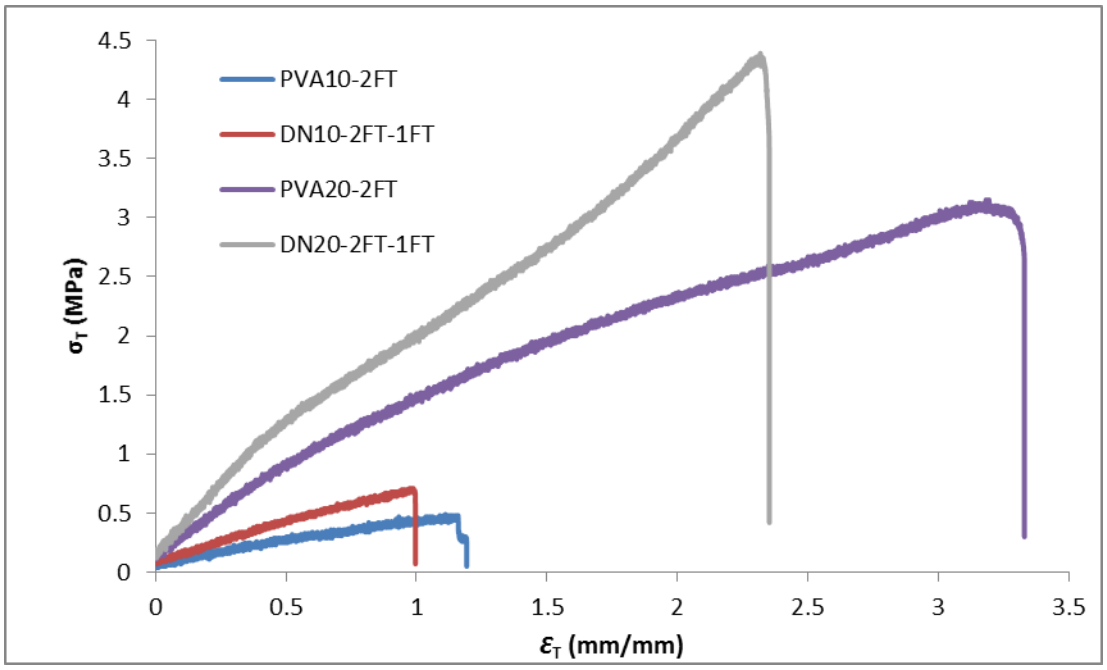

Figure 5-26: A comparison of the stress strain curves of PVA10 and 20 and their respective dual network hydrogels subjected to two freeze thaw cycles before a further crosslinking by 1 freeze-thaw cycle.

The modulus values of the dual networks indicated that they were dependent on the initial concentration of the first network, namely PVA. It can also be extrapolated that the stiffness of the single network hydrogels increases when SA is included in the network to form an IPN dual network.

Fracture toughness

A trouser tear test was performed on hydrogels with PVA base fabricated by two freeze thaw cycles.

Tearing tests are used as a measurement of fracture energy to qualify the mechanical strength of hydrogels. Fracture energies of the hydrogels (Figure 5-27) Showed that PVA20 dual network hydrogel had a significantly higher fracture energy of 6.5KJ/m^2 in comparison with all the other hydrogels. PVA10 dual network however had lower fracture energy than its base PVA10 hydrogel.

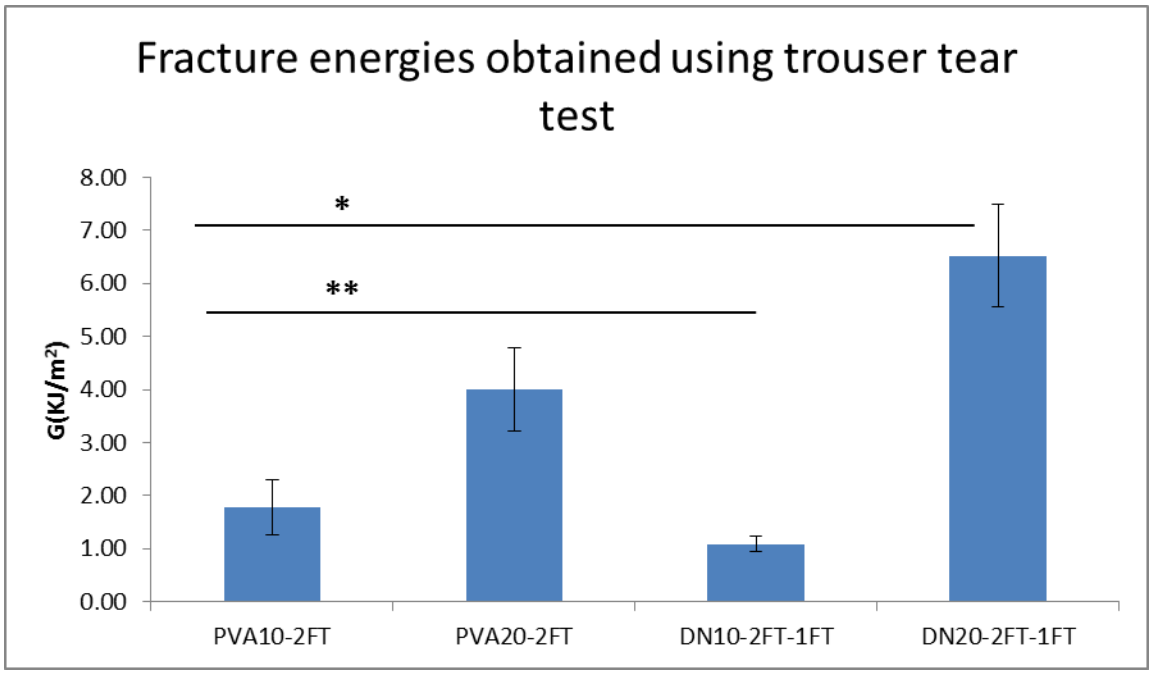

Figure 5-27: Fracture energy values of PVA10, 20-2FT and dual network hydrogels obtained from using a trouser tear test. (n=6); asterisk linked with lines indicate significant difference in values between the groups

Drug release

A preliminary study of these dual networks as potential drug carriers were evaluated using vancomycin, a widely used antibiotic. Vancomycin hydrochloride hydrate (Mw 1485.71 anhydrous basis) was incorporated within the hydrogels and its release rate calculated. FTIR spectra was recorded to determine the incorporation of the antibiotic drug within the hydrogels prior to release.

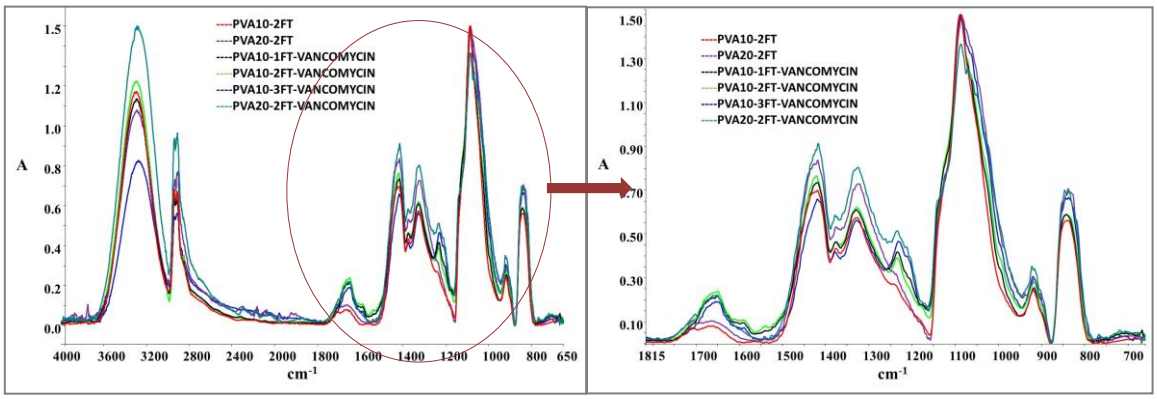

Figure 5-28: An overlay comparison of infrared absorbance peaks of PVA only hydrogels incorporated with and without vancomycin, subjected to different cycles of freeze thawing.

The spectra of the gels with and without vancomycin are shown in Figure 5-28, and the increase in the intensity of absorbance peaks between 1800-1600 cm^{-1} and 1500-1200 cm^{-1} confirmed the presence of vancomycin.

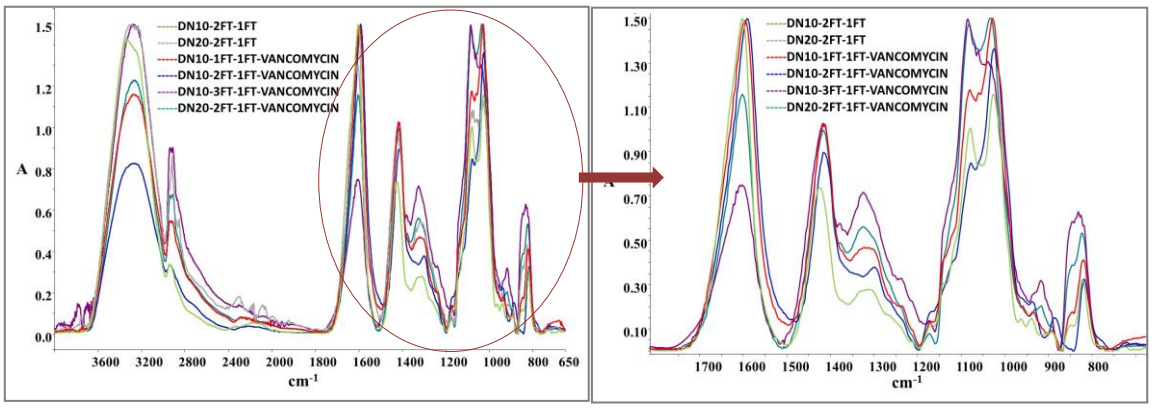

Figure 5-29: An overlay comparison of infrared absorbance peaks of dual network hydrogels incorporated with and without vancomycin, subjected to different cycles of freeze thawing.

The FTIR spectra of the dual networks with and without vancomycin in Figure 5-29 showed the increase in intensity of the peaks between 1700-1500 cm^{-1} due to amide groups of the vancomycin as well as 1500-1200 cm^{-1} indicating the presence of vancomycin the base PVA network structure. As the concentration of the drug used is low in comparison to the dual network, the overlapping bands of the base components predominate hence it is difficult to assign the peaks, however the comparison of the spectra with and without the drug can be used to confirm the presence of vancomycin.

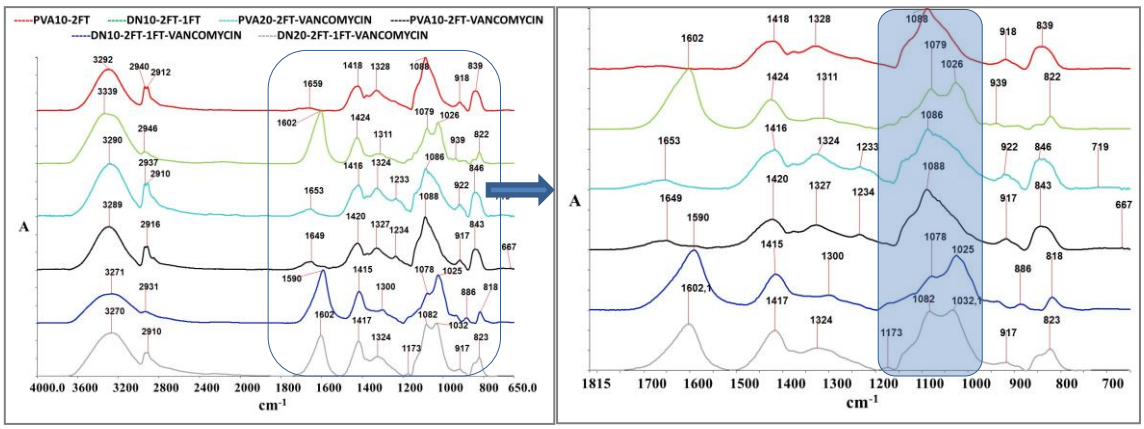

Figure 5-30: A split layer infrared absorption peak comparison of PVA10-2FT hydrogel with its precursor dual network with and without incorporation of vancomycin.

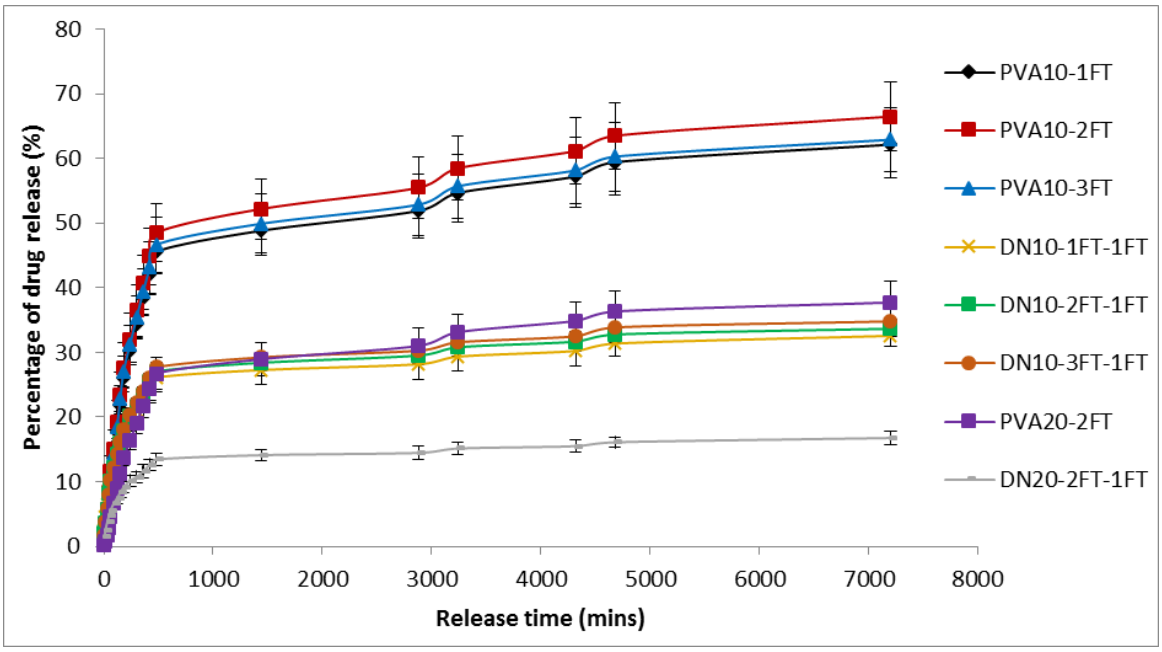

Figure 5-31: Percentage drug release as a function of time of the PVA only hydrogels subjected to different cycles of freeze thawing and their corresponding dual network hydrogels. (n=3)

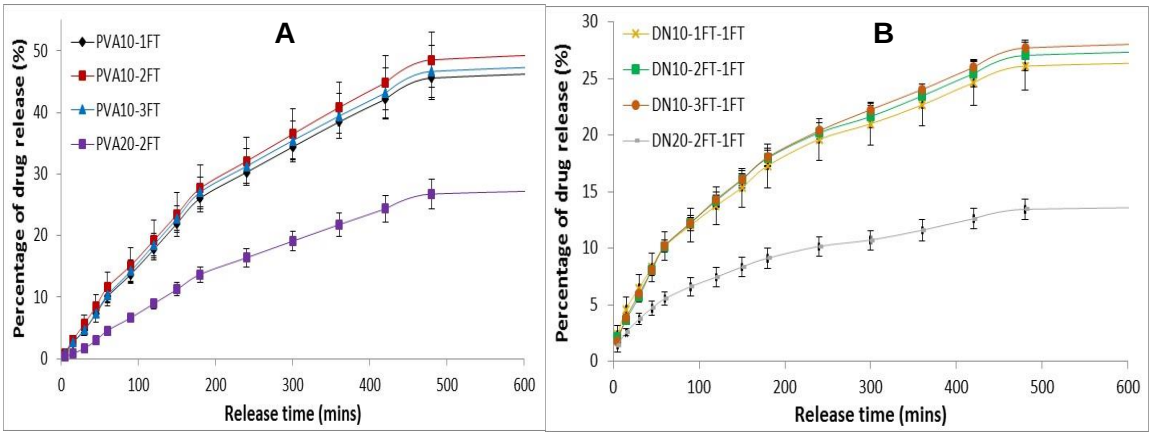

Figure 5-32: Expanded (first 600 mins) percentage drug release plot as a function of time representing **[A]**PVA only hydrogels subjected to different cycles of freeze thawing and their respective **[B]**dual network hydrogels. (n=3)

Figure 5-31 and Figure 5-32 display the percentage drug release plots of the hydrogels incorporated with vancomycin. Results show a linear drug release profile in the early stages, of up to between ~40-45% within the first 500 minutes the plateauing at ~60% release of the drug within 7000 mins. The dual networks exhibited a slower release in comparison to the single network ~17-25% of the drug being released within the first 500 mins and less than 40% of the drug being released after 7000 mins.

SEM analysis

Magnification			
Mag	100X	500X	2500X

PVA10-1FT

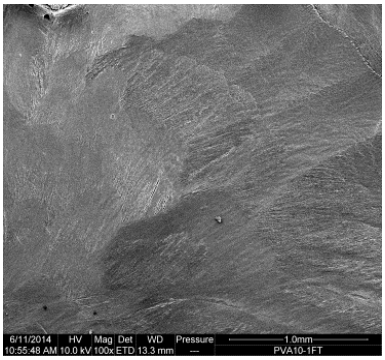

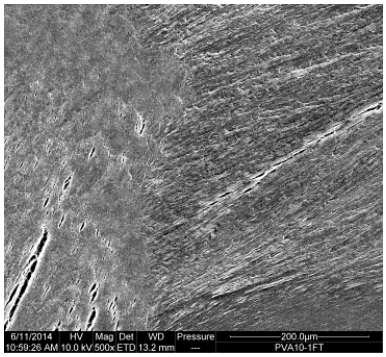

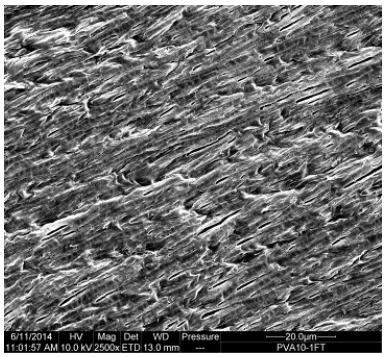

PVA10-2FT

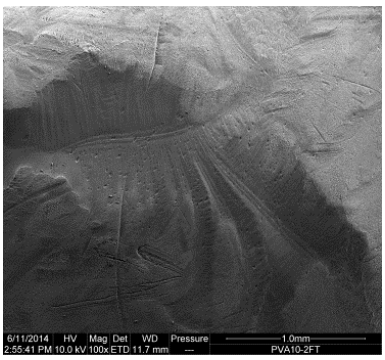

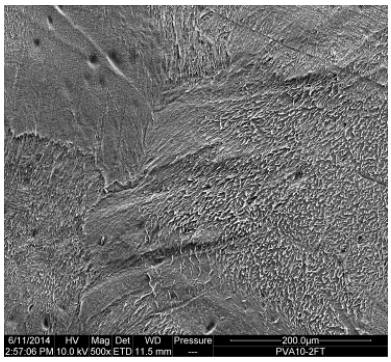

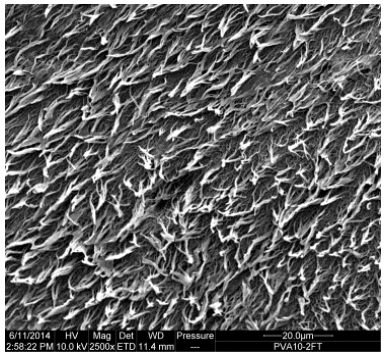

PVA10-3FT

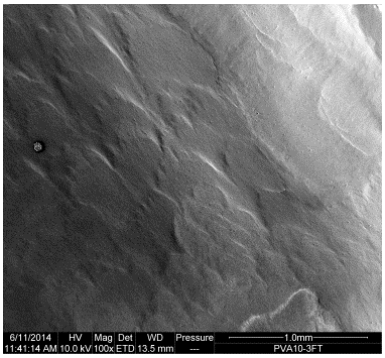

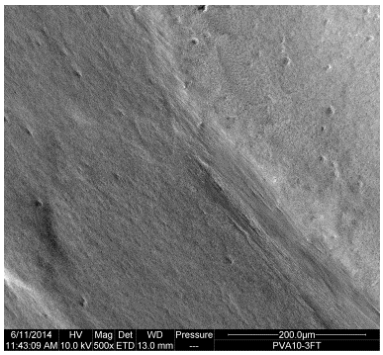

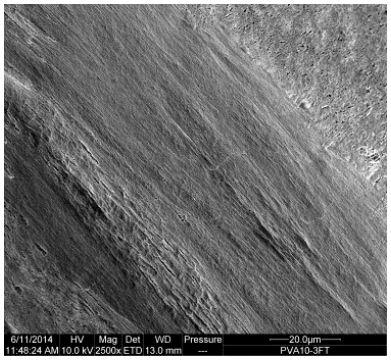

Magnification			
Mag	100X	500X	2500X

DN10-2FT-1FT

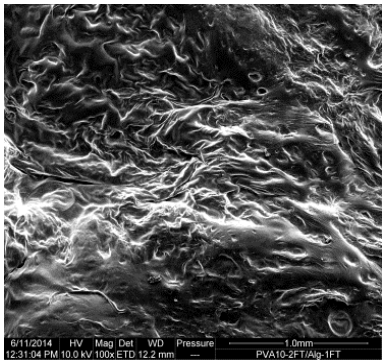

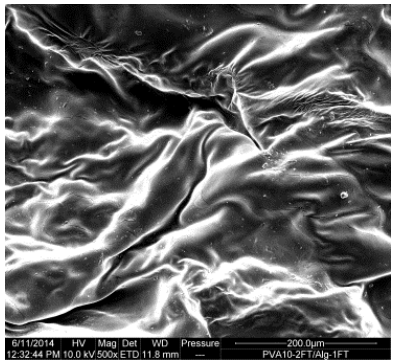

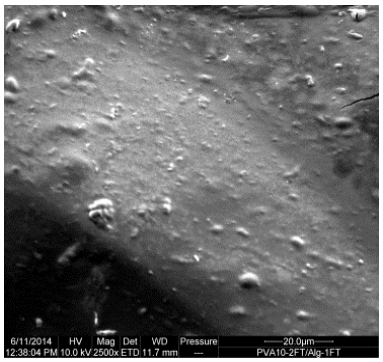

Tensile break

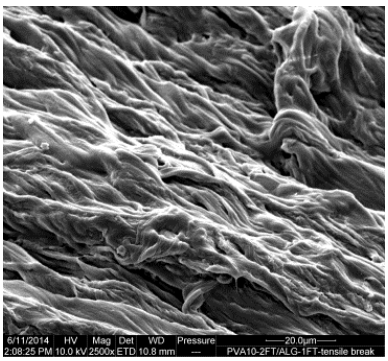

DN10-2FT-AD+1FT

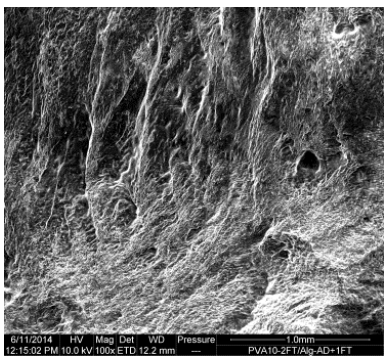

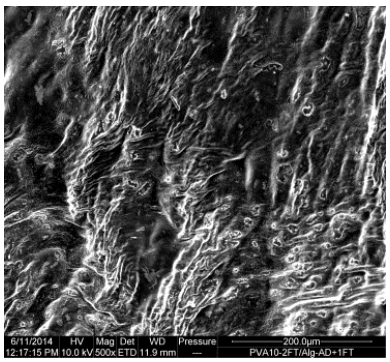

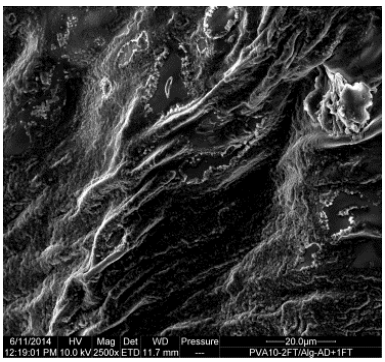

TENSILE BREAK

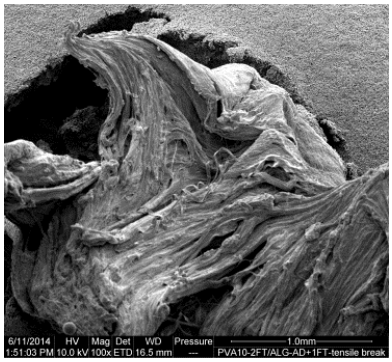

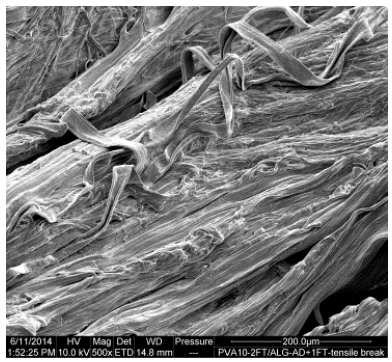

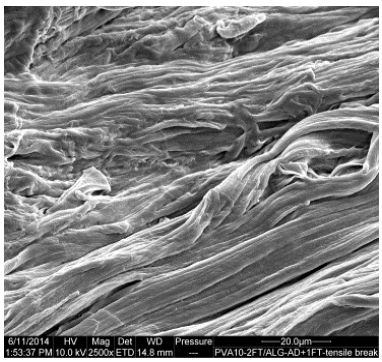

Magnification			
Mag	100X	500X	2500X

PVA20-2FT

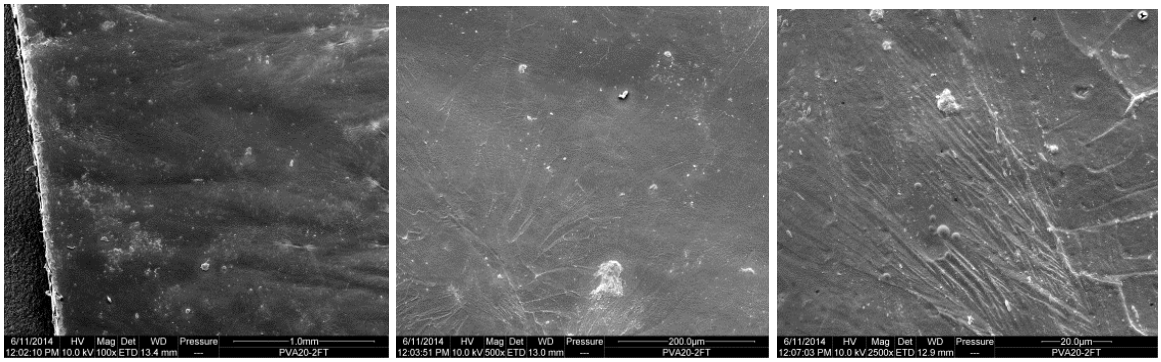

DN20-2FT-1FT

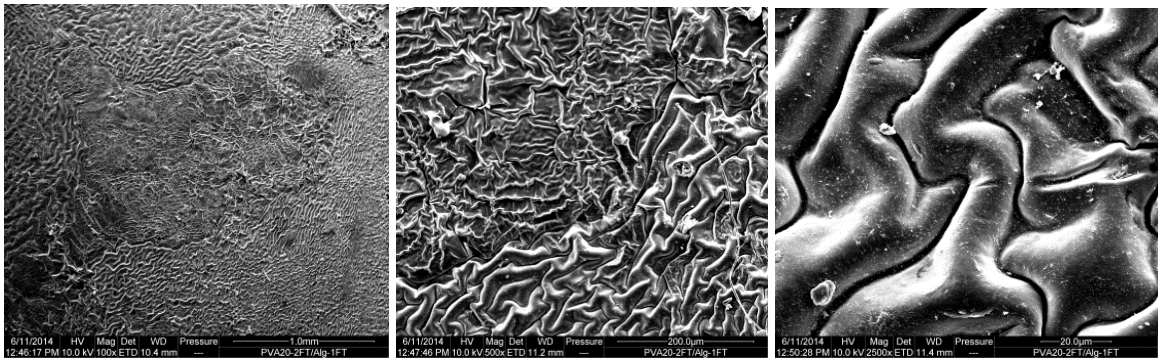

TENSILE BREAK

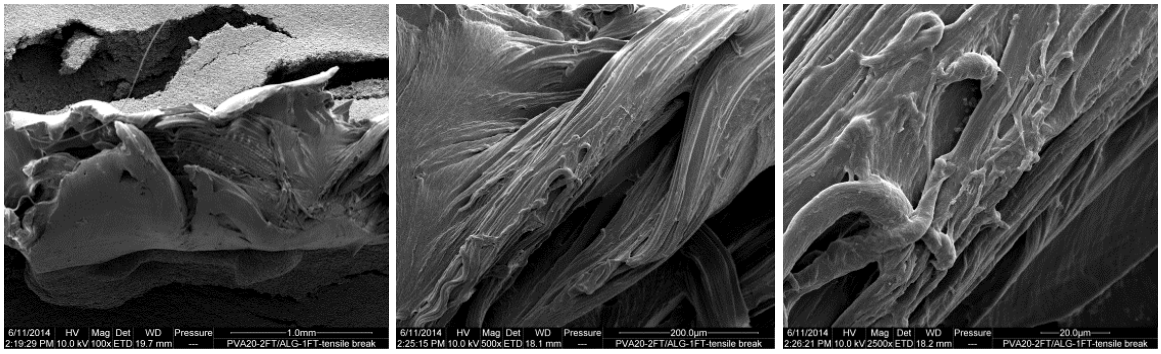

Figure 5-33: SEM micrographs of PVA10-(1,2,3)FT, DN(10,20)-2FT-1FT, DN-2FT-AD+FT, at different magnifications 100x, 500x and 2500x, as well as tensile specimens of the dual network hydrogels after tensile testing, presenting the different morphologies seen on the area of the tensile break.

The micrographs of PVA10 xerogels showed a microporous structure on the surface, with what appears to be crystallite domains, whereas the PVA20 xerogel showed a dense smooth surface with little to no visible porosity. The dual network hydrogels had a rough non-ordered surface area, this was attributed to the presence of alginate within the PVA network structure, of which was confirmed by FTIR results. The micrographs of the fractured surfaces of the tensile specimens show stretched elongated fibres of the

hydrogels indicating that the hydrogels are ductile, which is in agreement with tensile test results obtained from the study.

Cytocompatibility of hydrogels

Cell viability study by MTT assay

Human osteoblast like cells were used to test their viability in presence of the elutions of the hydrogels using MTT assay at 24, 48 and 72 hour exposure times of eluents collected after 24, 48 and 72 hours. The results showed that eluents from single networks of PVA and the dual networks did not have any toxicity, however DN hydrogels expressed a higher level of cell viability than the PVA hydrogels within the 24 and 48h culture exposure times.

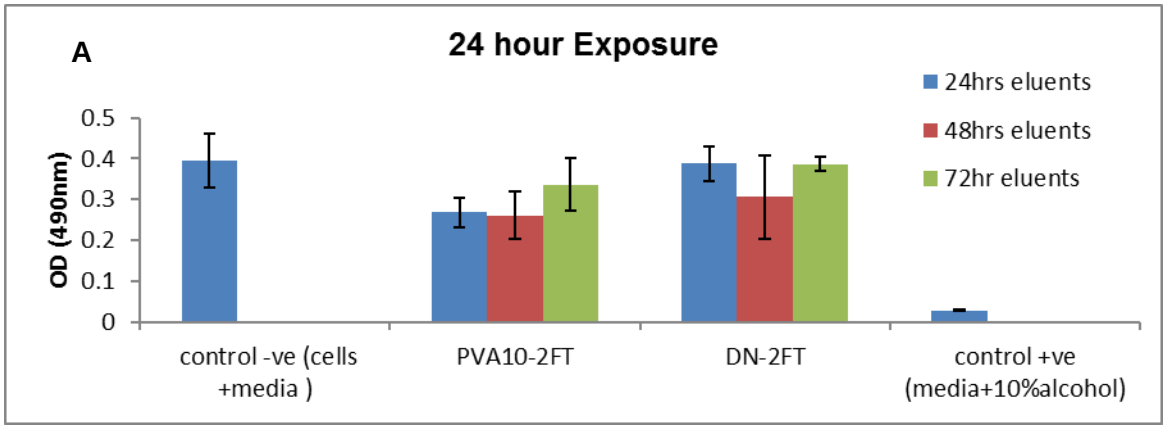

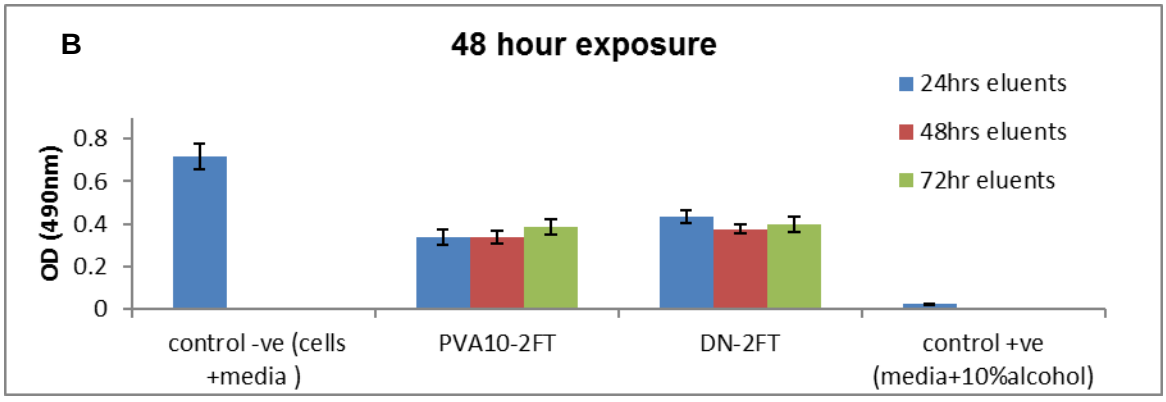

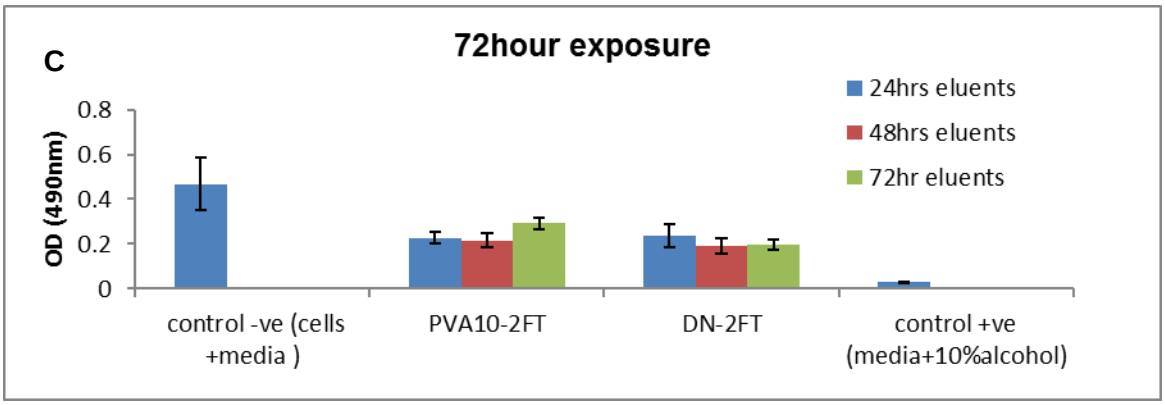

Figure 5-34: MTT test showing the response of human osteoblast cells following exposure to eluents from PVA10-2FT and DN10-2FT-1FT hydrogels. Cells were exposed for 24, 48 and 72h to a **[A].** 24h elution time **[B].** 48h elusion time and **[C].** 72h elusion time.

Live dead assay

HOB cells were stained with calcein AM and ethidium bromide solution, with the live cells displaying a green nucleus and dead cells fluorescing a red colour. Live cells were observed to be dispersed throughout the hydrogel networks. After 28 days in culture cells are observed to have a flattened morphology on the PVA10-2FT hydrogels, and observed to have formed something resembling a sheet cover on the surface of the dual network hydrogels (DN10-2FT).

PVA10-2FT hydrogel

Day 3

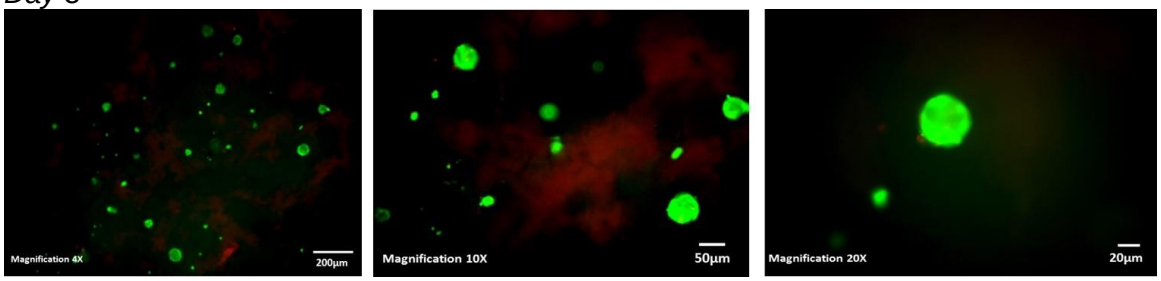

Day 7

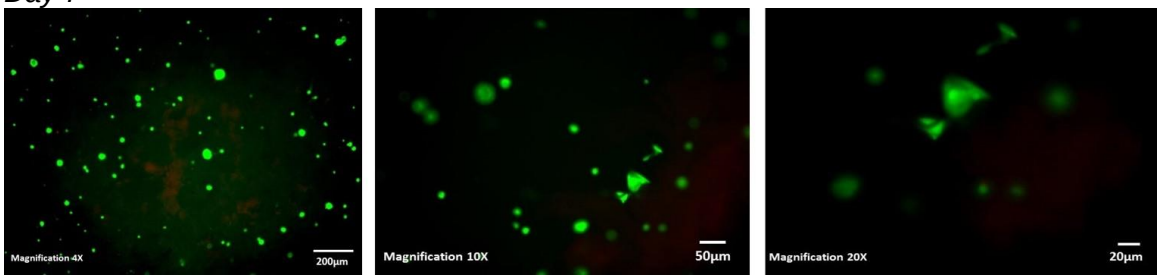

Day 14

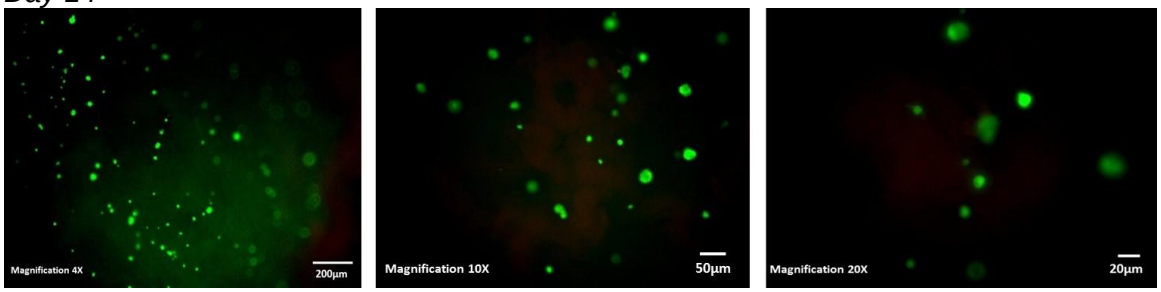

Day 28

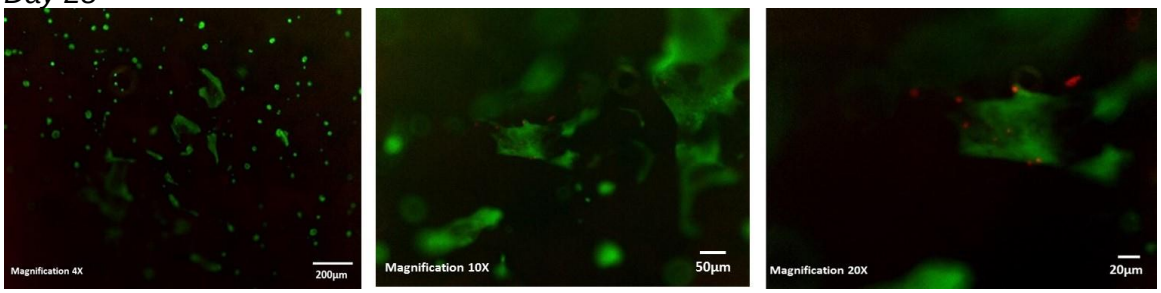

Figure 5-35: Images of live/dead staining of HOB cells (x4, 10 and 20 magnification on PVA10-2FT hydrogel at day 3, 7, 14 and 28.

DN10-2FT-1FT hydrogel

Day3

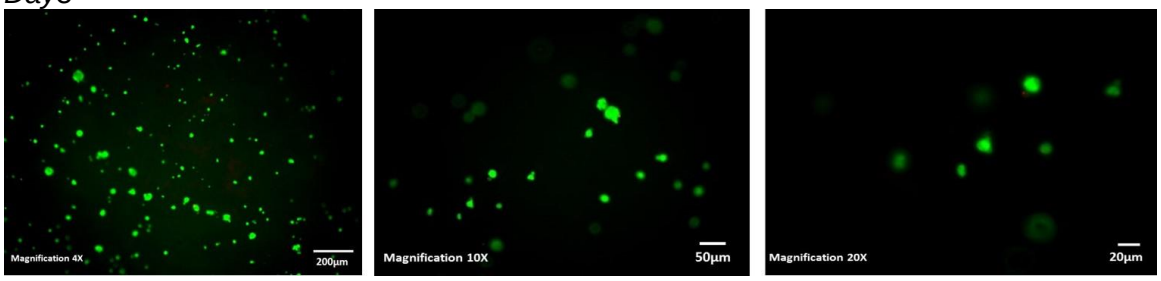

Day7

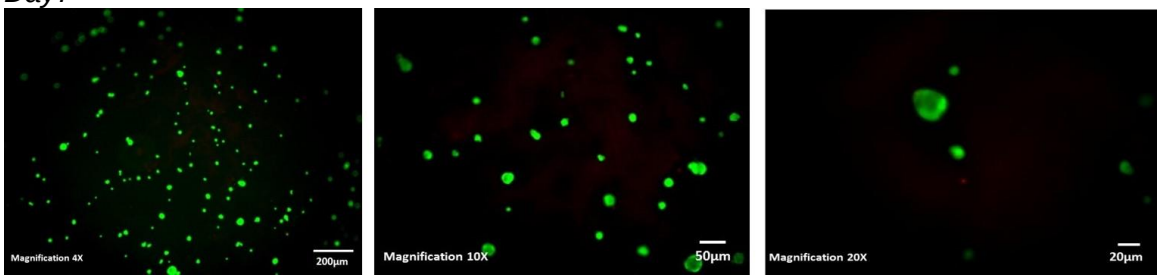

Day14

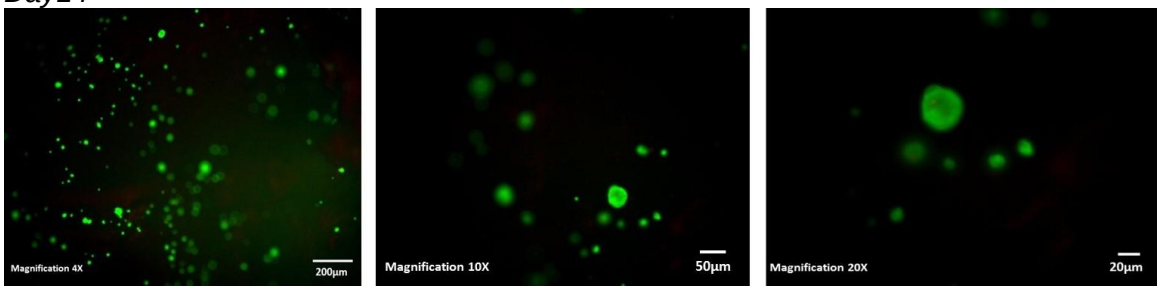

Day28

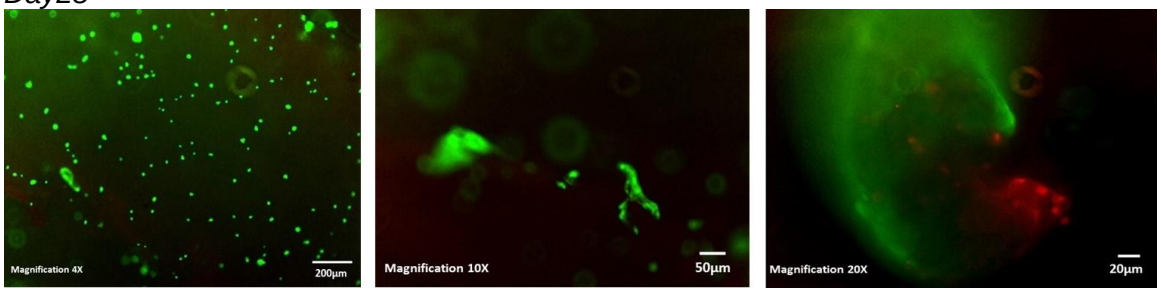

Figure 5-36: Images of live/dead staining of HOB cells (x4, 10 and 20 magnification on the DN10-2FT-1FT hydrogel at day 1, 3, 7, 14 and 28.

HOB cell differentiation by alkaline phosphatase activity and protein concentration

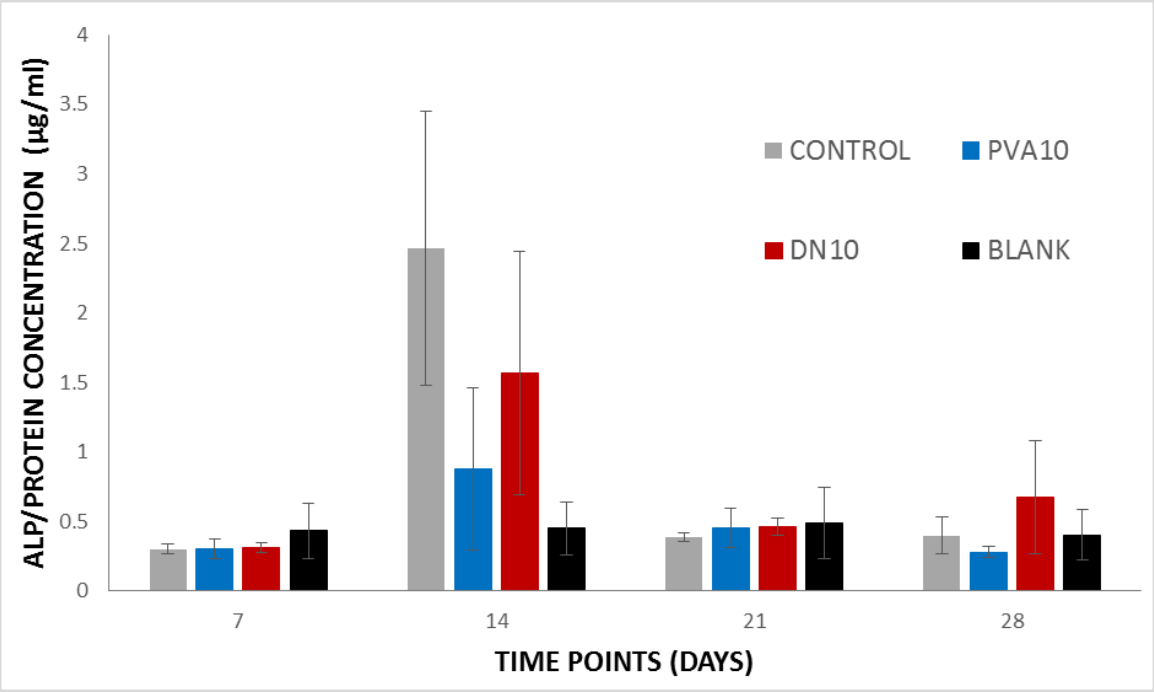

Figure 5-37: The alkaline phosphatase activity in balance with the protein concentration of humanosteoblast cells (HOB) on PVA10-2FT and DN10-2FT, with the tissue culture plate as the control. Tests were carried out on culture media supernatant of hydrogels at time points day (7, 14, 21 and 28). Data represents as mean±SD as n=4

HOB cells cultured on the PVA and DN hydrogels (Figure 5-37), expressed a peak in ALP concentration after 14 days culture period, which then decreased at 21 and 28 days in culture. The DN hydrogel had higher production of ALP than the PVA only network, indicating that more HOB cells in the dual network were progressing towards differentiation to mature osteoblasts.

Real time quantitative PCR: Molecular quantification of osteoblastic phenotypes, ALP and RUNX2

The expression of RUNX2 on the cells seeded within the PVA and dual network hydrogels at day 7, 14, 21 and 28 was determined using qRT-PCR.

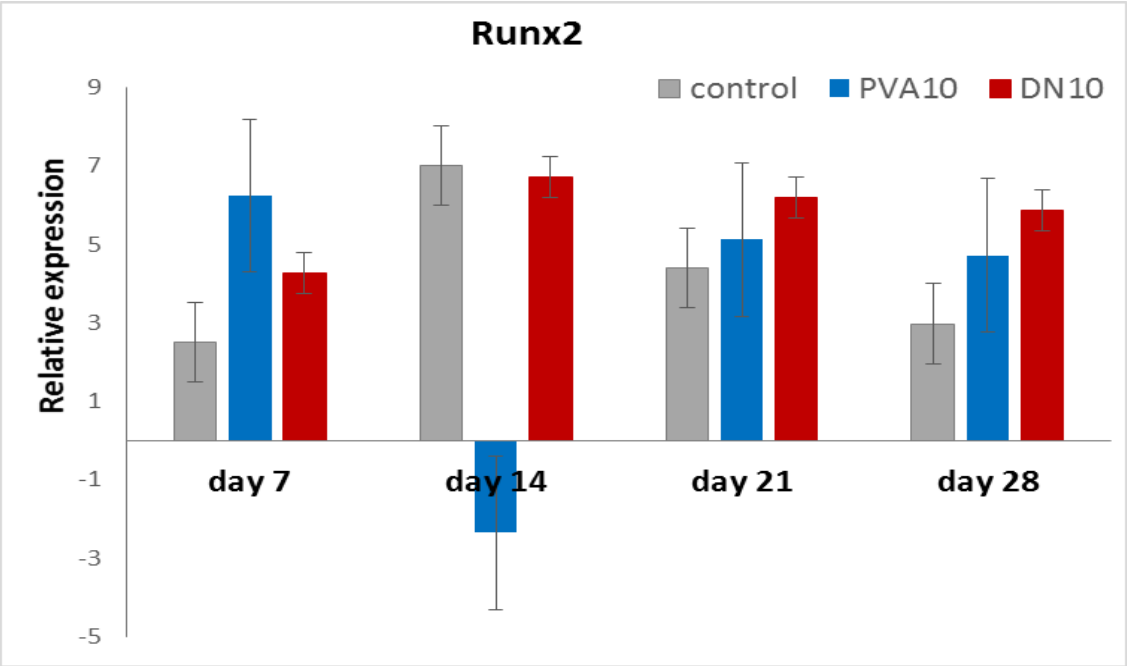

Figure 5-38: Relative expression of Runx2 of the HOB cells cultured on the PVA10-2FT and DN10-2FT-1FT hydrogels, analysis was carried out at time points day(7,14,21,28). NB: data presented is relative to day 7.

Relative expression of RUNX2 shown in Figure 5-38 indicated an increase in expression from day 7 to day 14 followed by a decrease, with exception of PVA10-2FT hydrogel which showed down regulation at day 14.

5.5 DISCUSSION

Hydrogels are able to provide a microenvironment for cells to adhere, proliferate and differentiate whilst providing exchange of nutrients, thus enabling their use in tissue engineering applications. The properties or design variables of hydrogels in biomedical applications are specified by the intended clinical scaffold application and the environment into which the scaffold is to be placed, hence tough networks with high water absorbency are expected to find applications in soft tissue engineering and wound dressing applications. Hydrogels possess a 3 dimensional matrix and constitutes of linear or branched hydrophilic networks that are either physically or chemically crosslinked with high water absorbency. Poly (vinyl alcohol)/PVA, is a synthetic biocompatible polymer that is water soluble due to its hydroxyl groups and is easily degradable in the environment, where the degradation depends on the amount of

hydroxyl groups. Alginate, on the other hand is an anionic linear polysaccharide composed of two saccharides composed of α-l-guluronic acid (G) and β-d-mannuronic (M) that are covalently bonded through 1,4-glycosidic linkage and arranged into either homopolymeric block (MM and GG) or alternating block (MGMG) along the polymeric backbone. Polymer blends and crosslinking of alginate with PVA have been reported to overcome the limitations of the individual polymers, however these still lead to fragile structures with low cell adherence due to the high water absorbency. With the aim of creating tough hydrogel networks, PVA was chosen as the base polymer for formation of dual networks due to its ability to form insoluble networks via hydrogen bonding and crystallite formation. The effect freeze drying on crystallite formation and the resultant consequences of freeze thaw cycles on the hydrogel was first investigated before incorporation of alginate into the network structure to form dual networks.

In this study the physical properties that were deemed appropriate for both soft tissue applications and to form tough, elastomeric matrices for composite formulation were evaluated:

- Mechanical strength at a macroscopic level must bear loads to provide stability to the tissue as it forms as well as fulfil its volume maintenance function.
- Fluid diffusion and degradation properties, which will directly translate to mass transport properties of the hydrogel and at a microscopic level influence cell growth, differentiation and ultimate tissue formation.
- Along with biocompatibility and nontoxicity, incorporation of drugs or growth factors, which can be released in vitro or in vivo as the gel degrades, aiding and facilitating in the process of new tissue formation.

Effect of different freeze drying and thawing cycles on the PVA single hydrogel network

It is known that freeze thawing produces stable PVA hydrogels that are physically crosslinked in the presence of crystallite regions. At a molecular level PVA chains present as a layered structure with a simple zig zag configuration where the double layer

of molecules is held together by hydroxyl bonds whilst weaker van der Waals forces operate between the double layers as shown in Figure 5-39.

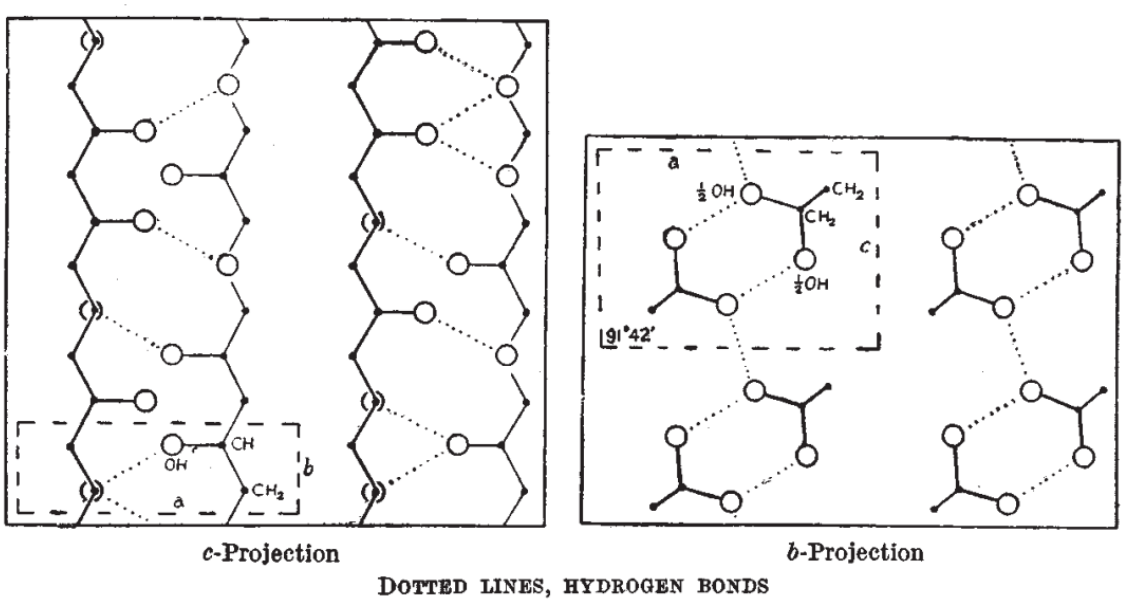

Figure 5-39: Zig zag configuration of hydrogen bonding in PVA structure. Adapted from Courtney et al [285].

A folded structure of PVA chains leads to small ordered regions called crystallites, scattered in a disordered amorphous polymer matrix. The increase in size of crystallites is directly proportional to increase in size of molecular weight [142] and the degree of crystallinity as well as the size of crystallites depends on drying conditions [192]. The molecular weight of PVA was not varied in this study and the crystallite formation was thus only dependent on the freeze-thawing cycles. The results (Table 5-3) showed that two freeze-thaw cycles led to a slightly more stable crystalline structure, indicated by the Tg and % crystallinity calculated, 73.4°C and 69.0% respectively, however the differences were not statistically significant, nevertheless they were different, considering DSC measurements are accurate This data was supported by an earlier study by Hassan et al. 2000 where a similar trend in crystallinity values of PVA 15 wt.% was observed when subjected to three, five and seven cycles of freeze thawing at approximately 60% [154]. It was noted that, increased number of cycles of freeze thawing does not necessarily increase the overall initial degree of crystallinity but

however reinforces the crystals that already exist, therefore enhancing stability of the hydrogels [154].

FTIR spectral analyses revealed crosslinking occurred when the PVA 10% solution was subjected to 1, 2 or 3 cycles of freeze-thawing, however only minor changes could be detected between the spectra with increasing number of freeze-thaw cycles as expected. The main difference was the decrease in the intensity of the O-H band due to loss of water from the consecutive cycles and the sharp intense peak of C-OH absorption band indicated an increase in the crystallinity.

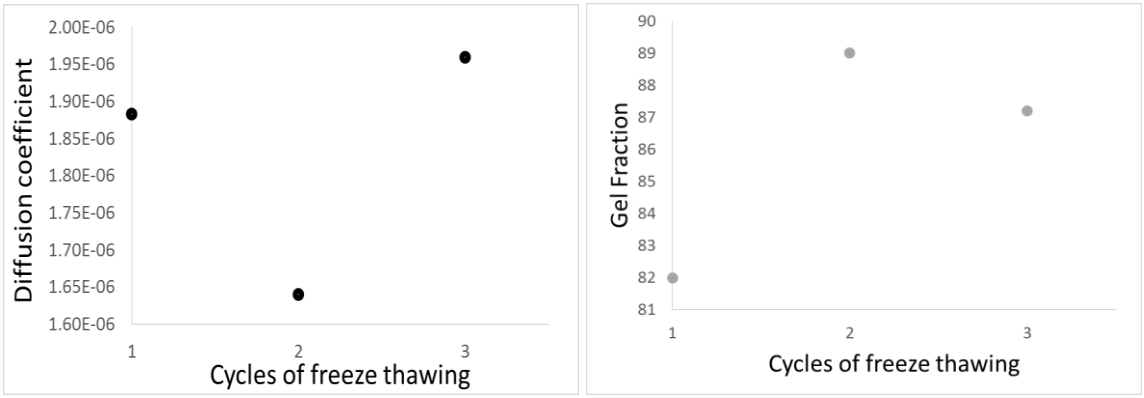

Figure 5-40: Diffusion Coefficient and Gel fraction as a function of number of freeze thaw cycles, carried out in distilled water at 37°C. (n=3)

When a hydrogel is placed in contact with water, it diffuses into the hydrogel resulting in swelling and saturation with water. Diffusion involves migration of water into pre-existing or dynamically formed spaces between the hydrogel polymer chains, whereas swelling of a hydrogel involves a larger scale segmental motion resulting in a bigger separation between the hydrogels. Hence, a critical analysis of the swelling process aids in revealing the underlying molecular processes of hydration and subsequent dehydration. Diffusion coefficients as well as gel fractions were determined to provide further insight on the hydration dynamics of the PVA10 hydrogels, relating directly to the effect of cycles of freeze thawing on the crystalline structure. The lowest diffusion coefficient was observed with two freeze thaw cycles, indicating less diffusion of water ions into the PVA10 hydrogel structure due to the presence of more crystalline regions. The gel fraction of the hydrogels were calculated, therefore PVA chains that were not incorporated into the overall crystalline structure dissolved in solution and thus the

resulting gel fraction indicated percentage of crosslinked regions within the overall PVA structure. Results showed that there was initial dissolution of PVA with all cycles of freeze thawing, due to the PVA chains that did not participate in the crystallite formation process, however the highest gel fraction retained was with two freeze thaw cycles at 89.0%. This supports the findings of the thermal analysis, that enhanced stability is obtained when PVA is subjected to an increased number of freezing thawing cycles (observed with 2FTcycles), but once the limit is reached to which crystallinity can be reinforced, further cycles of freeze thawing impact and reduce the stability of the hydrogel (observed with 3FT cycles).

Synthesis and development of the dual network Hydrogels

Double network gels essentially consist of two interpenetrating networks with contrasting structures, one a densely cross-linked, brittle network of low concentration and the other a lightly cross-linked ductile network of high concentration. The first network is rigid with cross-linked short chains whilst the second network is soft and ductile as illustrated in Figure 5-41, adapted from Gong et al [286]. However one of the requirements to form such networks is that the first network needs to be a strong polyelectrolyte that limits the polymers that maybe used, especially in tissue engineering applications.

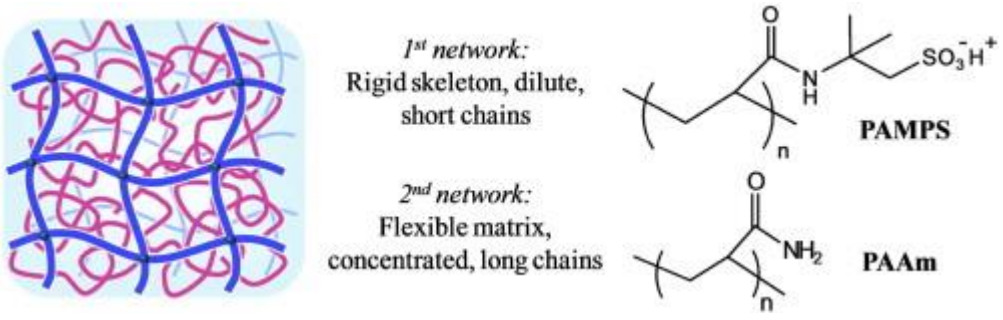

Figure 5-41: A double network with blue strands indicating the first network and pink the second ductile network [286].

More recently, a molecular stent method has been reported by Gong et al [287], proposing a more general method of toughening hydrogels. Unlike DbN gels, the method of synthesis involves using a neutral hydrogel to create the first network and then by swelling it in a linear polyelectrolyte they expand the first network akin to stent. This

occurs as the polyelectrolyte functions as a dangling chain that produces a high osmotic pressure, which leads to high swelling and rigidity of the neutral gel. Our approach of forming 'Dual networks' is analogous to double networks, but use two water soluble polymers where the first network is crosslinked and this is allowed to entrap the second linear polymer, which can be gelated and then subjected to crosslinking. The first polymer is essentially allowed to swell in the second water soluble polymer and chelated followed by crosslinking. Hence, two polymers are used and a new polymer is not synthesized by entrapping the monomers in the first network unlike the double or molecular stent networks.

Dual networks of PVA as a 1st network and alginate as a second network were successfully formed by first forming the PVA network and then the second polymer was allowed to ingress in the network. Dilute solutions of alginate were used such that the high viscosity did not impede diffusion within the polymer network. PVA could be swollen substantially in the second network component due to the ionizable carboxylate groups present in sodium alginate and due to porosity of the PVA network that was formed through freeze-drying. The percentage of alginate within the PVA networks post chelation with $CaCl_2$ and one cycle of freeze drying was obtained by the difference in weight of the PVA xerogel and the xerogel weight of dual network formed. The average overall amount of alginate present was found to be 36% and 23% respectively for PVA 10 and 20 dual networks.

FTIR spectra

The FTIR spectra (Figure 5-12) showed the ionic binding as calcium ions replaced the sodium ions in the alginate blocks, by the shift in the SA peak at 1400 cm^{-1} to 1420 cm^{-1} in the dual network, as well as the development of a more pronounced peak at 1300 cm^{-1}. This indicated that calcium ions were able to penetrate and chelate the alginate within the PVA structure. The second network post cross linking did not show variation in the spectra with the main difference being an increase in the intensity of the 1FT second

crosslinking as compared to the AD+1FT (absorbance range at 1700 – 800 cm^{-1}) in the spectra.

The FTIR spectra of the dual networks also confirmed the presence of the alginate within the network due to the appearance of the ~1600 cm^{-1} carboxylate peaks of SA units and the interaction of PVA and SA molecules as can be observed from the shift in the COO^- peaks from 1418 to 1426 cm^{-1}. Crosslinking between PVA and sodium alginate was indicated by the anti-symmetric stretch of the C-OH in PVA forming a doublet peak in the dual network observed at 1080 and 1026 cm^{-1} revealing the presence of alginate within the structure as well as crosslinking of the PVA, indicating that there may be some interaction between the two polymers.

Thermal analysis

One of the most commonly used methods to estimate polymer–polymer interaction is the determination of the Tg of the polymer networks. The Tg of PVA hydrogels increased from an average of ~72.3°C (Table 5-3) for all the 3 cycles of FT to an average of 162.6°C and 174.4°C (Table 5-9) for DN with a second crosslinking of just 1FT and AD+1FT respectively. A similar finding was reported where blends of PVA and alginate showed a single Tg that increased with alginate concentration. However, the onset of Tg obtained for the dual networks were considerably higher, which was dependent on the concentration of the alginate in the network and a repression in the degree of crystallinity of the crystallizable component was observed due to the presence of the alginate. This increase in glass transition indicates that indeed SA was incorporated within the PVA network structure, as SA has been reported to have and decomposition endothermic peak of close to 200°C [282]. It can be reported that increase in the Tg was due to formation of a tighter network structure on the DN than the PVA only hydrogels. These results were found to be in agreement with data obtained from studies by Kulkarni et al [288] who developed interpenetrating network hydrogel membranes of SA and PVA by solvent casting, and observed a shift in the endothermic peaks of their IPN hydrogels towards a higher temperature. They reported that their observations could be due to “the

formation of more rigid polymeric network as a result of increasing crosslinking and formation of IPN structure due to chain entanglements". Kim et al [143] developed blends of PVA and SA for wound dressing applications via freeze thawing method. They reported that the melting temperature of their hydrogels increased with increasing SA proportion. The dual networks in this study were obtained either solely by a 2nd crosslinking of one cycle of freeze-thawing or subjected to air drying followed by freeze-thawing. The Tg values showed higher values for the latter, which can be attributed to the hydrogels incurring a combination of physical chain entanglements by air-drying in addition to the hydrogen bonding that occurs on freeze drying of the network structures. The DN20-2FT-1FT hydrogel presented with a lower Tg than the DN10 hydrogels, this could be due to limited penetration of SA into the tight and dense network structure of PVA20 single network hydrogel.

Water uptake of hydrogels

Hydrogels have the ability to retain water in their network structure and their affinity to water varies with composition and the polymer architecture. The EWC of the PVA10 hydrogels subjected to 1,2 and 3 FT cycles decreased from an average of ~80.2% to ~70.2 and 71.9% for the dual network hydrogels networks with a second crosslinking of 1FT and AD+1FT respectively (Table 5-4 and Table 5-10). This decrease in EWC was found to be significant enough ($P<0.001$) to indicate that addition of SA to the network structures followed by the different forms of second crosslinking resulted in hydrogels with a tighter network structure than the base single network PVA hydrogels, which would in turn lead to less swelling of the hydrogels in fluids due to the hindered mobility of polymer chains as compared to hydrogels with a loosely cross-linked network structure.

Swelling ratio is negatively related to crosslink density and as with EWC the swelling ratio decreased with addition of SA into the PVA network structure. PVA is known to form hydrogels through freeze-thawing methods that result in porous architecture and it has been reported with PVA-gelatine blends that the swelling ratio decreases with increasing

PVA content, which is explained by the fact that with an increase in PVA concentration, the volume fraction of polymer in the cryogel increases, which enhances the degree of interaction between the PVA–PVA and PVA–gelatine molecules [182]. It was observed that the swelling ratio of the dual networks decreased with addition of SA into the network structure, which can be attributed to both the hydrophilic nature of PVA and the enhanced interaction between the SA and PVA [289]. However, in the dual network SA is first ionically crosslinked with Ca^{2+} ions followed by further crosslinking by either 1FT or AD+1FT, which lead to the rise in crosslink junctions resulting in lower EWC and SR. In agreement with these results is a study by Hua et al. 2010 [283] who reported that their dual crosslinked PVA/SA beads exhibited a lower swelling rate than the PVA/SA beads crosslinked by $CaCl_2$. Also Chhatri et al. 2011 [144], fabricated PVA and alginate blends via freeze thawing and reported that swelling ratio of their hydrogels decreased with increase in concentration of PVA within their blends, which is in agreement with results from this study where the water uptake of the PVA and DN hydrogels decreased with increase in PVA concentration.

Figure 5-16 and Figure 5-17 present typical plots of the behaviour of water absorption and desorption versus $t^{1/2}$ for the PVA10, 20 and DN10, 20 hydrogels subjected to two FT cycles. The initial stages of absorption and desorption conformed well to a linear $t^{1/2}$ relationship, the slope of which enabled the calculation of the diffusion coefficients.

Diffusion coefficient of the hydrogels indicated that there was limited migration of water molecules into the pre-existing spaces of the dual network hydrogels as compared to the PVA base hydrogel. These values decrease from an average of ~1.8 ($10^{-6}cm^2s^{-1}$) in PVA to ~0.5 and 0.7($10^{-6}cm^2s^{-1}$) for the DN networks with 1FT and AD+1FT second crosslinking.

The influence of addition of SA to the network on gel fraction was also investigated, the average gel fraction in the absence of SA was found to be ~86.1% for all the cycles of FT, this being relatively high suggesting PVA was almost completely crosslinked. With incorporation of SA the average gel fraction was found to be ~73.3% and 72.3% for the DN networks with 1FT and AD+1FT second crosslinking respectively. This result on

reduction of gel fraction with incorporation of SA may be due to the loss of unchelated and unreacted alginate within the network structure, this trend in results was found to be in agreement with results reported in a study by Kim et al. 2008 [143] on PVA alginate blends. Furthermore the cycles of FT did not show a significant difference in gel fraction within the different groups. Generally, with a decrease in gel fraction, hydrogels are weak and less flexible, however the EWC, SR and diffusion coefficient in this study indicated that this is not the case.

Increase in concentration of PVA from 10%(w/v) to 20%(w/v) resulted in decreased EWC and SR as well as increase in gel fraction as compared to the PVA10 and DN10 hydrogels. This is can be attributed to the increase in the interaction between the alginate and PVA due to the presence of higher number of hydroxyl groups available for interaction.

Hydrolytic degradation of hydrogels

Hydrogels can slowly degrade under physiological conditions due to hydrolytic or enzymatic chain breakages occurring within the network chains of the hydrogels, but under controlled in vitro conditions degradation is mainly due to breakdown of weak crosslinks between polymer chains. PVA, crosslinked by physical means can undergo dissolution with time via the breakdown of the crosslinks. Likewise calcium alginates breakdown fairly rapidly as the process of chelation is reversible and in presence of sodium ions this can slowly be reversed resulting in the dissolution and elimination of the product by the renal pathway.

Weight loss in phosphate buffer saline was monitored to determine the disintegration of the networks and evaluate the effect of the dual network formation. Figure 5-18, Figure 5-19 and Figure 5-20 show typical plots of weight loss (%) as a function of time, with the dual network hydrogels exhibiting a higher weight loss than the PVA10, 20 hydrogels. This is attributed to the presence of the calcium alginate chains, which probably begins to go through the reversible reaction forming sodium alginate that is subsequently lost. However the DN20-2FT-1FT hydrogel exhibited lower degradation values as compared

the to all the dual network hydrogels, this is attributed to the higher concentration of PVA that leads to the interaction of carboxylate groups of the alginate to form more H bonded links with the hydroxyl groups of the PVA due to their higher abundance in the network structure, which is also in agreement with the EWC and swelling ratio obtained

Generally hydrogels with lower crosslinking density undergo degradation at a faster rate while those with higher crosslink density degrade at a slower rate. Higher overall degradation of the dual networks is attributed to the early degradation of alginate in the network structure, although the alginate has been crosslinked twice ionically and covalently by either FT or AD+FT, these crosslink junctions are weaker than those of the OH bonds within the PVA hydrogels. Similar observations were reported in studies on PVA-Alginate blends by Hau et al. 2010 [283], Kamoun et al. 2015 [162] and IPN networks by Thankam et al. 2013 [284].

Tensile strength and modulus

The hydrogels obtained by freeze-thawing 10% PVA exhibited statistically significantly lower tensile strength ($P<0.001$) than all the dual networks irrespective of the number of FT cycles. The presence of alginate in the PVA network to form a dual network led to significant improvement in the tensile strength of the hydrogels, which is attributed to the interpenetration of alginate into the PVA structure, followed by its chelation and subsequent crosslinking within that structure. This crosslinked interpenetration within PVA by alginate may have led to the formation of hydrogen bonds between the hydroxyl groups of PVA and the hydroxyl groups of the alginate network, this resulting in enhanced tensile properties of the dual network hydrogels.

When evaluating the effect of the different types of the second crosslinking on the tensile properties, it was found that AD+1FT did not significantly enhance the tensile strength as compared to only 1FT crosslinking. Analysis on the effect of number of FT cycles within each group of the individual groups (PVA only network, DN-1FT, DN-AD+1FT), showed that PVA and DN-AD+1FT hydrogels were found to have tensile strength values with no significant difference between freeze thaw cycles within each group, whereas two FT

cycles of DN-1FT hydrogels yielded superior tensile strength (0.73MPa) significantly higher ($P<0.001$) than all the hydrogels. It would be expected that increasing the number of freeze thaw cycles (degree of crosslinking in the networks) would result in higher ultimate tensile strength, however it has been observed from the results that a higher degree of crosslinking i.e. cycles of FT greater than 2FT results in a more brittle network structure, hence the lowered UTS. PVA-alginate blends for wound dressings have been reported by Kim et al. 2008 [143] where they found the addition of SA into blends resulted in decrease in tensile strength of their hydrogels with UTS values of 0.07MPa with *E* of ~0.009MPa for 5%(w/w%) and 3%(w/v) of SA. Xie et al. 2012 [289] reported a similar observation with a drop in tensile strength of their PVA-SA blends with addition of SA to PVA. Their highest recorded tensile strength was with blends containing 25 % SA with 4FT cycles 0.2MPa. A comparison of the blends with the dual networks also clearly indicate that the formation of a dual network has a significant effect on the tensile properties and it is the first brittle network that has a bearing on the tensile properties as is evident with the higher concentration of PVA. Kulkarni et al. 2010 [288] formed IPN's of PVA and SA for drug release and found that tensile strength improved with the formation of IPN networks with maximum UTS values of ~0.4MPa, whilst Gnanaprakasam et al. 2013 whose study on growth and survival of cells on biosynthetic PVA and SA reported a similar trend with tensile values of semi IPN and IPN hydrogel network of 0.8 MPa (disodium hydrogen phosphate and Ca^{2+} crosslinks) and 1.2MPa (3% glutaradehyde crosslink) respectively [284]. These values were significantly lower than that obtained for the dual networks in this study that were above 4MPa.

Stiffness of the hydrogels was found to increase with formation of the dual networks, with no significant difference between the two methods of the second crosslinking used in formation of the dual networks. The typical stress strain curve of the hydrogels illustrated in Figure 5-23 indicates that hydrogels had the ability to undergo strains of ~≥1 (mm/mm). Figure 5-24 Figure 5-25 and Figure 5-26 demonstrate that hydrogels with higher tensile strength and stiffness can be achieved by increasing concentration of

PVA, however there is a limitation of increasing the concentration that yields high viscosity solutions not conducive for handling.

Fracture toughness

Fracture properties are related to specific material parameters such as critical fracture toughness, energy release rate, fracture energy and crack propagation resistance which can be determined using a fracture mechanical test method such as a trouser tear test. Tearing energy includes surface energy, energy dissipated in plastic flow processes, and energy dissipated irreversibly in viscoelastic processes.

Fracture energies of the hydrogels showed that (Figure 5-27), the PVA 20 dual network (DN20-2FT-1FT) had a statistically significantly ($P<0.001$) highest fracture energy (6.3 KJ/m^2) in comparison to its base PVA20 hydrogel as well as the PVA10 hydrogel and their corresponding dual network. This was within expectations as tensile strength tests indicated that increase in concentration of PVA lead to significantly higher strengths as well as incorporation of SA into the PVA base network structure. The opposite result however was observed with the PVA10 dual network where a lower fracture energy was obtained than its parent base PVA10 hydrogel. This could be attributed to the fact that more alginate is absorbed in the PVA10 network structure as compared to the PVA20, and with alginate being weaker than PVA in turn resulted in a decreased fracture toughness. Fracture toughness energies obtained in this study were compared with those obtained from double network hydrogels and the toughness values of the dual networks were ~≥ 2 fold than those reported in literature [290, 291].

In vitro drug release study

The dual networks developed exhibited properties that ere suited for potential wound dressing applications, hence a preliminary study using vancomycin was carried out. Vancomycin is a commonly effective antibiotic, recommended for chronic wounds, including those with moderate to severe osteomyelitis, is highly effective against gram positive bacteria and used in hospital epidemics as a first line of defence against deadly

resistant streptococcal and staphylococcal strains such as *Staphylococcus aureus*, which are becoming resistant to penicillin, methicillin and other b-lactam antibiotics[163-165].

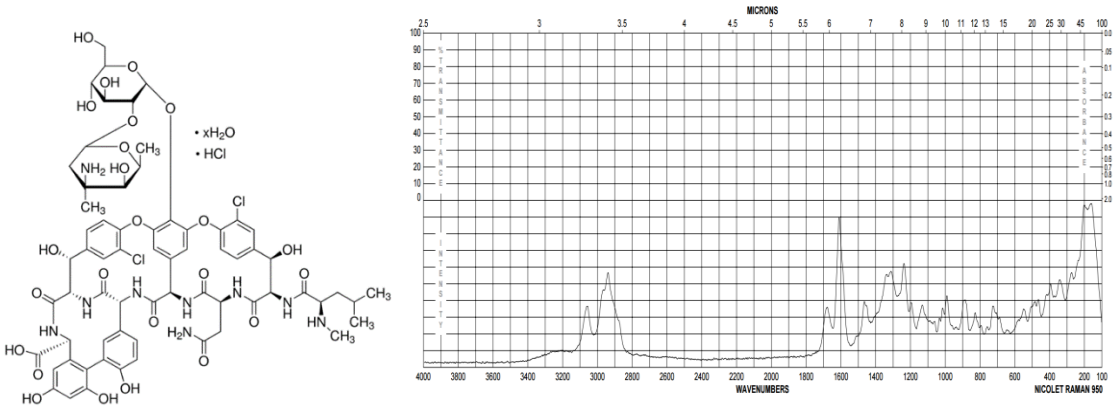

Figure 5-42: Molecular structure of vancomycin hydrochloride and FT Raman spectra [Source: Sigma Aldrich].

Drug and polymer Interaction

Vancomycin has a complex structure consisting of a seven membered peptide chain linked to two unique sugar moieties. The drug is known to bind to peptides and polymer surfaces, as well as act at a chelator. Vancomycin has also been reported to dimerize with itself specifically due to amide-amide hydrogen bonding, hydrophobic and ionic interactions, therefore it is expected to have hydrogen bonding as well as hydrophobic interactions with alginate. The drug and polymer interaction was studied by FTIR analysis represented on Figure 5-28 and Figure 5-29, where it was observed than not only was vancomycin incorporated into the network structures of the hydrogels, there were also some interactions as shifts in the intensity of the C=O, C-H symmetric peaks in PVA were observed along with the COO- symmetric and C-O-C stretching in the dual networks.

In-vitro drug release profile

Figure 5-31 and Figure 5-32 illustrate the release profile of entrapped vancomycin within the hydrogels. A linear (high) release rate is observed with the PVA10 single network hydrogels with up to 59% vancomycin being released from the hydrogels within the first 8

hours. This linear release is attributed to the porous structure of the PVA10 hydrogels attained during the sublimation process of water ice crystals within the network. This then in turn led to a large surface area of the hydrogel exposed to dissolution of the vancomycin drug into the PBS solution. Increase in concentration of PVA10 to PVA20 led to a decrease in total drug released (27%) after 500 minutes, this due to the dense network structure of PVA formed off higher concentrations.

DNs presented with lower drug release rate with a maximum of ~27% after 500minutes, this attributed to the tight interpenetrating network structure attained in formation of the dual networks as well as reduced porosity within those networks, thereby hindering the transport of drug molecules through the membrane. It was observed that drug release rate is closely related to EWC and SR of the hydrogels, therefor the higher the swelling ratio of the hydrogel the higher the %drug release and vice versa. Similar observations have been reported in other studies, where Kulkarni et al reported that their PVA hydrogels loaded with prazosin hydrochloride showed a maximum release of ~ 99.3% after 12 h, with a high release rate observed in the initial hours, where as their PVA/SA IPN membranes had an extended drug release for up to 24 h. They also reported that the drug release in their hydrogels decreased with increase in PVA concentration [288]. Hau et al reported that their dual crosslinked beads (chelated blend of PVA/SA subjected to 2 cycles of freeze thawing) showed a lower initial drug release profile of diclofenac sodium as compared to the PVA/SA $CaCl_2$ crosslinked beads [283]. Variation of freeze thaw cycles in this study did not show a significant difference in drug release rates within the individual groups.

It has been reported that high initial linear drug release profiles are useful for immediate irradication of bacteria while slower release profiles are appropriate for preventing infection or recolonisation of the wound by bacteria [163]. Therefore the initial linear followed by slower drug release profile of the DN hydrogels would prove suitable for simultaneously irradicating an existing infection while preventing recolonisation of the wound by bacteria.

SEM analysis

SEM (Figure 5-33) identified crystallite domain in the PVA 10 hydrogels post freeze-thawing, which is expected and in agreement with literature as PVA forms crosslinks via hydrogen bonding and crystallite formation. The higher magnification identifies fibrous strands in the PVA10 hydrogels as well as micropores. This observation supports the high EWC and SR results obtained in the hydration studies. PVA20 micrograph displays a dense network structure with no to much lower porosity, which is in agreement with the low EWC and SR results. The dual networks in contrast show a fibrillar morphology, with entwined fibrils and there is appearance of a difference in the morphology within the network. The fracture tensile surfaces of the dual networks indicate a ductile fracture compared to PVA networks that show a brittle fracture. This observation is in agreement with results obtained from tensile test where strains of the hydrogels were >1 mm/mm

The differences in the appearance of the PVA10 and 20 hydrogels is that (this may not be clearly visible with SEM images but is demonstrated with images of the hydrogels), PVA10 hydrogels appear to be more opaque in nature whereas the PVA20 hydrogels appear to be translucent. This difference in appearance was also reported in another study[200], which can be explained by the fact that the polymer solution is less viscous with low concentration of PVA therefore there is less restriction on the movement of the PVA chains in solution thus making it easier for them to crystallise more effectively. This results in a hydrogel with large crystallites that scatter more visible light which makes the hydrogels look opaque (will however have a lower crystallinity than hydrogel of higher polymer content). Increase in PVA concentration results in an aqueous solution with high viscosity and more PVA chains to form crystallites, however the crystallite size decreases as there will be restricted growth and therefore scatters less visible light which translucent hydrogels [200].

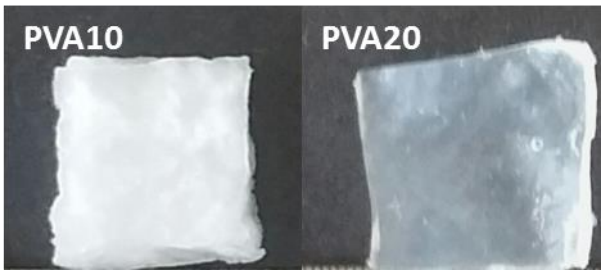

Figure 5-43: picture image of freeze thawed PVA hydrogels with 10 and 20%w/v concentration, demonstrating the difference in final appearance of the hydrogels.

Cytocompatibility

Cell proliferation and viability of seeded cells on the elusion extracts the hydrogels was quantitatively assessed by **MTT assay**. Relative growth rate of the HOB cells was calculate from the average optical density (OD) values.

$$Relative\ growth\ rate\ (RGR) = \left[\frac{average\ of\ tested\ group\ OD\ -\ average\ of\ blank\ control\ OD}{(\text{average of negative control OD}\ -\ \text{average of blank control OD})}\right] \times 100\%$$

Hydrogel System	Eluents (hr)	Relative growth rate (RGR)(%)		
		24 exposure	48 exposure	72 exposure
PVA10-2FT	24	65.6	45.4	45.2
	48	63.5	45.2	42.6
	72	84.2	52.4	59.8
DN10-2FT-1FT	24	98.2	58.9	47.7
	48	75.9	50.7	37.0
	72	97.9	54.2	38.6

Table 5-11: Relative growth rate percentage of PVA10-2FT and DN10-2FT-1FT demonstrating viability of HOB cells within the hydrogels.

Where:

Non-cytotoxic >90% cell viability;

Slightly cytotoxic = 60–90% cell viability;

Moderately cytotoxic = 30–59% cell viability;

Severely cytotoxic ≤30% cell viability

24hr exposure to 24, 48 and 72hr eluents indicated that the HOB cells found the degradation products of the hydrogels to be slightly toxic increasing to moderately toxic with 48 and 72 hour exposure. These results are contradictory to those obtained in a study by Gnanaprakasam et al. 2013 [284], where they reported a higher viability of

fibroblast cells on their hydrogel extracts indicating that the degradation products for their PVA-alginate IPN were not toxic.

However **live/dead staining** over a period of 28 days (Figure 5-35 and Figure 5-36) showed that HOB cell were able migrate from the surface into the internal structure of the hydrogels. Difficulty was encountered when imaging, as cell were at different depths within the hydrogels and change in focus and magnification led the cells at different depth going out of focus. This illustrates and confirms the ability of the hydrogels to not only present as biocompatible, with good cell adhesion and attachment, but also the ability of the cells to migrate and proliferate within the hydrogel networks. Earlier time point observation (day 1-14) of the cell morphology showed cells aggregating to form bollus shape, cells of which later spread out along the surface of the hydrogel, beginning to form a sheet like structure over the surface as observed with the DN on Figure 5-36 x20magnification. Literature reports that surface aspects of a biomaterial such as, topography, chemistry and surface energy determine cell behaviour upon contact. Cells in contact with a surface will first attach, adhere and spread, the quality of adhesion will influence their morphology and their capacity to proliferate and differentiate [166].

Active proliferation of HOB cells occurs within the first 10-12 days, from 12 to 18 days the extra cellular matrix undergoes a series of modifications in composition and organisation that renders it competent for mineralisation. During this matrix maturation phase, every cell becomes alkaline phosphatase positive **(ALP)** [169, 170]. Hence ALP concentrations on cell supernatants were determined and presented on Figure 5-37. Control and hydrogel samples indicated a sharp increase in ALP at day 14. The dual networks presented with a higher increase in ALP production than the PVA10 only hydrogels. This indicates that the HOB cells in culture were on the onset of progression to the next phase being mineralisation. This observation is a reflection of functional activities of the HOB cells necessary for the progressive formation of bone tissue.

Runx2 is down regulated in mature osteoblasts during bone development, meaning that Runx2 expression increases during osteoblast differentiation validating involvement in maturation of osteoblasts. Results (Figure 5-38) were found to be inconclusive however,

results indicated an increase in expression of DN10-2FT-1FT from day 7 to 14, which indicated an increase in osteoblast differentiation, this was followed by a decrease after day 21 indicating that the osteoblast on the hydrogels may be maturing.

Applications of the formed hydrogels

Given the properties of the fabricated dual network hydrogels, various applications are proposed where the hydrogels can integrate with surrounding tissues and induce new tissue formation: hydrogels can be loaded with soluble signalling molecules such as bone morphogenetic proteins or platelet rich plasma as well as antibiotics, and be used in areas such as wound dressing.

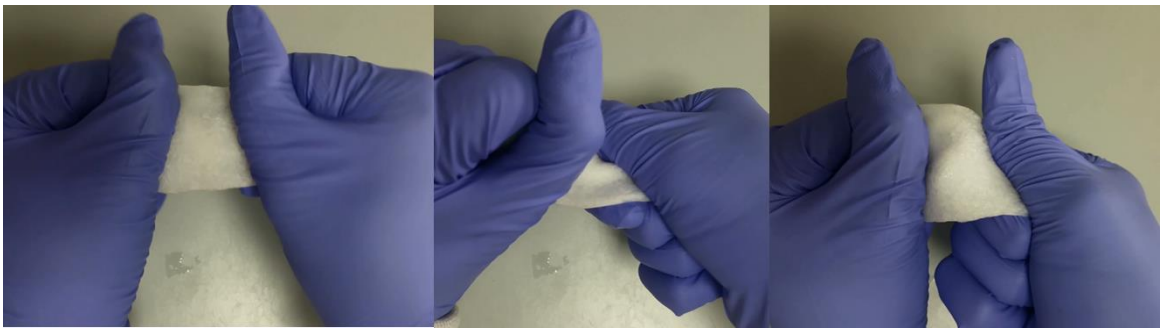

Figure 5-44: Picture images illustrating the nature and flexibility of the dual network hydrogels.

With addition of a calcium phosphate filler and increase in PVA concentration dual network hydrogels can be used for osteochondral defect applications, as well as in areas of bone repair where stimulation of bone regeneration is required. It can also be noted that to allow for enhanced cell attachment and proliferation, peptide-coupled alginates can be used for the formation of dual network hydrogels [292].

5.6 CONCLUSION

The present study demonstrated that dual network hydrogels of PVA and alginate can be successfully and easily fabricated as well as be tailored to desired tensile strength and stiffness.

The methodology was optimised and showed that two cycles of freeze-thawing yielded optimum properties of DNs demonstrated by higher UTS than their base PVA hydrogel

or counterpart AD+1FT hydrogels, also confirmed by their lower EWC and higher Tg. The hydrogels were also characterised by FTIR and SEM. SEM images of the hydrogels showed a clear difference in their morphologies. This approach in fabricating dual network hydrogels could be useful and properties tailored for applications in different biomedical fields such as drug delivery or soft tissue engineering purposes. Additionally this hydrogel network system can be incorporated with fillers such as calcium phosphates and bioglass to further advance their development for applications in wider fields such as bone tissue regeneration.

Chapter 6
Dual network composite bone grafts

6.1 INTRODUCTION

Single network hydrogels have been studied extensively for biomedical applications [9], however the focus in the last decade has been on enhancing the mechanical properties to favour cell based applications. The mechanical properties of hydrogels formed solely via physical interactions are usually too weak for application in load bearing tissues, thus new platforms are required to create hydrogels with diverse chemical composition and physical properties to satisfy the demands of different cell types and tissues.

This has led to the synthesis of a range of different type of smart hydrogels that have different interpenetrating polymer architectures. Double networks are being increasingly investigated as a convenient method of synthesizing tougher hydrogels. The mechanical properties of hydrogels can be enhanced by the generation of a double-network and this approach can produce hydrogels that are considerably tougher than the corresponding single-network gels, with optimised double-network hydrogels that are hard (0.1–1 MPa), strong (tensile stress 1–10 MPa, compressive stress 20–60 MPa), tough (tearing fracture energy 100–9000 J m^{-2}), and the ability to be stretched up to 20 times their own length [293, 294]. Double-network combinations including poly(2-acrylamido-2-mehtylpropanesulfonic acid), alginate, or poly(ethylene oxide) (PEO) as the highly cross-linked first network with poly(acrylamide) or poly(acrylic acid) (combined with PEO) as the loosely cross-linked second network have been reported for cartilage repair due to its tissue like properties [68, 293, 295]. Double networks as described earlier (Chapter 5) utilize two interpenetrating networks with contrasting structures; one which is a densely crosslinked polyelectrolyte to imbibe the brittle characteristics which is then interpenetrated with second ductile network having a low degree of crosslinking. In our approach, we use the same concept but use two water soluble polymers where the first

network is crosslinked and this is allowed to entrap the second linear polymer that can be crosslinked under physiological conditions, hence we term it as a ‘dual network’. Based on this concept, novel dual hydrogel networks formed using PVA and sodium alginate were designed to form for the first time novel composites for bone regeneration. A totally novel approach has been used to form composites with bioactive fillers specifically using 45S5Bioglass® as the filler due to the established ability of this glass to bond with bone [296].

Bioactive glass: The composition of bioactive glasses typically includes, Na_2O-CaO-SiO_2 with addition of P_2O_5, MgO and CaF_2 in the system. The glass compositions are denoted with names that signify the wt. % of silica in the network for example the ratio of Ca/P in Bioglass® 45S5 is 5 to 1. These compositional features make the surface highly reactive when exposed to an aqueous medium and therefore lead to in vitro and in vivo bioactivity [297]. All the bioactive materials developed form mechanically strong bonds with bone however the rate of bone bonding depends on the composition of the material as lower molar ratios do not bond to bone. Examples of common bioactive glass compositions are presented on Table 6-1.

	45S5	52S4.6	55S4.3	58S Sol-gel glass	S53P4	A-W Glass-ceramic
SiO_2	45	52	55	60	53	34
P_2O_5	6	6	6	4	4	16.2
CaO	24.5	21	19.5	36	20	44.7
CaF_2					0	0.5
MgO					0	4.6
Na_2O	24.5	21	19.5		23	0
Phases	Glass				Glass	Apatite β-wollastonite glass
Class of bioactivity	A				A	B

Table 6-1: Composition of bioactive glasses and glass-ceramics (wt. %) used clinically for medical and dental applications.

Class A bioactivity is reported to lead to both osteoconduction and osteostimulation as a consequence of rapid reactions on the bioactive glass surface. Therefore, compositions of bio active glass such as 45S5 are reported to have the highest rate of bioactivity, hence result in the fastest rate of bone bonding as well as bonding to soft tissues [298]. This mechanism of bonding is attributed to the formation of a hydroxycarbonate apatite (HCA) layer on the surface of the glass, following glass dissolution [299, 300].

Bioactive bioceramic materials have found many clinical applications in orthopaedic and dental areas, where they have been used as bone grafts as well as powders to fill various types of bone defects, and implant coatings. It has been reported that Bioglass® 45S5 has been used in more than a million patients to repair bone defects in the jaw and orthopaedic application [301]. Bioglass® currently finds use in a number of clinical applications and more than a dozen commercial products either solely composed of bioglass or adapted with binders (i.e. Perioglass® [302] and NovaBone® [303]). The use in tooth pastes such as Novamin (2004) [300] which are designed to occlude dental

tubles and remineralise the surface of the teeth thereby eliminating the cause for dental hypersensitivity.

BIOGLASS® COMPOSITES

Using bioceramics as a reinforcing phase in polymeric composites was first introduced by Bonfield et al [304], wherein polyethylene was reinforced with hydroxyapatite to form bone analogue materials. The inclusion of Bioglass® 45S5 to form composites was later investigated due to the bioactivity conferred, however there were concerns related to the glass particles being smeared by the polymer during processing that would hamper bioactivity. The inclusion of Bioglass® in polymers can increase the stiffness and compressive strength to an extent, since polymeric scaffolds usually tend to have low strength and bioactivity. Bioglass® on the other hand has low fracture toughness, is brittle when used alone. In order to mitigate this structural weakness various methods have been employed for fabricating porous composite scaffolds with tuned pore sizes and interconnectivity. Some of the common methods used in fabrication of porous Bioglass® scaffolds include particulate leaching, Solid free form (SFF) and replication technique (Sponge method) [305] as these provide more reproducible scaffolds with control over structural properties.

Bioglass® has been reported in composite formulations with polymer matrices such as polylactide (PLA), polyglycolide (PGA) and their copolymers (PLGA), as well as poly - caprolactone (PCL) [306]. Cannillo et al, fabricated PCL-Bioglass® 45S5 composites via salt leaching technique and to develop scaffolds with good interconnected porosity, suited for bone regeneration and vascularisation, however due to the porogen removal process in water, these composites had supressed development of HA in vitro [307]. Another study on Bioglass® nano particles (5–20wt.%) with PCL fabricated via particle leaching and freeze extraction using polyethylmethacrylate (PEMA) beads as a porogen, resulted in porous composites with 0.04 - 0.12MPa strength in compression, and with low Bioglass content exhibited higher yield strength but a larger filler content resulted in decrease in yield strength, which was lower than that of the parent polymer [264].

Ryszkowska et al, fabricated porous polyurethane composites containing 5-20wt. % of Bioglass® via polymer coagulation and salt leaching method. Their composites showed a higher storage modulus (0.12 – 0.81 MPa) than the parent polyurethane foams, and they were able to achieve good formation of HCA layer in SBF [308].

Limitations of current Bioglass® materials and composites

Bioglass® 45S5 remains the gold standard within the class of bioactive glasses but as a material it has limitations in that:

- They cannot be made into amorphous bioactive glass scaffolds because they crystallize during sintering, due to the narrow window between Tg and onset of crystallisation for 45S5, this makes it difficult to fabricate porous structures by sintering which would bond particles into a strong glass phase creating inter connected porous 3D structures.
- Glass devitrification during sintering results in the formation of a predominantly crystalline phase (Na_2O-2CaO-3SiO_2), which results in reduced rate of conversion to HA. Slow degradation rate and conversion to an HA like material makes it difficult to match the degradation rate of the scaffold with the rate of new tissue formation [298].

The rationale for this study is to develop an osteoconductive bone substitute with good structural properties that can be combined with an osteoinductive biological stimulus. Thus, to enhance the elastic and expandable properties of the composites, in addition to localising orthobiologic factors with controlled swelling, dual networks were selected as the matrix and 45S5Bioglass® was the filler to form bone substitutes. The dual network was established to be a tough interpenetrating polymer network as detailed in Chapter 5 provides an added advantage to the continuous phase of the composite. The type of filler that can be incorporated in the hydrogel network is not limited to just Bioglass® but encompasses the various forms of calcium phosphates as well as bioactive glasses but

the current study was limited to the use of 45S5 Bioglass® to understand the mechanical and physical features of these novel composites

Objectives of the study

- To develop a biocompatible and bioactive dual network Bioglass® composite with an interconnected porous structure, designed to allow fluid flow, cell migration, bone ingrowth and vascularisation.
- To characterise the mechanical properties and understand the physical features of these novel systems prior to in vivo testing.
- The ability to promote osteogenic cell attachment and osteogenesis.

6.2 MATERIALS AND METHODS

MATERIAL	CONCENTRATION
PVA	10 & 20wt./v
Sodium alginate	2%wt./v
Bioglass® 45S5	30%wt with respect to PVA
Porogen	10%wt with respect to PVA

Table 6-2: The concentration of the precursors for fabrication of the experimental composites.

Hydrogel composites were prepared by thoroughly mixing a solution of PVA with Bioglass® 45S5 using a magnetic stirrer for at-least an hour until a homogenous mixture with a slurry like consistency was obtained. This was then subjected to 1, 2, and 3 cycles of freeze thawing at -59.4°C, vacuum 17mT for 24hrs. The physically crosslinked hydrogels were swollen in a solution of sodium alginate until equilibrium was reached and chelated with a 10% solution of calcium chloride. The hydrogel composites were then further crosslinked by 1 freeze thaw cycle.

Acronym of composite	Description of formulation composition of the composites
DN10-(1, 2 or 3FT)BG	PVA10 network incorporated with Bioglass® subjected to a 1st crosslinking of either 1, 2 or 3 cycles of FT followed by a 2nd crosslinking of 1 cyle of FT after swelling in alginate and chelation with $CaCl_2$.
DN10-2FTBG-10%Porogen	PVA10 network incorporated with Bioglass®, subjected to a 1st crosslinking of 2 FT and a 2nd crosslinking of 1FT after swelling in alginate and chelation with $CaCl_2$. The composite contains 10% porogen with respect to PVA content.
DN20-BG-10%Porogen	PVA20 network incorporated with Bioglass®, subjected to a 1st crosslinking of 2 FT and a 2nd crosslinking of 1FT after swelling in alginate and chelation with $CaCl_2$. The composite contains 10% porogen with respect to PVA content.

Table 6-3: Description of formulation composition ascribed to the acronyms used for different composite formulations in this chapter.

6.3 CHARACTERISATION

Particle size analysis

The particle size of the ceramic 45S5 Bioglass® phase was analysed. The experimental procedure is detailed in the materials and method section of chapter 4.

FTIR spectroscopy

FTIR was used to characterize the presence of specific chemical groups in the PVA/Bioglass® hydrogel composites, reflecting the effectiveness of the method used to fabricate them. FTIR spectra were obtained within the range between 4000 and 400 cm^{-1} (Perkin–Elmer, Paragon 1000), using diffuse reflectance spectroscopy method (DRIFTS-FTIR). The experimental details are similar as detailed in the materials and method section of chapter 3.

Raman spectroscopy

The Raman spectra of the hydrogels composites were recorded on a Renishaw Invia Raman microscope. The experimental procedure is detailed in the materials and method section of chapter 3.

DSC analysis

DSC thermograms of the composite samples were recorded on a PerkinElmer DSC jade analyser, as detailed in the materials and method section of chapter 3.

Equilibrium Water Content (EWC)

The hydration studies were performed as detailed in the materials and method section of chapter 3 and 5.

Ultimate Tensile Strength

The tensile strength was determined using the methodology as detailed in the materials and method section of chapter 3.

Trouser Tear test

The toughness of the hydrogel composites was determined using the methodology as detailed in the materials and method section of chapter 5.

Compression & cyclic compression

Compression tests were carried out on samples that were hydrated to equilibrium. Cylindrical specimens with dimensions *d=8, h=5* were tested in compression using a universal testing machine (Instron 5569A) with a 500N load cell and cross head speed of 1mm/min.

Cyclic compression was carried out at 40% strain and rate 0.01MPa/sec.

SEM-EDAX analysis

The morphology was determined using the methodology as detailed in the materials and method section of chapter 3.

BIOACTIVITY OF COMPOSITES (MINERALISATION)

The simulated body fluid (SBF) solution was prepared by following the recipe reported by Kokubu and co-workers [309], which was used to conduct mineralisation studies of the composites due to its similarity in ionic concentration to that of human plasma.

Briefly reagents from 1 to 8 were dissolved one by one in distilled water at 37°C, reagents 9 and 10 were dissolved in small amounts with care taken not to exceed pH 7.45. Samples were then placed in SBF solution which was maintained at 37°C. At periodic intervals samples were removed from the solution and analysed for desired characterisations i.e. tensile, cyclic compression, FTIR, Raman SEM and EDAX. The immersion medium, SBF was refreshed weekly to better simulate in vivo conditions by maintaining the ionic concentration of the solution.

Order	Reagent	Amount (g)
1	NaCl	8.035
2	$NaHCO_3$	0.355
3	KCL	0.225
4	$K_2HPO_4 \cdot 3H_2O$	0.231
5	$MgCl_2 \cdot 6H_2O$	0.311
6	1.0M HCl	39ml
7	$CaCl_2$	0.292
8	Na_2SO_4	0.072
9	Tris	6.118
10	1.0M HCl	0-5ml

Table 6-4: The reagents listed in order of mixing used to prepare 1000ml of SBF.

CYTOCOMPATIBILITY

MTT, Live/Dead Staining, Protein concentration, qPCR

Biocompatibility of the hydrogel composites was determined using the methodology as detailed in the materials and method section of chapter 5.

6.4 RESULTS

Particle size distribution

The particle size distribution percentiles (10, 50 and 90 %) of Bioglass® 45S5 powder are presented in Table 6-5, whilst the histogram of particle size distribution and the cumulative percentage of the data are shown in Figure 6-1. The histogram of the tested powder exhibited a normal distribution.

	Diameter at 10% (µm)	Diameter at 50% (µm)	Diameter at 90% (µm)
Bioglass 45S5	1.4	7.2	17.1

Table 6-5: Particle size distribution of bioglass® 45S5 powder.

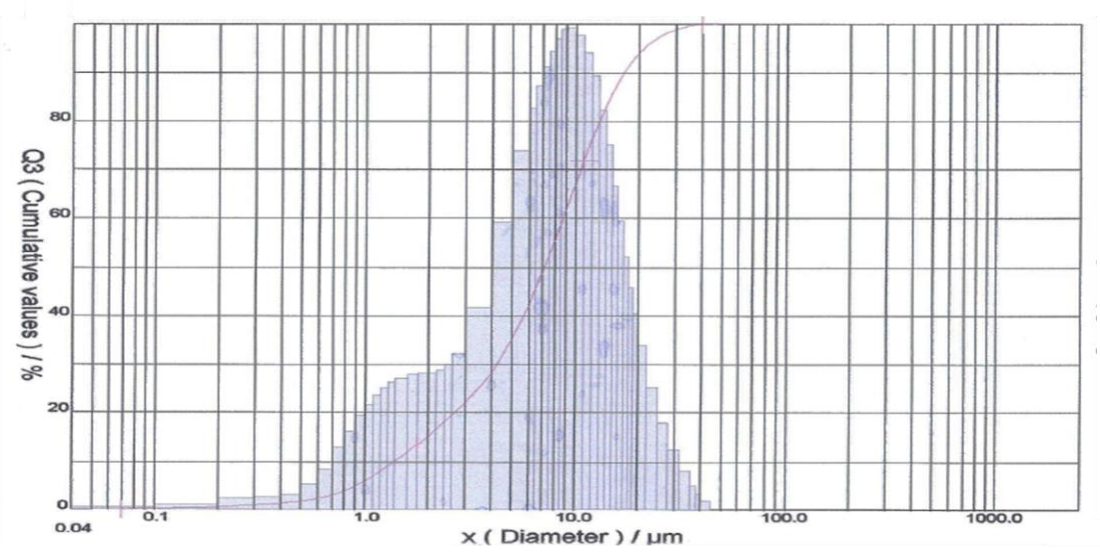

Figure 6-1: The particle size distribution of 45S5 Bioglass powder in cumulative percentage (red line) and in frequency percentage (bars).

FTIR analysis

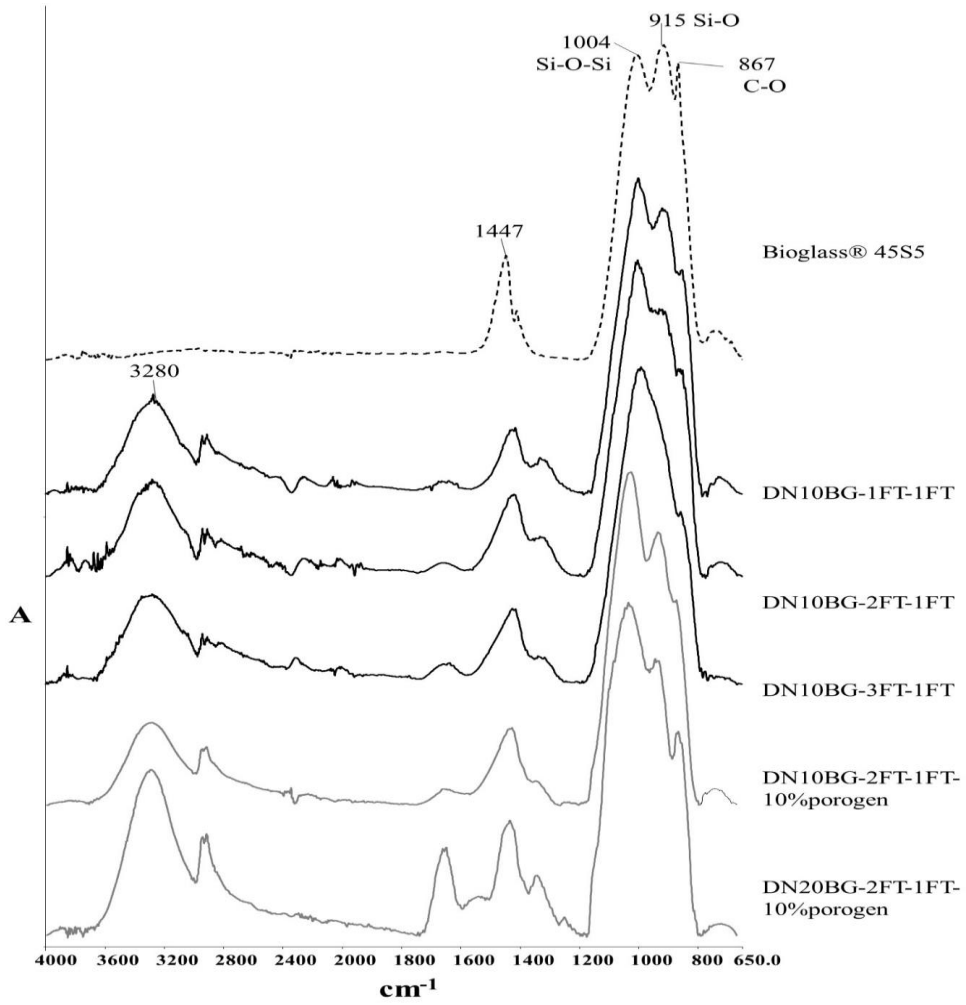

Figure 6-2: FTIR spectra comparing Bioglass® powder with the non-porous dual network bioglass composites fabricated by 1,2 and 3 freeze thaw cycles and the porous dual network composites of PVA concentration (10 and 20)wt.%, fabricated by two cycles of freeze thawing.

The FTIR spectra of the dual network Bioglass® composites with and without the porogen showed strong absorption peaks at 1004 and 915 cm^{-1}, attributed to Si-O-Si and Si-O stretching modes respectively. The Si-O-Si bending mode and the amorphous phosphate is not apparent in this spectra as the scales were till 650 cm^{-1} but are expected at 480 and 600 cm^{-1} respectively [310]. The characteristic absorption bands of PVA at 3280 cm^{-1}, 2946 cm^{-1}, 2908 cm^{-1}, was attributed to the stretching of OH, asymmetric stretching of $-CH_2$ and symmetric stretching of $-CH_2$. Absorption bands also arising from PVA in the composites were identified at 1416-1447 cm^{-1} (wagging of CH_2 and bending of OH), 992-1019 cm^{-1} (stretching of -CO and bending of -OH from amorphous sequence of PVA), 914-928 cm^{-1} (bending of -CH2) and 846-868 cm^{-1}

(rocking of -CH). Characteristic peaks of alginate at 1639 and 1423 cm^{-1} corresponding to –COO- group were prominent for the porous DN20 Bioglass® composite in comparison to the rest of the composites. Minor shifts in the Si-O and C-O peaks were observed on the spectra of DN10BG composites, where they decreased in intensity with increasing number of cycles of freeze thawing.

DSC analysis

Hydrogel composite network	Cycles of FT	Tg 1 (°C) ± SD	Tg 2 (°C) ± SD
DN10BG	1	74.2 ± 9.1	169.0 ± 5.5
	2	75.0 ± 3.7	211.1 ± 10.8
	3	81.1 ± 1.0	202.7 ± 9.5
DN10BG-10%Porogen	2	80.0 ± 12.8	218.5 ± 1.5
DN20BG-10%Porogen	2	85.6 ± 8.6	167.0 ± 5.5

Table 6-6: Glass transition temperature (Tg°C) of the dual network bioglass composites fabricated by different cycles of freeze thawing and porous dual network composites with a composition of PVA at 10 and 20%wt./v concentration. (n=3). DNBG: Dual network Bioglass® composites.

DNBG composites as shown in Table 6-6, were found to display two glass transition temperatures, the first between 74-85°C, corresponds to the Tg of PVA whilst the second between 167-218°C, corresponds to the Tg of the presence of alginate in the network. The inclusion of a porogen did not have a significant effect on the Tg as expected, however it was noted that the increasing concentration of the PVA led to an increase in Tg for the porous networks.

Equilibrium Water Content (EWC)

The water uptake of the DNBG composites over a period of 4 weeks (Figure 6-3) clearly demonstrated that the porous networks had a significantly higher uptake due to the

larger surface area.

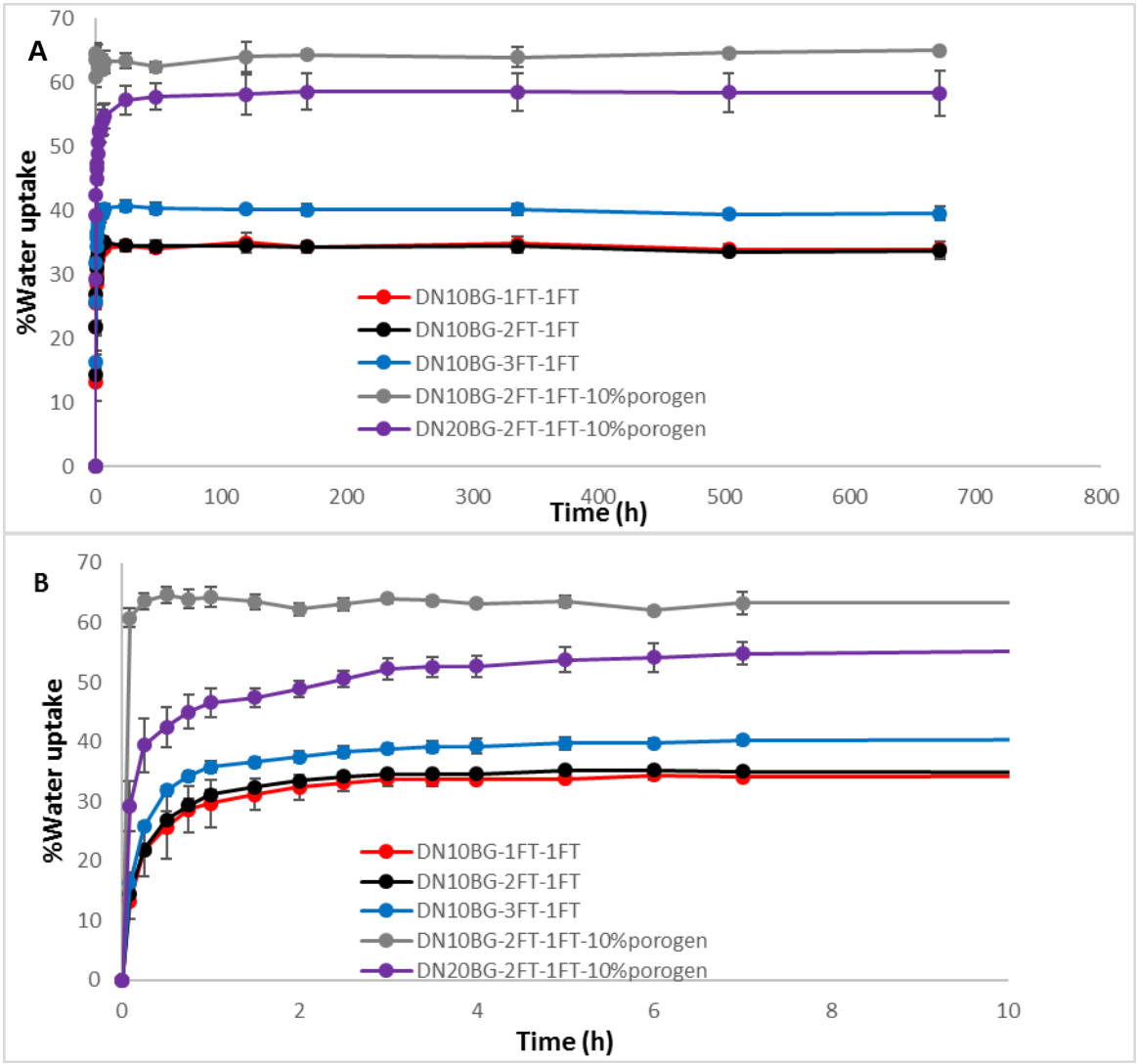

Figure 6-3: Water uptake of the non-porous DNBG composites fabricated by 1,2 or 3 cycles of freeze thawing and porous DNBG composites fabricated with PVA of concentrations 10 and 20wt./v%. A represents a full scale plot of water uptake from the initial time point to the final 4weeks time point. B represents an expanded version of water uptake in the first 10 hours. (n=3)

All the composites attained equilibrium uptake within 8 hours and as expected the rate of water uptake was highest for the porous networks, which was also dependent on the starting concentration of PVA.

NON-POROUS DUAL NETWORK COMPOSITES

Ultimate Tensile Strength

The ultimate tensile strength and Young's modulus of non-porous DN10BG composites shown in Figure 6-4, indicated that fabrication using 2 freeze thaw cycles resulted in the

highest ultimate tensile strength, whilst further freeze–thaw process had no discernible effect, whilst the Young's modulus was found to decrease with increasing cycles of freeze thawing.

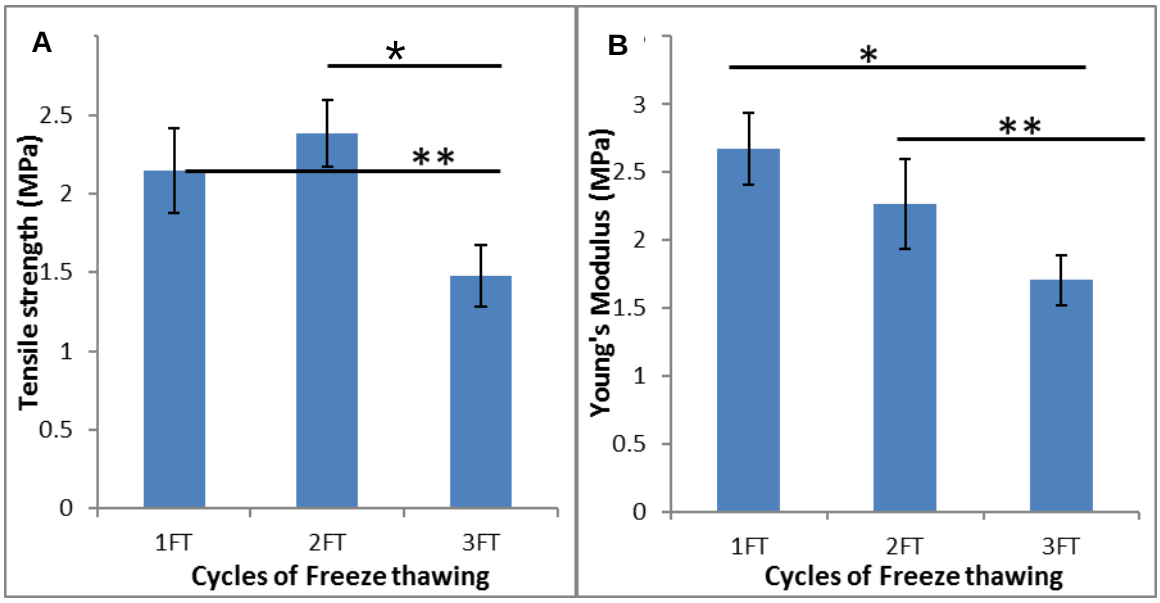

Figure 6-4: Tensile strength **[A]** and Young's modulus **[B]** of DN10BG composite networks fabricated using 1,2 and 3 cycles of freeze thawing. (n=6) (* P≤0.017 and ** P=0.004). The horizontal lines relate the groups and the asterisk shows the level of significant difference.

Trouser Tear test

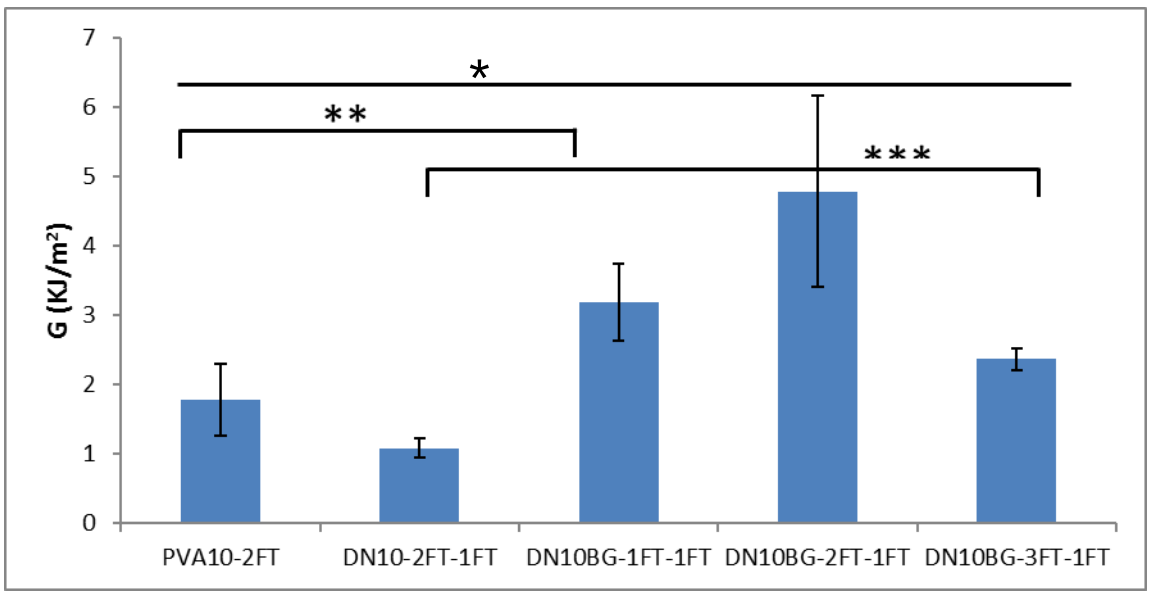

Figure 6-5: Fracture energies of the hydrogels and hydrogel composites obtained using the trouser tear method. The fracture energies of PVA10, DN10 with 2 cycles of freeze thawing and DN10BG fabricated by 1, 2 and 3 freeze thaw cycles. (n=6) (* and ** P<0.001, *** P=0.030). The horizontal lines relate the groups and the asterisk shows the level of significant difference

DNBG composite gels were found to have fracture energies higher than those of the PVA10 and DN10-2FT hydrogels (Figure 6-5) and amongst the DN10BG composites, fabricated by 2 cycles of freeze thawing yielded the highest fracture energy.

POROUS DUAL NETWORK COMPOSITES

The DN20BG composites exhibited significantly higher tensile strength and modulus in comparison to the DN10BG-1FT networks, clearly indicating that the initial concentration of PVA played a significant role. The strength and stiffness porous composites, however was lower than that obtained from the non-porous composites.

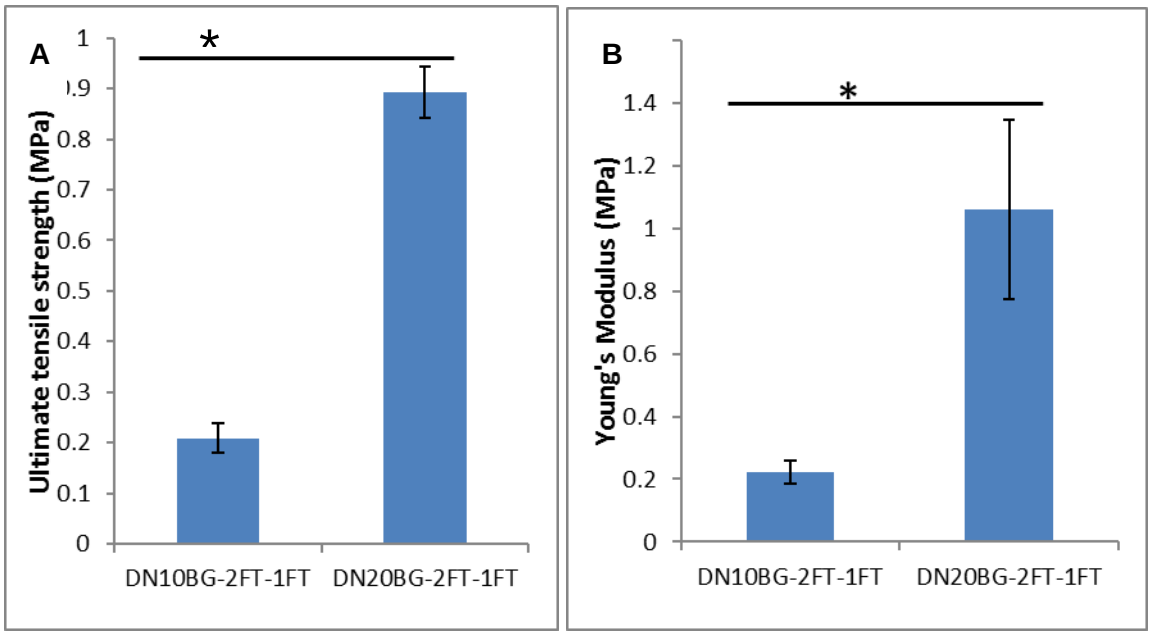

Figure 6-6: Tensile strength **[A]** and Young's modulus **[B]** of porous DN10, 20BG composites fabricated via 2 cycles of freeze thawing. (n=6) (* = P<0.001). The horizontal lines relate the groups and the asterisk shows the level of significant difference

Testing in Compression

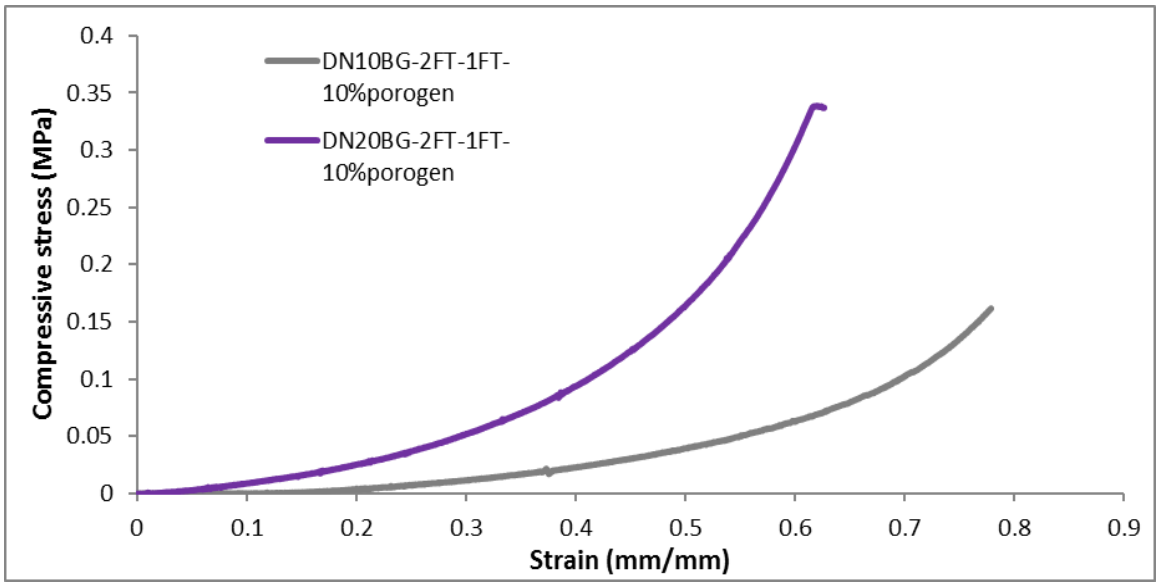

Figure 6-7: Compressive stress-strain curve of porous DNBG (10 and 20% PVA concentration by weight) composites fabricated via two cycles of freeze thawing.

Porous hydrogel composite	**Compressive stress (MPa)**	**Young's modulus (MPa)**
DN10BG-2F-1FT	0.2 ± 0.02	0.8 ± 0.1
DN20BG-2FT-1FT	0.3 ± 0.04 *	1.5 ± 0.4 *

Table 6-7: Compression and Young's modulus values of hydrated porous DN10, 20BG composites fabricated via two cycles of freeze thawing. (n=3) (* = P≤0.045)

The stress-strain curves of the porous DNBG composites are shown in Figure 6-7 and the values in Table 6-7. DN20BG was found to have higher compressive stress and stiffness values than the DN10BG composite, which was found to be able to undergo higher strain values than the DN20BG composite.

Uniaxial Cyclic compression

Figure 6-8 illustrates the repeated compressive force on the hysteresis and mechanical integrity of the composites of the porous DN10 and 20 BG composites. The experiments were performed with identical parameters, where loading and unloading cycles were carried out without allowing the composites to undergo a relaxation period.

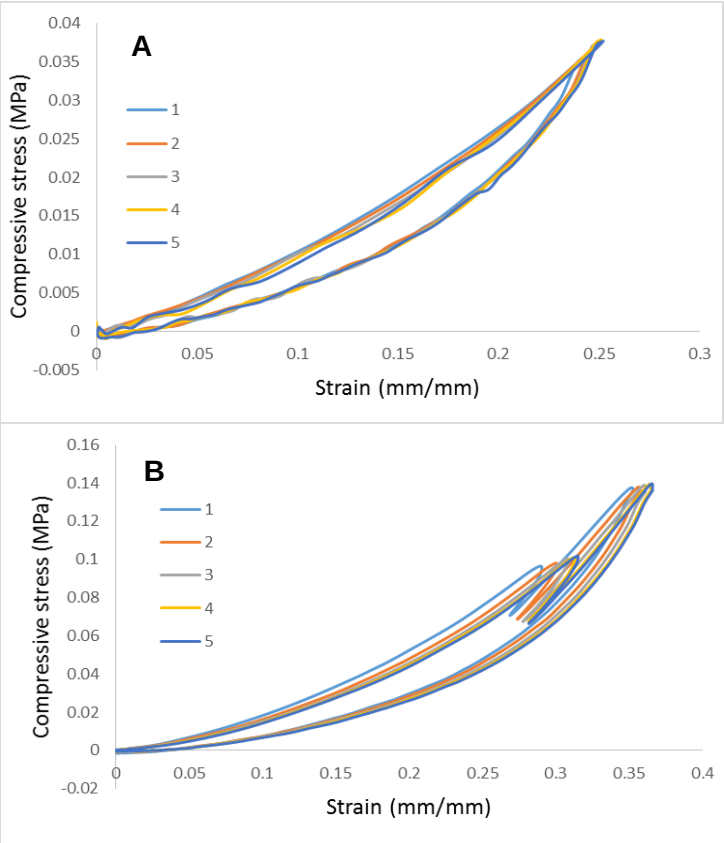

Figure 6-8: Cyclic compression showing stress vs strain plots of porous DN10BG **[A]** and DN20BG**[B]** composites for 5 cycles at 40% strain, calculated from maximum compression data.

The stretching and relaxation curves of both at low strain (40%) were superimposable and little to no hysteresis was observed, suggesting high resilience for both materials at low strains.

SEM analysis

	Magnification		
Mag	**100X**	**500X**	**2500X**

DN10BG-NO POROGEN

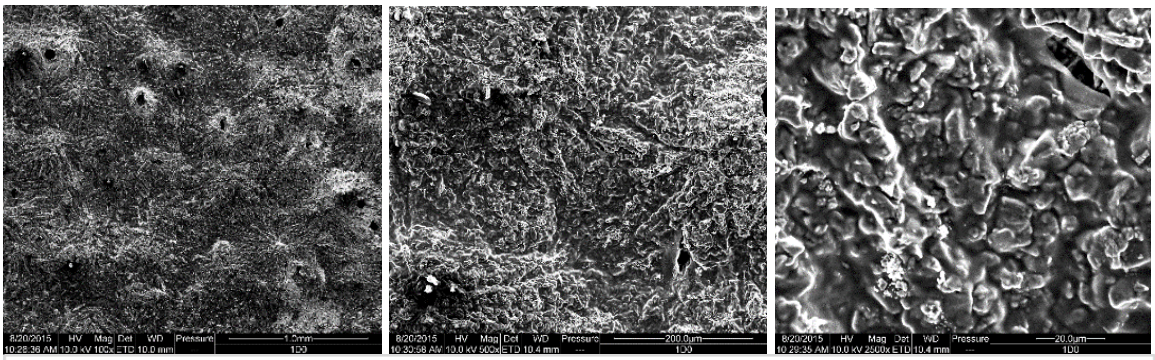

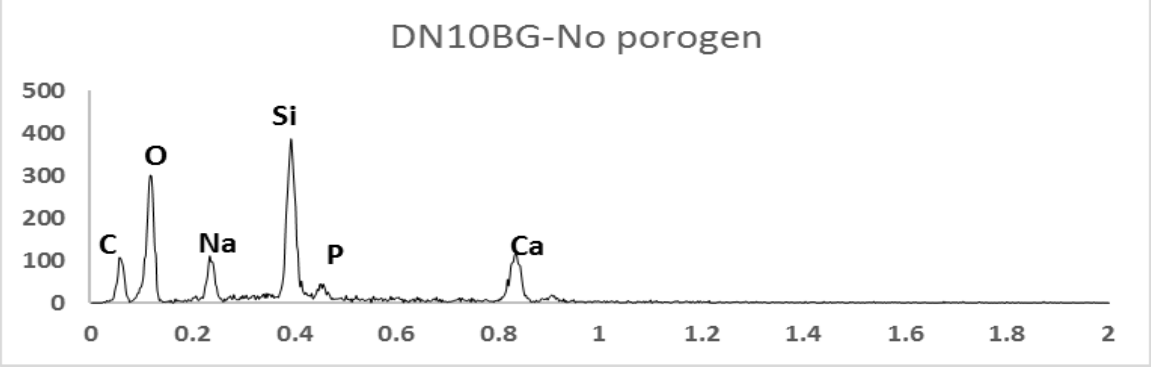

Magnification			
Mag	100X	500X	2500X

DN10BG-10%POROGEN

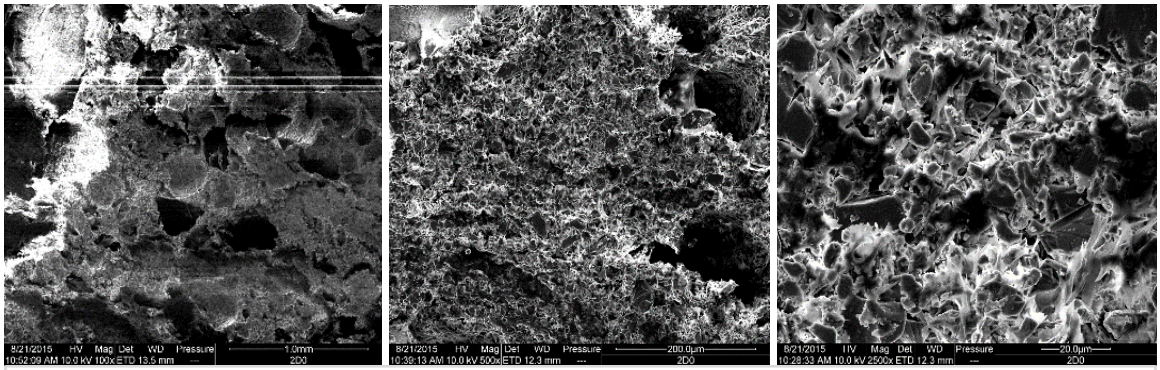

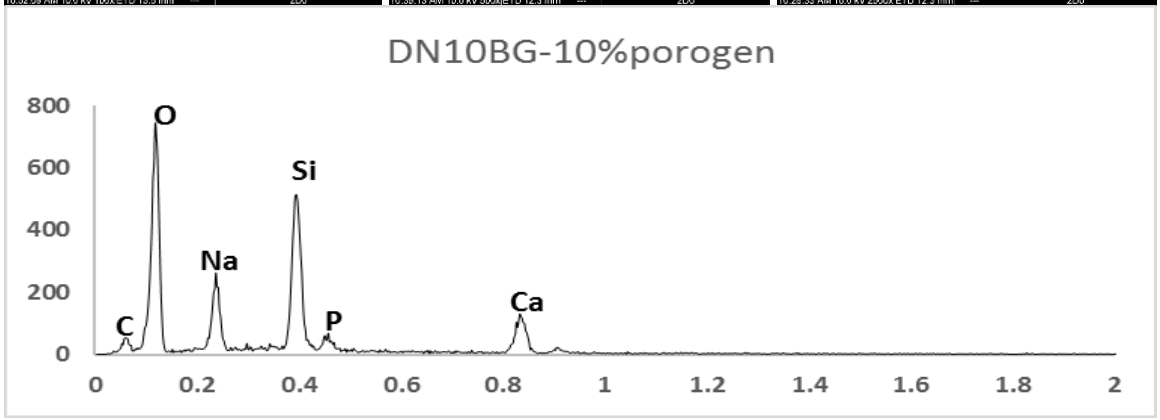

Magnification			
Mag	100X	500X	2500X

DN20BG-10%POROGEN

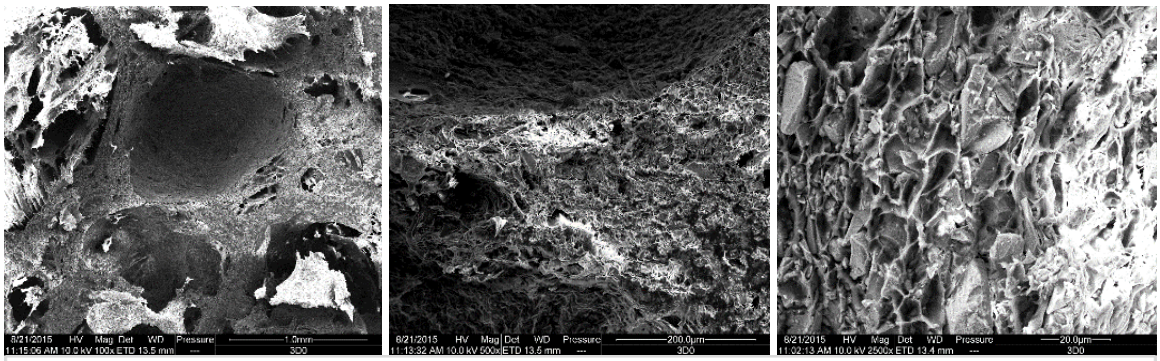

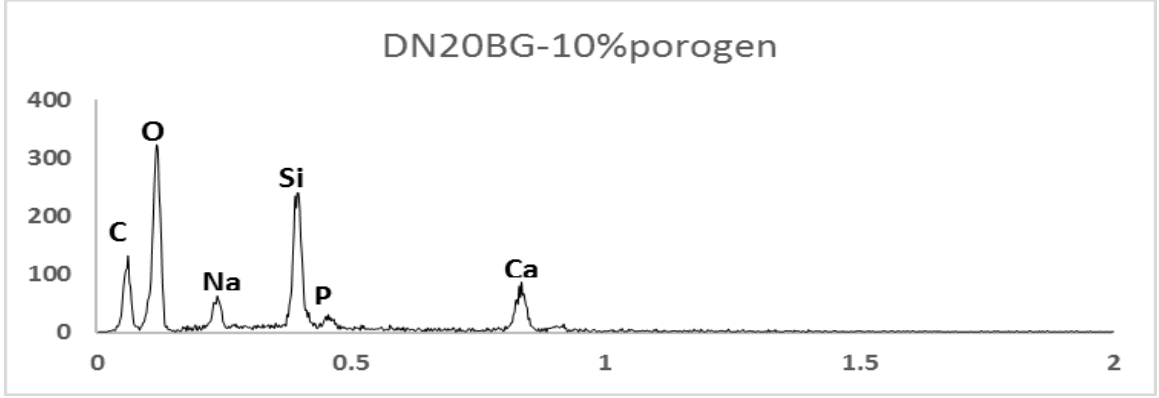

Figure 6-9: SEM microstructure images at magnification x100 500 and 2500, as well as EDX spectra of non-porous DN10BG composite and porous DN(10 and 20)BG composites fabricated via 2 freeze thaw cycles.

Scaffold microstructures and energy dispersive X-ray microanalysis of elements present in the DNBG composite networks shown in Figure 6-9, indicate that the non-porous DN10BG composite presents a compact structure with a rough surface area, whilst the porous DN(10 and 20)BG composites were found to have an interconnected porous structure, with varying pore sizes ranging from 1mm to < 20µm. EDX spectra confirmed the presence of silicon, calcium, phosphorus and sodium oxides in the composites as well as the presence of carbon due to the polymer content.

IN VITRO BIOMINERALISATION STUDY

The interaction of the selected hydrogel composites with simulated body fluid were studied in vitro by analysing the ability of the composite networks to form an apatite layer over a period of 4 weeks. The formation of an apatite layer is essential in assisting favourable intracellular and extracellular responses promoting rapid bone formation in vivo. DN hydrogels fabricated via 2 freeze thaw cycles and their respective DNBG composites were selected according to optimisation studies to be taken further and analysed for the level and effect of mineralisation on surface, tensile and stiffness properties on the hydrogels and hydrogel composites results are presented below.

Ultimate tensile strength and stiffness of dual network hydrogels and composites

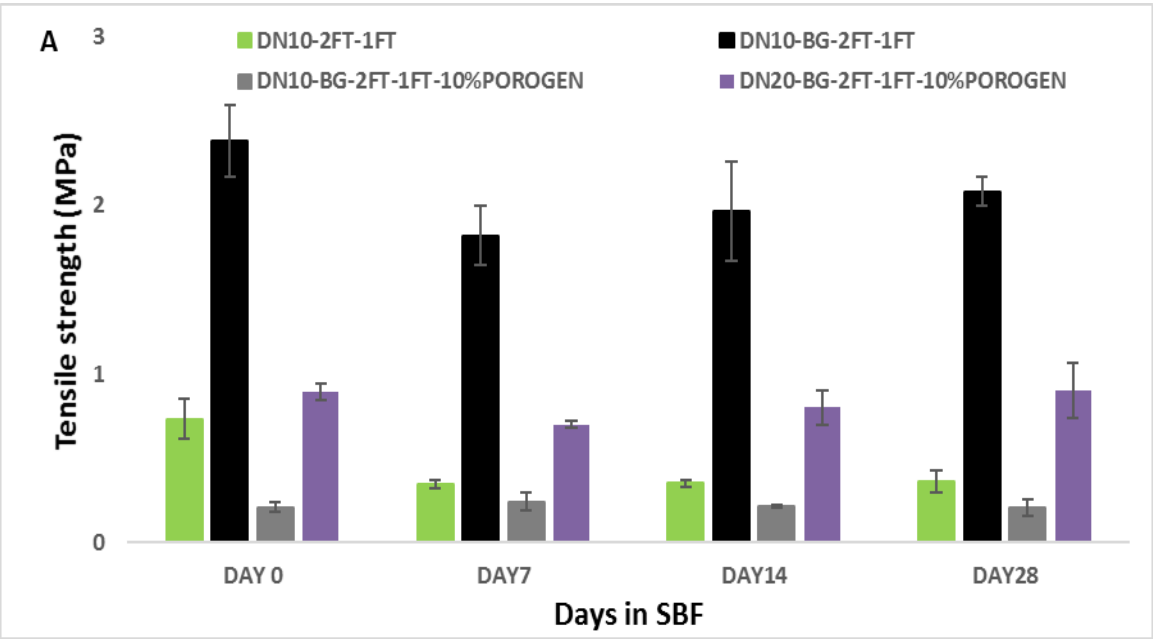

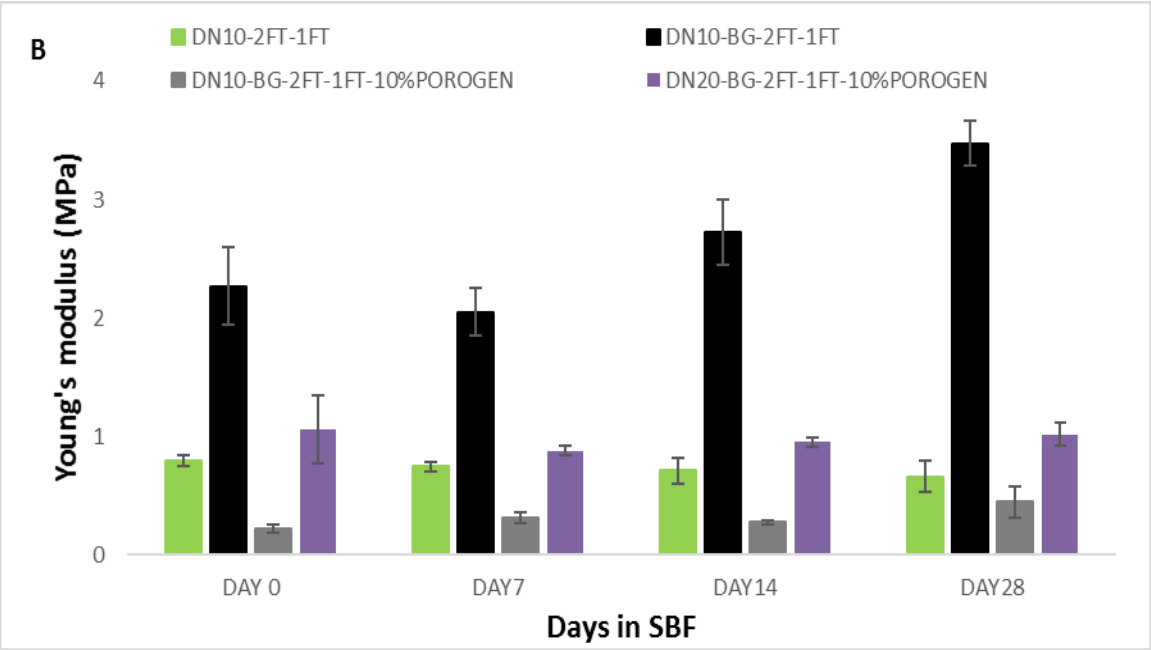

Figure 6-10: Tensile strength and Young's modulus changes after immersion in SBF at 7, 14 and 28 days, of the DN hydrogel, non-porous DN10BG and porous DN10, 20BG all fabricated via two cycles of freeze thawing. (n=4)

The effect of mineralisation on the tensile strength and Young's modulus of the hydrogels and composites (Figure 6-10) indicated that for all DNBG hydrogel composites there was an initial decrease in tensile strength and Young's modulus in the first 7 days, which was, then followed by a steady increase up to 28 days. The DN hydrogel itself however did not show and increase in tensile strength and stiffness when immersed in SBF over the stated time periods.

Cyclic compression
DN10BG-2FT-1FT

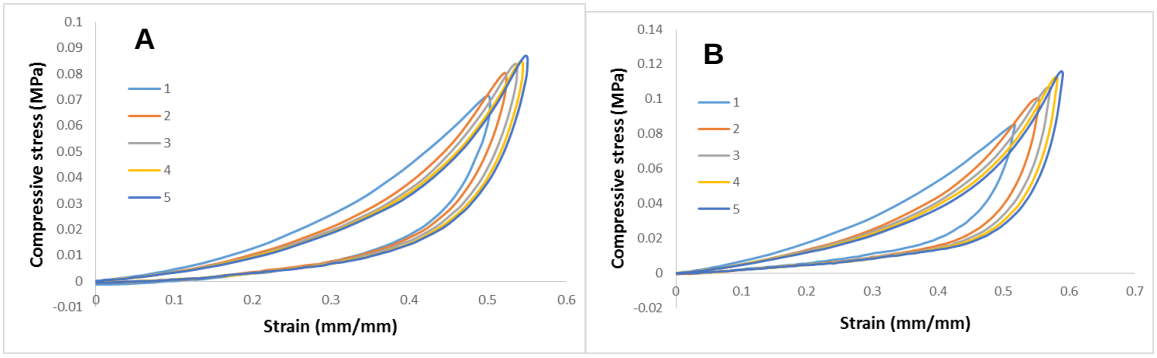

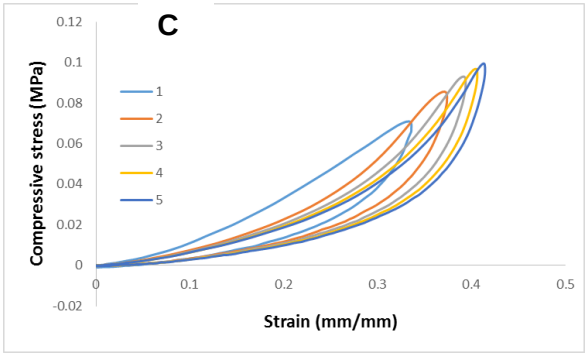

Figure 6-11: Cyclic compression showing stress vs strain plots of porous DN10BG composites for 5 cycles at 40% strain after 7 **[A]**, 14**[B]** and 28**[C]** days immersion in SBF.

DN20BG-2FT-1FT

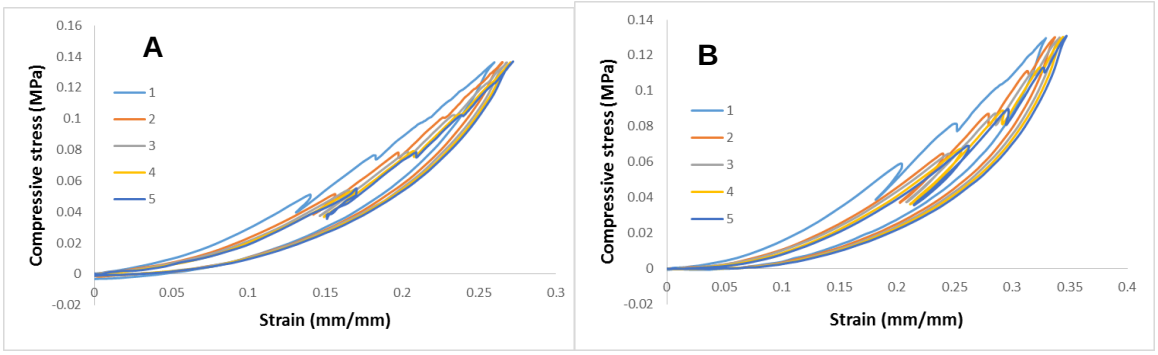

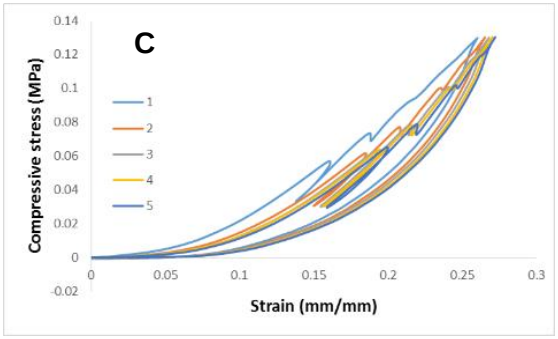

Figure 6-12: Cyclic compression showing stress vs strain plots of porous DN10BG composites for 5 cycles at 40% strain after 7**[A]**, 14**[B]** and 28**[C]** days immersion in simulated body fluid.

The DN10 and 20BG composites demonstrated hysteresis which was attributed to the effect of mineralisation on the porous composites after 7, 14 and 28 days immersion in SBF (Figure 6-11 and Figure 6-12).The change in the loading and unloading curves of the DN10BG composites was found to increase with increasing immersion time in SBF. The DN20BGcomposite exhibited multiple fracture points which increased with increasing cycles of loading after immersion in SBF.

FTIR analysis

The FTIR spectra of DNBG composites before exposure to SBF and after 7, 14 and 28 days are shown in Figure 6-13, highlighting the changes on the composites due to formation of apatite on the surface layers. The formation of HCA layer on the composites was identified and characterised by appearance of absorption bands at ~604 and ~565 cm^{-1} attributed to the P-O bending vibrations, as well as the P-O asymmetric stretching vibration bands between 1000 and 1150 cm^{-1}. The P-O stretching is superimposed on the Si-O stretching band corresponding to bioactive glasses, but however became more visible on the porous composites after 28 days immersion in SBF. The peak centred at 800-890 cm^{-1} was attributed to the C-O stretch vibrations.

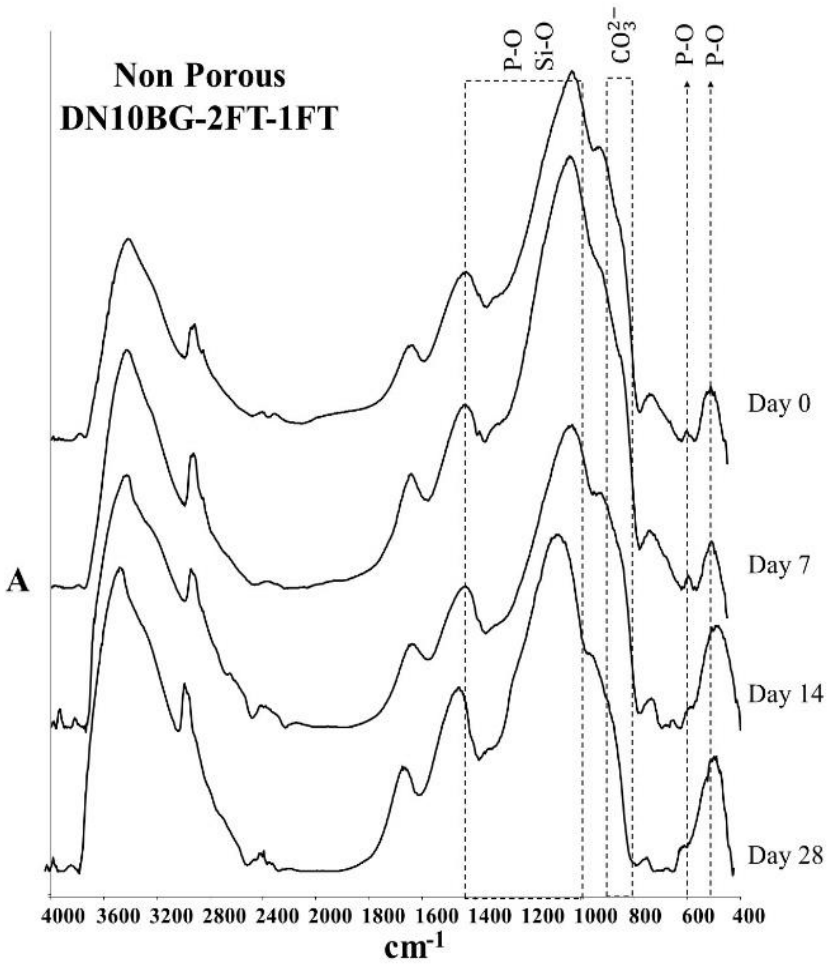

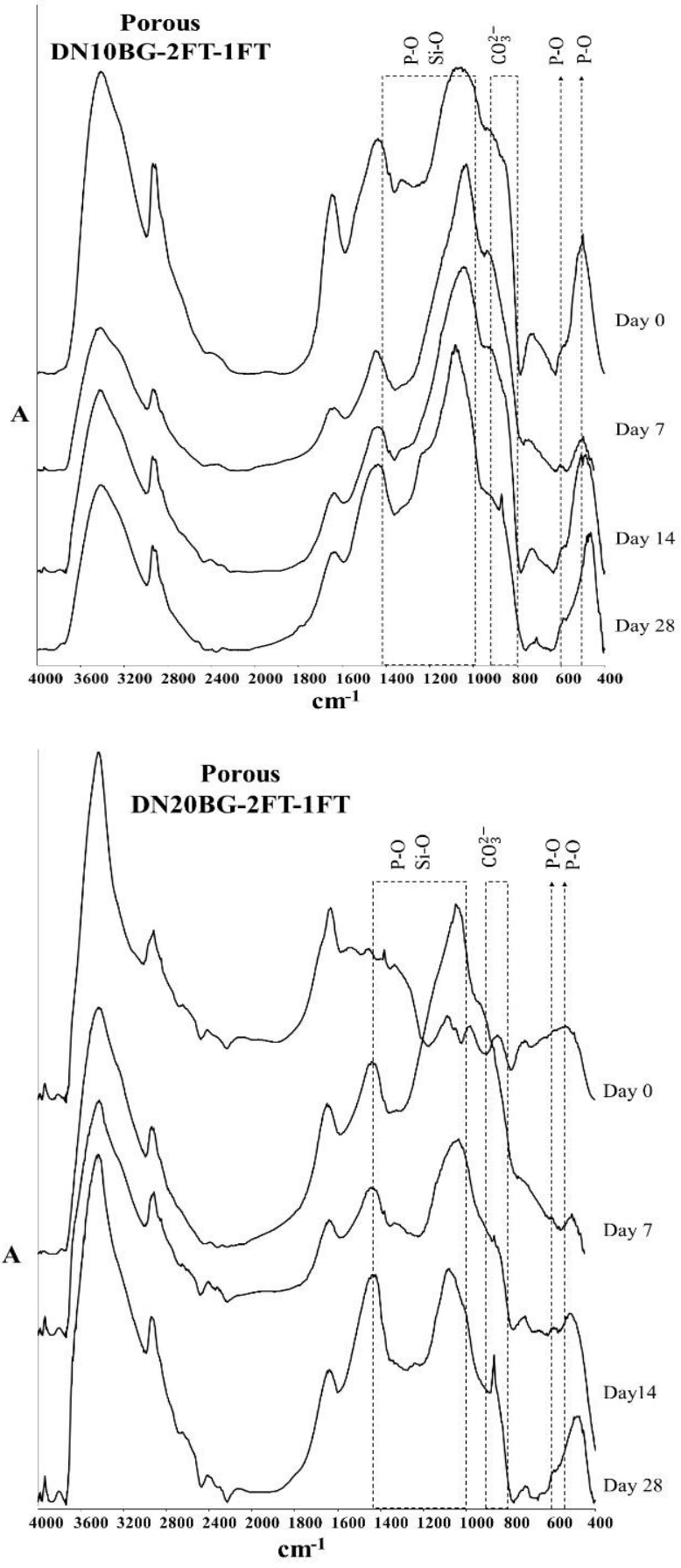

Figure 6-13: FTIR spectra non-porous DN10BG and porous DN10, 20BG composites fabricated by two cycles of freeze thawing, after 0, 7, 14 and 28 days exposure in simulated body fluids.

Raman spectra analysis

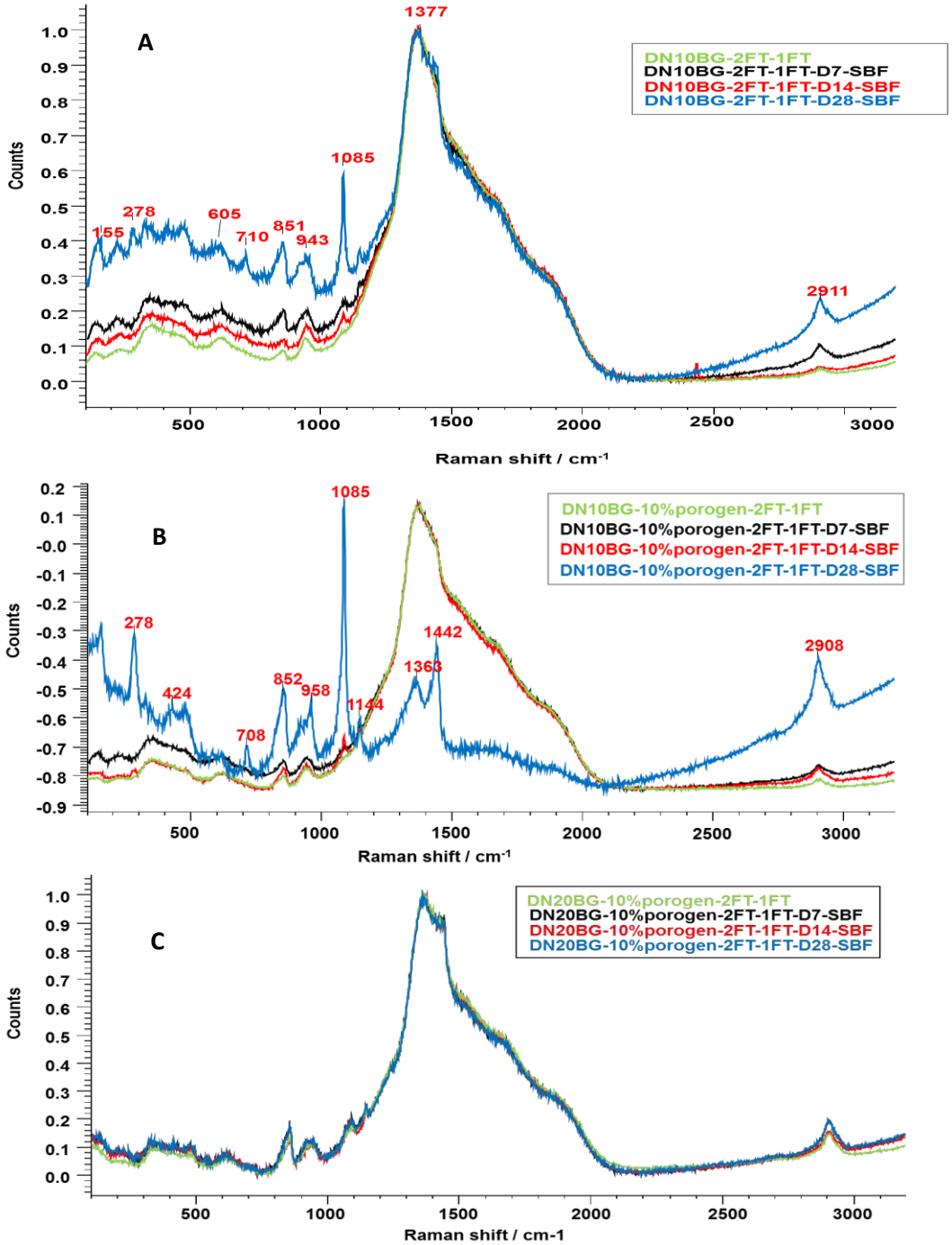

Figure 6-14: Raman spectra DNBG composites after 0, 7, 14 and 28 days immersion in SBF. **[A]** Represents non-porous DN10BG composite, **[B]** & **[C]** represent porous DN10, 20BG composites respectively.

Raman spectroscopic analysis of the DNBG composites after 7, 14 and 28 days in SBF is presented on Figure 6-14. Major differences in the spectra of the composites were observed at day 28 after immersion in SBF, with the exception of the porous DN20BG composite. Hydroxy carbonated apatite was identified by the symmetric PO_4^{3-} peaks at

943 and 958 cm^{-1} for non-porous and porous composite respectively. The asymmetric bending PO_4^{3-} and the asymmetric PO_4^{3-} stretching peak were identified at ~424 and 1085cm^{-1} respectively [296, 311].

SEM analysis

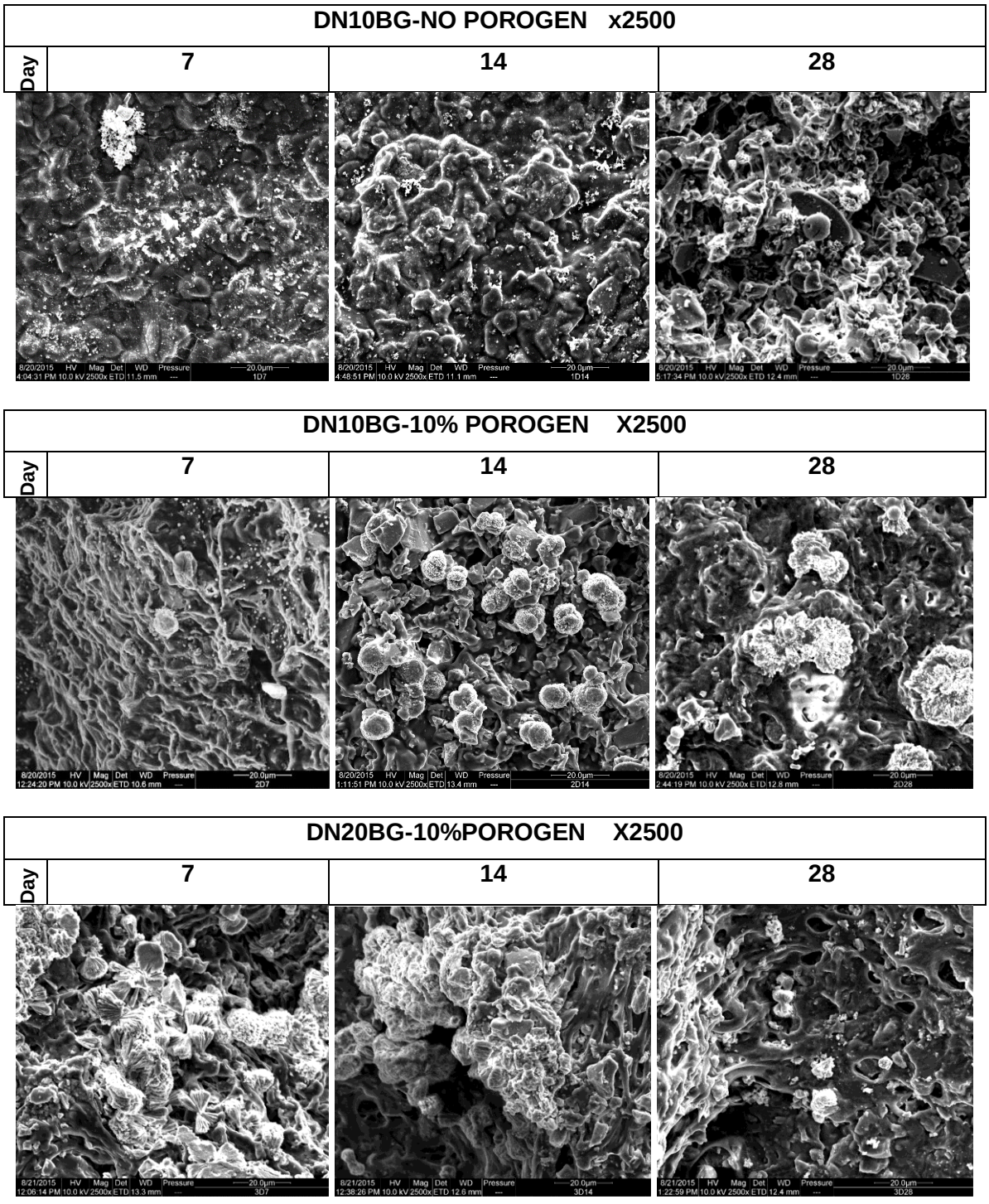

Figure 6-15: SEM micrographs of mineral deposition on both the non-porous and porous DNBG composites soaked in SBF over a period of 28 days.

The formation of HCA crystals on the DNBG composites is demonstrated in Figure 6-15. Results indicated that there was formations of crystallites on all the composites due to immersion in SBF.

CYTOCOMPATIBILITY

Cell viability study by MTT assay

Human osteoblast like cells were seeded on the eluents obtained from the composites in tissue culture medium for 24, 48 and 72 hours. An MTT assay was carried out at 24, 48 and 72 hour exposure times (Figure 6-1).

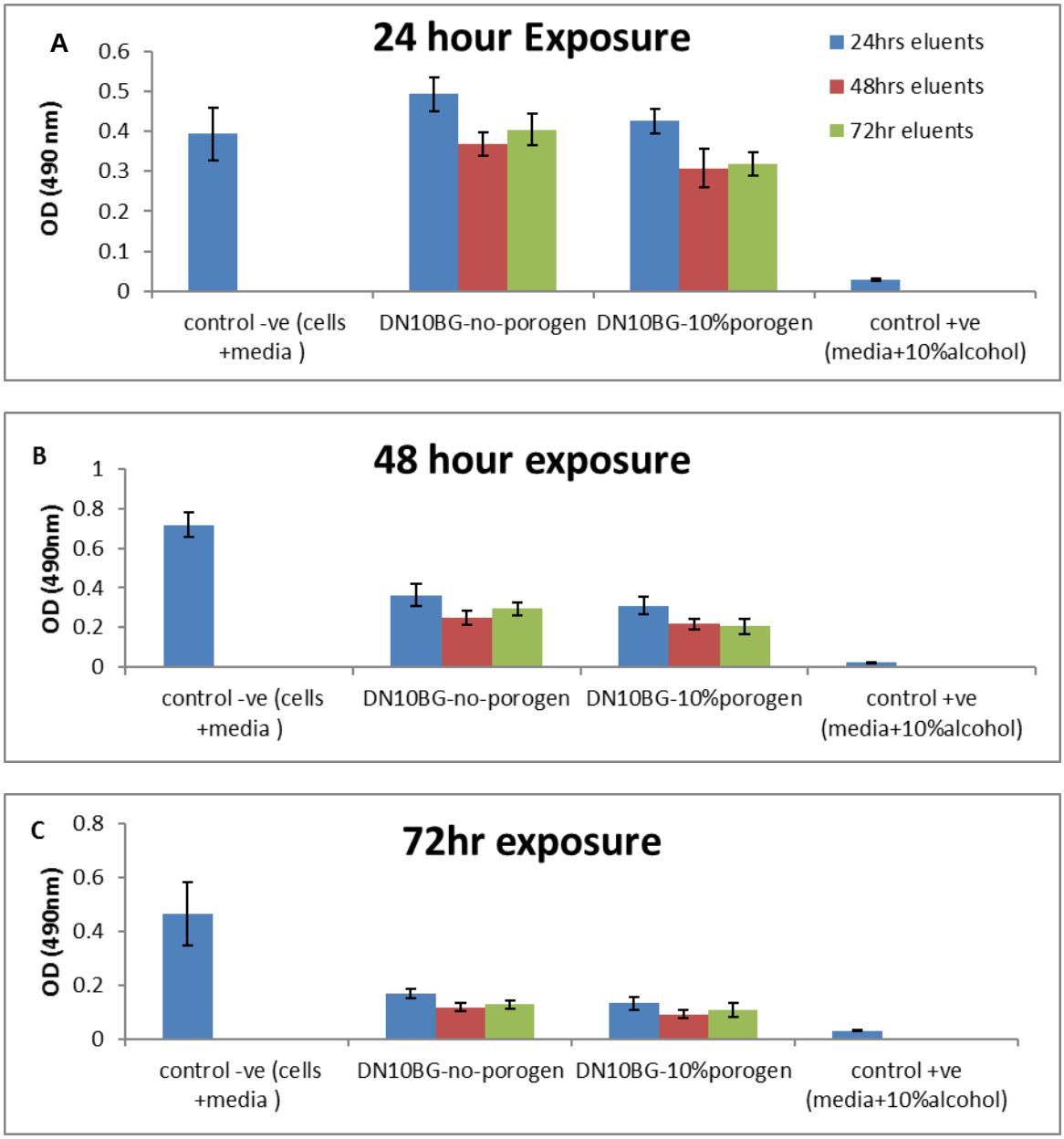

Figure 6-16: MTT assay test showing the response of human osteoblast cells following exposure to eluents from PVA10-2FT and DN10-2FT-1FT hydrogels. Cells were

exposed for 24, 48 and 72hrs to a **[A]**. 24hr elusion wash time **[B]**. 48hr elusion wash time and **[C]** 72hr elusion wash time.

The results indicated that prolonged exposure caused a drop in cell viability, which is likely to be related to the alkaline environment caused by the presence of Bioglass®.

LIVE/DEAD STAINING

Figure 6-17 displays superimposed live and dead staining images of the porous and non-porous DN10BG composites.

DN10BG-2FT-1FT No Porogen

Day 1

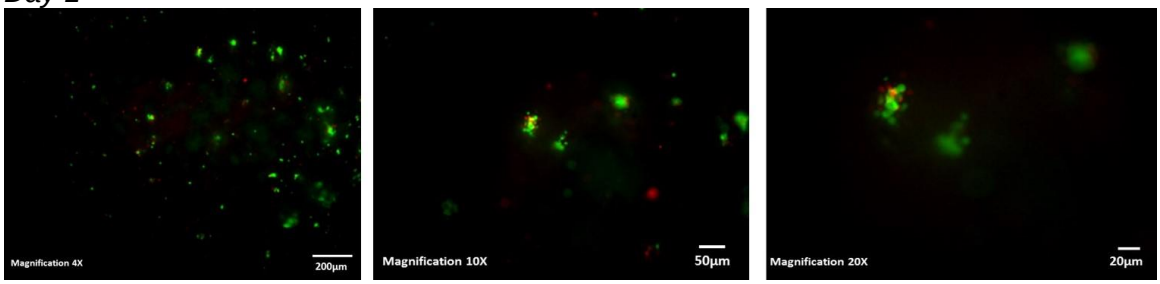

Day 7

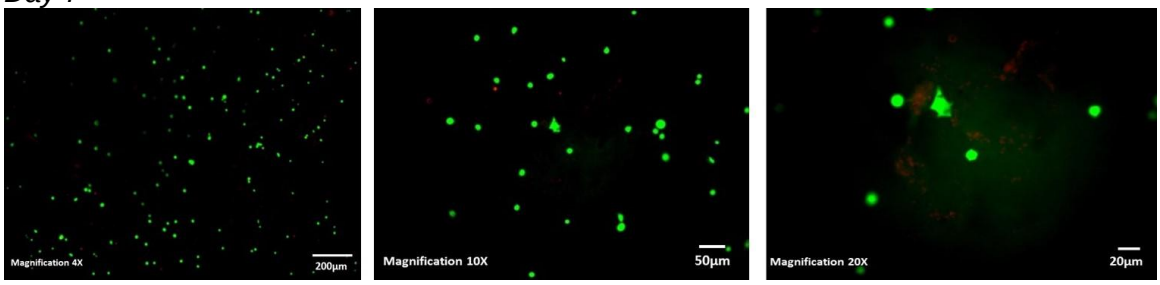

Day 14

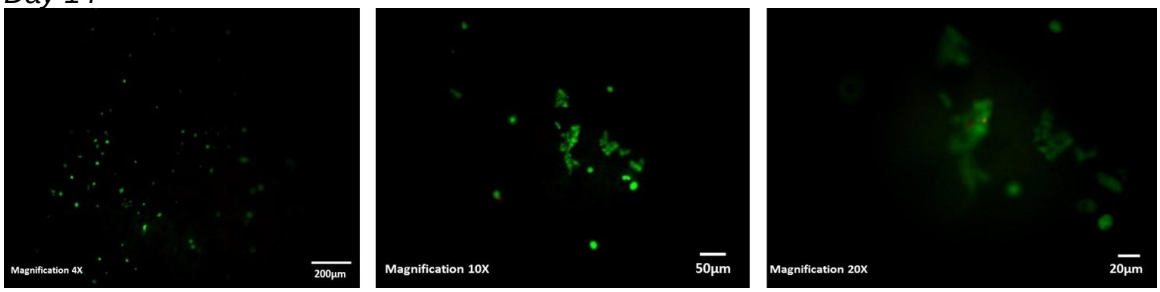

Day 28

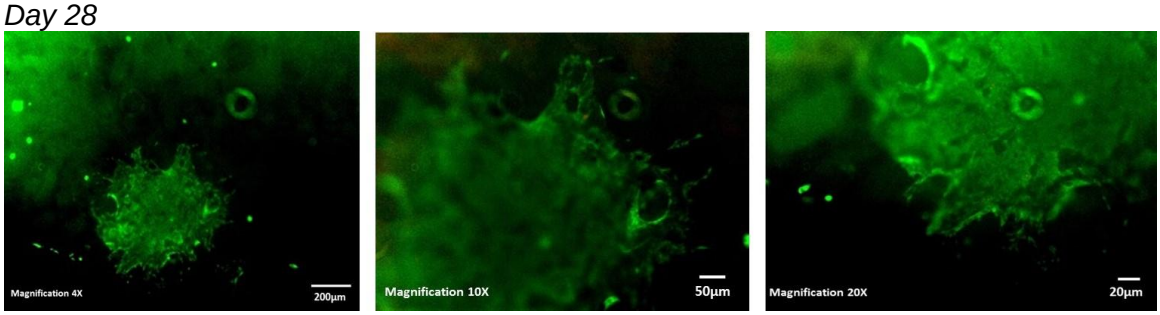

DN10BG-2FT-1FT 10% POROGEN

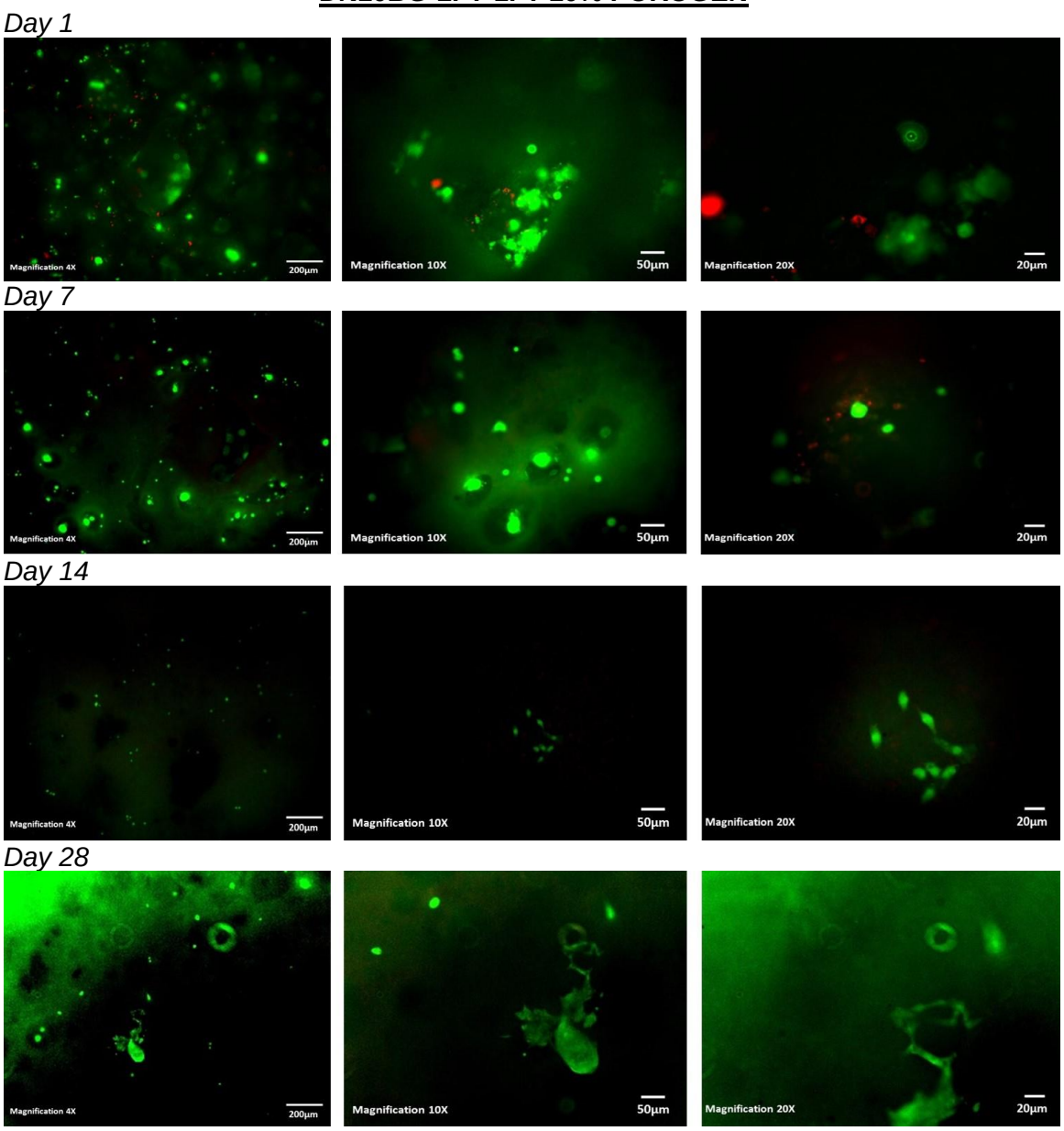

Figure 6-17: Images of live/dead staining of HOB cells (x4, 10 and 20 magnification) on the non porous and porous DN10BG-2FT-1FT hydrogel at day 1, 3, 7, 14 and 28 in culture.

Live cells were observed on all the hydrogels over a period of 28 days. This was also observed as a positive indication of good cell attachment, proliferation and migration of cells on the surface and within the internal structures of the composites.

Cell Morphology analysed via SEM

The adherence and morphology of the HOB cells on the surface of the composites was analysed at day 7 and 14 and the SEM micrographs are presented on Figure 6-18.

Mag	500X	2000X	5000X

DN10BG-NO POROGEN – Day 7

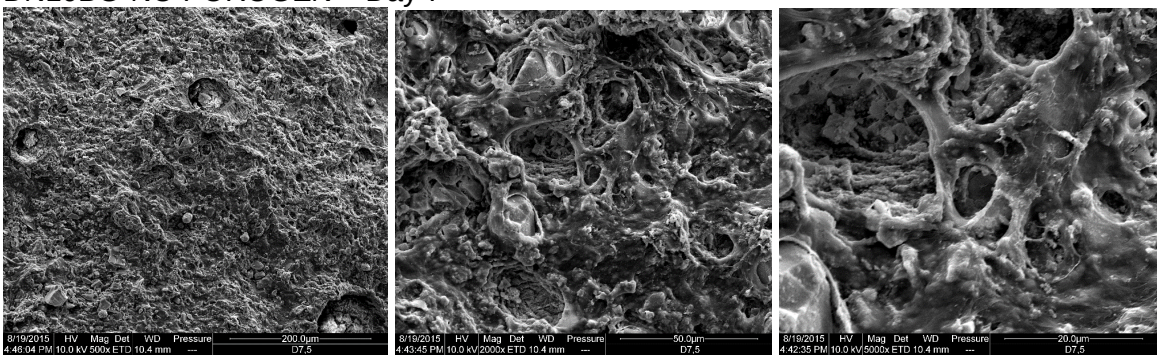

DN10BG-10%POROGEN – Day 7

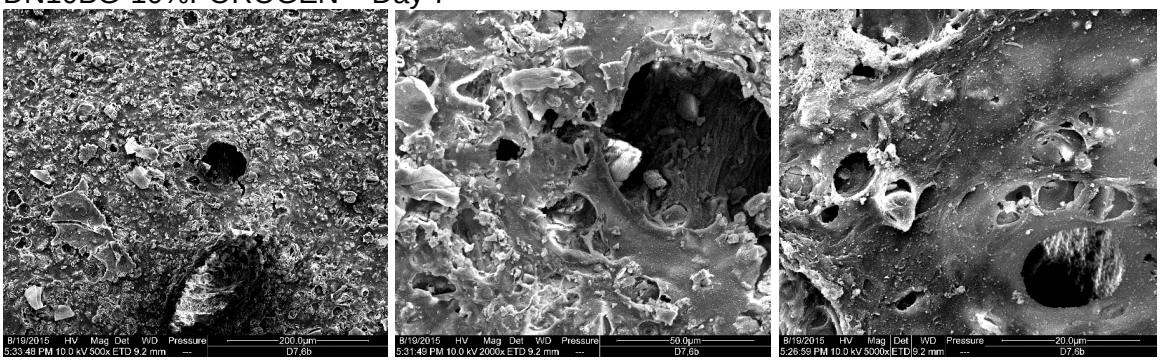

DN10BG-NO POROGEN – Day 14

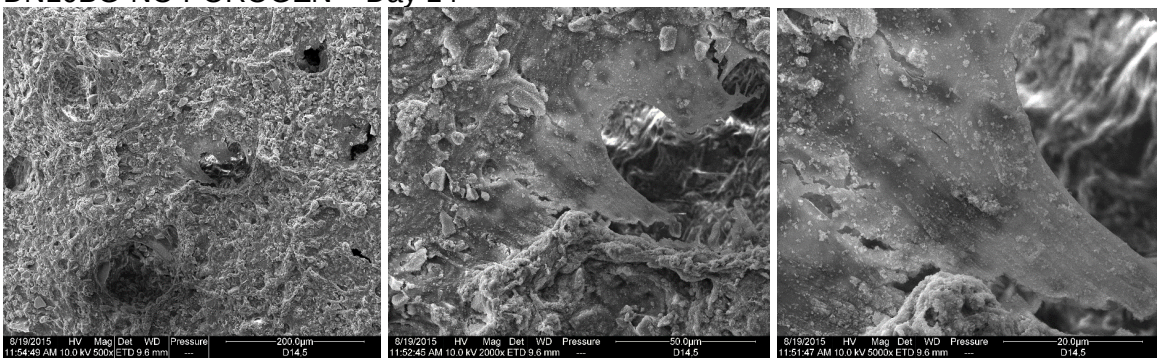

DN10BG-10%POROGEN – Day 14

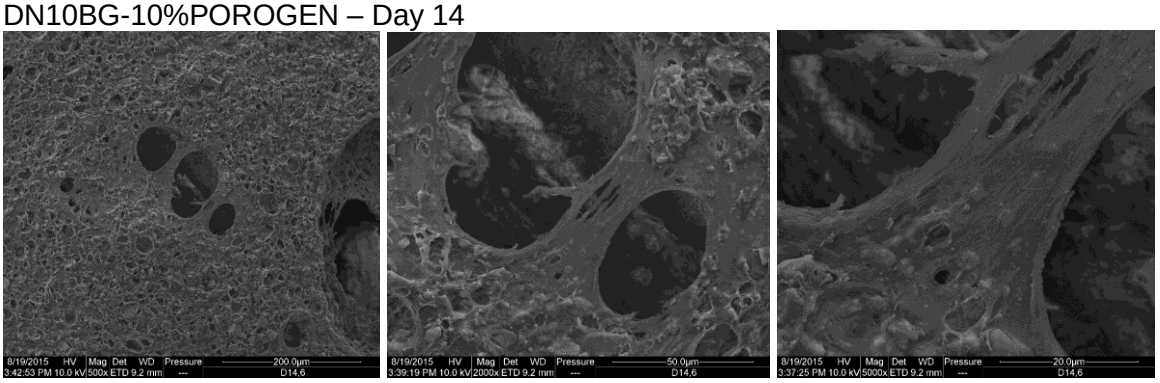

Figure 6-18: SEM micrographs showing HOB cell attachment and coverage on DNBG composites after 7 and 14 days in culture.

The results showed that the cells adhered well to the surface of the scaffolds. This was confirmed by the flat stretched morphology of the cells. It was also observed that on the porous composites the cells were able to spread across the pores of the composites, eventually entirely covering the pores entirely. It was noted that there seemed to be a deposition of a mineral layer on the surface as the cells were spreading and proliferating resulting mineral deposition over the cells.

HOB cell differentiation by alkaline phosphatase activity and protein concentration

The ALP/Protein concentration is used as a bone marker and has been implicated in the initiation of mineralisation. A peak in alkaline phosphatase activity was observed at 14 days in culture indicating early cell differentiation, after which ALP levels declined. This indicates differentiation of HOB cells and the onset of mineralisation.

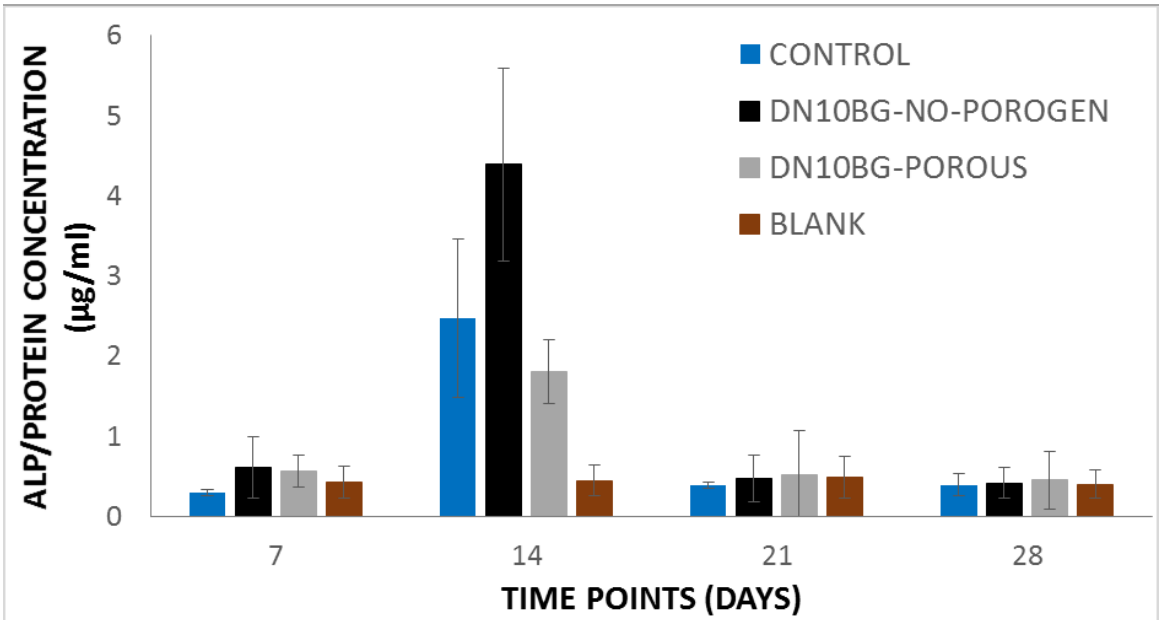

Figure 6-19: The alkaline phosphatase activity in balance with the protein concentration of human osteoblast cells (HOB) on non-porous and porous DN10BG composites, with the tissue culture plate as the control. Tests were carried out on culture media supernatant of hydrogels composites at day (7, 14, 21 and 28). Data represents as mean±SD (n=4)

6.5 DISCUSSION

Dual networks were successfully fabricated based on the principles of double networks using 2 water soluble polymers (PVA and sodium alginate) that are FDA approved and have been widely used in the biomedical field. This resulted in achievement of a tough

interpenetrating polymer network with potential for further development for applications in reinforcing long segmental bone defects. It is known that brittle, rigid bone substitutes often induce micro-movement at the bone-bone substitute interface, consequently interfering with bone regeneration. In contrast elastic materials that can exhibit controlled swelling have the ability to evoke an intimate contact with the wound bed edges under pressure. This alleviates the problems that can occur due to micro-motion of grafts/substitutes providing an environment favourable for bone formation. In this chapter the DN network system was taken forward to develop composite networks with a view to create a composite that would be suitable for applications in bone augmentation.

Scaffolds fabricated from inorganic materials such as calcium phosphate based bioceramics and Bioglass® possess higher mechanical strength than polymeric scaffolds, however such materials have been found to be very brittle and in most cases result in failure of the scaffold material on application of service loads. To overcome the common problems of brittle ceramics and weak hydrogels, several options have been developed to combine polymers with ceramics or glasses to form composite materials. This strategy has proved to be attractive as it combines the controlled degradation kinetics of the polymer phase with the high bioactive potential induced by the incorporation of ceramic or glass particles, which promote the formation of mineralisation sites. Additionally this combination allows for the mechanical properties of the composites to be improved as compared to the parent hydrogel networks, the brittle behaviour directly ascribable to the ceramic phase can be softened when coupled with a polymeric phase. This therefore offers valid and viable solution to mimic the composite behaviour of natural tissue response to external stimuli.

Bioglass® 45S5 was chosen as a filler for the formation of the dual network bone substitutes, as the 45S5 formulation of Bioglass® is known to bond rapidly with bone in vivo as well as stimulate bone growth away from bone implant interface. Bioactive glass has been used clinically in bone repair and regeneration in orthopaedics, alveolar ridge augmentations, maxillofacial reconstruction and spinal surgery. The novelty of this work

is that for the first time, a dual network that was also developed in this study was being used to create a tough, elastomeric hydrogel composite with the inclusion of a bioactive component within the system. Although the hydrogel composites were fabricated by using different cycles of freeze thawing, the high tensile strength and toughness of the dual networks (Chapter 5) obtained after two cycles of freeze-thawing process was anticipated to yield optimum properties, for the Bioglass® composites. The bioglass composites were also taken further to develop porous composites with a structure mimicking cancellous bone.

The effect of incorporation of Bioglass® into the dual network hydrogel system

The idea in this study was to incorporate a bioactive phase within the tough dual network hydrogel matrix without compromising the mechanical properties. The inclusion of Bioglass® would impact the amounts of fluids absorbed in that, higher concentrations of Bioglass® filler in the network would result in reduced water uptake of the composite, which would directly impact the ability of the composite to absorb biological fluids which would aid in enhancing regeneration and repair of the bone tissue. The particle size selected was optimum as larger particles would disrupt the mechanical integrity of the networks.

Therefore based on this 30% wt. Bioglass® with particle size 17µm was incorporated within the dual network hydrogel systems formulated with a PVA base of 10%w/v. This concentration of PVA had easy handling properties and low viscosity allowing for ease of fabrication when conducting optimisation studies.

FTIR analysis

The PVA, alginate and Bioglass® absorption bands were identified in the final composite structures. The spectra in Figure 6-2 compares Bioglass® powder with the non-porous DN10BG composites fabricated by 1, 2 and 3 cycles of freeze thawing and the DN10 and 20BG composites fabricated by 2 cycles of freeze thawing. The spectra revealed characteristic broad peaks of –OH stretching at 3280 cm^{-1}, -CH- stretching of alkanes at

~2946 cm^{-1} indicating the presence of PVA. Peaks at ~1602 and ~1420 cm^{-1} corresponding to –COO- group reveal the presence of alginate in the network structure. Broad peaks at ~1003 and ~846 cm^{-1} corresponding to Si-O stretching and Si-O-Si bending respectively [127, 312, 313]. This indicated that Bioglass® was successfully incorporated within the network structure of the DN hydrogel structure. Minor shifts observed in the Si-O-Si and Si-O peaks of the non-porous composites suggest that cycles of freeze thawing did not have a significant effect on the overall composite formulation. Similar observations in the spectra of PVA-alg-BG composites have been observed and reported on biocomposite foams [314], composite coatings on stainless steel [313] and PVA sol gel derived foams [315]. Trace elements of the porogen used to fabricate the porous composites were detected on the DN20BG composite as compared to the DN10BG composite. This may have been attributed to the fact that as PVA of 20%wt/v is more viscous than 10%wt/v, thus resulting in a denser and tighter network structure which makes it difficult to eliminate all remnants of the porogen due to the limited diffusion of water molecules within the polymeric network. However it was noted that the porogen used in this study is a biocompatible FDA approved material, and therefore these remnants were not of any consequence and the biocompatibility of the composites was not compromised.

DSC analysis

The effect of addition of Bioglass® into the DN hydrogel system resulted in the composite systems displaying two distinct glass transitions (Table 6-6). In the case of non-porous DN10BG composites fabricated by various cycles of freeze thawing, the first Tg was observed in the range of temperatures between 81.1 – 74.2°C which corresponds to the Tg of PVA. The second Tg was found in range of temperatures 202.7 – 169°C, corresponding to the temperature range where alginate has been reported to undergo decomposition (Amorphous polymers show only softening point which could not be considered as thermodynamic transition. It's a chain "slipping “of polymers chains that becomes possible at some thermal agitation). The Tg of Bioglass® has been reported to

be ~500°C [316], thus it was not observed in this study. The Tg of the non-porous composites increased with increasing cycles of freeze thawing. The porous composites exhibited the same trend of two Tg's, which increased with increasing concentration of PVA in the case of the first Tg, however there was a decrease in the case of the second Tg due to the fact that higher concentrations of PVA required more energy to change from a semi crystalline to amorphous state. These results clearly indicated that alginate was successfully incorporated in the PVA-BG network.

Equilibrium Water Content (EWC)

When developing dual network bioglass composites, it was vital to produce scaffolds that would be able to absorb biological fluid and retain them, allowing for their local delivery at the wound site. These composite should be able to absorb fluids but not swell to excessive amounts which would in turn heavily affect the dimension of the scaffold and also compromise its mechanical integrity. Excessive swelling is an undesirable feature as it would result scaffold pressure on the wound edges when implanted invivo and this could lead to cell death and necrosis of the affected tissue.

Figure 6-3 demonstrates the water uptake profile of the non-porous and porous composites over a period of four weeks, which showed that for all the composites there was a rapid uptake of water within the first 3 hours, whilst equilibrium was reached by 10 hrs. For the non-porous composites fabricated by 1, 2 and 3 cycles of freeze thawing EWC was found to be below 40%, this value was significantly lower than the EWC values obtained from DN hydrogels (Chapter 5) which were reported to be above 60%. This indicated that incorporation of Bioglass® into the DN system resulted in a dramatic decrease of the hydrogel composite's swelling ability as a result Bioglass® occupying the empty voids within the polymeric scaffold that would have otherwise been occupied by water upon swelling when hydrated. This decrease in EWC upon addition of Bioglass® is an advantage as increase in percentage swelling negatively affects the mechanical properties of hydrogels and also the distance between polymer chains which influences cell migration and neovascularisation. EWC of the non-porous DN10BG composite

networks showed that 3 cycles of freeze thawing resulted in composites with a significantly higher ($P<0.001$) than 1 and 2 cycles of freeze thawing. This result was within expectations as previous studies in Chapter 5 demonstrated that PVA base network when subjected to more than 2 cycles of freeze thawing did not further enhance the stability of the network. The EWC of the porous DN10BG (62.5%) and DN20BG (57.8)% was found to be significantly higher ($P<0.001$) than that of the non-porous DN10BG (1, 2 and 3FT) with EWC of (34.1, 34.4 and 40.4%) respectively. This result was expected because the porous structure of the composites introduces a larger surface area for water absorption, as well as providing an increased area for bulk water entrapment. It was also noted that the porous DNBG composites had a lower EWC than the DN hydrogels reported in Chapter 5. This can be explained due to the formation of strong bonding between hydrophilic groups of Bioglass and the alginate -COOH groups and also the P–O and O–H groups of the Bioglass particles can interact with the carboxylate groups of the alginate chains thereby firmly attaching to the surface of the Bioglass particles. Similar trends have been reported for blends of chitosan and gelatin with sol–gel derived nano-bioglass (SiO_2–CaO–P_2O5) prepared by a freeze-drying techniques [317]. The porous DN10BG composite had a significantly higher EWC than the porous DN20BG, which was attributed to the higher concentration of PVA resulting in a much dense network, with limited mobility of polymer chains owing to decrease in water uptake. A study by Pon-On et al, on PVA-BG/chitosan-collagen composite scaffolds for bone tissue engineering applications, reported their biocomposites with the best beneficial properties to have a swelling percentage of 120% after 1 day immersion in water, with a maximum of ~130% reached at 3 days [318], which is excessively high in comparison with that of the DNBG composites and would therefore negatively impact on the mechanical stability of the composites.

Ultimate Tensile Strength

In this study (Figure 6-4) the highest tensile strength was obtained for DN10BG-2FT composites with a value of 2.4MPa, found to be statistically significantly higher ($P<0.001$)

than the DN10BG-3FTcomposites. This trend in results was in agreement with that of tensile strength results obtained from the DN hydrogels (chapter 5), reinforcing the conclusion drawn before that 2 cycles of freeze thawing yield optimum tensile properties of the hydrogels. The stiffness of the DN10BG composites with no porogen was found to decrease with increasing cycles of FT. These tensile and stiffness values were higher than those of the DN hydrogels, which was due to the incorporation of Bioglass® within the network system. The small ~17µm particle size of the bioglass particles also enables a firm attachment of the polymeric matrix mainly by virtue of the carboxyl groups of the alginate interacting with the P-O and –OH group in the filler. A composite comprising of 45S5Bioglass® and alginate with a 3D multi-layered structure was reported by Nooeaid et al [319] for application in osteochondral tissue regeneration. These scaffolds were fabricated via polyurethane (PU) sponge method with a slurry of 3.5w/v% PVA and 40w/v% Bioglass®, the scaffold was then coated 3 times with 3% alginate and bonded with a layer of alginate foam, which was then chelated and dried at room temperature. These composites had tensile strength of 0.1MPa, substantially lower than the DNBG's, however it was deemed as sufficient mechanical competence and structural stability for osteochondral tissue engineering applications.

The tensile and stiffness properties of the porous composites, showed a statistically significant ($P<0.001$) rise with increase in concentration of PVA with 0.2 and 0.9MPa for porous DN10BG and DN20BG respectively. However, the porous network resulted in lower tensile and stiffness values as compared to the composites with no porogen, due to pores that can act as points of failure. Tensile strength values obtained in this study were found to be higher than the 0.1MPa [319] and 0.2MPa [320], values reported in literature on BG-PVA-alginate and BG-PVA composites respectively. Tensile strength obtained by Nooeaid et al [319] were also lower than those obtained for the porous composites in this study, by up to 6 fold in comparison with the DN20BG composites, which can be related to the double network formation. Bertolla et al, reported on Bioglass® based scaffolds reinforced by PVA/microfibrillated cellulose composite

coating. The Bioglass scaffolds were formed by PU sponge method, and were coated twice with a solution of PVA and microfibrillated cellulose (MFC). The composites exhibited tensile strength values of 0.2MPa which is ~ 4 folds lower than the tensile strength obtained with the DN20BG composites [320].

Trouser Tear test

The toughness of the DN10BG composites fabricated via 1, 2 and 3FT was tested along with the PVA only and dual network hydrogel fabricated via 2 cycles of freeze thawing, so as to serve as a control. Results in Figure 6-5 showed that 2 cycles of FT resulted in the DN10BG composites (4.8KJ/m^2) with statistically significantly ($P \leq 0.005$) higher fracture energy as compared to the PVA single network (1.8KJ/m^2), DN hydrogel (1.1KJ/m^2) and DN10BG composites fabricated via 1 and 3 FT cycles (3.2 and 2.4KJ/m^2) respectively. This result of DN10BG fabricated via 2FT cycles yielding the highest toughness is in agreement and solidifies tensile test results obtained from DN hydrogels and DN10BG composites where it was observed that 2FT cycles yield optimum mechanical properties for the hydrogels and composites, whereas 3FT cycles did not serve to further enhance the mechanical properties. The results were also found to be in agreement with those obtained in Chapter 5, where it was demonstrated that 2 cycles of freeze thawing resulted in higher fracture toughness for the DN network hydrogels.

Compression and cyclic compression

A statistically significant ($P \leq 0.045$) increase in compressive strength and stiffness of the composites were observed with increase in the concentration of PVA with values of 0.2 and 0.3MPa for DN10BG and DN20BG respectively. A change in the slope of the stress-strain curves of (Table 6-7) the composites were noted, initially small increases in stress gave large extensions however, at larger extensions the material became stiffer and more difficult to extend. This behaviour is typical of biomaterials whose microstructure evolves during compression to provide an increased stiffness. Porous multi-layered scaffolds of PVA, alginate and BG, designed for osteochondral applications have been

reported in literature with average compressive strength values in the range 0.01 - 3MPa, that were suited for osteochondral tissues, however the hydrogel like nature combined with the mechanical properties of these composites further lend themselves for osteochondral applications [319]. Several studies have reported compressive strength data on composites of Bioglass; Bertolla et al, 2014 on BG scaffolds reinforced by a composite coating of PVA and micro-fibrillated cellulose with values of 0.3 MPa [320]; PCL-BG composites by Rodenas-Rochina et al, 0.1 and 0.04MPa for 10% 20%BG respectively in the composite and elastic modulus 0.9 and 0.5MPa respectively [264]; BG-PVA-alginate biocomposite foams prepared via sol gel process were reported to have a higher compressive strength of 1.6MPa with elastic modulus of 0.02GPa [127]. A study on hybrid PVA/BG scaffolds reported compressive strength values of 9.1MPa however the authors did not state whether their scaffolds were tested under dry or hydrated conditions [321]. The DNBG composites either had values superior or comparable to the compressive behaviour reported for similar type of systems reported in literature, hence there is good potential to expand the biomedical applications.

It was observed during the compression test that once the applied load was removed from the composites, they sprung/returned back to their initial state, thus to understand if loading was completely reversible and elastic, cyclic compression tests were carried out. Although the composites returned to their original position and shape upon unloading, it was assumed that there must be some microscopic failures that occur in the composite before it can reach a level where it incurs macroscopic failure. This type of event should be mechanically detectable through the presence of a hysteresis loading-unloading curve.

Systematic loading-unloading experiments (Figure 6-8) were carried out on the composites at a constant load for 5 consecutive cycles. In both the DN10&20BG composites the loading curve of the 1st compressive cycle was different from the unloading curve, and equally different from the 2nd loading-unloading curve. The 2nd loading-unloading cycles were nearly elastic and followed the path of the 1st cycle, whilst

the 3rd, 4th and 5th cycles seemed to reach a steady state where there seemed to be no further changes in the loading-unloading curves of the composites. This behaviour is typical to that of Mullins effect whereby, the mechanism of stress softening is characterised by a decrease of the stress on unloading compared to the stress when loading at the same strain, this is as long as the maximum strain of the first loading is not reached. The stress drop between successive loading cycles is especially important during the first and second cycles and becomes negligible after about 5-10cycles. At a stationary state with constant stress amplitude, a stabilised hysteresis loop is then reached after several cycles [322]. However it is known that in filled rubbers (elastomeric materials) the behaviour of the virgin sample can be recovered when a sample is left to rest typically for 1hour [323] but the DNBG composites were found to be able to recover after application of a given load without the need for relaxation time. In recording the level of hysteresis during the experiments, the heterogeneous structure of the network of the composite was investigated and the most likely explanation is that the macromolecular chains of the polymers slip and slide with friction over one another, whilst the chains connected to the Bioglass® particles are slipping and sliding with friction over these particles (Figure 6-20). The hysteresis curves of the DN20BG composites can be further explained by the macromolecular chains connected to the surfaces of the Bioglass® particles undergo deformation close to macroscopic deformation state [322].

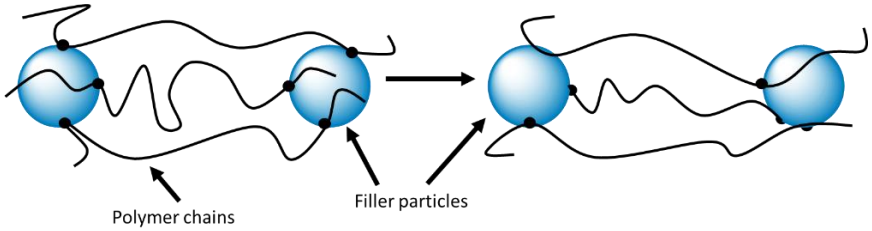

Figure 6-20: Ceramic or glass filler particle interactions with polymer chains.

SEM analysis

The non-porous DN10BG composite (Figure 6-9) showed a compact network structure with porosity that was primarily due to freeze drying. The heterogeneity of the composite was observed at higher magnification, the polymer phase was seen coating the Bioglass® particles. The micrographs of the DN10&20BG composites displayed a porous structure with interconnected pores of varying sizes ranging from ~1mm to < 20µm. Such large pores should in principle encourage bone cell adhesion and proliferation, enable mass transfer and providing increased surface area for cells to grow and act as a carrier for growth factors, very small pore sizes are known to hamper neovascularisation. Ideal pore size for bone tissue engineering has been reported to be in the ranges 300 – 500µm [28] or 200 - 800µm [127]. Pore size plays a very important role on the mechanical properties of the scaffold, large pore sizes weaken the mechanical properties of the scaffold, and this justifies the lower tensile and compressive strength values obtained from the composites.

BIOACTIVITY OF COMPOSITES (MINERALISATION)

A bioactive material is one that elicits a specific biological response at the interface of the material which results in the formation of a bond between the human tissue and the biomaterial [324]. The key compositional features that are responsible for the bioactivity of bioglass® 45S5 are its low SiO_2 content, high Na_2O and CaO content and high Ca/P_2O_5 ratio. The bonding of bioglass® 45S5 to bone has been attributed to the formation of a carbonate substituted hydroxyapatite (HCA) like layer on the glass surface in contact with body fluid, and this HCA layer is generally believed to form as a result of a sequence of reactions on the surface of the bioglass implant. The surface reactions involves dissolution of critical concentrations of soluble Si and Ca ions that give rise to both intracellular and extracellular responses at the interface of the glass with its physiological environment [300, 306]. Solution mediated dissolution of bioglass results in the accumulation of dissolution products, which cause both the chemical composition and pH of the solution to change. This change results in surface sites and pH levels

inductive for HCA nucleation. There is a sequence of 11 reactions stages that occur on the surface of Bioglass® after implantation. To understand the processes that occur when Bioglass® is placed in SBF resulting in mineralisation, the first five stages on the mechanism of HCA layer formation are summarised.

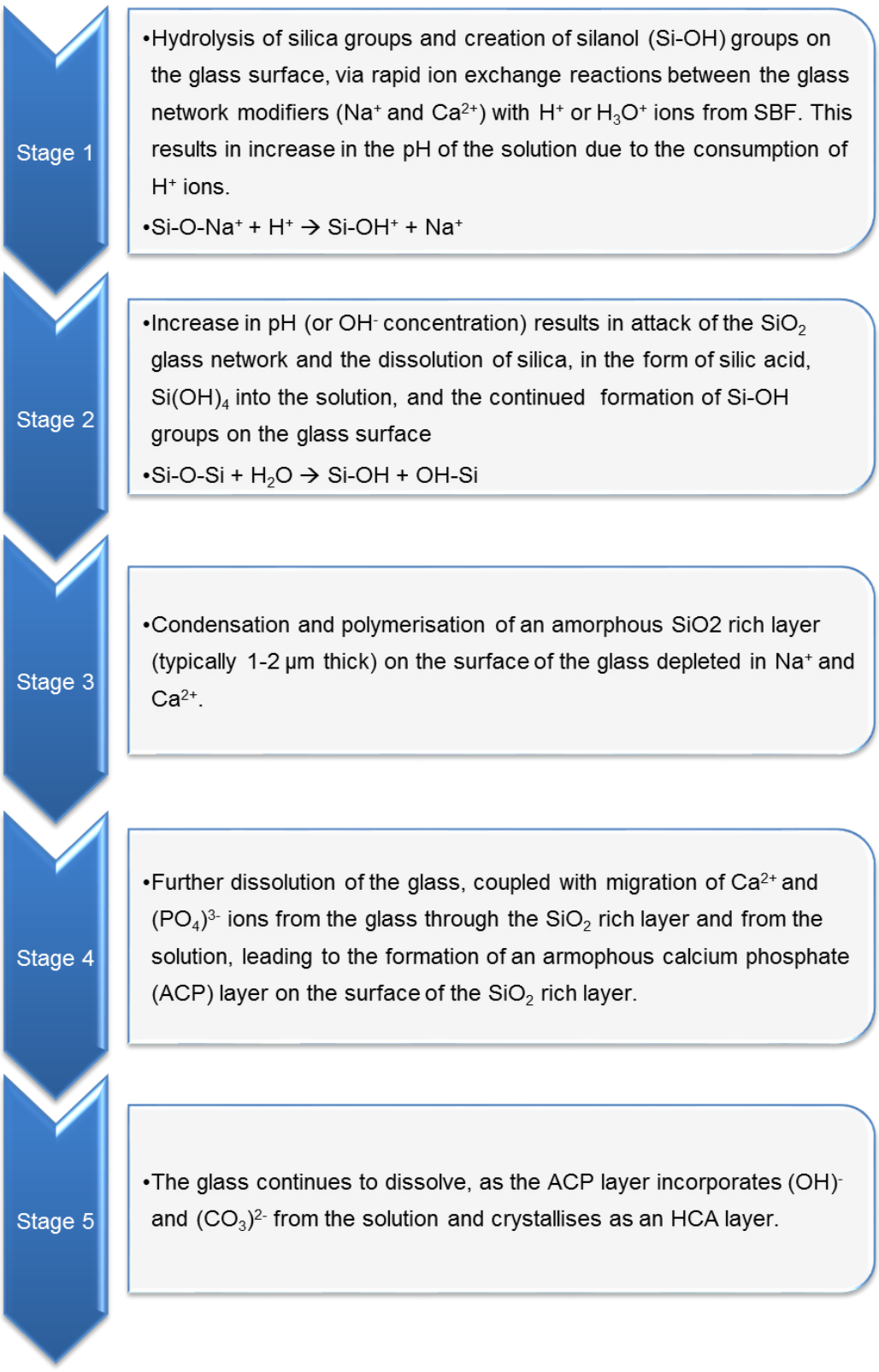

The DNBG composites on interaction with simulated body fluid, clearly exhibited the formation of a mineral layer on the surface of the composites as shown in the SEM micropgraphs. Furthermore, tensile strength tests were carried out to investigate the effect of mineralisation on the composite networks after immersion in SBF for 7, 14, and 28 days. The tensile strength after 7 days of immersion showed a decrease in the tensile strength (Figure 6-21) of both non-porous and porous composites, which was attributed to the initial degradation of unreacted and uncrosslinked PVA and alginate chains in the network.

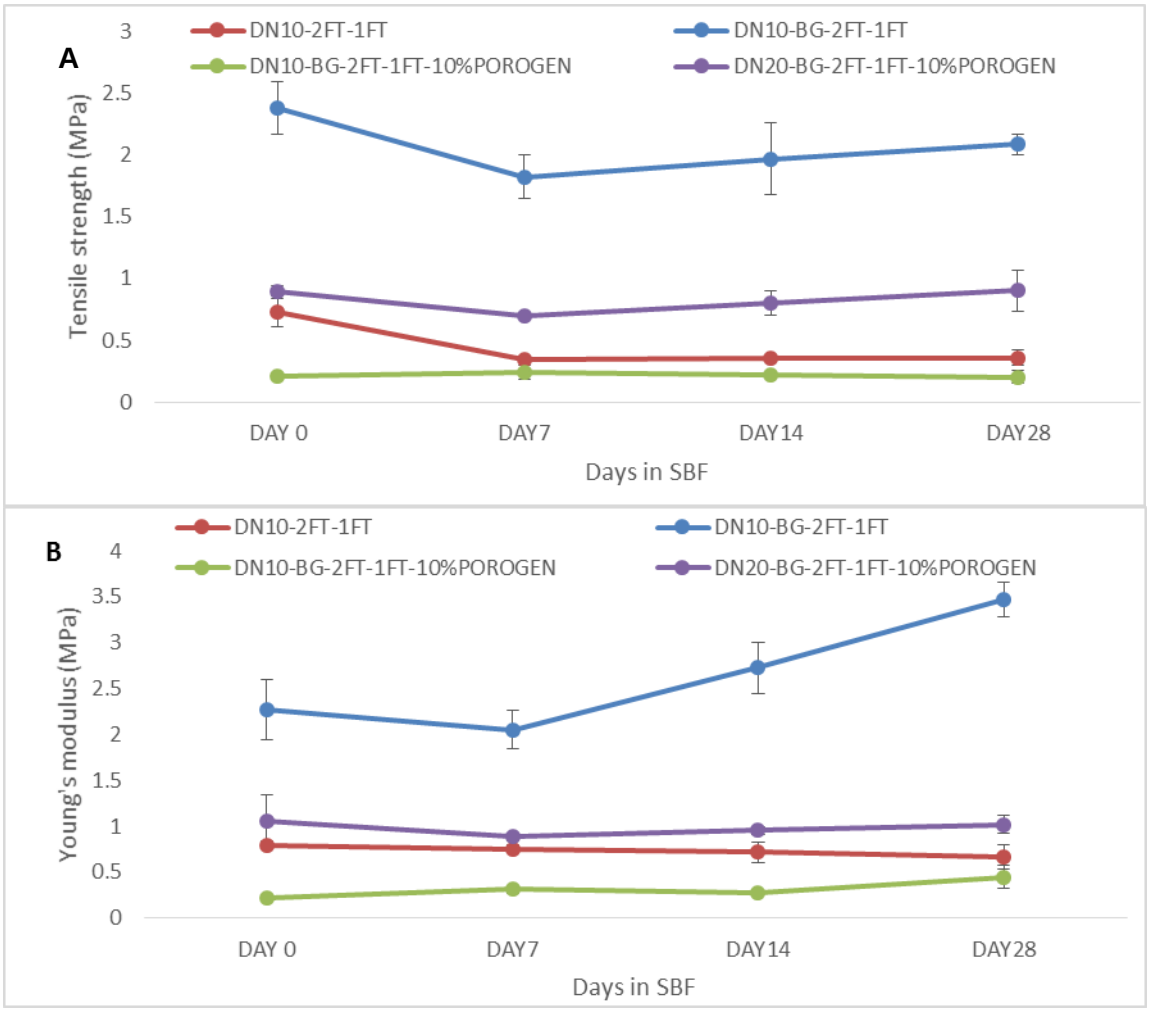

Figure 6-21: The effect of mineralisation on the tensile strength **[A]** and Young's modulus **[B]**, observed from the DN10, non-porous DN10BG and porous DN10 and 20 BG composites, all fabricated via two cycles of freeze thawing.

Tensile strength of the non-porous DN10BG composite at day 0 (2.4MPa) was significantly higher (P=0.005 and 0.038) than at day7 (1.8MPa) and day 14 (2.0MPa) respectively, but not significantly higher than that at day28 (2.2MPa). The stiffness at day 28 (3.5MPa) was found to be significantly higher (P<0.001 and P=0.006) than after 7

(2.1MPa) and 14 (2.7MPa) days immersion in SBF respectively. This indicated that there was an increase in strength and stiffness in the non-porous DN10BG-2FT-1FT composite, due to the reinforcement of the composite network by the HCA crystals formed on the surface area of the composite. For the porous DN10BG-2FT-1FT composite there was no significant increase in tensile strength however, the stiffness at day 28 (0.5MPa) was found to be significantly higher ($P<0.001$, $P=0.048$, $P=0.014$) than at days 0, 7 and 14 (0.2, 0.3 and 0.3MPa) respectively. For the porous DN20BG-2FT-1FT, the tensile strength at day 0 (0.9MPa) was found to be significantly higher ($P=0.043$) than the strength at day 7 (0.7MPa), and was not found to be significantly higher than at day 14 and 28 (0.8 and 0.9MPa) respectively. The tensile strength at day 28 was significantly higher ($P=0.049$) than after 7 days immersion in SBF, however no significant difference was found in stiffness values of the composite.

These results indicated that mineralisation did occur in both porous and non-porous composites, however the non porous composites showed a marked improvement. The DN hydrogels were used as the control group in this study, for which the tensile strength of 0.7 MPa before immersion in SBF was significantly higher ($P<0.001$) than after all immersion periods, whereas there was no significant difference in stiffness between all periods. Therefore, no significant stiffening or increase in tensile strength occurred in the DN hydrogels, hence the enhancement in tensile and stiffness properties of the composites was mainly due to the mineralisation process that resulted in mineralisation of the composite which would reinforce and enhance the already existing mechanical properties of the composites. Similar results were reported by Pon-On et al, 2014 where they prepared poly(vinyl alcohol)–bioglass/chitosan–collagen composite scaffolds with various compositions via 3 freeze thaw cycles followed by freeze drying process to impart porosity on the scaffolds. The authors 1st created PVA/BG powder of ratio 2:1 with 7wt.% PVA solution, they then used this PVA/BG powder to create composites of PVABG/ChiCol of ratios 0.5:1, 1:1 and 2.1. The authors found that the compressive strength and modulus of the PVA/BG-Chitosan-collagen scaffolds decreased after 7

days immersion in SBF for all composite formulations, the study however did not report on mechanical properties further than 7 days immersion in SBF [129].

The bioactivity of composite networks was also assessed by monitoring the rate of HA formation on samples after immersion in SBF using FTIR and Raman spectroscopy and further validated by the mechanical behaviour of the composites theorised to be enhanced due to the mineralisation process. The P-O bending bands (Figure 6-13) located at ~604 and ~565 cm^{-1} can be considered to be the main characteristics of HA and thus they were used for confirming the formation of HA layer. However, weak absorption bands were also observed in the FTIR spectra for day 0 at ~604 and ~565 cm^{-1} that is typical of the P-O bending of HA, which can be explained that some level of interaction had occurred during the formulation of the composite because the PVA-Bioglass was subjected to immersion in a sodium alginate. A new carbonate band at 800-890cm^{-1} was observed on the porous composites after 28 days in SBF, which suggests the formation of an apatite like layer. Similar observations on absorption bands identifying the formation of apatite on Bioglass® and Bioglass® containing composites have been reported [311, 314, 325-327].

Identification of HCA layer on the composites was supplemented by FTIR-ATR spectra in Figure A-1 (see appendix) where: The peaks at ~1400 cm^{-1} increased in intensity after 28 days immersion in SBF, these peaks were due to the υ_3 vibrational mode of carbonate ions. The distribution of the carbonate υ_3 sites is said to depend on the maturation and formation of the apatite crystals, as well as on the competition between phosphate and carbonate ions. After 28 days immersion in SBF, the phosphate peaks (υ_3) on the composites were observed at 1024, 1051 and 1023 cm^{-1} for non-porous DN10BG and porous DN10, 20BG respectively. Peaks centred at ~914 cm^{-1} were due to mixed stretching and bending vibrations of Si-O-Si bonds, which overlapped the bend mode of phosphate vibrations. Resonances attributed to the carbonate $(CO_3)^{2-}$ group have generally been interpreted as indicating the formation of carbonated substituted

HA, whereby some of the $(PO_4)^{3-}$ ions in HA are substituted by $(CO_3)^{2-}$ due to the dissolved CO_2 in aqueous solution [327, 328].

The results obtained from Raman analysis (Figure 6-14) showed little to no changes after 7 and 14 days in SBF. Peaks attributed to the P-O stretching and asymmetric stretching at 960 cm^{-1} and 1085 cm^{-1}, corresponding to HCA formation were clearly observed after 28 days immersion in SBF. The DN20BG porous composite were an exception and the absence of HCA formation peaks on the DN20BG composite was attributed possibly to the random area of mushrooming crystals caused by a high ratio of polymer contents as compared to Bioglass® content in the composites. The Raman and IR results confirmed the presence of HCA layer formation on the composites, results which are supported by the tensile strength and stiffness value trends obtained from the composites after immersion in SBF for 7, 14 and 28 days.

SEM micrographs provide a visual presentation of the formation of cauliflower like structures with some fan-like crystallite outgrowths which probably as the Bioglass particles are entrapped in polymer matrix, hence the mineralisation mirrors that pattern. . The increase in density of the crystals with immersion time in SBF was clearly observed. Micro-chemical analysis was carried out on the crystals at each time point and the Ca/P ratios calculated to determine the proximity of the formed crystal stoichiometric ratios to that of HA which is known to be 1.67 [298]. Results obtained from analysis did not display any particular trends with Ca/P ratios. It however was observed that the initial Ca/P ratio was high with values in the ranges 2.23 – 2.44, indicative of Bioglass® where the Ca to P ratio is 5:1, this value was then observed to decrease with increase immersion times in SBF. After 28 days immersion in SBF, the EDX of the porous composites displayed calcium deficient HA in which the Ca/P ratio was lower than 1.67. The presence of carbonate was however established through FTIR and Raman analysis. It has been noted from this study that the composites comprise of only 30% Bioglass® and that this would consequently have an over-all effect on the amount of HCA produced and detected. The levels of HCA on the surface were therefore not expected to be to those within the internal structure of the composite.

Cyclic compression tests were carried out to understand the effect of mineralisation on the hysteresis of the composites. Initially before immersion in SBF the composites were found to have superimposable curves with little to no hysteresis, implying very little energy dissipation at a molecular level. However, from the results displayed in Figure 6-11 and Figure 6-12 show substantial hysteresis on all the cycles (mostly observed well between cycle 1 and 2), which was probably due to molecular friction between the composite and new crystal formation due to the process of mineralisation. It was clear that the loading and unloading curves were all different, strongly suggesting that the hysteresis observed in the first cycle is related to irreversible fracture events taking place in the composites. However the nature of these fractures could be investigated further by conducting studies were the samples would be allowed relaxation time before applying load for the second cycle, before concluding that the fracture incurred and observed here was irreversible. It can be stated that “The number of fracture events is directly dependant on the maximum strain achieved during the first cycle.” This is to say “if a second loading-unloading cycle is performed at a lower or equivalent strain the material behaves very elastically, however if the maximum strain of the second cycle surpasses that of the first cycle, the loading curve has two parts.” In this case it is the latter.

CYTOCOMPATIBILITY

Research has shown that glasses with especially high levels of bioactivity can also be used to activate genes to stimulate the body to repair itself, this means that Bioglass® 45S5, which has the highest rate of bioactivity would impact regeneration of trabecular bone. This rapid regeneration of bone is due to a combination of osteostimulation and osteoconduction, a consequence of rapid reactions on the bioactive glass surface. However, the level of regeneration would be influenced by the ratio of polymer to glass content in the composite. To understand how human osteoblast cells would behave on the scaffolds, a series of in vitro cell culture tests were carried out.

MTT results displayed in Figure 6-16 indicated that there was a decrease in cell proliferation with increased exposure time to eluents. Calculations of the RGR confirmed

the level of cytotoxicity of the degradation products and ions released in the media due to mineralisation process that occurred during sample wash time periods.

Hydrogel System	Eluent extraction (hr)	Relative growth rate (RGR) (%)		
		24 exposure	48 exposure	72 exposure
DN10BG No porogen	24	127.0	48.9	31.9
	48	92.9	32.6	19.9
	72	102.8	39.2	22.3
DN10BG 10%porogen	24	108.6	41.5	23.3
	48	76.3	28.0	14.3
	72	79.3	26.3	17.9

Table 6-8: Relative growth rate percentage of non-porous DN10BG and porous DN10BG demonstrating viability of HOB cells within the hydrogels.

Results in Table 6-8 indicated that elution products were cytotoxic to the cells after 72 hours exposure (culture period) which resulted in cell death. This result was mediated by changing the media solution of the composites with cells seeded on them, during culture period every 2-3 days to prevent cell death. This proved to be a major limitation in the application of in vitro analysis of scaffolds with a composition of Bioglass® 45S5 within their network as the local biological environment can be influenced significantly by their chemical degradation products of Bioglass®. Release and increases in the concentration of ions such as Na^+ and Ca^{2+} as well as $Si(OH)_4$ and changes in the pH occur as a result of degradation particularly in the early stages due to fast degradation of the glass component. However it is theorised that, in animal and clinical trials this would not pose a big problem because living tissues have a constant flow and diffusion of fluids and ions as well as migration of cells all of which allow for extraction of degraded toxic elements at the wound site. For example small pieces of $Si(OH)_4$ released during degradation are eaten by phagocytes and extracted out [298]. Mishra et al, 2009 assessed the cell viability of fibroblasts on their BG-PVA-alginate biocomposite prepared by sol gel process and reported that their material indicated good cell viability using MTT assay

under in vitro conditions [314]. This is attributed to the fact that sol gel process recreates to the same degree of nanoscale order and organisation, the mineral organic components as found in vivo.

Live/Dead Staining of the HOB cells cultured on the composites for up to 28 days (Figure 6-17) showed cell attachment and proliferation on all the composites. On the porous composites good cell penetration and proliferation within the porous network of the composite was observed. It was noted that due to the formation of an HCA layer formed on the surface areas of the composites, visualisation of live/dead cells on the composites became difficult, as this HCA layer formed over the surface of already attached and proliferating cells. Instead what was observed was a glowing green colour on the whole surface of the composites resulting in limited visualisation of actual cell structures or morphologies. At 28 days in culture a flat layer of HOB cells was clearly observed on the surface of the composite fabricated with no porogen. On the porous composites at day 28, a cell structure through one of the pores that had a connected structure through the depths of the composite was observed. This indicated that a communication and connection of cells had occurred through the pores to the different depths of the composite.

SEM was utilised to observe and characterise the cell morphology of the HOB cells on the composites after 7 and 14 days in culture, results have been displayed in Figure 6-18. Cellular attachment, adhesion, and spreading are of vital importance in living biological processes and belong to the first phase of cell/material interactions. This process is involved in various natural phenomena such as embryogenesis, wound healing, immune response, the maintenance of tissue structure, metastasis, as well as the integration of tissue with biomaterials. After 7 days in culture it was observed osteoblast attached to the surface of the composites and spread across the whole surface colonising the scaffold and displaying a flattened morphology. Also observed was the flattened morphology of cells spreading across pores and forming a sheet over them, cells were multi-layered and elongated.

Proliferation and differentiation is influenced by the quality of this phase, and Costa et al, 2012 reported that cell spreading has been divided into three main interaction levels:

I. Unspread; cells observed to be spherical in appearance, and protrusions or lamellipodia were not yet produced.
II. Partially spread; cells are observed to begin spreading laterally on one or more sides, but the extensions of the plasma membrane were not completely confluent.
III. Fully spread; cells are spread laterally with extensions, represents the best result of material hosting. [321]

The observations of the HOB cell morphology indicated that the composites are a good cell host scaffold allowing for cell attachment and proliferation on the surface and internal structure of the scaffold.

Higher levels of ***ALP*** activity were observed at day 14 for both composites. ALP is essential in bone maturation and it is produced at high levels during bone formation activity [329]. Bioglass® 45S5 has been reported to show a marked effect on its ability to support the proliferation and functions of cells in vitro [298]. On reaching osteoblast maturity, initiation of mineralisation protein is signalled, thus results have indicated that the HOB cells cultured on the composite scaffolds were progressing towards bone maturation.

6.6 CONCLUSION

Novel dual network composites of PVA-alginate-bioglass were successfully fabricated. These composites have the advantage to be easily tailored to have either high or limited macroporosity, expanding their potential use in applications as membranes or porous plugs. The composites have the potential to function as bone substitutes that can absorb and retain biological fluids rich in growth factors allowing for their delivery at the wound site, whilst retaining their shape, mechanical strength with limited swelling expansion. This has been demonstrated by their water uptake levels and exhibit remarkable increase in tensile strength, stiffness and fracture toughness in response to mechanical

deformation. The added advantage of the composites is their bioactive component which was demonstrated by means of FTIR, Raman, SEM and EDAX analysis and resulted in enhanced mechanical tensile properties. The fabricated novel composite systems are designed to function as three dimensional frameworks for augmentation of bone voids in non-load bearing areas that can have exogenous orthobiologics introduced to them before implantation or be obtained endogenously after implantation.

Chapter 7
Conclusion and future work

The design strategies for bone substitutes used in this study involved two strategies (i) fabrication of elastomeric composites that would have controllable expansion to fit the bone defect overcoming the problem of rigid bone substitutes that tend to induce micro-movement at the bone-substitute interface, adversely impacting bone regeneration and (ii) the porous composite scaffolds to suit vascularisation and orthobiologic approaches via the potential for inclusion of platelet rich plasma or bone marrow aspirates within them that are rich in biologics and known to promote bone healing.

Hydrogels were selected as the matrix for the composites to enable fluid uptake and dual networks formed to enhance toughness and impart elastomeric properties whilst using phosphate calcium phosphate as fillers, in view of their transient role and effectiveness in bone regeneration. The base polymer selected was poly(vinyl alcohol), which is an FDA approved polymer for medical use and can be crosslinked using physical methods alleviating problems associated with use of chemical cross linking agents in devices for biomedical applications. Previous studies in our laboratories demonstrated that calcium metaphosphate (CMP) scaffolds with mixed porosity promoted bone formation whilst undergoing total resorption within 8 weeks in rabbits. In addition the in vitro cell-material interaction studies by Buranawat (Buranawat thesis 2012) showed that CMP exhibited an osteoinductive potential even in non-induced conditions and Von Kossa staining exhibiting nodule formation in non-induced medium. This was further confirmed by gene expression of proteins, Runx 2, Osteocalcin, ALP and procollagen. Based on these results, this phase of calcium phosphate was selected as the filler and 45S5 Bioglass®, which has an established history of bone regeneration capabilities, for designing the hydrogel composites towards clinically viable materials to repair, regenerate and enhance bone healing across small and large bone defects. In particular, the role of the hydrogel matrix would be to allow imbibition and retention of biological fluids such as

autologous PRP or growth factors, and allow for their delivery at the wound site. The design parameters of the grafts included incorporation of hydrophilic polymers that could be cross-linked by physical means, with the ability to be tailored to increase or decrease hydrophilicity, allowing for their potential to absorb biological fluids. The overall study was carried out in four developmental stages leading to the achievement of the final bone graft substitutes, which are now being considered by a commercial enterprise towards clinical translation.

Stage 1: The concentration of PVA and the most effective physical crosslinking method between freeze thawing, air drying and a combination of both that yielded optimum mechanical properties of PVA single network hydrogels were identified and utilised in the development of PVA-CMP composites, interpenetrating dual network hydrogels and their composites. A concentration of 10% wt/vol of PVA yielded the viscosity suited for composite formulation with freeze-thawing for physical crosslinking.

Stage 2: Composites of PVA with a high concentration of CMP filler particles were fabricated and through freeze-drying, and a porous network was obtained. The inclusion of the filler in the composite decreased both swelling and water uptake as compared to the parent PVA single network hydrogel. The mechanical properties of the composites could be tailored by varying the concentration of PVA in the composite formulation and the hydrated composites with 30% concentration of PVA yielded compressive strength of 48 MPa and modulus of 725 MPa, which were 7 and 2 times higher than composites of PVA with hydroxyapatite [239]. The diametral compressive strength was also found to be highest for the 30% concentration of PVA, the water uptake being lowest, indicating the formation of a tight network with interaction between the filler and matrix which is attributed to some H bonding between the PVA and CMP on freeze thawing. The inclusion of CMP in the PVA matrix led to a decrease in water uptake and could be regulated to low values of 25% EWC with low swelling and enhanced mechanical properties in the hydrated form. This study for the first time formed porous hydrogel composites of PVA with direct incorporation of the new calcium metaphosphate filler and subjecting to physical crosslinking, suited as bone plugs and cavity fillers for bone

defects. PVA hydrogels with hydroxyapatite inclusions have been mainly reported for articular cartilage where in situ formation of hydroxyapatite is carried out that limits the amount of HA that can be incorporated due to agglomerations forming even with concentrations of 15% of PVA.

Stage3: Double network hydrogels are being increasingly used as a convenient method of synthesizing tougher hydrogels, which comprises of a first network, in which a second interpenetrating polymer network is formed within the first network. Based on this concept, for the first time dual network hydrogels were formed with two biocompatible FDA approved polymers to create tougher hydrogels than single network PVA hydrogels. Unlike double networks, two water soluble polymers were used where the first network was a brittle network formed by physical crosslinking of PVA and intrusion of sodium alginate was conducted and chelated to yield the neutral gel, which was further freeze thawed to create the dual network. These hydrogel networks were successfully formed with lower swelling characteristics and increased tensile strength and ductility due to the formation of a second network within the first brittle network. The evaluation of the properties of the dual network provided the information required to formulate the composites using the tough network as the matrix. Interestingly, the texture, water uptake and elasticity of these networks highlighted the potential application to form wound dressings and as matrices for soft tissue engineering. Although this will be a future research project, a preliminary drug release study was carried out using vancomycin to study the drug release profile. The drug release was found to be ~proportional to the swelling ratio of the hydrogels (i.e high swelling ratio resulted in high drug release) that showed a steady increase in the release with time, thus could be suited for local applications of high doses of vancomycin. The ability to tailor the hydration dynamics makes this dual network an attractive system for delivery of drugs. The dual network hydrogels demonstrated the multifunctional capability to function not only as the initial polymeric phase to serve as a base matrix for the development of composites, but with potential for soft tissue applications as well as drug delivery matrices.

Stage 4: Elastomeric composites facilitate surgical handling and the intimate contact with the wound also allows a gradual load transfer to the bone, until it can be mechanically capable of enduring loading. Dual networks that were formed in this study were further used for formulation of the composites due to their controllable swelling and mechanical properties. 45S5 Bioglass® was selected as the filler due to its bioactivity as well as its reported ability to form mechanically strong bonds with bone as well as soft tissue. Both non porous and porous composites were fabricated Bioglass® 45S5 and the porous networks were spongy and found to exhibit hysteresis behaviour typical of that described by Mullins effect, a preconditioning condition typically exhibited by soft tissues. The interaction with simulated body fluid identified the deposition of an HCA mineral layer on both the composites with good biocompatibility, low cytotoxicity and good mechanical properties. These novel composites were found to exhibit a potential to overcome current biological challenges of bone substitutes and holds great promise as effective bone substitutes and drug delivery devices.

One of the most important design parameters for scaffolds in this study was their ability to absorb and retain fluids. This parameter aids in determining the functionality and limits thereof of the scaffolds. The trend in comparison of the water uptake of the networks fabricated was observed as follows:

PVA single network > Dual networks > DNBG composites

PVA single network > PVA-CMP composite

The novel dual network hydrogels fabricated with PVA and sodium alginate exhibited properties to suit a diverse range of applications in soft tissue applications and it will be of future interest to explore, especially as these systems can be used for bio therapeutics. Hydration properties of these network gels show potential for wound dressing applications, not only to keep the wound hydrated while preventing build-up of bacteria and maintain its structural integrity. This could be achieved by incorporating

antimicrobial peptides that can bind to the alginate in the dual network, employing similar methods as reported in a study by Chan et al, 2004 [330]. Similar clinical studies have been reported on hydrogels impregnated dressings for graft fixation, where patients treated for skin grafting have been treated with hydrogel impregnated dressings. The dressings were coated with hydrophobic fatty acids that irreversibly binds to the bacterial surface and mechanically removes bacteria from the wound, so as to prevent infections and the skin grafts from drying. The authors concluded by suggesting the dressing to be used as a superior alternative over tie-over dressings [331].

It is postulated that these dual network hydrogels can be applied as internal stabilisation devices to provide torsional stability and allow a localised delivery of autologous growth factors that would aid and enhance healing time. The composites are elastic and it is known that elastic bone substitutes decrease shear forces on the bone-implant interface and a study on polyurethanes have shown to be successful in repairing critical bone defects [332]. The PU systems however are slow to degrade whilst the dual networks with PVA-Alginate/CMP composites are erodible with a CaP phase that assists in bone formation.

A recent study by Baker et al, 2016 reported [333] on self-deploying shape memory polymer (SMP) scaffolds for grafting and stabilizing mouse femoral segmental defects, in which they concluded that their SMP sleeves used in combination with allografts provided torsional stability to the bone defect, and showed promise as internal stabilisation devices that could be used as supplementary fixation to current strategies. The polymer systems used in the study by Baker et al use acrylate based monomers with crosslinking agents, tetraethylene glycol dimethacrylate, which yield stable polymeric entities, hence will have limitations, however the strategies of their study is similar to this study in terms of the ability to absorb fluids rich in growth factors, which would allow for their localised delivery at the wound site. Furthermore, the surgical handling of the dual networks were assessed by two orthopaedic surgeons and oral communications suggested that their placement would be far superior than any other

existing bone substitutes (oral communication with consultant orthopaedic surgeon Dr Reichert).

The ability to tune the swelling and EWC of the DN hydrogels, DNBG and PVA-CMP composites combined with the fact that all exhibited lower water uptake than their corresponding PVA single network hydrogel counter parts is clinically desirable, since excessive swelling negatively affects the mechanical stability as well the expansion of the graft, which may result in undue pressure on the edges of the wound site, eventually resulting in cell death and tissue necrosis.

The mechanical stability and integrity of scaffolds has been a major challenge and have been one of the causes of limited translation of scaffolds from the laboratory to clinical practice. Scaffolds with mechanical properties matching those of native tissue, aid in providing the desired mechanical stability at the defect sites, especially in load bearing areas.

The trend in comparison of the mechanical properties of the networks fabricated was observed as follows:

Tensile strength: - PVA10 < DN10 < DN10BG

Compression: - DN10, 20BG < PVA-CMP

Composite grafts reported on the DNBG (Chapter 6) and PVA-CMP (Chapter 4) were designed specifically for orthopaedic applications. Both composites had a porous structure with a highly interconnected porous structure in the DNBG composites, which facilitates nutrient transport, bone ingrowth and vascularisation. The mechanical properties of the composites were found to more closely resemble cancellous bone. The scaffolds were found to have low brittleness and therefore pose a limited risk of catastrophic failure under load. The easy handling and the ability to reshape the

composites using a scalpel under hydrated conditions, will ensure that they can be easily cut or shaped by the surgeon if need be during surgical procedures.

With a view to highlight the advantages of the composites developed in this study, a comparison of selected current grafts reported in recent literature is presented. The SMP grafts mentioned earlier, were tested in femoral segmental bone defects in a mouse model, however, the grafts did not result in bone regeneration as compared to the allografts and it was concluded that incorporation of ceramics or bioglass fibres may improve mechanical properties and enable the next generation of SMP sleeve to function as a stand-alone bone graft fixation strategy [333]. This is significant as the lack of a porous and mechanically stable structure, as well as a bioactive component in a graft suggested for bone bridging or augmentation, highly impedes the regeneration of new bone into the graft as the environment is unsuitable for osteoblast cell recruitment, attachment and proliferation.

Another novel highly porous ceramic scaffold termed ‘Baghdadite’ ($Ca_3ZrSi_2O_9$) containing zirconium in the crystal structure of calcium silicate was reported however were later modified to improve their mechanical properties by introducing a PCL coating containing bioglass nano-particles. The resultant compressive strength of the modified scaffold was reported to be 1.1MPa which was higher than the 0.2MPa of the unmodified scaffold. On implantation into critical sized segmental bone defects in sheep, the scaffolds were reported to be able to withstand physiological loads at the defect site, and induced substantial bone formation in the absence of supplements and growth factors [334]. These scaffolds can relatively be easily compared to the composites in this study, especially with the DNBG composites. While the compressive strength of the modified baghdadite is relatively close to the DN10BG composite, they however remain lower than those for all DNBG and PVA-CMP composites. Figure 7-1 illustrates a comparison and demonstrates the differences in brittle behaviour under load of the baghdadite scaffolds with the DNBG composite. It clearly shows that whilst the modified baghdadite scaffold does not undergo catastrophic failure under load, it does still undergo total

collapse. In contrast, the DNBG composites neither undergo catastrophic failure or total collapse when placed under loading conditions, and was observed to spring back to its original height when the load placed on it is removed.

.

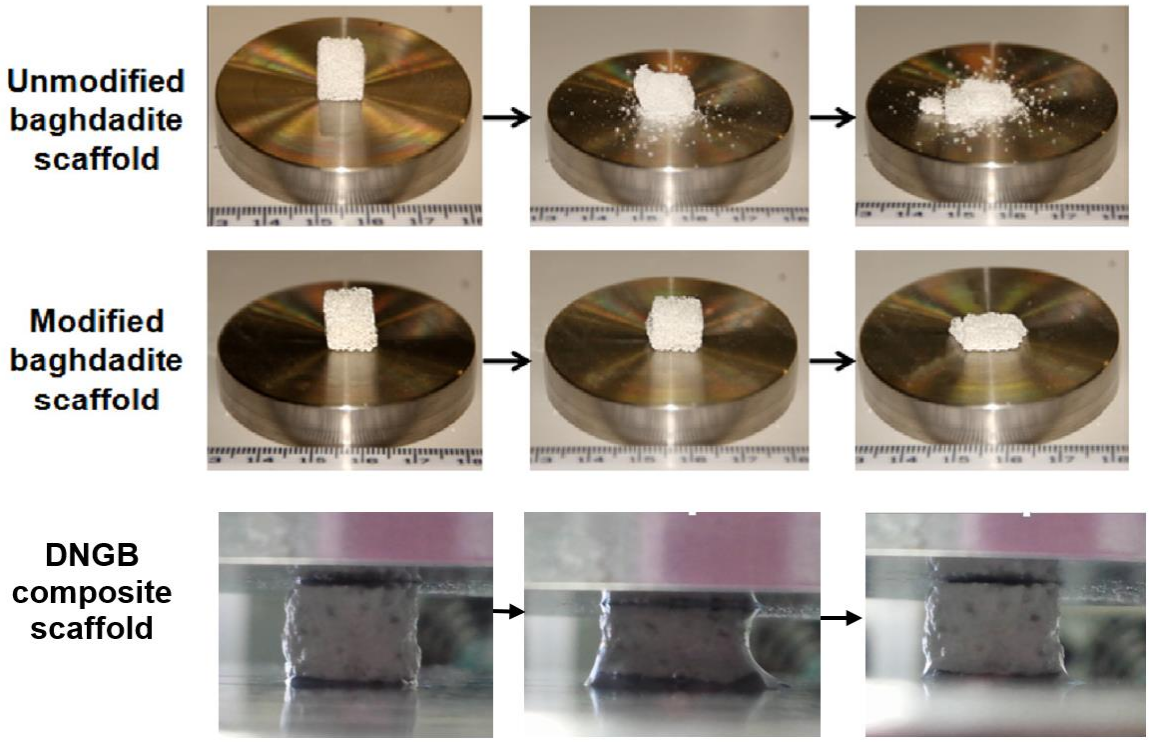

Figure 7-1: Comparison images demonstrating the differences in brittleness and lack of, of the baghdadite and modified baghdadite scaffolds [334], with the DNBG composites before and after loading.

As discussed in the literature review a number of bone substitutes based on ceramics are used clinically and their limitations mainly pertain to their brittle nature and in some cases very slow resorbability. Most clinically used bone substitutes are dispensed either as granules and blocks, which are either packed into defects or plugged into defects and the rigidity causes micromovement. However, the DNBG and PVA-CMP composites can be made as whole block grafts that can be easily cut by surgeons during operations if desired is a distinct advantage over other existing materials.

Both the DNBG and PVA-CMP composites offer the versatility to be fabricated with different types of ceramic and glass fillers. Properties of the composites can be tailored to desired needs by changing the polymer concentration used in their fabrication. DNBG

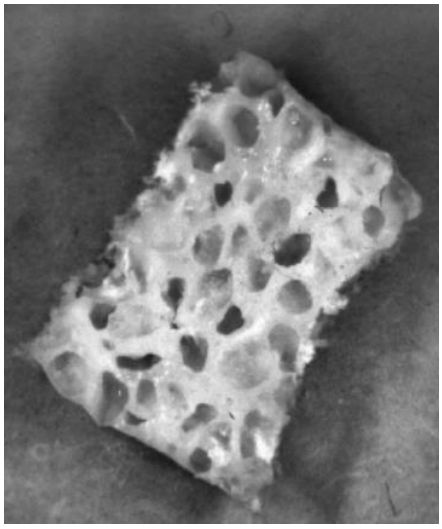

Figure 7-2: Image of DNBG composite demonstrating the porous internal structure, and the similar biomimicry to trabecular bone.

composites provide an interconnected porous structure that closely mimics the structure of trabecular bone. Clinical and animal studies have been carried out with scaffolds fabricated from the same materials as in the DNBG and PVA-CMP composites, demonstrating the biocompatibility of the individual components chosen in this study, of which has provided further solidification of the biocompatibility of the DN hydrogels, DNBG and PVA-CMP composites. The hydrogels and composites can be fabricated in moulds of different forms to expand their applications. For example the DN hydrogel can be fabricated in channelled moulds to be utilised as scaffolds applicable for nerve regeneration, with channels that can guide the regenerating axons. This is comparable to a study by Gunter et al, 2015 who developed alginate hydrogel scaffolds with anisotrpic structure, aimed at regenerating axons after spinal cord injury[335]. The non-porous DNBG composites as well as the DN hydrogels have the versatility to be fabricated to function as membranes, which can be used to seal wounds after graft placement.

7.1 CONCLUSIONS

This study has explored the use of two polymer networks being PVA and sodium alginate, to evaluate their suitability for engineering bones substitute grafts via incorporation of CMP and Bioglass® to form either a single network of PVA or an interpenetrating dual network of PVA and alginate. The characterisation of the materials in each stage of the study, suggest that suitable water uptake and mechanical properties as well as cellular interactions can be achieved by varying the concentration of polymers used in the fabrication of the composites. Thus, bone graft systems were developed that can function both mechanically as well as biologically that allow for absorption and

retention of biological fluids rich in growth factors. Simple and methods that did not involve use of any chemical crosslinking agents were employed in this study.

PVA displayed a viscous behaviour which increased with increase in concentration. The freeze thawing technique was found to yield PVA hydrogels with optimum properties. The hydrophilicity of PVA was demonstrated by its high water uptake. The tensile strength properties of PVA were found to be easily altered by increasing the concentration of PVA.

Interpenetrating network of PVA and alginate were successfully fabricated to form dual network hydrogels, which were initially proposed to function as a continuous polymer phase that would allow for incorporation of fillers to form bone graft substitutes. The hydrogels were found to have reduced swelling properties and increased tensile strength. Their biocompatibility and elasticity with a rubber like nature that resembles elastin in soft tissue, implied an expansion of applications from the polymer base for filler incorporation to form bone-graft substitutes, to applications in soft tissue areas.

Bioglass® was successfully incorporated into the DN hydrogel structure to form porous and non-porous DNBG composites. The composites were found to be suitable for bone graft augmentation in non-load bearing areas. Tensile strength of the non-porous composites were found to be significantly higher than those of the DN hydrogels. The composites were found to be biocompatible and their bioactivity in SBF demonstrated.

PVA-CMP composites with high mineral content were found to have increased compressive and diametral strength with increase in concentration of PVA. The composites were found to be biocompatible, and seemed to undergo a small level of hydrolysis when placed in SBF and culture media. Their properties determined them to be suitable for bone graft applications low and non-load bearing areas.

In conclusion this study has developed systems that can be beneficially applied in the advancement of Bio Medical engineering solutions in search for a better quality of life for humanity. Systems fabricated in this study show positive and beneficial applications for soft and bone tissue regeneration, they have demonstrated potential for good internal

bonding of host tissue to the biomaterials and this has been attributed to their good biocompatibility, water uptake, elastic and mechanical properties.

7.2 FUTURE WORK

Overall, a platform has been formed for continual development of the systems reported for further tissue engineering applications. The emphasis of the current research was to develop osteoconductive bone substitutes with good structural properties that would be able to absorb and retain biological fluids rich in growth factors, and allow for their delivery at the wound site. This thesis presented detailed studies on steps taken to fabricate and achieve hydrogel and composite systems with optimum properties suitable for soft tissue and bone augmentation applications. Therefore in future:

- Detailed in vitro studies on inclusion of PRP within selected hydrogels and composite systems with optimum mechanical and physical properties will enable to optimise the systems to provide the maximum clinical efficacy for bone healing. The kinetics of absorption of PRP and subsequent release in the surrounding environment will provide information on the effect of the inclusion of PRP. Selected mechanical properties will need to be characterised post absorption of PRP and detailed fatigue behaviour of the constructs will need to be characterised. The activity of the PRP within the constructs will need an evaluation, especially as the construct may provide binding sites for the proteins/peptides in the PRP, thus standard assays for growth factors such as PDGF and TGFβ should be assessed.

- The hydrogels and the composite hydrogels are versatile materials and can be further exploited for other applications such as nerve regeneration and wound healing. Forming the composite in fibre form with aligned bundles can be explored for nerve regeneration, especially as the materials can be easily moulded and expected to provide the requisite properties for the same. The

morphology of the fibres can be tailored for guided cell regeneration, for example hydrogels fabricated in a striated mould would be suited in axonal growth for nerve regeneration.

- Rapid prototyping fabrication techniques can be explored, for more patient specific design applications. Different designs from rapid prototyping may also result in improved mechanical properties, especially in the case of highly porous composite systems.

- Detailed in vivo studies in small animal models will be carried out using the optimised scaffolds in combination with and without autologous PRP. This study will help elucidate the effects and benefits of the scaffolds in regeneration of the bone tissue, and demonstrate advantages of the scaffold's ability to allow for localised delivery of PRP. The results would form the basis of extending this to large animal models in future towards clinical translation.

- Osteochondral defects that involve both cartilage and the underlying subchondral bone are particularly challenging to repair. Current treatment options provide limited success that often eventually need a joint replacement. The complex architecture through the articular cartilage to subchondral bone pose a significant challenge in developing tissue engineering strategies to regenerate this tissue. The fact, that there are integrated tissue sites involved in osteochondral defects, the continuum of this complex architecture is difficult to simulate. Literature suggests that there have been numerous attempts especially involving hydrogels, reinforced hydrogels with different fillers and interpenetrating networks have been explored, however the suitability is limited.

  Within this study, I have been able to create hierarchical structures and based on the fabrication of multilayer scaffolds of the PVA-CMP as well as the dual network composites, a combination can be adopted to develop scaffolds for

osteochondral plug applications without the delamination at the interface. The scaffolds would comprise of two layers, the fabricated PVA-CMP or DNBG layer (emulating bone) and a second tough hydrogel layer (emulating cartilage). These new systems can be tailored to the physical and mechanical requirements to suit a scaffold for multi-layered structures as the osteochondral defect. Most importantly determination of the integration and strength between the two layers would enable an understanding of the force or load limits the scaffold can undergo without rupture at the interface.

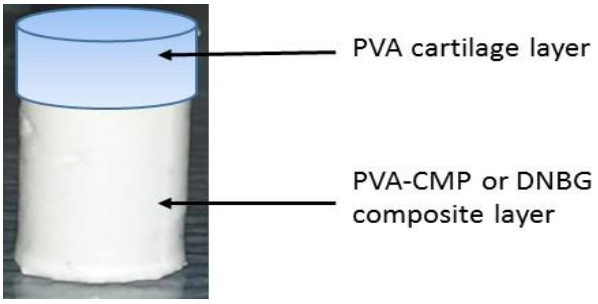

Figure 7-3: Illustration of the two layer composite to be fabricated, consisting of a composite and polymer layer.

- Tissue engineering strategies are an advancing area in healthcare. Bone tissue engineering is a promising field and extensive research on both development of scaffolds and cell based technologies are being progressed to achieve clinically viable translation. To increase the clinical relevance of my study the next step will be to utilize the elastomeric properties of (PVA-CMP and DNBG) scaffolds and subject them to mechanical loading in a bioreactor whilst using perfusion to allow the transport of nutrients and oxygen through the cell seeded scaffolds. The bioreactor essentially is able to maintain a culture environment for the cells, however as the mechanical loading also plays a role on the behaviour of cells a simultaneous application of fluid flow and mechanical loading will help determine the relationship between mechanical loading, perfusion parameters, cell proliferation and differentiation to provide an insight into the feasibility and optimisation of the constructs prior to in vivo studies.

- The dual network hydrogel could be studied for further applications, such as wound dressings and wound healing applications. The benefits of using hydrogel based dressings for wound care, include provision of moisture to a dry lesion which in turn simplifies common healing phases such as granulation, epidermis repair and removal of excess dead tissue. Drug loaded hydrogel wound dressings also aide in providing pain relief to the patient during the healing process. A new type of dual network was developed within this study, a ductile and flexible material with an interconnected micro porosity. Drug release studies on the dual network hydrogels demonstrated the ability of the hydrogels to be loaded with drugs, and potential to function as drug delivery matrices. The initial linear followed by the slower drug release profile of the DN hydrogels would prove to be suitable for simultaneously irradicating an existing infection while preventing recolonisation of the wound by bacteria. The study also demonstrated that swelling ratio as well as tensile strengths of the DN hydrogels could be tailored for desired specific functions. Water uptake studies of the DN hydrogels, demonstrated that these hydrogels would be suited to absorb biological fluids such as PRP. This allows the hydrogels to play an enhanced role in simple yet effective methods of enhanced recovery, by allowing the retained growth factors in the scaffold to be delivered locally at the wound site and injured tissue area. If possible studies could be conducted using wound healing simulations to allow for a more accurate interpretation on the performance of the hydrogel, as well as highlighting areas which may need further improvements.

- To further enhance the healing performance of the DN hydrogels and the DNBG composites, crosslinking of sodium alginates in the network could be carried out with different ions such as zinc or strontium. Zinc with trace elements found in the human body, has been demonstrated to have a beneficial effect on wound healing, with functions on the immune system, cell division as well as formation, mineralisation, development and maintenance of healthy bones. Strontium has

also been reported to have beneficial effects on bone regeneration, with potential as an anti-osteoporotic factor at low doses. Studies demonstrating the effect of using these ions to crosslink the alginate, on the resultant properties of the DN hydrogel and DNBG composite, would enable a clear understanding of the hydrogel and composite properties. Cell culture studies aimed at determining whether healing is enhanced due to the incorporation of these ions in the network would enable identification and expansions for applications of the hydrogels and composites.

Appendix

IN VITRO BIOMINERALISATION

FTIR-ATR analysis

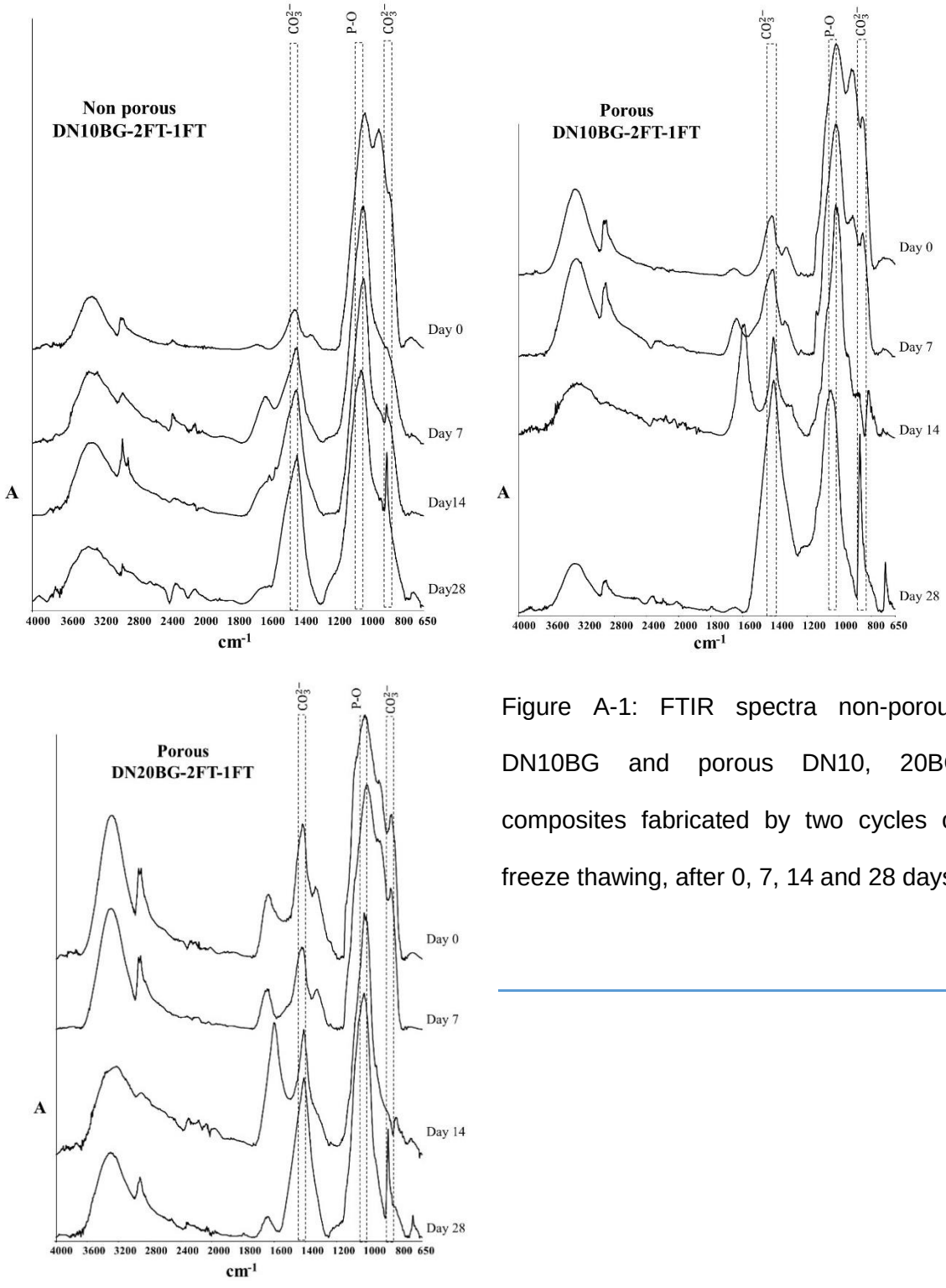

Figure A-1: FTIR spectra non-porous DN10BG and porous DN10, 20BG composites fabricated by two cycles of freeze thawing, after 0, 7, 14 and 28 days

Day	EDAX
	DN10BG-NO POROGEN
7	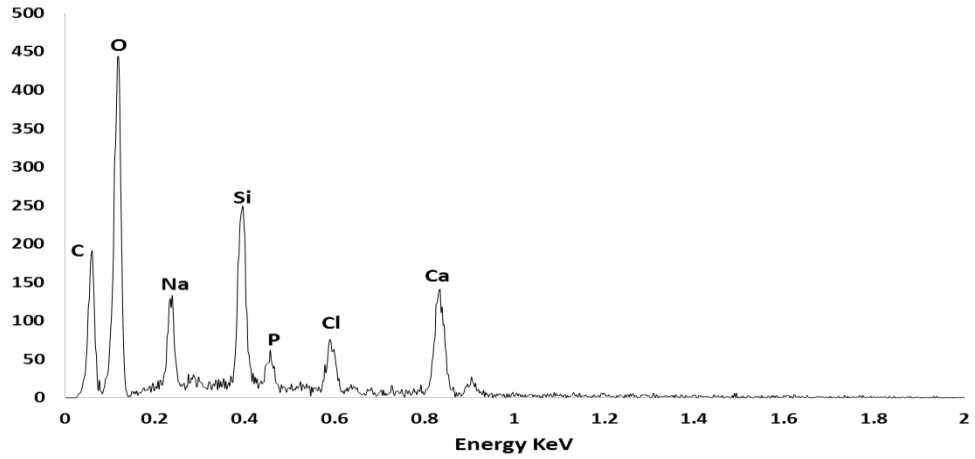
14	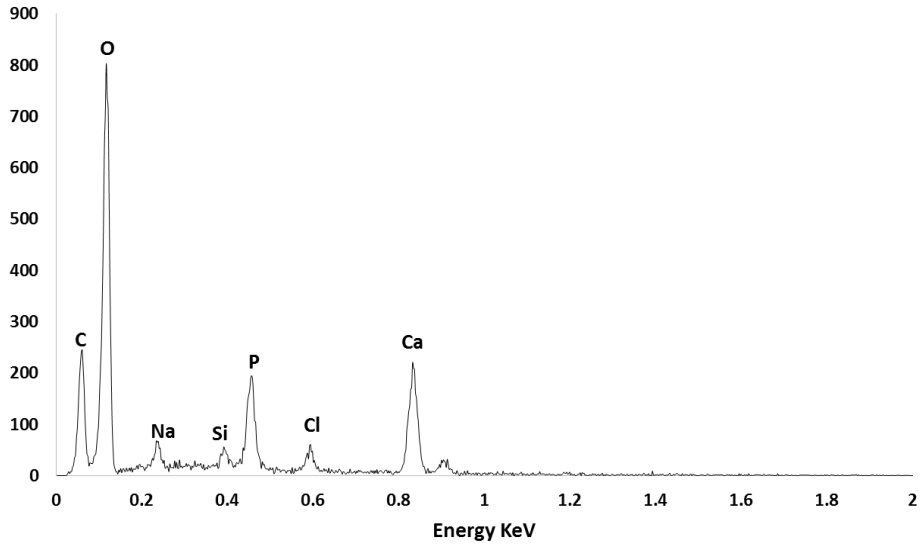
28	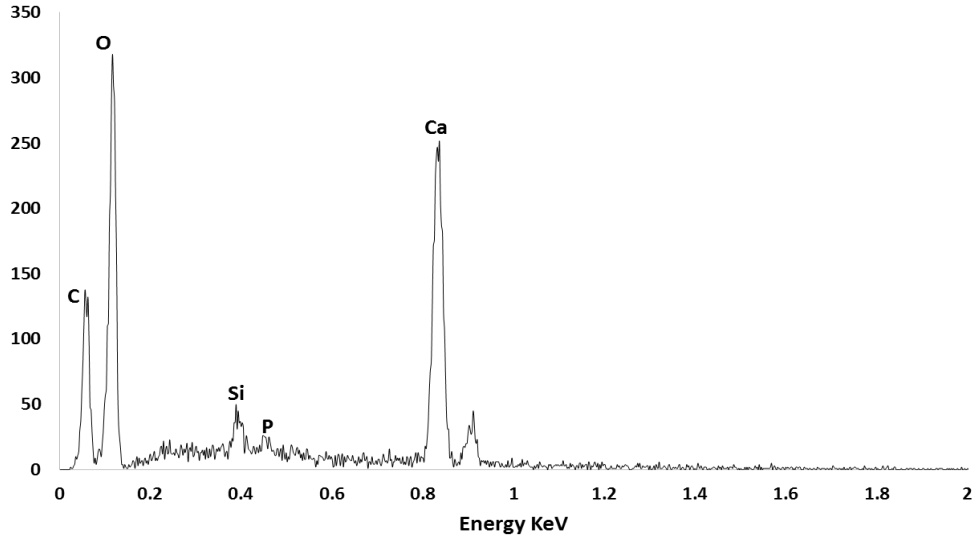

	DN10BG-10% POROGEN
7	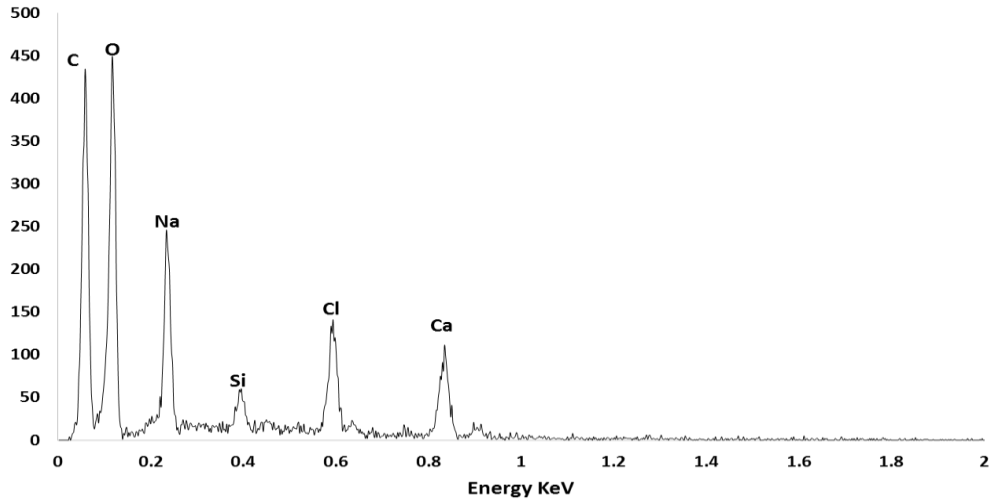
14	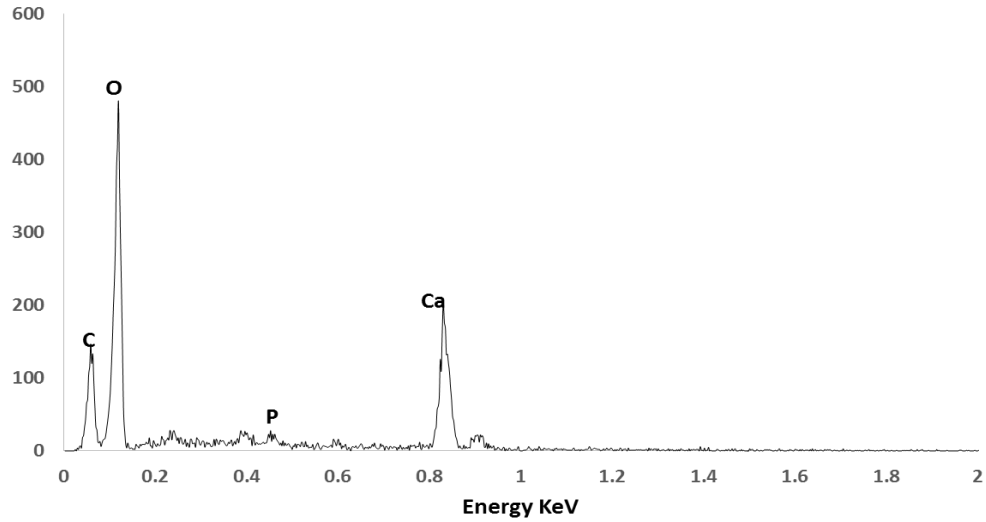
28	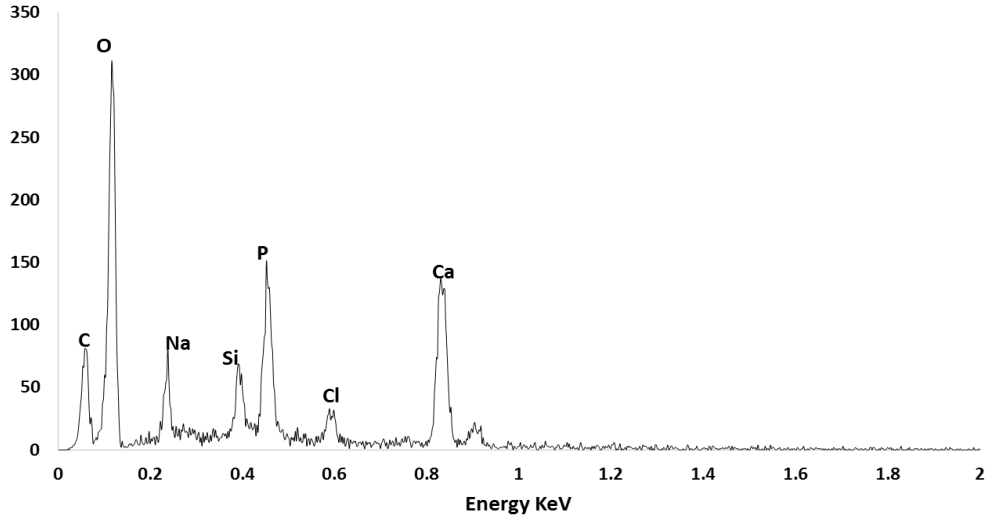

	DN20BG-10%POROGEN
7	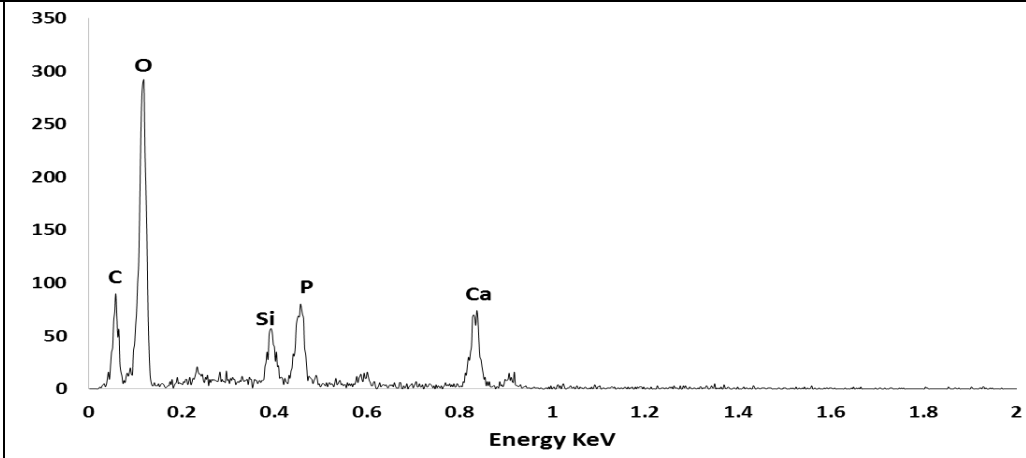
14	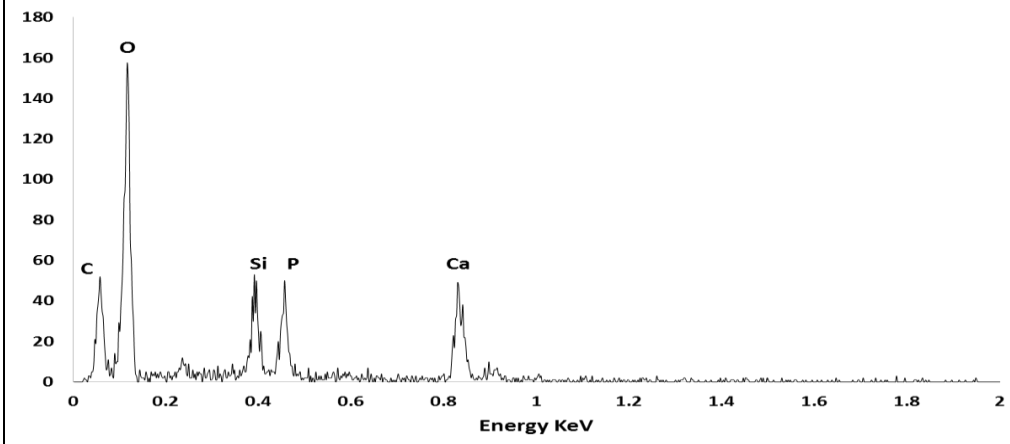
28	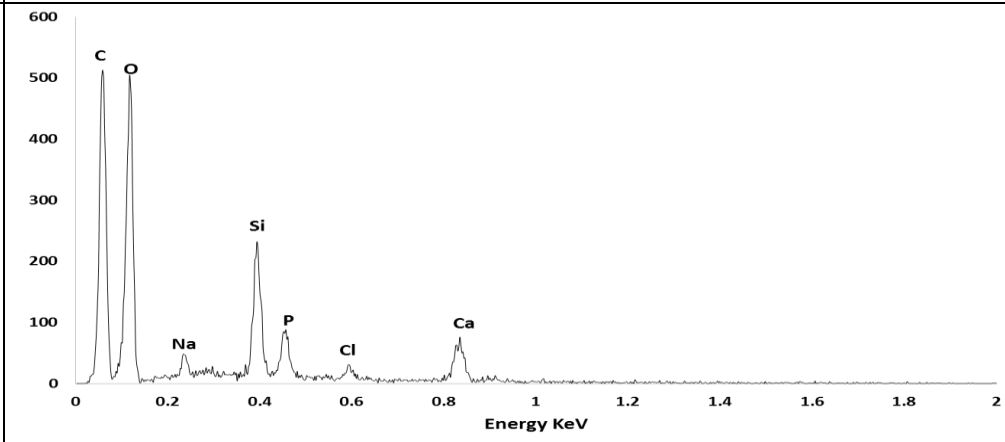

Figure A-2: EDX spectra of mineral deposition on both the non-porous and porous DNBG composites soaked in SBF over a period of 28 days.

References

1. Antonucci, J.M., B.O. Fowler, and S. Venz, *Filler systems based on calcium metaphosphates.* Dental Materials, 1991. **7**(2): p. 124-129.
2. Proff, P. and P. Romer, *The molecular mechanism behind bone remodelling: a review.* Clin Oral Investig, 2009. **13**(4): p. 355-62.
3. Horner, E.A., et al., *Long bone defect models for tissue engineering applications: criteria for choice.* Tissue Eng Part B Rev, 2010. **16**(2): p. 263-71.
4. Woolf, A.D. and B. Pfleger, *Burden of major musculoskeletal conditions.* Bull World Health Organ, 2003. **81**(9): p. 646-56.
5. Lidgren, L., *The bone and joint decade 2000-2010.* Bulletin of the World Health Organization; the International Journal of Public Health, 2003. **81**(9): p. 629.
6. Organization, W.H., *Global burdern of Disease 2004 update* available at http://www.who.int/healthinfo/global_burden_disease/GBD_report_2004update_full.pdf. accessed 06 June 2013, 2004.
7. Amini, A.R., C.T. Laurencin, and S.P. Nukavarapu, *Bone tissue engineering: recent advances and challenges.* Crit Rev Biomed Eng, 2012. **40**(5): p. 363-408.
8. Place, E.S., N.D. Evans, and M.M. Stevens, *Complexity in biomaterials for tissue engineering.* Nat Mater, 2009. **8**(6): p. 457-470.
9. Buwalda, S.J., et al., *Hydrogels in a historical perspective: From simple networks to smart materials.* Journal of Controlled Release, 2014. **190**: p. 254-273.
10. Sun, Y., et al., *Biomimetic engineering of nanofibrous gelatin scaffolds with noncollagenous proteins for enhanced bone regeneration.* Tissue Eng Part A, 2013. **19**(15-16): p. 1754-63.
11. Hofmann, S., et al., *Remodeling of tissue-engineered bone structures in vivo.* European Journal of Pharmaceutics and Biopharmaceutics, 2013. **85**(1): p. 119-129.
12. Discher, D.E., D.J. Mooney, and P.W. Zandstra, *Growth factors, matrices, and forces combine and control stem cells.* Science, 2009. **324**(5935): p. 1673-7.

13. Dhivya, S., et al., *Nanohydroxyapatite-reinforced chitosan composite hydrogel for bone tissue repair in vitro and in vivo.* Journal of Nanobiotechnology, 2015. **13**: p. 40.

14. Gentile, P., et al., *Bioactive glass/polymer composite scaffolds mimicking bone tissue.* Journal of Biomedical Materials Research Part A, 2012. **100A**(10): p. 2654-2667.

15. Lacroix, J., E. Jallot, and J. Lao, *Gelatin-bioactive glass composites scaffolds with controlled macroporosity.* Chemical Engineering Journal, 2014. **256**: p. 9-13.

16. Diogo, G.S., et al., *Manufacture of beta-TCP/alginate scaffolds through a Fab@home model for application in bone tissue engineering.* Biofabrication, 2014. **6**(2): p. 025001.

17. Huang, X., et al., *Biomineralization regulation by nano-sized features in silk fibroin proteins: Synthesis of water-dispersible nano-hydroxyapatite.* Journal of Biomedical Materials Research Part B: Applied Biomaterials, 2014. **102**(8): p. 1720-1729.

18. Nie, L., et al., *Physicochemical characterization and biocompatibility in vitro of biphasic calcium phosphate/polyvinyl alcohol scaffolds prepared by freeze-drying method for bone tissue engineering applications.* Colloids and Surfaces B: Biointerfaces, 2012. **100**: p. 169-176.

19. Lareau, C.R., et al., *Does autogenous bone graft work? A logistic regression analysis of data from 159 papers in the foot and ankle literature.* Foot Ankle Surg, 2015. **21**(3): p. 150-9.

20. Sbordone, C., et al., *Volume changes of autogenous bone after sinus lifting and grafting procedures: A 6-year computerized tomographic follow-up.* Journal of Cranio-Maxillofacial Surgery, 2013. **41**(3): p. 235-241.

21. Smolka, W., et al., *Changes in the volume and density of calvarial split bone grafts after alveolar ridge augmentation.* Clin Oral Implants Res, 2006. **17**(2): p. 149-55.

22. Liu, Y., J. Lim, and S.H. Teoh, *Review: development of clinically relevant scaffolds for vascularised bone tissue engineering.* Biotechnol Adv, 2013. **31**(5): p. 688-705.

23. O'Keefe, R.J. and J. Mao, *Bone tissue engineering and regeneration: from discovery to the clinic--an overview.* Tissue Eng Part B Rev, 2011. **17**(6): p. 389-92.

24. Henkel, J., et al., *Bone regeneration based on tissue engineering conceptions—a 21st century perspective.* Bone research, 2013. **1**(3): p. 216.

25. Nandra, R., L. Grover, and K. Porter, *Fracture non-union epidemiology and treatment.* Trauma, 2015: p. 1460408615591625.

26. Mills, L.A. and A.H. Simpson, *The relative incidence of fracture non-union in the Scottish population (5.17 million): a 5-year epidemiological study.* BMJ Open, 2013. **3**(2).

27. Zimmermann, E.A., B. Busse, and R.O. Ritchie, *The fracture mechanics of human bone: influence of disease and treatment.* BoneKEy Rep, 2015. **4**.

28. Cartmell, S., A. Rupani, and R. Balint, *Osteoblasts and their applications in bone tissue engineering.* Cell Health and Cytoskeleton, 2012. **49**.

29. Jahan, K. and M. Tabrizian, *Composite biopolymers for bone regeneration enhancement in bony defects.* Biomater Sci, 2015. **4**(1): p. 25-39.

30. Webber, M.J., et al., *A perspective on the clinical translation of scaffolds for tissue engineering.* Ann Biomed Eng, 2015. **43**(3): p. 641-56.

31. Wu, S., et al., *Biomimetic porous scaffolds for bone tissue engineering.* Materials Science and Engineering: R: Reports, 2014. **80**: p. 1-36.

32. Schindeler, A., et al., *Bone remodeling during fracture repair: The cellular picture.* Seminars in Cell & Developmental Biology, 2008. **19**(5): p. 459-466.

33. Schmidt-Bleek, K., et al., *Initiation and early control of tissue regeneration - bone healing as a model system for tissue regeneration.* Expert Opin Biol Ther, 2014. **14**(2): p. 247-59.

34. Marsell, R. and T.A. Einhorn, *The biology of fracture healing.* Injury, 2011. **42**(6): p. 551-5.

35. ©Pearson Education, I., *http://slideplayer.com/ (Accessed 12-04-2016).*

36. Kalfas, I.H., *Principles of bone healing.* Neurosurg Focus, 2001. **10**(4): p. E1.

37. Carano, R.A.D. and E.H. Filvaroff, *Angiogenesis and bone repair.* Drug Discovery Today, 2003. **8**(21): p. 980-989.

38. Hernandez, R.K., et al., *Patient-related risk factors for fracture-healing complications in the United Kingdom General Practice Research Database.* Acta Orthop, 2012. **83**(6): p. 653-60.

39. Jahagirdar, R. and B.E. Scammell, *Principles of fracture healing and disorders of bone union.* Surgery (Oxford), 2009. **27**(2): p. 63-69.

40. Gómez-Barrena, E., et al., *Bone fracture healing: Cell therapy in delayed unions and nonunions.* Bone, 2015. **70**: p. 93-101.

41. Dimitriou, R., et al., *Bone regeneration: current concepts and future directions.* BMC Med, 2011. **9**: p. 66.

42. Nandi, S.K., et al., *Orthopaedic applications of bone graft & graft substitutes: a review.* Indian J Med Res, 2010. **132**: p. 15-30.

43. Giannoudis, P.V., H. Dinopoulos, and E. Tsiridis, *Bone substitutes: An update.* Injury, 2005. **36**(3, Supplement): p. S20-S27.

44. Sivarajasingam, V., et al., *Secondary bone grafting of alveolar clefts: a densitometric comparison of iliac crest and tibial bone grafts.* Cleft Palate Craniofac J, 2001. **38**(1): p. 11-4.

45. Iturriaga, M.T. and C.C. Ruiz, *Maxillary sinus reconstruction with calvarium bone grafts and endosseous implants.* J Oral Maxillofac Surg, 2004. **62**(3): p. 344-7.

46. Kurien, T., R.G. Pearson, and B.E. Scammell, *Bone graft substitutes currently available in orthopaedic practice: the evidence for their use.* Bone Joint J, 2013. **95-b**(5): p. 583-97.

47. Schroeder, J.E. and R. Mosheiff, *Tissue engineering approaches for bone repair: concepts and evidence.* Injury, 2011. **42**(6): p. 609-13.

48. Calori, G.M., et al., *The use of bone-graft substitutes in large bone defects: Any specific needs?* Injury-International Journal of the Care of the Injured, 2011. **42**: p. S56-S63.

49. Drosos, G.I., et al., *Safety and efficacy of commercially available demineralised bone matrix preparations: a critical review of clinical studies.* Injury, 2007. **38 Suppl 4**: p. S13-21.

50. Bueno, E.M. and J. Glowacki, *Cell-free and cell-based approaches for bone regeneration.* Nat Rev Rheumatol, 2009. **5**(12): p. 685-97.

51. Kim, Y., H. Nowzari, and S.K. Rich, *Risk of Prion Disease Transmission through Bovine-Derived Bone Substitutes: A Systematic Review.* Clinical Implant Dentistry and Related Research, 2012: p. no-no.

52. Ziran, B.H., W.R. Smith, and S.J. Morgan, *Use of calcium-based demineralized bone matrix/allograft for nonunions and posttraumatic reconstruction of the appendicular skeleton: preliminary results and complications.* J Trauma, 2007. **63**(6): p. 1324-8.

53. Petruskevicius, J., et al., *No effect of Osteoset, a bone graft substitute, on bone healing in humans: a prospective randomized double-blind study.* Acta Orthop Scand, 2002. **73**(5): p. 575-8.

54. Chu, P.J. and J.T. Shih, *Arthroscopically assisted use of injectable bone graft substitutes for management of scaphoid nonunions.* Arthroscopy, 2011. **27**(1): p. 31-7.

55. Nauth, A., et al., *Bone Graft Substitution and Augmentation.* J Orthop Trauma, 2015. **29 Suppl 12**: p. S34-8.

56. Muramatsu, K., et al., *Recalcitrant posttraumatic nonunion of the humerus: 23 patients reconstructed with vascularized bone graft.* Acta Orthop Scand, 2003. **74**(1): p. 95-7.

57. Soucacos, P.N., et al., *Vascularised bone grafts for the management of non-union.* Injury, 2006. **37 Suppl 1**: p. S41-50.

58. Wheeler, D.L. and W.F. Enneking, *Allograft bone decreases in strength in vivo over time.* Clin Orthop Relat Res, 2005(435): p. 36-42.

59. Ratner, B.D., *The Biocompatibility Manifesto: Biocompatibility for the Twenty-first Century.* Journal of Cardiovascular Translational Research, 2011. **4**(5): p. 523-527.

60. Lichte, P., et al., *Scaffolds for bone healing: concepts, materials and evidence.* Injury, 2011. **42**(6): p. 569-73.

61. Liu, Y., J.K. Chan, and S.H. Teoh, *Review of vascularised bone tissue-engineering strategies with a focus on co-culture systems.* J Tissue Eng Regen Med, 2015. **9**(2): p. 85-105.

62. Muschler, G.F., C. Nakamoto, and L.G. Griffith, *Engineering principles of clinical cell-based tissue engineering.* J Bone Joint Surg Am, 2004. **86-a**(7): p. 1541-58.

63. Simon, J.L., et al., *Engineered cellular response to scaffold architecture in a rabbit trephine defect.* J Biomed Mater Res A, 2003. **66**(2): p. 275-82.

64. Bose, S., et al., *Understanding in vivo response and mechanical property variation in MgO, SrO and SiO(2) doped beta-TCP.* Bone, 2011. **48**(6): p. 1282-90.

65. Bose, S., M. Roy, and A. Bandyopadhyay, *Recent advances in bone tissue engineering scaffolds.* Trends Biotechnol, 2012. **30**(10): p. 546-54.

66. Jinku, K., et al., *Tyrosine-derived polycarbonate scaffolds for bone regeneration in a rabbit radius critical-size defect model.* Biomedical Materials, 2015. **10**(3): p. 035001.

67. Hafeman, A.E., et al., *Injectable biodegradable polyurethane scaffolds with release of platelet-derived growth factor for tissue repair and regeneration.* Pharm Res, 2008. **25**(10): p. 2387-99.

68. Gong, J.P., et al., *Double-Network Hydrogels with Extremely High Mechanical Strength.* Advanced Materials, 2003. **15**(14): p. 1155-1158.

69. Gong, J.P., *Why are double network hydrogels so tough?* Soft Matter, 2010. **6**(12): p. 2583-2590.

70. Bhakta, G., et al., *The influence of collagen and hyaluronan matrices on the delivery and bioactivity of bone morphogenetic protein-2 and ectopic bone formation.* Acta Biomater, 2013. **9**(11): p. 9098-106.

71. Hokugo, A., et al., *Stimulation of bone regeneration following the controlled release of water-insoluble oxysterol from biodegradable hydrogel.* Biomaterials, 2014. **35**(21): p. 5565-71.

72. Moreira Teixeira, L.S., J. Patterson, and F.P. Luyten, *Skeletal tissue regeneration: where can hydrogels play a role?* Int Orthop, 2014. **38**(9): p. 1861-76.

73. Shields, C.L., et al., *Experience with the Polymer-Coated Hydroxyapatite Implant after Enucleation in 126 Patients.* Ophthalmology, 2007. **114**(2): p. 367-373.

74. Finke, B., et al., *Plasma Polymer Coating of Titanium for Improved Bone Implants*, in *14th Nordic-Baltic Conference on Biomedical Engineering and Medical Physics: NBC 2008 16–20 June 2008 Riga, Latvia*, A. Katashev, Y. Dekhtyar, and J. Spigulis, Editors. 2008, Springer Berlin Heidelberg: Berlin, Heidelberg. p. 30-33.

75. Pertici, G., et al., *Composite polymer-coated mineral grafts for bone regeneration: material characterisation and model study.* Annals of Oral & Maxillofacial Surgery, 2014.

76. Shrivats, A.R., M.C. McDermott, and J.O. Hollinger, *Bone tissue engineering: state of the union.* Drug Discov Today, 2014. **19**(6): p. 781-6.

77. Fillingham, Y. and J. Jacobs, *Bone grafts and their substitutes.* Bone & Joint Journal, 2016. **98-B**(1 Supple A): p. 6-9.

78. Shie, M.Y., S.J. Ding, and H.C. Chang, *The role of silicon in osteoblast-like cell proliferation and apoptosis.* Acta Biomater, 2011. **7**(6): p. 2604-14.

79. Banerjee, S.S., et al., *Understanding the influence of MgO and SrO binary doping on the mechanical and biological properties of β-TCP ceramics.* Acta Biomaterialia, 2010. **6**(10): p. 4167-4174.

80. Fielding, G.A., A. Bandyopadhyay, and S. Bose, *Effects of silica and zinc oxide doping on mechanical and biological properties of 3D printed tricalcium phosphate tissue engineering scaffolds.* Dent Mater, 2012. **28**(2): p. 113-22.

81. Jones, J.R., L.M. Ehrenfried, and L.L. Hench, *Optimising bioactive glass scaffolds for bone tissue engineering.* Biomaterials, 2006. **27**(7): p. 964-73.

82. San Miguel, B., et al., *Enhanced osteoblastic activity and bone regeneration using surface-modified porous bioactive glass scaffolds.* J Biomed Mater Res A, 2010. **94**(4): p. 1023-33.

83. Utech, S. and A. Boccaccini, *A review of hydrogel-based composites for biomedical applications: enhancement of hydrogel properties by addition of rigid inorganic fillers.* Journal of Materials Science, 2016. **51**(1): p. 271-310.

84. Habraken, W.J.E.M., J.G.C. Wolke, and J.A. Jansen, *Ceramic composites as matrices and scaffolds for drug delivery in tissue engineering.* Advanced Drug Delivery Reviews, 2007. **59**(4–5): p. 234-248.

85. De, M., P.S. Ghosh, and V.M. Rotello, *Applications of Nanoparticles in Biology.* Advanced Materials, 2008. **20**(22): p. 4225-4241.

86. Haraguchi, K., *Development of soft nanocomposite materials and their applications in cell culture and tissue engineering.* J Stem Cells Regen Med, 2012. **8**(1): p. 2-11.

87. Kokabi, M., M. Sirousazar, and Z.M. Hassan, *PVA–clay nanocomposite hydrogels for wound dressing.* European Polymer Journal, 2007. **43**(3): p. 773-781.

88. Desai, P.N., Q. Yuan, and H. Yang, *Synthesis and characterization of photocurable polyamidoamine dendrimer hydrogels as a versatile platform for tissue engineering and drug delivery.* Biomacromolecules, 2010. **11**(3): p. 666-73.

89. Daniel, M.C. and D. Astruc, *Gold nanoparticles: assembly, supramolecular chemistry, quantum-size-related properties, and applications toward biology, catalysis, and nanotechnology.* Chem Rev, 2004. **104**(1): p. 293-346.

90. Murali Mohan, Y., et al., *Hydrogel networks as nanoreactors: A novel approach to silver nanoparticles for antibacterial applications.* Polymer, 2007. **48**(1): p. 158-164.

91. Yi, D.K., et al., *Silica-coated nanocomposites of magnetic nanoparticles and quantum dots.* J Am Chem Soc, 2005. **127**(14): p. 4990-1.

92. Kumar, C.S. and F. Mohammad, *Magnetic nanomaterials for hyperthermia-based therapy and controlled drug delivery.* Adv Drug Deliv Rev, 2011. **63**(9): p. 789-808.

93. Meenach, S.A., J.Z. Hilt, and K.W. Anderson, *Poly(ethylene glycol)-based magnetic hydrogel nanocomposites for hyperthermia cancer therapy.* Acta Biomater, 2010. **6**(3): p. 1039-46.

94. Cha, C., et al., *Carbon-based nanomaterials: multifunctional materials for biomedical engineering.* ACS Nano, 2013. **7**(4): p. 2891-7.

95. Zhang, L., et al., *High strength graphene oxide/polyvinyl alcohol composite hydrogels.* Journal of Materials Chemistry, 2011. **21**(28): p. 10399-10406.

96. Salgado, A.J., O.P. Coutinho, and R.L. Reis, *Bone tissue engineering: state of the art and future trends.* Macromol Biosci, 2004. **4**(8): p. 743-65.

97. Cao, H. and N. Kuboyama, *A biodegradable porous composite scaffold of PGA/β-TCP for bone tissue engineering.* Bone, 2010. **46**(2): p. 386-395.

98. Motamedian, S.R., et al., *Smart scaffolds in bone tissue engineering: A systematic review of literature.* World Journal of Stem Cells, 2015. **7**(3): p. 657-668.

99. Alsousou, J., et al., *The biology of platelet-rich plasma and its application in trauma and orthopaedic surgery: a review of the literature.* J Bone Joint Surg Br, 2009. **91**(8): p. 987-96.

100. Hogan, B.L., *Bone morphogenetic proteins: multifunctional regulators of vertebrate development.* Genes Dev, 1996. **10**(13): p. 1580-94.

101. Xiao, Y.-T., L.-X. Xiang, and J.-Z. Shao, *Bone morphogenetic protein.* Biochemical and Biophysical Research Communications, 2007. **362**(3): p. 550-553.

102. Marukawa, E., et al., *Functional reconstruction of the non-human primate mandible using recombinant human bone morphogenetic protein-2.* Int J Oral Maxillofac Surg, 2002. **31**(3): p. 287-95.

103. Herford, A.S. and P.J. Boyne, *Reconstruction of mandibular continuity defects with bone morphogenetic protein-2 (rhBMP-2).* J Oral Maxillofac Surg, 2008. **66**(4): p. 616-24.

104. Asahina, I., *Bone Morphogenetic Proteins: Their History and Characteristics.* Journal of Hard Tissue Biology, 2014. **23**(3): p. 283-286.

105. Yaremchuk, K., M. Toma, and M. Somers, *Acute airway obstruction associated with the use of bone-morphogenetic protein in cervical spinal fusion.* Laryngoscope, 2010. **120 Suppl 4**: p. S140.

106. Boraiah, S., et al., *Complications of recombinant human BMP-2 for treating complex tibial plateau fractures: a preliminary report.* Clin Orthop Relat Res, 2009. **467**(12): p. 3257-62.

107. Shields, L.B., et al., *Adverse effects associated with high-dose recombinant human bone morphogenetic protein-2 use in anterior cervical spine fusion.* Spine (Phila Pa 1976), 2006. **31**(5): p. 542-7.

108. Carter, T.G., et al., *Off-label use of recombinant human bone morphogenetic protein-2 (rhBMP-2) for reconstruction of mandibular bone defects in humans.* J Oral Maxillofac Surg, 2008. **66**(7): p. 1417-25.

109. Wong, D.A., et al., *Neurologic impairment from ectopic bone in the lumbar canal: a potential complication of off-label PLIF/TLIF use of bone morphogenetic protein-2 (BMP-2).* Spine J, 2008. **8**(6): p. 1011-8.

110. Sampson, S., M. Gerhardt, and B. Mandelbaum, *Platelet rich plasma injection grafts for musculoskeletal injuries: a review.* Curr Rev Musculoskelet Med, 2008. **1**(3-4): p. 165-74.

111. Wasterlain, A.S., H.J. Braun, and J.L. Dragoo, *Contents and Formulations of Platelet-Rich Plasma.* Operative Techniques in Orthopaedics, 2012. **22**(1): p. 33-42.

112. Eppley, B.L., W.S. Pietrzak, and M. Blanton, *Platelet-rich plasma: a review of biology and applications in plastic surgery.* Plast Reconstr Surg, 2006. **118**(6): p. 147e-159e.

113. Dohan Ehrenfest, D.M., L. Rasmusson, and T. Albrektsson, *Classification of platelet concentrates: from pure platelet-rich plasma (P-PRP) to leucocyte- and platelet-rich fibrin (L-PRF).* Trends Biotechnol, 2009. **27**(3): p. 158-67.

114. Foster, T.E., et al., *Platelet-rich plasma: from basic science to clinical applications.* Am J Sports Med, 2009. **37**(11): p. 2259-72.

115. Anitua, E., et al., *Platelet-Rich Plasma: Preparation and Formulation.* Operative Techniques in Orthopaedics, 2012. **22**(1): p. 25+.

116. Marx, R.E., et al., *Platelet-rich plasma: Growth factor enhancement for bone grafts.* Oral Surg Oral Med Oral Pathol Oral Radiol Endod, 1998. **85**(6): p. 638-46.

117. Bi, L., et al., *Reconstruction of goat tibial defects using an injectable tricalcium phosphate/chitosan in combination with autologous platelet-rich plasma.* Biomaterials, 2010. **31**(12): p. 3201-11.

118. Chen, J.C., et al., *Calcium phosphate bone cement with 10 wt% platelet-rich plasma in vitro and in vivo.* J Dent, 2012. **40**(2): p. 114-22.

119. Singh, I., et al., *Role of platelet-rich plasma in combination with alloplastic bone substitute in regeneration of osseous defects.* Journal of Oral Biology and Craniofacial Research, 2011. **1**(1): p. 17-23.

120. Bibbo, C., C.M. Bono, and S.S. Lin, *Union rates using autologous platelet concentrate alone and with bone graft in high-risk foot and ankle surgery patients.* J Surg Orthop Adv, 2005. **14**(1): p. 17-22.

121. Acebal-Cortina, G., et al., *Evaluation of autologous platelet concentrate for intertransverse lumbar fusion.* European Spine Journal, 2011. **20**(Suppl 3): p. 361-366.

122. Tsai, C.H., et al., *Using the growth factors-enriched platelet glue in spinal fusion and its efficiency.* J Spinal Disord Tech, 2009. **22**(4): p. 246-50.

123. Weiner, B.K. and M. Walker, *Efficacy of autologous growth factors in lumbar intertransverse fusions.* Spine (Phila Pa 1976), 2003. **28**(17): p. 1968-70; discussion 1971.

124. Hsu, W.K., et al., *Platelet-rich plasma in orthopaedic applications: evidence-based recommendations for treatment.* J Am Acad Orthop Surg, 2013. **21**(12): p. 739-48.

125. Padilla, S., et al., *Platelet-rich plasma in orthopaedic applications: evidence-based recommendations for treatment.* J Am Acad Orthop Surg, 2014. **22**(8): p. 469-70.

126. Barbucci, R., *Hydrogels: Biological Properties and Applications*. 2009: Springer.

127. Peppas, N.A., et al., *Hydrogels in pharmaceutical formulations.* European Journal of Pharmaceutics and Biopharmaceutics, 2000. **50**(1): p. 27-46.

128. Hoffman, A.S., *Hydrogels for biomedical applications.* Advanced Drug Delivery Reviews, 2012. **64, Supplement**: p. 18-23.

129. Peppas, N.A., et al., *Hydrogels in biology and medicine: from molecular principles to bionanotechnology.* ADVANCED MATERIALS-DEERFIELD BEACH THEN WEINHEIM-, 2006. **18**(11): p. 1345.

130. Ullah, F., et al., *Classification, processing and application of hydrogels: A review.* Materials Science and Engineering: C, 2015. **57**: p. 414-433.

131. Singhal, R. and K. Gupta, *A Review: Tailor-made Hydrogel Structures (Classifications and Synthesis Parameters).* Polymer-Plastics Technology and Engineering, 2016. **55**(1): p. 54-70.

132. Ratner, B.D., et al., *Biomaterials science: an introduction to materials in medicine*. 2004: Academic press.

133. Reis, R.L., et al., *Natural-based polymers for biomedical applications*. 2008: Elsevier.

134. Peppas, N.A. and S.R. Stauffer, *Reinforced uncrosslinked poly (vinyl alcohol) gels produced by cyclic freezing-thawing processes: a short review.* Journal of Controlled Release, 1991. **16**(3): p. 305-310.

135. Oetjen, G.-W., *Freeze-Drying*, in *Ullmann's Encyclopedia of Industrial Chemistry*. 2000, Wiley-VCH Verlag GmbH & Co. KGaA.

136. Haweel, C. and S. Ammar, *Preparation of polyvinyl alcohol from local raw material.* Iraqi J. Chem. Pet. Eng.(IJCPE), 2008. **9**: p. 15-21.

137. Matricardi, P., et al., *Interpenetrating Polymer Networks polysaccharide hydrogels for drug delivery and tissue engineering.* Advanced Drug Delivery Reviews, 2013. **65**(9): p. 1172-1187.

138. J. Alemán, A.V.C., J. He, M. Hess, K. Horie, R. G. Jones, P. Kratochvíl, I. Meisel, I. Mita, G. Moad, S. Penczek, And R. F. T. Step, *Definitions of terms relating to the structure and processing of sols, gels, networks, and inorganic–organic hybrid materials (IUPAC Recommendations 2007).* Pure Appl. Chem, 2007. **79**(10): p. 1801-1829.

139. Myung, D., et al., *Progress in the development of interpenetrating polymer network hydrogels.* Polymers for advanced technologies, 2008. **19**(6): p. 647-657.

140. Hoare, T.R. and D.S. Kohane, *Hydrogels in drug delivery: Progress and challenges.* Polymer, 2008. **49**(8): p. 1993-2007.

141. Dragan, E.S., *Design and applications of interpenetrating polymer network hydrogels. A review.* Chemical Engineering Journal, 2014. **243**: p. 572-590.

142. Mandelkern, L., *Thermodynamic and morphological properties of bulk crystallized polymers.* Polymer Engineering & Science, 1967. **7**(4): p. 232-252.

143. Kim, J.O., et al., *Development of polyvinyl alcohol-sodium alginate gel-matrix-based wound dressing system containing nitrofurazone.* Int J Pharm, 2008. **359**(1-2): p. 79-86.

144. Chhatri, A., et al., *Cryogenic fabrication of savlon loaded macroporous blends of alginate and polyvinyl alcohol (PVA). Swelling, deswelling and antibacterial behaviors.* Carbohydrate Polymers, 2011. **83**(2): p. 876-882.

145. Gnanaprakasam Thankam, F., et al., *Growth and survival of cells in biosynthetic poly vinyl alcohol-alginate IPN hydrogels for cardiac applications.* Colloids Surf B Biointerfaces, 2013. **107**: p. 137-45.

146. Ricciardi, R., et al., *X-ray Diffraction Analysis of Poly(vinyl alcohol) Hydrogels, Obtained by Freezing and Thawing Techniques.* Macromolecules, 2004. **37**(5): p. 1921-1927.

147. Ricciardi, R., et al., *Investigation of the Crystallinity of Freeze/Thaw Poly(vinyl alcohol) Hydrogels by Different Techniques.* Macromolecules, 2004. **37**(25): p. 9510-9516.

148. Ricciardi, R., et al., *Structural Organization of Poly(vinyl alcohol) Hydrogels Obtained by Freezing and Thawing Techniques: A SANS Study.* Chemistry of Materials, 2005. **17**(5): p. 1183-1189.

149. Nakaoki, T. and H. Yamashita, *Bound states of water in poly(vinyl alcohol) hydrogel prepared by repeated freezing and melting method.* Journal of Molecular Structure, 2008. **875**(1–3): p. 282-287.

150. Alves, M.H., et al., *Poly(vinyl alcohol) physical hydrogels: new vista on a long serving biomaterial.* Macromol Biosci, 2011. **11**(10): p. 1293-313.

151. Jiang, H., et al., *Design and manufacture of a polyvinyl alcohol (PVA) cryogel tri-leaflet heart valve prosthesis.* Med Eng Phys, 2004. **26**(4): p. 269-77.

152. Suciu, A.N., et al., *A Study upon Durability of the Artificial Knee Joint with PVA Hydrogel Cartilage.* JSME International Journal Series C Mechanical Systems, Machine Elements and Manufacturing, 2004. **47**(1): p. 199-208.

153. Święszkowski, W., et al., *An elastic material for cartilage replacement in an arthritic shoulder joint.* Biomaterials, 2006. **27**(8): p. 1534-1541.

154. Hassan, C.M. and N.A. Peppas, *Structure and Morphology of Freeze/Thawed PVA Hydrogels.* Macromolecules, 2000. **33**(7): p. 2472-2479.

155. Hassan, C.M. and N.A. Peppas, *Cellular PVA hydrogels produced by freeze/thawing.* Journal of Applied Polymer Science, 2000. **76**(14): p. 2075-2079.

156. Vashisth, P., et al., *A novel gellan–PVA nanofibrous scaffold for skin tissue regeneration: Fabrication and characterization.* Carbohydrate Polymers, 2016. **136**: p. 851-859.

157. Singh, B. and L. Pal, *Sterculia crosslinked PVA and PVA-poly(AAm) hydrogel wound dressings for slow drug delivery: Mechanical, mucoadhesive, biocompatible and permeability properties.* Journal of the Mechanical Behavior of Biomedical Materials, 2012. **9**: p. 9-21.

158. Chhatri, A., J. Bajpai, and A.K. Bajpai, *Development of Savlon Containing Polyvinyl Alcohol Based Cryogels as Potential Biomaterials for Burn Healing Applications.* International Journal of Polymeric Materials and Polymeric Biomaterials, 2014. **63**(7): p. 380-387.

159. Kim, J.O., et al., *Development of polyvinyl alcohol–sodium alginate gel-matrix-based wound dressing system containing nitrofurazone.* International Journal of Pharmaceutics, 2008. **359**(1–2): p. 79-86.

160. Jiang, H., et al., *Property-based design: optimization and characterization of polyvinyl alcohol (PVA) hydrogel and PVA-matrix composite for artificial cornea.* J Mater Sci Mater Med, 2014. **25**(3): p. 941-52.

161. DeMerlis, C.C. and D.R. Schoneker, *Review of the oral toxicity of polyvinyl alcohol (PVA).* Food and Chemical Toxicology, 2003. **41**(3): p. 319-326.

162. Kamoun, E.A., et al., *Poly (vinyl alcohol)-alginate physically crosslinked hydrogel membranes for wound dressing applications: Characterization and bio-evaluation.* Arabian Journal of Chemistry, 2015. **8**(1): p. 38-47.

163. Shukla, A., et al., *Tunable vancomycin releasing surfaces for biomedical applications.* Small, 2010. **6**(21): p. 2392-404.

164. Hernandez, R., *The use of systemic antibiotics in the treatment of chronic wounds.* Dermatol Ther, 2006. **19**(6): p. 326-37.

165. Schäfer, M., T.R. Schneider, and G.M. Sheldrick, *Crystal structure of vancomycin.* Structure, 1996. **4**(12): p. 1509-1515.

166. Anselme, K., *Osteoblast adhesion on biomaterials.* Biomaterials, 2000. **21**(7): p. 667-81.

167. Ansar Ahmed, S., R.M. Gogal, and J.E. Walsh, *A new rapid and simple non-radioactive assay to monitor and determine the proliferation of lymphocytes: an alternative to [3H]thymidine incorporation assay.* Journal of Immunological Methods, 1994. **170**(2): p. 211-224.

168. Bonnier, F., et al., *Cell viability assessment using the Alamar blue assay: A comparison of 2D and 3D cell culture models.* Toxicology in Vitro, 2015. **29**(1): p. 124-131.

169. Lian, J.B. and G.S. Stein, *Concepts of osteoblast growth and differentiation: basis for modulation of bone cell development and tissue formation.* Crit Rev Oral Biol Med, 1992. **3**(3): p. 269-305.

170. Stein, G.S., J.B. Lian, and T.A. Owen, *Relationship of cell growth to the regulation of tissue-specific gene expression during osteoblast differentiation.* Faseb j, 1990. **4**(13): p. 3111-23.

171. Yuksel, E., et al., *Challenges in Soft Tissue Engineering.* Seminars in Plastic Surgery, 2005. **19**(3): p. 261-270.

172. Wijeyaratne, S.M., R.A. Ubayasiri, and C. Weerasinghe, *Fatal pulmonary embolism of polyvinyl alcohol particles following therapeutic embolisation of a peripheral arteriovenous malformation.* BMJ Case Reports, 2009. **2009**: p. bcr02.2009.1635.

173. Moretto, A., et al., *Slow release of two antibiotics of veterinary interest from PVA hydrogels.* Il Farmaco, 2004. **59**(1): p. 1-5.

174. Besheer, A., et al., *Tracking the urinary excretion of high molar mass poly(vinyl alcohol).* Journal of Biomedical Materials Research Part B: Applied Biomaterials, 2007. **82B**(2): p. 383-389.

175. http://www.mondomed.be/en/key-products/wound-management *(Accessed 03/12/2015).*

176. http://www.mondomed.be/en/key-products/otology-rhinology *(Accessed 03/12/2015).*

177. http://www.mondomed.be/en/key-products/surgery *(Accessed 03/12/2015).*

178. http://www.networkmedical.co.uk/ophthalmic_pva_sponge_range.html *(Accessed 03/12/2015).*

179. http://pvaroller.com/case_study_two.html *(Accessed 03/12/2015)*

180. https://www.plmedical.com/index.php/products/ophthalmic-products/accessories-eye-sponge-pva/ *(Accessed 03/12/2015)*

181. https://www.cookmedical.com/products/di_pva_webds/ *(Accessed 03/12/2015)*

182. Nkhwa, S., et al., *Poly(vinyl alcohol): Physical Approaches to Designing Biomaterials for Biomedical Applications.* Conference Papers in Science, 2014. **2014**: p. 7.

183. Leone, G., et al., *A PVA/PVP hydrogel for human lens substitution: Synthesis, rheological characterization, and in vitro biocompatibility.* Journal of Biomedical Materials Research Part B-Applied Biomaterials, 2011. **97B**(2): p. 278-288.

184. Thomas, L.V., et al., *A biodegradable and biocompatible PVA-citric acid polyester with potential applications as matrix for vascular tissue engineering.* Journal of Materials Science-Materials in Medicine, 2009. **20**: p. 259-269.

185. A. ROGOJANU, E.R., N. OLARU, M. DOBROMIR, D.O. DOROHOI, *DEVELOPMENT AND CHARACTERIZATION OF POLY(VINYL ALCOHOL) MATRIX FOR DRUG RELEASE.* 2011. **Vol. 6**(No 2): p. p.809 - 818

186. Ali, Z.I., F.A. Ali, and A.M. Hosam, *Effect of electron beam irradiation on the structural properties of PVA/V2O5 xerogel.* Spectrochimica Acta Part A: Molecular and Biomolecular Spectroscopy, 2009. **72**(4): p. 868-875.

187. Gamal S. El Bahy, E.-S.M.E.-S., Abdel Aziz Mahmoud and Noha M. Gweily, *Preparation and Characterization of Poly Vinyl Alcohol /Gelatin Blends.* Journal of Applied Sciences, 2012. **8(7)**: p. 3544-3551.

188. Bajpai, A.K. and R. Saini, *Preparation and characterization of biocompatible spongy cryogels of poly(vinyl alcohol)-gelatin and study of water sorption behaviour.* Polymer International, 2005. **54**(9): p. 1233-1242.

189. Liu, X., et al., *Characterization of associating hydrogels of poly(vinyl alcohol) and poly(vinyl pyrrolidone).* Journal of Applied Polymer Science, 2009. **112**(1): p. 541-549.

190. Cassu, S.N. and M.I. Felisberti, *Poly(vinyl alcohol) and poly(vinyl pyrrolidone) blends: miscibility, microheterogeneity and free volume change.* Polymer, 1997. **38**(15): p. 3907-3911.

191. Thomas, P.S. and B.H. Stuart, *A Fourier transform Raman spectroscopy study of water sorption by poly(vinyl alcohol).* Spectrochimica Acta Part A: Molecular and Biomolecular Spectroscopy, 1997. **53**(13): p. 2275-2278.

192. Hassan, C. and N. Peppas, *Structure and Applications of Poly(vinyl alcohol) Hydrogels Produced by Conventional Crosslinking or by Freezing/Thawing Methods*, in *Biopolymers · PVA Hydrogels, Anionic Polymerisation Nanocomposites*. 2000, Springer Berlin Heidelberg. p. 37-65.

193. Berthomieu, C. and R. Hienerwadel, *Fourier transform infrared (FTIR) spectroscopy.* Photosynthesis Research, 2009. **101**(2-3): p. 157-170.

194. Leone, G., et al., *A PVA/PVP hydrogel for human lens substitution: Synthesis, rheological characterization, and in vitro biocompatibility.* Journal of Biomedical Materials Research Part B: Applied Biomaterials, 2011. **97B**(2): p. 278-288.

195. Gabbott, P., *Principles and applications of thermal analysis*. 2008: John Wiley & Sons.

196. Gabbott, P., *A Practical Introduction to Differential Scanning Calorimetry*, in *Principles and Applications of Thermal Analysis*. 2008, Blackwell Publishing Ltd. p. 1-50.

197. Willcox, P.J., et al., *Microstructure of poly(vinyl alcohol) hydrogels produced by freeze/thaw cycling.* Journal of Polymer Science Part B: Polymer Physics, 1999. **37**(24): p. 3438-3454.

198. Gauthier, M.A., et al., *Degree of crosslinking and mechanical properties of crosslinked poly(vinyl alcohol) beads for use in solid-phase organic synthesis.* Polymer, 2004. **45**(24): p. 8201-8210.

199. Peppas, N.A., et al., *Physicochemical foundations and structural design of hydrogels in medicine and biology.* Annu Rev Biomed Eng, 2000. **2**: p. 9-29.

200. Hong, H., et al., *Facile method to prepare self-healable PVA hydrogels with high water stability.* Materials Letters, 2014. **122**: p. 227-229.

201. Gupta, S., S. Goswami, and A. Sinha, *A combined effect of freeze--thaw cycles and polymer concentration on the structure and mechanical properties of transparent PVA gels.* Biomed Mater, 2012. **7**(1): p. 015006.

202. Fukumori, T. and T. Nakaoki, *High-tensile-strength polyvinyl alcohol films prepared from freeze/thaw cycled gels.* Journal of Applied Polymer Science, 2014. **131**(15): p. n/a-n/a.

203. Bonfield, W., *Designing porous scaffolds for tissue engineering.* Philosophical Transactions of the Royal Society A: Mathematical, Physical and Engineering Sciences, 2006. **364**(1838): p. 227-232.

204. Dorozhkin, S.V. and M. Epple, *Biological and Medical Significance of Calcium Phosphates.* Angewandte Chemie International Edition, 2002. **41**(17): p. 3130-3146.

205. Huang, J. and S.M. Best, *1 - Ceramic biomaterials A2 - Boccaccini, Aldo R*, in *Tissue Engineering Using Ceramics and Polymers*, J.E. Gough, Editor. 2007, Woodhead Publishing. p. 3-31.

206. C. Chow, L., *Next generation calcium phosphate-based biomaterials.* Dental Materials Journal, 2009. **28**(1): p. 1-10.

207. Ginebra, M.P., T. Traykova, and J.A. Planell, *Calcium phosphate cements as bone drug delivery systems: A review.* Journal of Controlled Release, 2006. **113**(2): p. 102-110.

208. Barinov, S. and V. Komlev, *Calcium phosphate bone cements.* Inorganic Materials, 2011. **47**(13): p. 1470-1485.

209. Ginebra, M.-P., et al., *Calcium phosphate cements as drug delivery materials.* Advanced Drug Delivery Reviews, 2012. **64**(12): p. 1090-1110.

210. Navarro, M., et al., *Biomaterials in orthopaedics.* Journal of The Royal Society Interface, 2008. **5**(27): p. 1137-1158.

211. Rodrigues, C.V.M., et al., *Characterization of a bovine collagen–hydroxyapatite composite scaffold for bone tissue engineering.* Biomaterials, 2003. **24**(27): p. 4987-4997.

212. Dorozhkin, S.V., *Biphasic, triphasic and multiphasic calcium orthophosphates.* Acta Biomaterialia, 2012. **8**(3): p. 963-977.

213. Yuan, H., et al., *Osteoinductive ceramics as a synthetic alternative to autologous bone grafting.* Proceedings of the National Academy of Sciences, 2010. **107**(31): p. 13614-13619.

214. Rezwan, K., et al., *Biodegradable and bioactive porous polymer/inorganic composite scaffolds for bone tissue engineering.* Biomaterials, 2006. **27**(18): p. 3413-3431.

215. Beck-Coon, R.J., C.W. Newton, and A.H. Kafrawy, *An in vivo study of the use of a nonresorbable ceramic hydroxyapatite as an alloplastic graft material in periapical surgery.* Oral Surgery, Oral Medicine, Oral Pathology, 1991. **71**(4): p. 483-488.

216. Champion, J., A. Walker, and S. Mitragotri, *Role of Particle Size in Phagocytosis of Polymeric Microspheres.* Pharmaceutical Research, 2008. **25**(8): p. 1815-1821.

217. Bohner, M., L. Galea, and N. Doebelin, *Calcium phosphate bone graft substitutes: Failures and hopes.* Journal of the European Ceramic Society, 2012. **32**(11): p. 2663-2671.

218. Baker, M.I., et al., *Bone properties surrounding hydroxyapatite-coated custom osseous integrated dental implants.* Journal of biomedical materials research. Part B, Applied biomaterials, 2010. **95**(1): p. 218-24.

219. Walsh, W.R., et al., *β-TCP bone graft substitutes in a bilateral rabbit tibial defect model.* Biomaterials, 2008. **29**(3): p. 266-271.

220. Horch, H.H., et al., *Synthetic, pure-phase beta-tricalcium phosphate ceramic granules (Cerasorb®) for bone regeneration in the reconstructive surgery of the jaws.* International Journal of Oral and Maxillofacial Surgery, 2006. **35**(8): p. 708-713.

221. Jung, Y., et al., *A poly(lactic acid)/calcium metaphosphate composite for bone tissue engineering.* Biomaterials, 2005. **26**(32): p. 6314-6322.

222. Grynpas, M.D., et al., *Porous calcium polyphosphate scaffolds for bone substitute applications in vivo studies.* Biomaterials, 2002. **23**(9): p. 2063-2070.

223. Baksh, D., J.E. Davies, and S. Kim, *Three-dimensional matrices of calcium polyphosphates support bone growth in vitro and in vivo.* Journal of Materials Science: Materials in Medicine, 1998. **9**(12): p. 743-748.

224. Pilliar, R.M., et al., *Porous calcium polyphosphate scaffolds for bone substitute applications — in vitro characterization.* Biomaterials, 2001. **22**(9): p. 963-972.

225. Lee, Y.M., et al., *Tissue-engineered growth of bone by marrow cell transplantation using porous calcium metaphosphate matrices.* J Biomed Mater Res, 2001. **54**(2): p. 216-23.

226. Hill, W.L., et al., *Acid Pyro- and Metaphosphates Produced by Thermal Decomposition of Monocalcium Phosphate.* Industrial & Engineering Chemistry, 1947. **39**(12): p. 1667-1672.

227. Buranawat, B., et al., *Evaluation of a beta-calcium metaphosphate bone Graft containing bone morphogenetic protein-7 in rabbit maxillary defects.* J Periodontol, 2014. **85**(2): p. 298-307.

228. Shi, Y., et al., *Swelling, mechanical and friction properties of PVA/PVP hydrogels after swelling in osmotic pressure solution.* Materials Science and Engineering: C, 2016. **65**: p. 172-180.

229. Tadavarthy, S.M., J.H. Moller, and K. Amplatz, *Polyvinyl alcohol (Ivalon)--a new embolic material.* Am J Roentgenol Radium Ther Nucl Med, 1975. **125**(3): p. 609-16.

230. Di-Silvio, L. and N. Gurav, *Osteoblasts*, in *Human Cell Culture*, M. Koller, B. Palsson, and J.W. Masters, Editors. 2001, Springer Netherlands. p. 221-241.

231. Mosmann, T., *Rapid colorimetric assay for cellular growth and survival: application to proliferation and cytotoxicity assays.* J Immunol Methods, 1983. **65**(1-2): p. 55-63.

232. Venkatesan, J., et al., *Alginate composites for bone tissue engineering: a review.* Int J Biol Macromol, 2015. **72**: p. 269-81.

233. Rowley, J.A., G. Madlambayan, and D.J. Mooney, *Alginate hydrogels as synthetic extracellular matrix materials.* Biomaterials, 1999. **20**(1): p. 45-53.

234. Yao, N., et al., *The effect of phosphoric acid concentration on the synthesis of nano-whiskers of calcium metaphosphate by chemical precipitation Method.* IOP Conference Series: Materials Science and Engineering, 2011. **18**(6): p. 062022.

235. Abo-Naf, S.M., M.S. El-Amiry, and A.A. Abdel-Khalek, *FT-IR and UV–Vis optical absorption spectra of γ-irradiated calcium phosphate glasses doped with Cr2O3, V2O5 and Fe2O3.* Optical Materials, 2008. **30**(6): p. 900-909.

236. Kasuga, T., et al., *Surface modification of calcium metaphosphate fibers.* Journal of Materials Science: Materials in Medicine, 2000. **11**(4): p. 223-225.

237. Pemberton, J.E., et al., *Raman spectroscopy of calcium phosphate glasses with varying calcium oxide modifier concentrations.* Chemistry of Materials, 1991. **3**(1): p. 195-200.

238. Nannmark, U. and L. Sennerby, *The bone tissue responses to prehydrated and collagenated cortico-cancellous porcine bone grafts: a study in rabbit maxillary defects.* Clin Implant Dent Relat Res, 2008. **10**(4): p. 264-70.

239. Gonzalez, J.S. and V.A. Alvarez, *Mechanical properties of polyvinylalcohol/hydroxyapatite cryogel as potential artificial cartilage.* J Mech Behav Biomed Mater, 2014. **34**: p. 47-56.

240. Zhang, J., et al., *Biodegradable poly (lactic acid)/hydroxyl apatite 3D porous scaffolds using high-pressure molding and salt leaching.* Journal of Materials Science, 2014. **49**(4): p. 1648-1658.

241. Melton, J.T.K., et al., *A biomechanical analysis of the material properties of the TRUFIT CB PLUG for osteochondral defects of the knee.* Orthopaedic Proceedings, 2010. **92-B**(SUPP III): p. 420-421.

242. Zhou, C., et al., *Biomimetic fabrication of a three-level hierarchical calcium phosphate/collagen/hydroxyapatite scaffold for bone tissue engineering.* Biofabrication, 2014. **6**(3): p. 035013.

243. Gay, S., S. Arostegui, and J. Lemaitre, *Preparation and characterization of dense nanohydroxyapatite/PLLA composites.* Materials Science and Engineering: C, 2009. **29**(1): p. 172-177.

244. BIOMATLANTE, *http://biomatlante.com/wp-content/uploads/2015/08/FT2015021MOSD1-Biomatlante-EZ-Cure-Plug-Brochure-BD.pdf (accessed 15-07-2016).*

245. OsteoGen, *http://www.impladentltd.com/v/vspfiles/images/OsteoGenPlugBrochureFinalsmall.pdf (accessed 15-07-2016).*

246. Nephew, S., *https://www.smith-nephew.com/global/assets/pdf/temp/e-2012_advanced_biomaterials_(copy-1).pdf (accessed 15-07-2016).*

247. Gao, C., et al., *Fabrication of calcium sulfate/PLLA composite for bone repair.* J Biomed Mater Res A, 2005. **73**(2): p. 244-53.

248. Yamashita, J., et al., *The use of dynamic mechanical analysis to assess the viscoelastic properties of human cortical bone.* Journal of Biomedical Materials Research, 2001. **58**(1): p. 47-53.

249. Barbieri, D., et al., *Controlling dynamic mechanical properties and degradation of composites for bone regeneration by means of filler content.* J Mech Behav Biomed Mater, 2013. **20**: p. 162-72.

250. Schmidt, C., et al., *A scanning electron microscopy study of human osteoblast morphology on five orthopedic metals.* J Biomed Mater Res, 2002. **63**(3): p. 252-61.

251. http://www.biohorizons.com/memlok-pliable.aspx *(Accessed 03/12/2015)*

252. http://www.zimmerdental.com/Products/Regenerative/rg_WoundDressingsOverview.aspx *(Accessed 11/12/2015)*

253. http://www.straumann.co.uk/en/dental-professionals/straumann-products-and-solutions/regenerative-solutions-incl-botiss/soft-tissue-grafts/mucoderm.html *(Accessed 11/12/2015)*

254. http://www.straumann.co.uk/en/dental-professionals/straumann-products-and-solutions/regenerative-solutions-incl-botiss/collagen-fleeces.html *(Accessed 11/12/2015)*

255. http://www.botiss-surgical.com/ *(Accessed 11/12/2015)*

256. http://surgery.ucsd.edu/som/surgery/divisions/trauma-burn/about/burn-center/Documents/85-TransCyte.pdf *(Accessed 03/12/2015)*

257. http://www.smith-nephew.com/professional/products/advanced-wound-management/algisite-m/ *(Accessed 15/12/2015)*

258. Williams, C., *3m Tegasorb Thin: A hydrocolloid dressing for chronic wounds.* British Journal of Nursing, 2000. **9**(11): p. 720-723.

259. http://www.apligraf.com/professional/what_is_apligraf/index.html *(Accessed 11/12/2015)*

260. http://www.dermagraft.com/home/ *(Accessed 11/12/2015)*

261. http://www.goremedical.com/resources/dam/assets/AR2659-EN1.pdf *(Accessed 15/12/2015)*

262. http://www.goremedical.com/resources/dam/assets/AP2975-EN1.pdf *(Accessed 15/12/2015)*

263. Courtney, T., et al., *Design and analysis of tissue engineering scaffolds that mimic soft tissue mechanical anisotropy.* Biomaterials, 2006. **27**(19): p. 3631-8.

264. Miserez, A., J.C. Weaver, and O. Chaudhuri, *Biological materials and molecular biomimetics - filling up the empty soft materials space for tissue engineering applications.* Journal of Materials Chemistry B, 2015. **3**(1): p. 13-24.

265. Feng, Q., et al., *Mechanically resilient, injectable, and bioadhesive supramolecular gelatin hydrogels crosslinked by weak host-guest interactions assist cell infiltration and in situ tissue regeneration.* Biomaterials, 2016. **101**: p. 217-228.

266. Haque, M.A., T. Kurokawa, and J.P. Gong, *Super tough double network hydrogels and their application as biomaterials.* Polymer, 2012. **53**(9): p. 1805-1822.

267. Yasuda, K., et al., *Biomechanical properties of high-toughness double network hydrogels.* Biomaterials, 2005. **26**(21): p. 4468-75.

268. Hagiwara, Y., et al., *Ligament-like tough double-network hydrogel based on bacterial cellulose.* Cellulose, 2010. **17**(1): p. 93-101.

269. Jang, S.S., W.A. Goddard, and M.Y.S. Kalani, *Mechanical and Transport Properties of the Poly(ethylene oxide)−Poly(acrylic acid) Double Network Hydrogel from Molecular Dynamic Simulations.* The Journal of Physical Chemistry B, 2007. **111**(7): p. 1729-1737.

270. Fei, R., et al., *Thermoresponsive nanocomposite double network hydrogels.* Soft matter, 2012. **8**(2): p. 481-487.

271. Yasuda, K., et al., *A novel double-network hydrogel induces spontaneous articular cartilage regeneration in vivo in a large osteochondral defect.* Macromol Biosci, 2009. **9**(4): p. 307-16.

272. Azuma, C., et al., *Biodegradation of high-toughness double network hydrogels as potential materials for artificial cartilage.* J Biomed Mater Res A, 2007. **81**(2): p. 373-80.

273. Bajpai, S.K. and S. Sharma, *Investigation of swelling/degradation behaviour of alginate beads crosslinked with Ca2+ and Ba2+ ions.* Reactive and Functional Polymers, 2004. **59**(2): p. 129-140.

274. Nakamura, K., et al., *Thermal properties of water insoluble alginate films containing di- and trivalent cations.* Thermochimica Acta, 1995. **267**: p. 343-353.

275. Marriott, A.S., et al., *A natural template approach to mesoporous carbon spheres for use as green chromatographic stationary phases.* RSC Advances, 2014. **4**(1): p. 222-228.

276. Ruvinov, E. and S. Cohen, *Alginate biomaterial for the treatment of myocardial infarction: Progress, translational strategies, and clinical outlook: From ocean algae to patient bedside.* Advanced Drug Delivery Reviews, 2016. **96**: p. 54-76.

277. Andersen, T., P. Auk-Emblem, and M. Dornish, *3D Cell Culture in Alginate Hydrogels.* Microarrays, 2015. **4**(2): p. 133-161.

278. N.A. Peppas, D.T., *Semicrystalline poly(vinyl alcohol) films and their blends with poly(acrylic acid) and poly(ethylene glycol) for drug delivery applications.* J. DRUG DEL. SCI. TECH, 2004. **14** ((4)): p. 291-297.

279. Mansur, H.S., et al., *FTIR spectroscopy characterization of poly (vinyl alcohol) hydrogel with different hydrolysis degree and chemically crosslinked with glutaraldehyde.* Materials Science and Engineering: C, 2008. **28**(4): p. 539-548.

280. Sartori, C., et al., *Determination of the cation content of alginate thin films by FTi.r. spectroscopy.* Polymer, 1997. **38**(1): p. 43-51.

281. Leal, D., et al., *FT-IR spectra of alginic acid block fractions in three species of brown seaweeds.* Carbohydrate Research, 2008. **343**(2): p. 308-316.

282. Soares, J.P., et al., *Thermal behavior of alginic acid and its sodium salt.* Eclética Química, 2004. **29**: p. 57-64.

283. Hua, S., et al., *pH-sensitive sodium alginate/poly(vinyl alcohol) hydrogel beads prepared by combined Ca2+ crosslinking and freeze-thawing cycles for controlled release of diclofenac sodium.* International Journal of Biological Macromolecules, 2010. **46**(5): p. 517-523.

284. Gnanaprakasam Thankam, F., et al., *Growth and survival of cells in biosynthetic poly vinyl alcohol–alginate IPN hydrogels for cardiac applications.* Colloids and Surfaces B: Biointerfaces, 2013. **107**(0): p. 137-145.

285. Bunn, C.W., *Crystal Structure of Polyvinyl Alcohol.* Nature, 1948. **161**(4102): p. 929-930.

286. Ahmed, S., et al., *Brittle–ductile transition of double network hydrogels: Mechanical balance of two networks as the key factor.* Polymer, 2014. **55**(3): p. 914-923.

287. Nakajima, T., et al., *A Universal Molecular Stent Method to Toughen any Hydrogels Based on Double Network Concept.* Advanced Functional Materials, 2012. **22**(21): p. 4426-4432.

288. Kulkarni, R.V., et al., *Interpenetrating network hydrogel membranes of sodium alginate and poly(vinyl alcohol) for controlled release of prazosin hydrochloride through skin.* Int J Biol Macromol, 2010. **47**(4): p. 520-7.

289. Xie, L., et al., *Controlled mechanical and swelling properties of poly(vinyl alcohol)/sodium alginate blend hydrogels prepared by freeze–thaw followed by Ca2+ crosslinking.* Journal of Applied Polymer Science, 2012. **124**(1): p. 823-831.

290. Nakajima, T., et al., *True Chemical Structure of Double Network Hydrogels.* Macromolecules, 2009. **42**(6): p. 2184-2189.

291. Tanaka, Y., et al., *Determination of Fracture Energy of High Strength Double Network Hydrogels.* The Journal of Physical Chemistry B, 2005. **109**(23): p. 11559-11562.

292. Therese Andersen, B.L.S., Kjetil Formo, Eben Alsberg and Bjorn E. Christensen, *Alginates as biomaterials in tissue engineering.* Carbohydrate Chemistry, 2012(37): p. 227-258.

293. Sun, J.Y., et al., *Highly stretchable and tough hydrogels.* Nature, 2012. **489**(7414): p. 133-6.

294. Duffy, C., et al., *Arrays of 3D double-network hydrogels for the high-throughput discovery of materials with enhanced physical and biological properties.* Acta Biomater, 2016. **34**: p. 104-12.

295. Ronken, S., et al., *Double-network acrylamide hydrogel compositions adapted to achieve cartilage-like dynamic stiffness.* Biomechanics and Modeling in Mechanobiology, 2013. **12**(2): p. 243-248.

296. Hench, L.L., N. Roki, and M.B. Fenn, *Bioactive glasses: Importance of structure and properties in bone regeneration.* Journal of Molecular Structure, 2014. **1073**: p. 24-30.

297. Jones, J.R., *3 - Bioactive ceramics and glasses A2 - Boccaccini, Aldo R*, in *Tissue Engineering Using Ceramics and Polymers*, J.E. Gough, Editor. 2007, Woodhead Publishing. p. 52-71.

298. Rahaman, M.N., et al., *Bioactive glass in tissue engineering.* Acta Biomater, 2011. **7**(6): p. 2355-73.

299. Hench, L.L., *Chronology of Bioactive Glass Development and Clinical Applications.* New Journal of Glass and Ceramics, 2013. **Vol.03No.02**: p. 7.

300. Hench, L.L., et al., *Glass and Medicine.* International Journal of Applied Glass Science, 2010. **1**(1): p. 104-117.

301. Hench, L.L., *Bioactive materials for gene control.* New Materials and Technologies for Healthcare, 2011: p. 25-48.

302. works, H.P., *http://www.novabone.in/pdf/pggen.pdf (Accessed 16/03/2016)*

303. NovaBone, *http://www.novabone.com/NB/orthopedic.html (Accessed 16/03/2016)*

304. Bonfield, W., et al., *Hydroxyapatite reinforced polyethylene — a mechanically compatible implant material for bone replacement.* Biomaterials, 1981. **2**(3): p. 185-186.

305. Chen, Q.Z., I.D. Thompson, and A.R. Boccaccini, *45S5 Bioglass®-derived glass–ceramic scaffolds for bone tissue engineering.* Biomaterials, 2006. **27**(11): p. 2414-2425.

306. Jones, J.R., *Review of bioactive glass: From Hench to hybrids.* Acta Biomaterialia, 2013. **9**(1): p. 4457-4486.

307. Cannillo, V., et al., *Production of Bioglass® 45S5 – Polycaprolactone composite scaffolds via salt-leaching.* Composite Structures, 2010. **92**(8): p. 1823-1832.

308. Ryszkowska, J.L., et al., *Biodegradable polyurethane composite scaffolds containing Bioglass® for bone tissue engineering.* Composites Science and Technology, 2010. **70**(13): p. 1894-1908.

309. Kokubo, T. and H. Takadama, *How useful is SBF in predicting in vivo bone bioactivity?* Biomaterials, 2006. **27**(15): p. 2907-2915.

310. Boccaccini, A.R., et al., *Sintering, crystallisation and biodegradation behaviour of Bioglass-derived glass-ceramics.* Faraday Discuss, 2007. **136**: p. 27-44; discussion 107-23.

311. Clupper, D.C., et al., *Bioactive evaluation of 45S5 bioactive glass fibres and preliminary study of human osteoblast attachment.* Journal of Materials Science: Materials in Medicine. **15**(7): p. 803-808.

312. Clupper, D.C., et al., *Bioactive evaluation of 45S5 bioactive glass fibres and preliminary study of human osteoblast attachment.* J Mater Sci Mater Med, 2004. **15**(7): p. 803-8.

313. Chen, Q., et al., *Electrophoretic co-deposition of polyvinyl alcohol (PVA) reinforced alginate–Bioglass® composite coating on stainless steel: Mechanical properties and in-vitro bioactivity assessment.* Materials Science and Engineering: C, 2014. **40**: p. 55-64.

314. Mishra, R., B. Basu, and A. Kumar, *Physical and cytocompatibility properties of bioactive glass-polyvinyl alcohol-sodium alginate biocomposite foams prepared via sol-gel processing for trabecular bone regeneration.* J Mater Sci Mater Med, 2009. **20**(12): p. 2493-500.

315. Oliveira, A.A.R.d., et al., *Effect of polyvinyl alcohol content and after synthesis neutralization on structure, mechanical properties and cytotoxicity of sol-gel derived hybrid foams.* Materials Research, 2009. **12**: p. 239-244.

316. Wu, Z.Y., et al., *Melt-derived bioactive glass scaffolds produced by a gel-cast foaming technique.* Acta Biomater, 2011. **7**(4): p. 1807-16.

317. Peter, M., et al., *Novel biodegradable chitosan–gelatin/nano-bioactive glass ceramic composite scaffolds for alveolar bone tissue engineering.* Chemical Engineering Journal, 2010. **158**(2): p. 353-361.

318. Pon-On, W., et al., *Mechanical properties, biological activity and protein controlled release by poly(vinyl alcohol)–bioglass/chitosan–collagen composite scaffolds: A bone tissue engineering applications.* Materials Science and Engineering: C, 2014. **38**: p. 63-72.

319. Nooeaid, P., et al., *Technologies for Multilayered Scaffolds Suitable for Interface Tissue Engineering.* Advanced Engineering Materials, 2014. **16**(3): p. 319-327.

320. Bertolla, L., I. Dlouhý, and A.R. Boccaccini, *Preparation and characterization of Bioglass®-based scaffolds reinforced by poly-vinyl alcohol/microfibrillated cellulose composite coating.* Journal of the European Ceramic Society, 2014. **34**(14): p. 3379-3387.

321. Costa, H.S., et al., *Engineered Hybrid Scaffolds of Poly(vinyl alcohol)/Bioactive Glass for Potential Bone Engineering Applications: Synthesis, Characterization, Cytocompatibility, and Degradation.* Journal of Nanomaterials, 2012. **2012**: p. 16.

322. Cantournet, S., R. Desmorat, and J. Besson, *Mullins effect and cyclic stress softening of filled elastomers by internal sliding and friction thermodynamics model.* International Journal of Solids and Structures, 2009. **46**(11–12): p. 2255-2264.

323. Webber, R.E., et al., *Large Strain Hysteresis and Mullins Effect of Tough Double-Network Hydrogels.* Macromolecules, 2007. **40**(8): p. 2919-2927.

324. Hench, L.L., *Bioceramics: From Concept to Clinic.* Journal of the American Ceramic Society, 1991. **74**(7): p. 1487-1510.

325. Zheng, K., et al., *Aging Time and Temperature Effects on the Structure and Bioactivity of Gel-Derived 45S5 Glass-Ceramics.* Journal of the American Ceramic Society, 2015. **98**(1): p. 30-38.

326. Notingher, I., et al., *Application of FTIR and Raman spectroscopy to characterisation of bioactive materials and living cells.* Spectroscopy, 2003. **17**(2-3).

327. Peitl Filho, O., G.P. LaTorre, and L.L. Hench, *Effect of crystallization on apatite-layer formation of bioactive glass 45S5.* J Biomed Mater Res, 1996. **30**(4): p. 509-14.

328. Rehman, I., J.C. Knowles, and W. Bonfield, *Analysis of in vitro reaction layers formed on Bioglass using thin-film X-ray diffraction and ATR-FTIR microspectroscopy.* J Biomed Mater Res, 1998. **41**(1): p. 162-6.

329. Gade, T.P., et al., *Imaging of alkaline phosphatase activity in bone tissue.* PLoS One, 2011. **6**(7): p. e22608.

330. Chan, C., L.L. Burrows, and C.M. Deber, *Helix induction in antimicrobial peptides by alginate in biofilms.* J Biol Chem, 2004. **279**(37): p. 38749-54.

331. Choi, J.S., et al., *Hydrogel-impregnated dressings for graft fixation: a case series.* J Wound Care, 2015. **24**(7): p. 326-8.

332. Lavrador, C., et al., *Elastomeric enriched biodegradable polyurethane sponges for critical bone defects: a successful case study reducing donor site morbidity.* J Mater Sci Mater Med, 2016. **27**(3): p. 61.

333. Baker, R.M., et al., *Self-deploying shape memory polymer scaffolds for grafting and stabilizing complex bone defects: A mouse femoral segmental defect study.* Biomaterials, 2016. **76**: p. 388-398.

334. Li, J.J., et al., *Efficacy of novel synthetic bone substitutes in the reconstruction of large segmental bone defects in sheep tibiae.* Biomed Mater, 2016. **11**(1): p. 015016.

335. Gunther, M.I., et al., *Cell-seeded alginate hydrogel scaffolds promote directed linear axonal regeneration in the injured rat spinal cord.* Acta Biomater, 2015. **27**: p. 140-50.